ORNL-3262
UC-4 – Chemistry
TID-4500 (17th ed.)

Contract No. W-7405-eng-26

REACTOR CHEMISTRY DIVISION ANNUAL PROGRESS REPORT

For Period Ending January 31, 1962

Director

W. R. Grimes

Associate Directors

E. G. Bohlmann
H. F. McDuffie
G. M. Watson

Senior Scientific Advisors

F. F. Blankenship
C. H. Secoy

DATE ISSUED

MAY 11 1962

OAK RIDGE NATIONAL LABORATORY
Oak Ridge, Tennessee
operated by
UNION CARBIDE CORPORATION
for the
U. S. ATOMIC ENERGY COMMISSION

DISCLAIMER

Summary

PART I. MOLTEN-SALT REACTOR PROGRAM

1. High-Temperature Phase Equilibrium Studies

Investigations of high-temperature phase equilibria were continued for systems having potential use in molten-salt reactor technology. Composition-temperature relationships of LiF-BeF_2-ZrF_4-ThF_4-UF_4 MSRE fuel mixtures were studied in the temperature range 400 to 600°C. Phase diagrams were constructed for the systems LiF-BeF_2-ZrF_4, KF-ThF_4, RbF-ThF_4, NaF-ThF_4-UF_4, NaF-YF_3, and CrF_2-CrF_3. Investigations of phase behavior were continued in the systems NaF-BeF_2-ZrF_4 and LiF-NaF-ThF_4, which are of potential use as reactor-fuel reprocessing solvents. X-ray diffraction studies of the $LiSbF_6$ crystal structure were completed. Unit-cell measurements and space group assignments were made for the compounds $NaF{\cdot}YF_3$, $3KF{\cdot}UF_4$, $3KF{\cdot}ThF_4$, chromium(II,III) fluoride, $LiF{\cdot}RbF$, $LiF{\cdot}CsF$, and $6LiF{\cdot}BeF_2{\cdot}ZrF_4$. Unsuccessful attempts were made to produce uranium(IV) oxyfluoride. Characteristic properties and/or methods of preparing the new compounds VF_3, $ZrOF_2$, $ZrCl$, $RbF{\cdot}SrF_2$, $CsF{\cdot}CaF_2$, and $CsF{\cdot}BaF_2$ were determined.

2. Compatibility of MSRE Components

In the Molten-Salt Reactor Experiment, a molten fluoride fuel containing UF_4 is exposed to a large area of graphite moderator surface. Because of the sensitivity of reactor behavior to the amount of uranium in the core, the extent to which fuel may penetrate the graphite is of considerable import. Since the fuel is nonwetting and pressure is a controlling variable in the permeation, a buoyancy balance has been constructed to study the penetration of graphite by fuel over a range of pressures. The influence of cesium deposition, which arises from decay and burnup of fission product xenon migrating into the graphite, has also been examined. The results, as established in the absence of radiation, continue to give evidence of favorable behavior for MSRE operation.

An experiment designed to determine whether fissioning fuel in contact with graphite exhibits interfacial characteristics different from the nonwetting behavior shown out-of-pile was operated for 1580 hr at a fuel power density of 200 w/cc. The fuel, LiF-BeF_2-ZrF_4-ThF_4-UF_4 (69.5-23-5-1-1.5 mole %), contained in encapsulated graphite boats, reached maximum temperatures of about 900°C in undergoing 8.5% burnup of U^{235} and still remained nonwetting toward graphite; the graphite was virtually undamaged.

Supplemental observations, some of which are still in progress, revealed that CF_4 was produced, that the frozen fuel appeared black because of discoloration by beta radiation, and that several other unusual or puzzling phenomena had occurred. The persistence of CF_4 was contrary to thermodynamic equilibrium and may have been favored by the experimental arrangement; the escape of CF_4 in the off-gas is potentially a serious problem, mainly because the effect is that of a strong reducing agent acting on the fuel.

3. Fluoride Salt Production

During 1961, approximately 4750 kg of various fluoride mixtures was prepared for the Molten-Salt Reactor Program and other Laboratory projects which utilize fused fluorides. In addition to production operations, various related services were performed to support engineering tests with molten-salt and liquid-metal systems, in-pile test programs, and experimental development projects. Continued efforts to improve both the fluoride purification procedure and the processing plant have resulted in substantial increases in the production rate of fused fluoride mixtures.

4. Chemical Aspects of MSRE Safety

Questions related to the safety of the MSRE are raised by the possibility of accidentally mixing the fuel or coolant salts with water. Both short-term and long-term effects are important. The solubilities of the reactor coolant and the nominal reactor fuel in water have been determined at 25°C and at higher temperatures up to 100°C. Uranium concentrations as high as 0.01 *m* were observed, suggesting that nuclear poisons be added to the water in case of an accidental fuel spill. Apparatus was devised and tested for laboratory studies of the short-term temperature and pressure effects of injecting molten fluoride salts into water. Calculations were made with respect to the possible release of radioactive iodine from MSRE fuel under various conditions; only in case of a spill in the presence of air does it appear that the liberation of free iodine would be expected.

5. Physical Chemistry of Molten-Salt Systems

Further studies of freezing-point depressions of sodium fluoride showed that solutes of trivalent fluorides caused negative deviations from ideality (the smaller the solute cation size, the greater the deviation) and that solutes of alkali fluorides caused mainly positive deviations (attributable to changes in London dispersion forces). Solutes of alkali fluorides caused freezing-point depressions in lithium fluoride somewhat different from those in sodium fluoride because of differences in Coulombic forces. Excess partial molal free energies of mixing, calculated from liquidus temperatures in the system NaF-LiF, were expressible in terms of concentration and two constants.

Densities of solid complex metallic fluorides were calculated, with an average error of 5.5%, by assuming that the molar volume of the complex is the sum of the molar volumes of the simple fluorides that formed the complex. This method of estimating densities facilitated the choice of number of molecules per unit cell for complex fluorides whose structures were under investigation.

All the published density data on molten fluoride mixtures were re-examined in order to develop a more useful method of predicting densities of related systems. To a good approximation, the molar volumes of these melts were found to be expressed by an additive function of the components. By using empirically adjusted values for the molar volumes of the components of the melt and assuming additivity, the densities could be calculated to within 2% of the experimentally reported values.

The enthalpy changes from 874.0 to 0°C were measured with a Bunsen ice calorimeter for samples of KF, LiF, and mixtures containing 0.193, 0.385, and 0.747 mole fraction of LiF. The calculated molar enthalpies of mixing when plotted vs composition gave an approximately symmetrical curve with a maximum at ~50 mole % LiF.

Equilibrium constants have been carefully measured at elevated temperatures for the reaction

$$NiF_2 + H_2 \rightleftharpoons 2HF + Ni ,$$

with the NiF_2 in unsaturated solution in an $LiF\text{-}BeF_2$ mixture and in several $NaF\text{-}ZrF_4$ solutions of varying NaF concentration, and with crystalline nickel present in large excess. These measurements all show the equilibrium constant, K_N, to vary with temperature and with solvent composition but to be independent of NiF_2 concentration; the activity coefficient of NiF_2 in these solutions is accordingly also independent of concentration of this compound. From the $LiF\text{-}BeF_2$ mixture (alone among those studied) the phase in equilibrium with the saturated solution is pure NiF_2; for such saturated solutions the activity coefficient (crystalline NiF_2 reference state) at any temperature is simply the reciprocal of the solubility at that temperature. Accordingly, from these activity coefficients and values of K_N in the $LiF\text{-}BeF_2$ solvent, free-energy values can be derived. Use of these values and of pertinent thermochemical data, either known or capable of reliable estimates in a third-law treatment, permits evaluation of $\Delta H^0_{298.16}$ and estimation of ΔF^0 values at other temperatures for the reaction with crystalline solid and (hypothetical) supercooled liquid NiF_2 as reference states. From the true equilibrium constant, obtainable directly from these free-energy values, and the K_N values, activity coefficients of NiF_2 have been obtained. These activity coefficients and their changes with solvent composition, especially those with supercooled NiF_2 as the reference state, offer suggestions as to the nature of such solutions.

The temperature coefficients of the association constants K_1, K_2, and K_{12} for the formation of the species AgBr, $AgBr_2^-$, and Ag_2Br^+ in molten KNO_3, and of K_1 and K_2 for the formation of $CdBr^+$, CdI^+, $CdBr_2$, and CdI_2 in alkali nitrate mixtures indicate that the entropies of these associations are consistent with the "configurational" entropy calculated from the quasi-lattice model. The entropy of association of Ag^+ with the polyatomic ion CN^- is much more positive than for the associations with monatomic anions. The influence of solvent on the association constants for the formation of the associated species AgBr or AgCl in the molten solvents $NaNO_3$ and KNO_3 is consistent with the *reciprocal Coulomb effect*.

The perturbation theory of Reiss, Katz, and Kleppa for systems with a common anion has been extended to the third- and fourth-order terms to yield the equation for the excess free energy of mixing of uniunivalent salt mixtures:

$$\frac{\Delta F^E}{kT} = X_1 X_2 P\delta^2 + X_1 X_2 (X_1 - X_2) Q\delta^3 + [X_1 X_2 R + X_1 X_2 (X_1 - X_2)^2 S]\delta^4 + \cdots ,$$

where X_i is a mole fraction of component i, δ is related to the ionic sizes, and P, Q, R, and S are constants. The third- and fourth-order terms are necessary to rationalize experimental measurements in molten salts.

An estimate of the contribution of London dispersion energy to the heats of mixing of mixtures of alkali nitrates with $AgNO_3$ or $TlNO_3$ is consistent with the observed differences between these mixtures and mixtures of alkali nitrates. This suggests a method of making estimates of this effect in mixtures containing other polarizable cations.

PART II. AQUEOUS REACTOR PROGRAMS

6. Chemistry of Pressurized-Water Reactor Systems

A study of the chemical and radiochemical behavior of the water in the pressurized-water loop at the Oak Ridge Research Reactor, in process, indicates that a large fraction of the water-borne activity (principally Mn^{54}, Fe^{59}, Co^{58}, and Co^{60}) is present as dissolved ionic material. The particulate material which can be removed by filtration is well crystallized and has the structure of magnetite. Appreciable radiochemical exchange may occur between the particulate and the dissolved material, suggesting that magnetite may be a suitable high-temperature filter, ion exchange medium for pressurized-water reactor coolant purification.

7. Phase Equilibria in Aqueous Systems at Elevated Temperatures

Solubilities of UO_3 hydrates in the system UO_3-SO_3-H_2O are presented at temperatures from 150 to 300°C. The stable hydrates are shown to be α-$UO_3 \cdot H_2O$ at 150°, β-$UO_3 \cdot H_2O$ at 225°, and $UO_3 \cdot \frac{1}{2}H_2O$ at 300°C.

In the five-component system UO_3-CuO-NiO-SO_3-H_2O, the compositions of solutions saturated simultaneously with the three solid phases, $UO_3 \cdot \frac{1}{2}H_2O$, $CuO \cdot 3UO_3$, and $NiO \cdot 3UO_3$, are given at 300, 325, and 350°C in solutions varying from 0.002 to 0.06 m in SO_3.

Solubilities of stoichiometric salts in H_2O at temperatures above 200°C were compiled and show that very little information exists for these systems at temperatures above 374°C. Sufficient study at high temperature on aqueous systems containing uranium might define regions of stability necessary to specify fuel compositions.

Critical phenomena and regions of liquid-liquid immiscibility were defined in the systems UO_3-CuO-SO_3-D_2O, UO_3-NiO-SO_3-D_2O, and UO_3-CuO-NiO-SO_3-D_2O at temperatures from 280 to 410°C. At a fixed concentration of SO_3, the temperature of liquid-liquid immiscibility rose as the concentration of metal oxide decreased. Critical phenomena (defined herein as the disappearance of the meniscus between liquid and vapor) occurred at molal ratios, metal oxide:SO_3, below approximately 0.3.

The effects of hydrostatic pressure in raising the temperature of liquid-liquid immiscibility were determined for several H_2O solutions of UO_3 and SO_3. The value of $\Delta t/\Delta p$ for stoichiometric UO_2SO_4 solutions was approximately constant at 0.08°C/atm at pressures up to 300 atm.

The solubilities of $NiSO_4 \cdot H_2O$ and several nickel oxysulfates in SO_3-H_2O at temperatures from 150 to 350°C and at SO_3 concentrations from 10^{-4} to 2 m are given. Comparative data in the D_2O systems are presented which show higher solubilities than in the H_2O system.

In connection with evaluation of possible breeding blankets, the solubilities of ThO_2 in HNO_3-H_2O at 150 and 200°C are presented and are compared with previous data at 200 and 300°C.

Details of a high-pressure vessel incorporating Teflon as a gasketing material, used for equilibrating liquid-solid mixtures, are given. Vessels of this design were used at temperatures up to 500°C and at pressures up to 1000 bars.

Data are shown for the solubility of H_2 in H_2O and of D_2 in D_2O from 260 to 300°C. Data are also given that show the effect on the solubility of H_2 in H_2O of a 2-1 and a 1-2 electrolyte at a concentration of 0.1 *M* from 0 to 120°C. The effect of 1 *M* $HClO_4$ in the same system from 20 to 120°C is also reported.

8. Physical Chemistry of Aqueous Solutions

A study of thorium(IV) hydrolysis at 94°C in 1 *M* $NaClO_4$ solution is in progress. Results thus far indicate that comparable hydrolysis occurs about one pH unit lower at 94° than at 25°C. While the hydrolysis mechanism, involving polynuclear species, is similar at the two temperatures, mononuclear species appear relatively more stable at the higher temperature.

A study of uranium(VI) hydrolysis at 25 and 94°C has been completed. Three hydrolysis products, in which the mole ratio UO_2^{2+}:OH^- = 1:1, 2:2, and 3:5, were found to account adequately for the results. The best values of the corresponding equilibrium quotients were evaluated at the two temperatures by a least-squares computer code. This hydrolysis scheme accounts qualitatively for the solubility behavior of UO_3 in nitric acid solutions at elevated temperatures. Analysis of the solubility data is being conducted to extend the temperature dependence of uranium(VI) hydrolysis to higher temperatures.

Isopiestic ratios with reference to NaCl solutions have been obtained for four alkali chlorides and for magnesium and uranyl sulfates at 140°C. Osmotic coefficients for these solutes have been estimated from the data and by extrapolation of boiling-point data for NaCl solutions. The temperature dependence of the osmotic coefficients has been qualitatively related to the comparative ability of the various ions to stabilize the ice structure of water.

The effects of pressure up to 3000 bars, upon the specific conductances of solutions, were determined for 0.005 *m* H_2SO_4 at 30.1°C, for 0.005 *m* K_2SO_4 at 24.3°C, for 0.00218 *m* K_2SO_4 from 25 to 750°C, and for 0.0005 *m* K_2SO_4 from 25 to 600°C.

The decomposition of peroxide in thorium nitrate–nitric acid solutions was only slightly catalyzed by ferric ion. Cupric-ion catalysis was similar to that observed in other systems. The insoluble thorium peroxynitrate formed by the addition of hydrogen peroxide to thorium nitrate solution corresponds to the stoichiometric formula $Th_6(OO)_{10}(NO_3)_4 \cdot 10H_2O$.

Exploratory experiments for the purpose of determining the stability of protactinium in thorium nitrate–nitric acid solutions were performed. The data obtained indicate that protactinium does not precipitate rapidly from these solutions at temperatures from 140 to 180°C, when in contact with Zircaloy and stainless steel surfaces.

Protactinium-231 was precipitated from 2 *M* $Th(NO_3)_4$–3 *M* HNO_3 by the addition of H_2O_2. Extraction of Pa^{231} from an aliquot of this same solution by diisobutyl carbinol indicated that the Pa^{231} was initially in true solution.

9. Chemical Aspects of Corrosion of Zircaloy-2

Examination has been completed on corrosion specimens exposed at locations in the core outlet, blanket, and circulating lines of the HRE-2 for various periods prior to run 20. Observations in near agreement with predictions from the in-pile loop program are as follows: (1) only small amounts of oxide remain on surfaces irradiated by fission recoils, with most of the oxide formed in such regions transported to other surfaces in the circulating system; (2) corrosion rates were 3 to 4 mpy for Zircaloy-2 exposed in the blanket side of the core and were negligible for specimens exposed elsewhere (none in the core); (3) corrosion rates were very low or negligible for titanium alloys; (4) corrosion rates were about 2.5 mpy for type 347 stainless steel in the blanket region; (5) penetration was comparable to that out-of-radiation for specimens in the circulating lines. The corrosion of stainless steel in the core outlet, however, was 3 to 5 times that predicted from the behavior of in-pile loops.

Two in-pile autoclave experiments, designed primarily to provide information on the radiation corrosion of Zircaloy-2 at temperatures to 360°C in 0.08 *m* UO_2SO_4, 0.02 *m* $CuSO_4$, and 0.24 *m*

D_2SO_4 in D_2O solution, failed by leakage before the design objectives could be achieved. However, the first autoclave, which remained intact for 350 hr out-of-pile at 360°C and for a short time at 280°C in beam hole HB-5 of the LITR, yielded some valuable information. The corrosion rate out-of-pile after the initial 50 hr was about 1.3 mpy, alpha counting of washed specimens after 124 hr exposure out-of-pile showed a very small amount of uranium sorption (0.24 $\mu g/cm^2$), and deuterium-oxygen recombination rate constants, K_{Cu} (from rates of pressure increase following initiation of irradiation), were shown to be 7×10^2, 1.9×10^3, and 6.6×10^3 liters(STP)/mole-hr at 230, 250, and 280°C respectively. All these data are consistent with previous observations or extrapolations.

Equipment has been assembled and tested for a study of the mechanism of corrosion of Zircaloy-2 after heavy-particle irradiation. Specimens will be irradiated in an inert environment and will subsequently be oxidized in 300°C steam with added oxygen. Weight-gain and capacitance measurements are expected to show variations which will yield valuable clues to the mechanisms of radiation corrosion.

Sorption of sulfate and of uranium by hydrous zirconia from D_2O solutions of UO_2SO_4 (0.02 to 0.17 *M*) and D_2SO_4 (0.02 to 0.2 *M*) has been determined over the temperature interval 100 to 300°C. Surface area of the residual oxides varied from 545 to 100 m^2/g with temperature and with solution composition. Total sulfate sorption at 100, 200, and 250°C was markedly higher at acidities above 0.01, 0.03, and 0.05 *M* than for lower acidities because of increased (and multilayer) sorption of acid; no such marked increase occurred up to 0.15 *M* D_2SO_4 at 280 and 300°C. Amounts sorbed at lower acidities at all temperatures probably represent near-monolayer adsorption. Uranium sorption per unit of surface area was nearly independent of temperature over the 100 to 300°C interval for solutions sufficiently acid to be truly stable. Sorption was less in solutions with 0.06 to 0.2 *M* acid than in solutions with 0.02 *M* excess acid, but no marked effects of the different initial acid concentrations of 0.06 to 0.2 *M* were observed. Sorption increased with increasing uranium concentration in the solution but did not exceed 0.004 millimole/cm^2. Acidities of the solutions generally decreased markedly during the exposure. Good values for the concentration of hydrogen ions and of other species in solution at temperature are probably required for complete interpretation of these results.

Corrosion currents were determined as a function of potential and temperature (150 to 300°C) on passive Zircaloy-2 in oxygenated 0.05 *M* H_2SO_4. From the results the activation energy for the anodic partial process (oxidation of zirconium) is 31.1 kcal/mole and is independent of potential and temperature in the range studied. The activation energy for the anodic partial process (reduction of O_2) is, however, a function of potential and temperature, being 10.8 kcal/mole at −1.400 v vs Pt between 220 and 300°C and changing to 5.4 kcal/mole at temperatures below 220°C. At −1.200 v vs Pt the activation energy is 5.4 kcal/mole over the entire temperature range. On the basis of the data at 298°C, a model proposed by Vetter for passive iron is suggested as an explanation for the corrosion behavior of passive Zircaloy-2.

10. Corrosion by Solutions

A program designed to study the stress-corrosion cracking behavior of type 347 stainless steel in a boiling, simulated HRE-2 fuel solution (0.04 *m* UO_2SO_4, 0.02 *m* H_2SO_4, and 0.005 *m* $CuSO_4$) containing chloride ions was completed. Cracking frequency was independent of chloride ion concentration in the range 25 to 500 ppm; no cracking occurred at 10 ppm or less. Two different heats of type 347 stainless steel were used, and although both were within AISI compositional limits, specimens from one heat consistently showed a cracking frequency twice that of the other. When chloride was added to the solution as mercuric chloride, no cracking was observed; however, the addition of chloride ions to the solution containing mercuric chloride increased the cracking frequency. The presence of as much as 100 ppm dichromate ions in the chloride-containing solution inhibited cracking, and exposure of the specimens to a chloride-free fuel solution prior to exposure to the chloride-containing solution was very effective in minimizing cracking.

Corrosion tests with QMV beryllium in deionized water at 250 and 300°C showed no significant attack after 120 days. Both with and without oxygen in the system, a thin tenacious film was formed and a few small pits were observed. The coupling of beryllium to itself, to Zircaloy-2, or to stainless steel produced no adverse effects in

degassed water. With oxygen in the system, however, beryllium coupled to Zircaloy developed pits up to 6 mils deep on contact surfaces in 120 days, and beryllium coupled to stainless steel showed very severe corrosion, with pits as much as 125 mils deep in 60 days. Beryllium oxide specimens corroded uniformly at 1.0 to 1.5 mpy at temperatures of 250 and 300°C.

Corrosion test assemblies exposed in the steam generators of the HRE-2 were examined after the final reactor shutdown. Specimens of titanium, three stainless steels, and three carbon steels were not significantly corroded. The specimens indicated that many more years of useful service life could have been expected for the HRE-2 steam generators.

A testing program to determine the adequacy of aluminum cladding for fuel elements in the High Flux Isotope Reactor was completed. It was shown that the corrosion of aluminum leads to the formation of an insulating layer of boehmite on the aluminum surface. Thus as aluminum, through which heat is being transferred at a constant rate, corrodes, the temperature of the aluminum increases. The rate at which the boehmite formed was constant under fixed conditions and was related to the temperature at the water interface and to the pH. The lower the temperature and the lower the pH (in the range 5.0 to 6.5 with HNO_3), the lower the rate of corrosion-product formation. Within the ranges of 300 to 900 psi and 31 to 51 fps, pressure and flow rate were without effect. It was concluded that 6061 aluminum will be a satisfactory cladding material for the HFIR fuel plates, provided the pH of the coolant is maintained at 5.0 or even 5.3 with nitric acid.

A testing program has been started to determine if aluminum can be used as cladding material for the fuel plates in the Advanced Test Reactor. Although the ATR is similar to the HFIR in many respects, the ATR fuel plates will operate at higher temperatures and for longer times. Tests to date have shown that at the higher temperatures the rate of oxide accumulation is not linear, as was the case at the lower HFIR temperatures, but is parabolic. Under the same conditions, X8001 and 6061 aluminum developed oxide layers at the same rate, and some oxide spontaneously spalled from both when thicknesses exceeded 2 to 3 mils. Specimens of 6061 aluminum from which oxide had spalled always showed localized attack, but under all conditions X8001 always corroded uniformly. Preliminary data suggest that the rate of oxide buildup on the aluminum specimens is related to the surface area of the stainless steel exposed to the coolant. Attempts to verify the observation are in progress.

Corrosion tests in support of the Power Reactor Fuel Element Processing Program have continued, and a screening program to select materials with adequate corrosion resistance for the transuranium processing facility has been initiated. During the year, 475 boiling 65% HNO_3 tests (ASTM:A262-55T) and 510 electrolytic oxalic acid tests (ASTM:A262-55T) were conducted. A continuation of the testing of aluminum alloys in various parts of the Oak Ridge Research Reactor has shown that many years of trouble-free service should be expected from the structural materials in the reactor, provided the present treatment practices are continued.

11. Surface Chemistry of Thoria in Dilute Aqueous Electrolytic Solutions

Self-consistent measurements of the adsorption of nitric acid on a particular thoria sample have been obtained after several changes in experimental technique. Probably the most significant of these was the use of a commercial paint shaker to accelerate the equilibration rate. Complete interpretation of the data will not be attempted until additional measurements have been made with other thoria samples.

Progress on the design and construction of the high-temperature adiabatic calorimeter is reported. Several measurements of the heat of wetting of thoria at 25°C have been made in a Dewar flask calorimeter with the instrumentation assembled for the high-temperature machine. The precision of the measurements is excellent, but the accuracy is not adequate. Changes in the design of the glass calorimeter are indicated and are being made.

PART III. HETEROGENEOUS SYSTEMS STUDIES

12. Investigation of the Compatibility of Coated Fuel Particles and Coated Matrices with Liquid Coolants

A program to study the compatibility of coated fuel particles and associated matrices with liquid

coolants has been initiated. Particles of UO_2 coated with Al_2O_3, and UC_2 coated with pyrolytic carbon, supported in graphite matrices of various qualities, are to be tested in pressurized water and organic moderator–coolants and in various molten fluoride salts.

Equipment capable of exposing electrically heated graphite rods to pressurized water has been developed. Operation at heat fluxes exceeding 200,000 Btu hr^{-1} ft^{-2} has been demonstrated.

In a brief test in molten LiF-NaF eutectic at 900°C in a torch-fired vacuum crucible furnace, no dimensional change was observed on small sapphire (Al_2O_3) spheres.

13. Hydriding of Zirconium-Base Alloys

An investigation was completed to determine the relative effects of variables associated with hydriding of zirconium-base alloys during exposure to circulating aqueous slurries of ThO_2 and thorium-uranium oxides in toroids at temperatures of 200, 280, and 330°C. Hydriding did not occur under oxidizing atmospheres. In reducing atmospheres with specimens exposed under conditions of slug flow in toroids, hydriding was not detected in 200°C tests, but severe hydriding occurred at 280°C, and moderate hydriding occurred at 330°C. The rate and severity of hydride formation increased with increasing hydrogen overpressure and exposure time, and increased with the U/Th ratio of the slurry oxide.

14. Thoria Pellet Test Program

The program for evaluation of the integrity of ThO_2 pellets and sol-gel fragments was continued by use of standardized ball mill, autoclave, and spouted-bed tests. The attrition characteristics of pellets in small fluidized beds were also investigated, as a function of flow velocity and resultant bed expansion. It was found that wear rates increased as flow velocity increased, until increasing bed expansion resulted in less frequent collisions and the wear rate reached a maximum and diminished with further increase in flow. Wear rates were generally constant with time. At a bed expansion of 30%, wear rates slightly above 0.01%/hr were observed for 0.2-in. pellets. The rate at 400% expansion was 0.08%/hr, and at 900% expansion (near elutriation) it slightly exceeded 0.04%/hr.

15. Examination of In-Pile Slurry Loop

Examination of cutup sections from in-pile slurry loop experiment L-2-27S, in which an aqueous thoria–0.4% urania slurry was circulated successfully for 2220 hr in beam hole HB-2 of the Low-Intensity Test Reactor, developing 7×10^{16} fissions per g of solids, did not reveal any instances of slurry deposition or localized attack. Slurry was found in the pressurizer and in the annulus of a sintered stainless steel filter which had cracked loose at one end, apparently prior to irradiation. The filter was not plugged. Recovery of all slurry drained from the loop and removed as samples permitted a material balance to be made: of 1590 g of solids put into the loop, 1579 g was recovered. Examination of corrosion specimens from the loop showed little effect of radiation and circulation velocity (at the levels of the experiment) on the attack of Zircaloy-2 or titanium alloys. Corrosion of type 347 stainless steel was increased, although not to excessive levels, by irradiation and by increased circulation.

Progressive degradation of thoria particles was evidenced by the examination of samples taken at intervals during the run. Particle size decreased from 1.7 μ to 0.3 μ average diameter, crystallite size diminished from 1900 A to about 220 A, and surface area increased to over 40 m^2/g. These changes were confirmed by observations of pore volume and area distribution and by electron microscope photographs.

Changes in particle properties in the loop experiment did not affect the slurry in ways leading to unsatisfactory handling.

16. Second In-Pile Loop Experiment

The development and the fabrication of a loop for insertion into beam hole HN-1 of the Oak Ridge Research Reactor were completed. In this second in-pile loop experiment, an attempt will be made to irradiate pure thoria to a fission dose with in-bred U^{233} similar to or exceeding that of the first in-pile slurry loop experiment. A number of improvements in the loop are expected to increase substantially the effective irradiation of the slurry.

17. In-Pile Slurry Autoclaves

For comparison with the first in-pile slurry loop, identical materials were irradiated to similar doses in an in-pile autoclave experiment. Comparable changes in crystallite size and surface

area occurred; however, only in the loop experiment, which involved pumped-slurry circulation, was the particle size reduced.

Cyclotron irradiation of dry targets of pure thoria and thoria–0.4% urania has been carried out to energy depositions in the particles of up to 6×10^5 w-sec per g of solids (exceeding that estimated for the in-pile slurry loop experiment) with the 28-Mev 63-in. nitrogen (3+) cyclotron and the 22.4-Mev 86-in. proton cyclotron. No change in crystallite size as indicated by x-ray line broadening has been detected in the irradiated materials.

PART IV. SUPPORT FOR HIGH-TEMPERATURE SOLID-FUELED REACTORS

18. Transport of Noble Gases in Graphites

Proposals have been advanced to operate gas-cooled reactors with unclad fuel elements within porous graphite sleeves through which helium flows from the main coolant stream to sweep radioactive fission product gases out of the reactor. In a system of this type, back-diffusion of radioactive gas through the sleeve wall, against the helium flow, must be minimized. An understanding of diffusive flow of a gas through a porous medium, against a forced flow of another gas, is especially important to such a reactor. This complex problem has been examined in a program of theoretical and experimental study. The magnitude of diffusive flow with and without forced flow of one component has been determined experimentally by careful study of systems in which flowing streams of helium and argon were separated by porous sleeves of graphite. Available theories of flow did not satisfactorily explain all the results obtained in these experiments. However, a new theoretical treatment of the problem, in which the porous medium is considered to be a collection of uniformly distributed "dust" particles which are constrained to be stationary, uses rigorous kinetic theory to permit derivation of suitable flow equations as special cases of well-known multicomponent-mixture equations. These equations predict the behavior observed experimentally over a wide range of low conditions and fail only after back-diffusion has been reduced to a minute fraction of its value, and with no forced flow. It appears that a difficult flow problem has been simplified and solved.

19. Diffusion of Fuel and Nonvolatile Fission Products in Fuel-Graphite Systems

The feasibility of using coated fuel particles for nuclear reactors depends, in part, on the rate at which uranium and nonvolatile solid fission products diffuse through the coating material. Currently, it is expected that the coating material will be pyrolytic carbon, graphite, or both materials. Diffusion studies have been made on high-permeability graphites, but there is very little definitive information available on diffusion rates in low-permeability coating materials. Solid-state diffusion studies have been initiated, which have as their ultimate aim the study of pyrolytic graphites.

The experimental program started with the fabrication of a uranium carbide–AGOT graphite diffusion couple. Satisfactory couples were made from uranium metal foil placed between two plane surfaces of graphite. The layer of UC formed when these materials were heated in a vacuum was thick enough to be considered infinitely thick in a theoretical treatment of the data. Present experimental work is concerned with reproducing experiments reported in the literature to test the procedure in use and to verify previously reported data. Emphasis is being placed on experimental methods at this stage of the program, since it is proposed to use a wedge technique frequently employed in autoradiographic diffusion studies of systems using tracers. This technique will amplify the penetration-concentration data considerably and should be an important device for obtaining good results.

20. Compatibility of Special Fueled Graphites with Water Vapor

The compatibility of pyrolytic-carbon-coated carbide fuel particles and of uncoated fuel bodies, which are being considered for possible use in the Pebble Bed Reactor Experiment, with water vapor is being studied. The studies are being made in the temperature range 800 to 1200°C with flowing helium containing a maximum partial pressure of water vapor of nearly 1 atm. The rate of removal of carbon is determined from weight changes, and the integrity of the coating on the fuel particle is evaluated by use of a nitric acid leach.

21. Gas-Graphite Reactions

Experimental studies were recently started for the purpose of measuring the reactivity of various grades of graphite with CO_2 and H_2O at low partial pressures (10 to 1000 volumes/million) in flowing helium, in the temperature range 800 to 1200°C. Reaction rates will be determined from changes in weight of the specimens measured by a recording balance and from the composition of the effluent gas measured by a sensitive gas chromatograph.

22. Evolution of Gas from Graphite

Additional studies were made of the degassing behavior of EGCR graphite. The release of sulfur compounds (SO_2, H_2S, CS_2) as a function of graphite temperature was established, and the rate of release of desorbate was determined in the temperature range 500 to 1000°C. The rate of gas release in this temperature interval was found to be quite variable and not completely described by the equation $v = A \log t + B$ above 600°C.

23. Measurement of Temperature in Reactor Environments

Tests to determine emf drift on bare-wire base-metal thermocouples in stagnant helium atmospheres at 1000°C showed that the 80 Ni–20 Cr type alloys were less susceptible to selective oxidation than the 90 Ni–10 Cr type. Geminol-P and Chromel-A or -AA gave reliable emf data. In these tests, Special Chromel-P was no more reliable than the regular Chromel-P, but Special Alumel remained in good physical condition longer than the regular Alumel. It was established that selective oxidation might be observed at temperatures over about 700°C in a marginally oxidizing atmosphere.

Chromel-P–Alumel couples sheathed with stainless steel were found to be of questionable reliability when exposed at 870°C to atmospheres containing gases desorbed from graphite. Hydrogen diffusion into the sheath resulted in selective oxidation of chromium, with a consequent negative emf drift. The emf output was more stable at 704°C, staying within the specified tolerance ($\pm\frac{3}{8}$% of the emf output) during long exposures. Exposure to carbon monoxide at 870°C resulted in damage to the thermocouple wires and sheath, but without appreciable change in emf during the time of exposure. The damage occurred in relatively isothermal regions near the hot junctions. The reliability was dependent upon the source of material and the test conditions. Varying amounts of water, hydrogen, air, and carbon oxides inside the sheath seemed responsible for the differences among the materials furnished by different vendors.

24. Beryllium Chemistry Studies

Measurements of the refractive indices of irradiated BeO specimens, made before and after thermal annealing, demonstrated that this technique affords a rapid method of measuring the extent of radiation damage to BeO.

Attempts were made to produce a stabilized cubic form of BeO by doping with small amounts of other oxides. No evidence of the formation or stabilization of a cubic BeO phase was observed.

A solvent-extraction process for making high-purity beryllium oxide has been developed, and a small-scale production operation has been demonstrated. About 1280 g of BeO has been prepared. Spectrographic analyses of this material showed that impurity concentrations were reduced to exceedingly low values. Several batches of this high-purity BeO have found use in the preparation of spectrographic standard mixtures. Reports that the tensile strength of beryllia increases markedly as the purity and the crystal perfection are improved suggest that ultrapure BeO might display greater resistance to radiation damage.

A spectrographic analysis method has been developed for the simultaneous determination of beryllium acetylacetonate and acetylacetone in organic solutions which occur in the solvent-extraction beryllium purification process. It is based on the ultraviolet absorption peaks of the two components (294 and 272 mμ respectively), which are sufficiently separated that measured sample absorbancies at two wavelengths (260 and 301.5 mμ) can be used in simultaneous equations to obtain the concentration of each component, usually within ±5%.

25. Effect of Radiation on Beryllium Oxide

Severe damage was observed when sintered BeO was irradiated to high neutron doses at low temperatures. Specimens receiving 1.5×10^{21} *nvt* at 110°C disintegrated to powder, and those receiving 2.6×10^{21} *nvt* at 800 to 950°C fractured, but some specimens survived which were exposed to neutron doses and at temperatures between these limits. Samples irradiated to doses of approximately

10^{21} *nvt* showed increases in linear dimensions ranging from 0.5 to 4%, anisotropic lattice expansion and lattice defects, a decrease in the refractive indices, intergranular fracture, and void formation. These effects generally increased with dose and decreased with temperature. Essentially all the internally generated helium was retained in the BeO, even at high temperatures with neutron doses up to 1.6×10^{21} *nvt*, but tritium was lost to an increasing extent above 120°C. Future experiments are designed to permit a better separation of variables in order to determine the relative importance of various possible mechanisms of irradiation damage.

26. Phase-Equilibrium Studies of the System UO_2-ThO_2-O_2

Equilibrium-phase relationships in the system UO_2-ThO_2-O_2 are being studied by long-term equilibration exposures to fixed conditions of temperature and oxygen pressure, followed by chemical and crystallographic analyses of the products and by determinations of the relationship between oxygen pressure and temperature in sealed systems of known original composition. Well-defined discontinuities in the relationship between oxygen content and crystallographic lattice parameter have been tentatively interpreted as marking the compositional boundaries to the single-phase solid-solution region.

PART V. NUCLEAR SAFETY PROGRAM

Data are needed on the amounts and on the form of radioactive species that may be released from a reactor when a loss-of-coolant accident occurs, in order to provide a sound scientific basis for evaluating the hazard of such an accident. Overheated fuel elements may release fission products by melting, diffusion, and reaction with their environment. Most attention is currently being devoted to UO_2 fuels because of their importance in power reactors. Knowledge of the behavior of released fission products in different atmospheres and geometries and of the methods of collecting them is essential in hazards evaluations and is also needed in connection with the routine operation of some types of reactors and related activities.

27. Fission Product Transport Evaluations

Equipment is being assembled for experiments designed to define conditions to be employed during the melting of irradiated miniature UO_2 fuel elements in a hot cell. These experiments, with unirradiated UO_2 or ThO_2 particles, are intended to provide a better understanding of the environmental factors that may change the physical and chemical form of fission products after their release and thus affect their deposition characteristics. No data have yet been obtained in this project, which was initiated during the latter part of the report period.

28. Influence of Irradiation Level on Fission Product Hazards Associated with UO_2-Fueled Reactors

Experiments were conducted with UO_2 fuel materials irradiated at tracer level, at 1000 Mwd/ton, and at 4000 Mwd/ton to study the effect of burnup on fission product release resulting from the melting of fuel specimens and from oxidation and diffusion at temperatures below the melting point of UO_2. The results showed that, in general, increased releases were obtained with increasing burnup of uranium. The burnup effect was most noticeable in the increased amount of iodine released and in the increased rate of oxidation of UO_2 when the fuel was heated in air. When fuel was heated for 5.5 hr in pure helium, however, the increase in diffusion of fission products with increased burnup was found to vary by a factor of 5 for iodine and tellurium and by a factor of 10 for cesium and strontium. A small but noticeable burnup effect on fission product release accompanying the melting of UO_2 in helium, air, and CO_2 was observed. Data were obtained which showed the effect of gas velocity on the deposition rate of fission products that volatilized from molten UO_2.

29. Release of Fission Products by the In-Pile Melting of Reactor Fuels

In-pile experiments are being conducted to determine the amounts and form of fission products released when miniature fuel elements are melted by fission and gamma heat. Two experiments have been completed in which stainless-steel-clad UO_2 fuel elements were heated in an experimental facility located in the Oak Ridge Research Reactor.

The specimens were irradiated in the reactor only long enough to accumulate tracer quantities of fission products and were then inserted in the high-flux region of the reactor. The first specimen, enriched to 3%, was in the maximum flux region for about 20 min. The steel cladding melted, and it seems probable that most of the center portion of the specimen reached a temperature above, or very near to, the melting point of UO_2. Postirradiation examination of the specimen revealed that it had a relatively large hole extending about three-fourths of its length. The surface was covered with well-crystallized UO_2 that had undoubtedly been formed by deposition from the vapor phase. Radiochemical data indicate that most of the Ce^{144}, Y^{91}, and Sr^{90} remained in the UO_2 specimen; Xe^{133} and Ru^{106} were largely released, while Ba^{140}, Sr^{89}, and Cs^{137}, all of which have volatile precursors, were partly released.

The specimen employed in the second experiment was 25% enriched to furnish more fission heat. It remained in the high-flux region of the reactor for about 10 min, and examination of the interior of the furnace after it was transferred to a hot cell showed that the specimen completely vaporized or melted and that most of the material collected as crystals on the wall of the thoria cylinder. A considerable amount of material deposited in the exit gas tube, and a portion of the thoria holder apparently melted. Radiochemical analyses of materials from this experiment are not available; consequently, release values remain to be determined.

30. Removal of Radioactive Fission Products from Air and Other Gases

The study of the containment, disposal, and removal of volatile or otherwise dispersible radioactive materials from gases continued. A method for removal of radioactive iodine from helium at temperatures up to 650°C was developed with Whetlerite (charcoal impregnated with silver, copper, and chromium salts) as an adsorber. This process permits decontamination of gas-cooled reactor coolants at high temperatures. The efficiency of activated charcoal for removal of iodine from steam-air mixtures is being investigated for application to the emergency off-gas system of the NS "Savannah." Tests of the efficiency of iodine collectors used for environmental monitoring on the NS "Savannah" were conducted.

An investigation of the transport and deposition of radioactive aerosols was initiated to provide information for aiding in the control of the radioactivity which occurs in this form. Thus far, the study has been mainly concerned with diffusion, both as an important mechanism in aerosol behavior and as a basis for the determination of particle-size distributions. Air containing radioactive iodine vapor or finely divided particulate matter labeled with I^{131} is passed through cylindrical or rectangular channels, and the resulting longitudinal activity profiles are determined by means of a gamma spectrometer. The deposition profile for an aerosol or vapor is governed by the diffusion coefficient, which, in turn, depends on particle diameter or molecular properties in the case of a vapor. The initial results obtained appear promising with regard to aerosol characterization, since iodine-labeled particles approximately 0.25 and 0.004 μ in diameter behaved in accordance with theoretical equations adapted from the literature.

Studies concerned with removal of radioactive krypton and xenon from coolants and other carrier gases continued at a slower rate than during the previous year. Equilibrium adsorption isotherms were obtained for krypton and xenon on charcoal at −45 and −78°C. Thermal-conductivity measurements were made with four types of charcoal containing He, N_2, or CO_2 in the voids. Apparent thermal conductivities decreased in the order He, N_2, and CO_2, in accordance with the behavior of the pure gases, but no significant differences were noted among the varieties of charcoal tested. A long-term krypton holdup test, with charcoal at liquid-nitrogen temperature and helium as the carrier gas, was initiated and has now been in progress for eight months with no evidence of krypton breakthrough; for comparison, the average krypton holdup time at 25°C for the same trap and flow rate would be 5 min. Equations were developed for estimating effective diffusion coefficients, for a fairly wide variety of adsorber parameters, from readily obtainable data.

PART VI. PREPARATION AND PROPERTIES OF PURE MATERIALS

31. Preparation of Pure Materials

In the research program on the preparation of very pure materials in crystalline form, emphasis has been placed on the purification of LiF and the production of defect-free single crystals, enriched in the Li^7 isotope. Solvent extraction of an aqueous lithium salt solution with perfluorooctanoic acid in diethyl ether was used to remove magnesium and other polyvalent cations; LiF was precipitated by the addition of the solution to aqueous hydrofluoric acid; the dried precipitate was dehydrated at elevated temperatures in a nickel container in the presence of hydrogen and HF gas streams. The purified material was melted under vacuum and slowly cooled in a purified helium atmosphere in a modified Stockbarger furnace to produce a 300-g ingot containing two crystals each of very high purity. Small single crystals of LiF were also grown from the vapor phase.

The growth of single crystals of refractory compounds, particularly oxides, from molten solvents was brought under study on the basis of previous experience with the determination of high-temperature phase equilibria in systems involving oxides. Molten molybdenum trioxide, although it has a conveniently low melting point, was found to form a number of intermediate compounds with refractory oxides and thus proved unsuitable. Simple eutectic systems are formed between ceramic oxides and $Na_2B_4O_7$; crystals of ThO_2, ZrO_2, and TiO_2 were produced from this solvent, and it proved possible to grow seed crystals directly on platinum stirring rods without the usual difficulties of mechanical attachment. Very encouraging results have been obtained with the growth of oxide crystals from molten fluoride mixtures; MgO and TiO_2 (rutile) have both been produced as good crystals, and evidence has been obtained that UO_2, ThO_2, and ZrO_2 should also be stable phases on exposure to the fluoride solvents.

A literature review of the solvent extraction of various metallic ions by dialkylphosphoric acids [of the structure $(RO)_2P(O)OH$, HX] has been carried out. At low loadings the extraction reaction

$$M^{z+}_{aq} + zH_2X_{2_{org}} \rightleftharpoons M(X_2H)_{z_{org}} + zH^{+}_{aq}$$

(in which the extractant is dimeric in the organic phase) appears to be quite general. The corresponding equilibrium quotient varies reasonably uniformly with ionic charge and radius when compared for the same reagent and diluent. At high loadings, various polynuclear extraction complexes, sometimes involving aqueous anions, often occur. These complexes, as well as mixed "synergistic" uranium(VI) complexes formed in the presence of neutral phosphates [e.g., R_3PO or $(RO)_3PO$], merit further study.

32. Radiation Chemistry of Organic Moderators

Samples of pure biphenyl were pyrolyzed at 490°C for 48 hr. After separation of the products of a given pyrolytic sample into three different boiling fractions in a vacuum system, they were analyzed gas chromatographically with helium as the carrier. The low-boiling fraction was resolved on a 6-ft column of a molecular sieve (Linde No. 5A) at room temperature and was shown to consist of hydrogen and methane. The intermediate-boiling material consisted solely of benzene, as identified on a 12-ft column of Chromosorb P with a static phase of 30 wt % Apiezon L and 2 wt % Carbowax 20 M, with temperature programming between 125 and 250°C. Finally, a 12-ft column of Chromosorb P with 20 wt % LiCl as the stationary phase was used to separate and, in some instances, to identify the components of the high-boiling fraction of the pyrolytic products. Through the use of temperature programming between 200 and 350°C, the presence of *o*-, *m*-, and *p*-terphenyl has been established.

PART VII. CHEMICAL SUPPORT FOR THE THERMONUCLEAR PROGRAM

33. Sherwood Project Chemistry

The experimental program of support for the Sherwood Project is largely devoted to studies of methods for obtaining and measuring high vacuum.

The response of conventional glass-enveloped ionization gages at low pressures has been compared under several test conditions with similar assemblies after substitution of a metal screen for the glass envelope. Plots of pressures read from these two types of gages show a curvature which diminishes with decreasing emission current on the screened gage and an absolute difference in reading which varies with several test conditions; the type of oil used in the diffusion pump was found to be an important factor.

The several available diffusion-pump oils have been examined for relative stability to thermal decomposition. A mixture of polyphenyl ethers appears most stable, with the esters (Octoil and Octoil-S) next, and the aliphatic hydrocarbon oils least stable. Polyphenyl ether has been shown to give appreciably lower pressures in simple vacuum systems with conventional pumps. A pump which should make optimum use of this favorable property is under test.

Small-scale experiments have substantiated the observation that titanium films on water-cooled substrates are more effective getters for H_2 if they are vapor-deposited in the presence of 2 to 10 μ of inert gas than if deposited in a good vacuum. Dramatic improvement, however, requires deposition in the inert atmosphere and use of liquid-nitrogen temperatures.

Lack of sputtering of titanium under bombardment with D^+ accelerated to 25 kev has been substantiated. A considerable fraction of the incident beam penetrates and is retained by the titanium specimen. Depth of penetration under bombardment suggests that the incident deuteron penetrates the usual surface layer and diffuses within the specimen.

A survey of materials requirements for a thermonuclear blanket system has been made, and the functions which such a blanket must fulfill have been outlined. No experimental efforts in this direction have been initiated.

Contents

PART V. NUCLEAR SAFETY PROGRAM

PART VI. PREPARATION AND PROPERTIES OF SPECIAL MATERIALS

PART VII. CHEMICAL SUPPORT FOR THE THERMONUCLEAR PROGRAM

Part I

Molten-Salt Reactor Program

1. High-Temperature Phase Equilibrium Studies

Experimental studies of many fluoride systems which have potential use in molten-salt-reactor technology have been continued. The data from which phase diagrams have been derived were obtained from thermal-gradient-quenching experiments, thermal analyses of melts (using both heating and cooling cycles), and visual observations of phase changes produced by heating and cooling. In samples from all experiments, the solid phases were identified by use of the polarizing light microscope and the x-ray diffractometer. The crystal structures of new compounds isolated in the course of these studies have been determined with single-crystal x-ray-diffraction techniques.

PHASE EQUILIBRIA AMONG THE FLUORIDES

R. E. Thoma

H. A. Friedman
H. Insley[1]
B. J. Sturm
G. M. Hebert
T. N. McVay[2]
C. F. Weaver
G. D. Robbins[3]

The System $LiF-BeF_2-ZrF_4$

In a previous report[4] crystallization equilibria for $LiF-BeF_2-ThF_4-UF_4$ mixtures were described. Incorporation of 5 mole % ZrF_4 into the MSRE fuel[5] caused ZrF_4 to become the principal tetravalent fluoride in the fuel mixture of nominal composition $LiF-BeF_2-ZrF_4-ThF_4-UF_4$ (70-23-5-1-1 mole %). Crystallization reactions should then be strongly influenced by the phase behavior in the system $LiF-BeF_2-ZrF_4$. Consequently, this system is being investigated. Results of the investigation, based on cooling-curve and thermal-gradient-quenching data, are summarized in the tentative phase diagram of the system (Fig. 1.1). A partial list of invariant points is shown in Table 1.1. The liquidus surfaces in the system are, in general, similar to those in the systems $LiF-BeF_2-ThF_4$ and $LiF-BeF_2-UF_4$, and somewhat lower because the melting point of ZrF_4 is considerably lower than that of ThF_4 or UF_4. Of the three $LiF-BeF_2-MF_4$ ternary systems, only $LiF-BeF_2-ZrF_4$ contains a ternary compound. This compound, $6LiF \cdot BeF_2 \cdot ZrF_4$ melts semicongruently to LiF and liquid at 475°C, and is the first solid phase to crystallize on cooling from the MSRE liquid fuel mixture. Crystal-structure studies of $6LiF \cdot BeF_2 \cdot ZrF_4$ are discussed in the section, "X-Ray Diffraction Study of $6LiF \cdot BeF_2 \cdot ZrF_4$" (this chapter).

The System $LiF-BeF_2-ZrF_4-ThF_4-UF_4$

Zirconium tetrafluoride serves as a scavenger for oxide ion and provides protection against precipitation of UO_2 in MSRE fuels containing LiF, BeF_2, and UF_4.[5,6] The nominal MSRE fuel mixture is composed of $LiF-BeF_2-ZrF_4-ThF_4-UF_4$ (70-23-5-1-1 mole %). Studies of this system and its limiting systems are continuing.[5] Investigations are continuing on the determination of temperature-composition relationships along various sections of special relevance to the MSRE fuel. Liquidus temperatures varying as a function of LiF/BeF_2 ratio with ZrF_4, ThF_4, and UF_4 concentrations held at 5, 1, and 1 mole %, respectively, are shown in Fig. 1.2. Liquidus temperatures varying as a function of the same ratio and

---

[1] Consultant, National Bureau of Standards (retired).

[2] Consultant, the University of Alabama (retired).

[3] Summer employee from the University of North Carolina.

[4] C. F. Weaver *et al.*, *Phase Equilibria in Molten Salt Breeder Reactor Fuels. I. The System $LiF-BeF_2-UF_4-ThF_4$*, ORNL-2896 (Dec. 27, 1960).

[5] *MSRP Progr. Rept. Feb. 28, 1961*, ORNL-3122, p 109.

[6] R. E. Thoma, "Scavenging of Oxide in $LiF-BeF_2-UF_4$ Mixtures by ZrF_4," August 22, 1960 (internal correspondence).

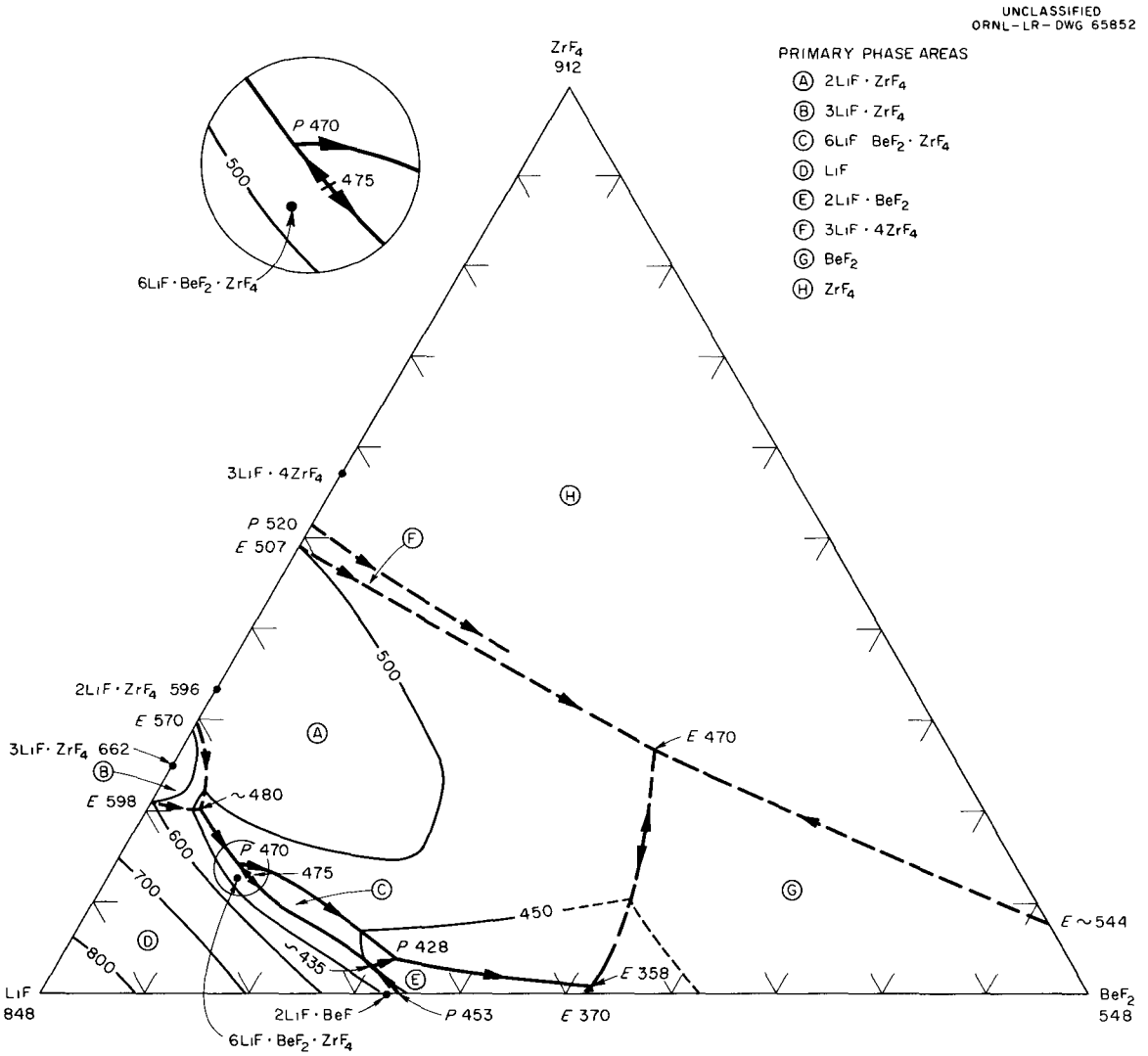

Fig. 1.1. The System $LiF\text{-}BeF_2\text{-}ZrF_4$.

Table 1.1. Invariant Equilibria in the System $LiF\text{-}BeF_2\text{-}ZrF_4$

Solid Phases Present	Composition (mole %)			Invariant Behavior	Temperature (°C)
	LiF	BeF_2	ZrF_4		
$3LiF \cdot ZrF_4$, LiF, $2LiF \cdot ZrF_4$	75	5	20	Peritectic	~480
LiF, $2LiF \cdot ZrF_4$, $6LiF \cdot BeF_2 \cdot ZrF_4$	74	12	14	Peritectic	470
LiF, $2LiF \cdot BeF_2$, $6LiF \cdot BeF_2 \cdot ZrF_4$	67	30	3	Peritectic	~435
$2LiF \cdot BeF_2$, $2LiF \cdot ZrF_4$, $6LiF \cdot BeF_2 \cdot ZrF_4$	64	32	4	Peritectic	428
$2LiF \cdot BeF_2$, BeF_2, $2LiF \cdot ZrF_4$	47	52	1	Eutectic	358
$2LiF \cdot BeF_2$, ZrF_4, BeF_2	~28	~45	~27	Eutectic	470

with ZrF_4, ThF_4, and UF_4 held at 7, 1, and 1 mole %, respectively, are shown in Fig. 1.3. The need for additional work on the investigation of phase relationships in the system $LiF\text{-}BeF_2\text{-}ZrF_4\text{-}ThF_4\text{-}UF_4$ was shown by results of recent in-pile tests with the nominal MSRE fuel mixture. In these tests, irradiated salt mixtures were exposed to temperatures as high as 1050°C, well above the upper temperatures specified in design criteria; LiF and BeF_2 were evaporated in approximately a 2:1 mole ratio from the mixtures. The resulting changes in composition and behavior of the remaining material require an understanding of the crystallization reactions along the composition section containing $2LiF \cdot BeF_2$ and the MSRE fuel. Removal of $2LiF \cdot BeF_2$ from the MSRE fuel mixture

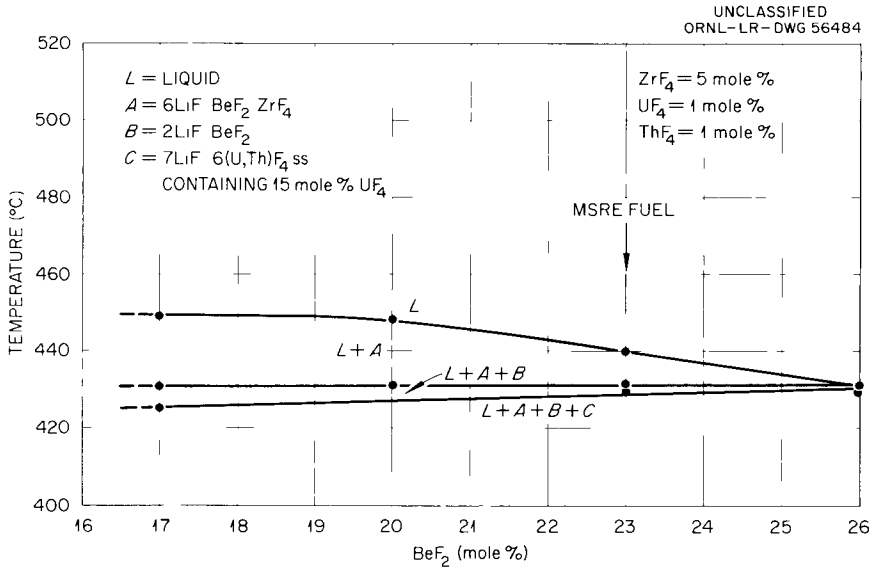

Fig. 1.2. The System $LiF\text{-}BeF_2\text{-}ZrF_4\text{-}UF_4\text{-}ThF_4$.

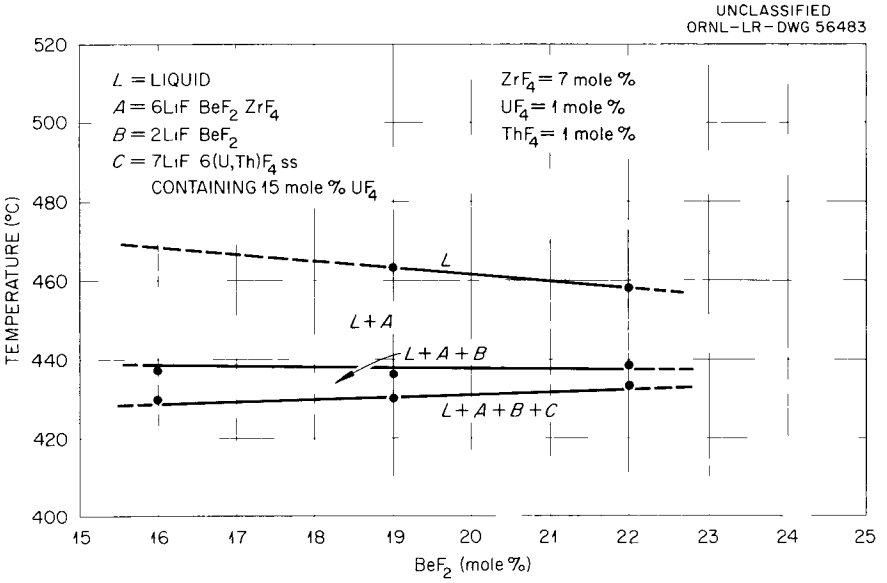

Fig. 1.3. The System $LiF\text{-}BeF_2\text{-}ZrF_4\text{-}UF_4\text{-}ThF_4$.

results in mixtures whose liquidus temperatures are increased by as much as 100°C, depending on the fraction of $2LiF \cdot BeF_2$ removed.

The Systems $KF\text{-}ThF_4$ and $RbF\text{-}ThF_4$

The cation-radius ratios K^+/Th^{4+} and Rb^+/Th^{4+} suggested that the compounds $7KF \cdot 6ThF_4$ and $7RbF \cdot 6ThF_4$ occur in the systems[7,8] $KF\text{-}ThF_4$ and $RbF\text{-}ThF_4$ rather than the reported compounds, $KF \cdot ThF_4$[9] and $RbF \cdot ThF_4$.[10] Preliminary experiments confirmed this conclusion and showed, as well, that several previously unreported compounds occur and that somewhat more intricate phase relationships exist than were reported by previous investigators.[10,11] Phase diagrams of the systems $KF\text{-}ThF_4$ and $RbF\text{-}ThF_4$, modified by the results of the ORNL investigations, are shown in Figs. 1.4 and 1.5. These are now considered complete with respect to definition of the phase relationships among the equilibrium compounds within the two systems.

[7] *Reactor Chem. Div. Ann. Progr. Rept. Jan. 31, 1960*, ORNL-2931, p 22.

[8] R. E. Thoma, *Inorganic Chemistry* (in press).

[9] W. H. Zachariasen, *J. Am. Chem. Soc.* **70**, 2147 (1948).

[10] E. P. Dergunov and A. G. Bergman, *Doklady Akad. Nauk S.S.S.R.* **60**, 391 (1948).

[11] W. J. Asker, E. R. Segnit, and A. W. Wylie, *J. Chem. Soc.* **1952**, p 4470.

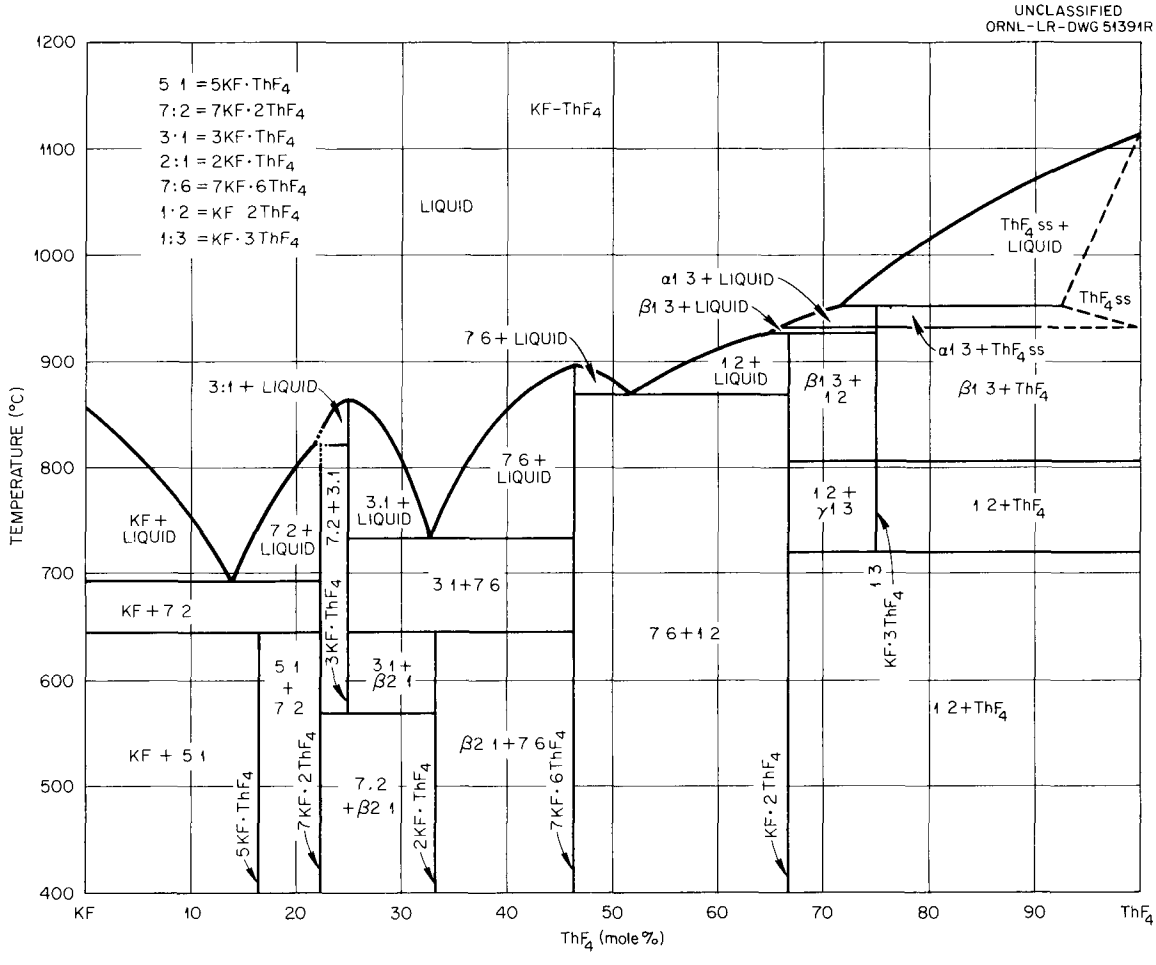

Fig. 1.4. The System $KF\text{-}ThF_4$.

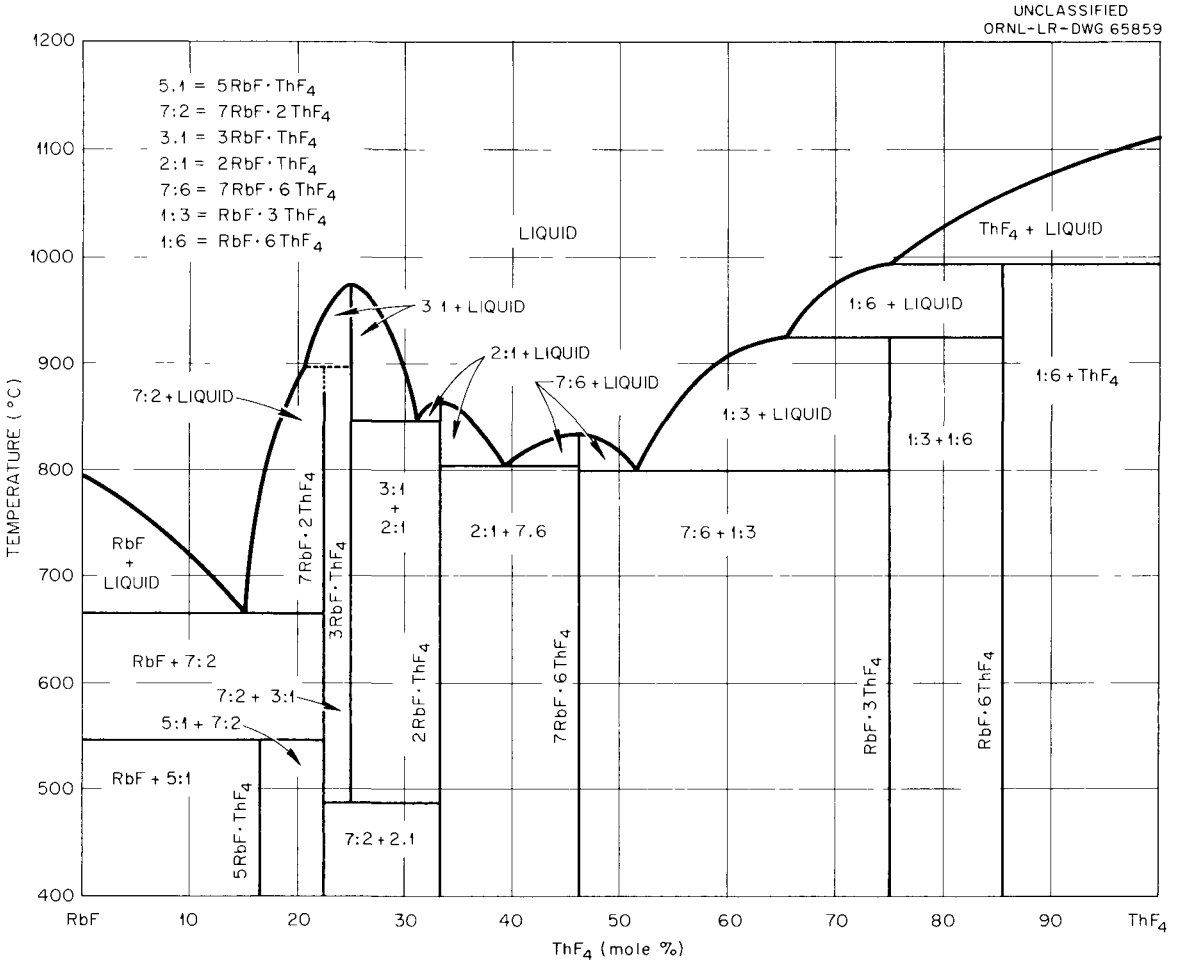

Fig. 1.5. The System RbF-ThF_4.

The System NaF-ThF_4-UF_4

For several years it was believed that continuous solid solution occurred between crystals thought to be the low-temperature forms of $4NaF \cdot ThF_4$ and $3NaF \cdot UF_4$.[12] This view had persisted because of the difficulty of isolating pure crystals of these materials, which are stable within only a limited temperature range and are formed only in solid-state reactions. Consequently, the presence of minor amounts of other fluoride phases, detected microscopically, was customarily interpreted as indicating that solid-state equilibria had not been attained. Recent reviews of a large number of phase data accumulated in studies of composition sections between $4NaF \cdot ThF_4$ and $3NaF \cdot UF_4$ suggested that a more satisfactory model should include $7NaF \cdot 2ThF_4$ and $7NaF \cdot 2UF_4$ as end members of a region of solid solution. Purified mixtures of NaF-ThF_4 and NaF-UF_4 were premelted, cooled, and homogenized, and were annealed in the solid state for three weeks at 500–600°C. Rapid cooling of the annealed mixtures preserved crystals of the pure single phases $7NaF \cdot 2ThF_4$ and $7NaF \cdot 2UF_4$. Revised phase diagrams of the systems NaF-ThF_4 and NaF-UF_4 are shown in Figs. 1.6 and 1.7. These discoveries removed the apparent anomalies related to the existence of solid solutions between the isomorphous crystals thought to be β-$4NaF \cdot ThF_4$ and β-$3NaF \cdot UF_4$. Continuous solid solution between the two fluorite phases $3NaF \cdot$

[12] *MSRP Progr. Rept. Aug. 31, 1961*, ORNL-3215, p 119.

$2ThF_4$ and $5NaF \cdot 3UF_4$ does not represent a comparable anomaly, for random cation distribution in a fluoride lattice is frequently observed. In addition, the compound $5NaF \cdot 3UF_4$ does not remain exactly stoichiometric within the binary system but is capable of dissolving a minor amount of NaF in the solid state. The phase-equilibrium diagram of the system $NaF\text{-}ThF_4\text{-}UF_4$ is shown in Fig. 1.8. As in the system $LiF\text{-}ThF_4\text{-}UF_4$,[13] the similarity in cation size of Th^{4+} and U^{4+} is believed to be the important factor responsible for the existence of extensive solid-solution regions. Eleven invariant points, including two eutectics and three singular points, occur in association with the primary phases of ten solid solutions and two pure solids. The minimum melting temperature in the system, 585°C, is found for the eutectic mixture $NaF\text{-}ThF_4\text{-}UF_4$ (75.5-10.5-14). No ternary compounds occur in the system.

[13] C. F. Weaver *et al.*, *J. Am. Ceram. Soc.* **43**, 213 (1960).

The System $NaF\text{-}BeF_2\text{-}ThF_4$

Studies of phase equilibria in the system $NaF\text{-}BeF_2\text{-}ThF_4$[14–16] have been completed. The phase diagram, showing solid-liquid relationships in the

[14] C. J. Barton *et al.*, *Reactor Chem. Div. Ann. Progr. Rept. Jan. 31, 1960*, ORNL-2931, pp 7–9.

[15] *MSRP Progr. Rept. Feb. 28, 1961*, ORNL-3122, pp 111–14.

[16] Presented at the 138th Meeting of the American Chemical Society, New York, N.Y., Sept. 11–16, 1960, Paper No. 83, Physical Chemistry Division.

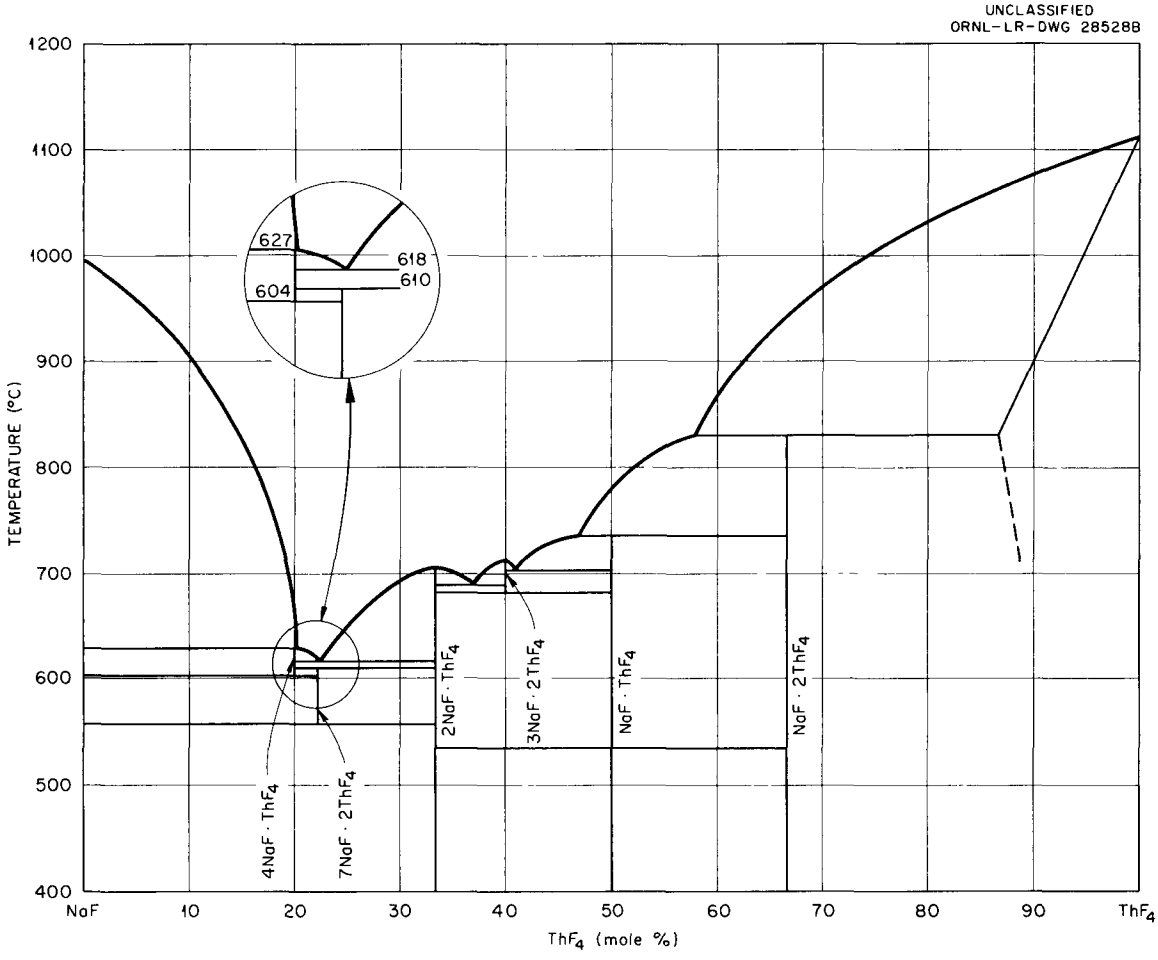

Fig. 1.6. The System $NaF\text{-}ThF_4$.

system, is shown in Fig. 1.9. Final revision was made possible by recent isolation of the single phase $7NaF \cdot 2ThF_4$ (see the immediately preceding section, "The System $NaF-ThF_4-UF_4$"). Primary phases of 12 compounds are crystallized from liquid mixtures of $NaF-BeF_2-ThF_4$. A single ternary compound, $NaF \cdot BeF_2 \cdot 3ThF_4$, occurring in the system[17] melts semicongruently to liquid and a solid solution of ThF_4 containing both dissolved NaF and BeF_2. Twelve invariant points occur in the system; the compositions and temperatures at which these occur are listed in Table 1.2. The system $NaF-BeF_2-ThF_4$ is divided into two independent subsystems by the quasi-binary system formed by $2NaF \cdot BeF_2$ and $2NaF \cdot ThF_4$. The composition section involving these two intermediate compounds is shown in Fig. 1.10.

[17] R. E. Thoma *et al.*, *J. Am. Ceram. Soc.* **43**, 608 (1960).

Possible Reprocessing Solvents

Reactor fuel recovery by the fluoride volatility process is dependent on the phase equilibria of the system in use. Economic dissolution of spent fuel elements by HF in molten fluoride mixtures depends on high capacity of an inexpensive fluoride solvent for the fuel material at temperatures sufficiently low to minimize corrosion of the container. Investigations of the systems $NaF-BeF_2-ZrF_4$ and $LiF-NaF-ThF_4$ were begun with the expectation that low-temperature composition paths would be found between $NaF-BeF_2$ mixtures and ZrF_4, as well as between LiF-NaF mixtures and ThF_4. Studies, not yet concluded, of the system $NaF-BeF_2-ZrF_4$[18] indicate that $NaF-BeF_2$ (71-29 mole %) is a potentially useful solvent for Zircaloy fuel elements; it dissolves approximately 50

[18] *Reactor Chem. Div. Ann. Progr. Rept. Jan. 31, 1960*, ORNL-2931, p 20.

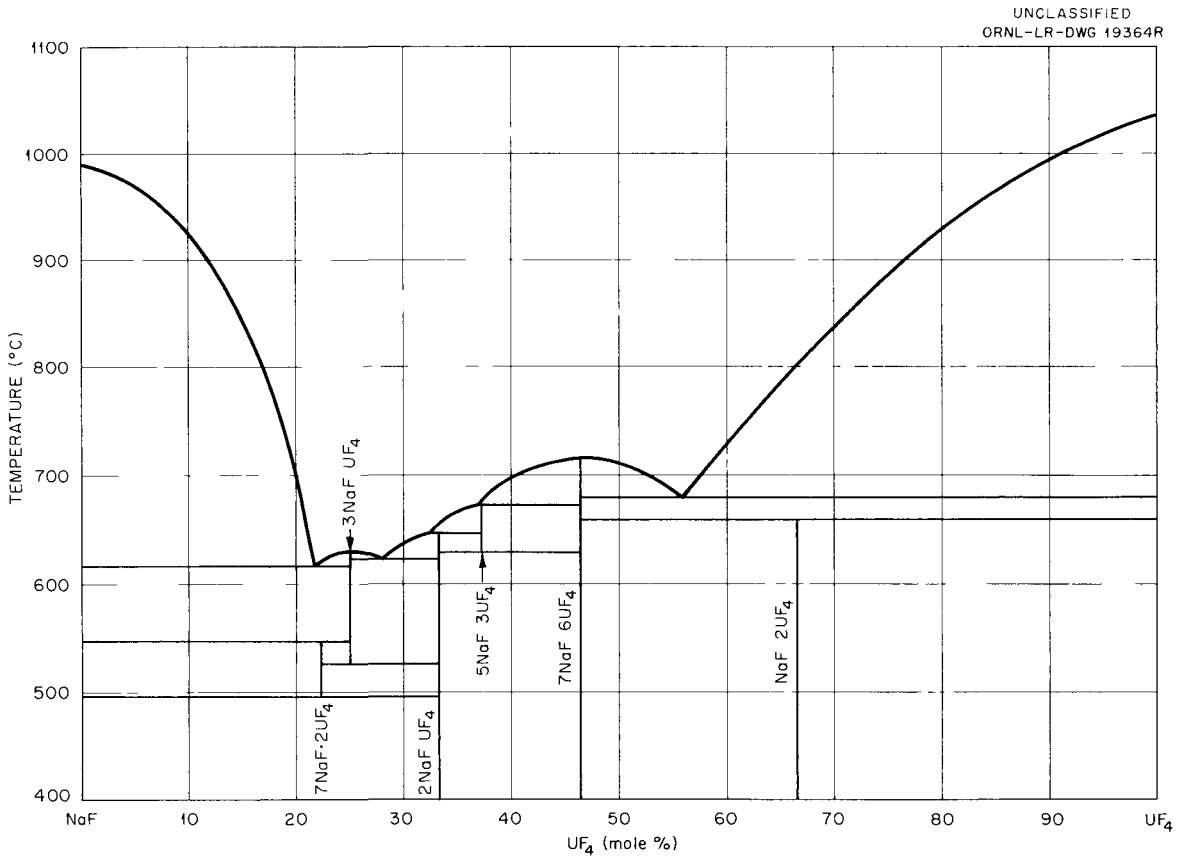

Fig. 1.7. The System $NaF-UF_4$.

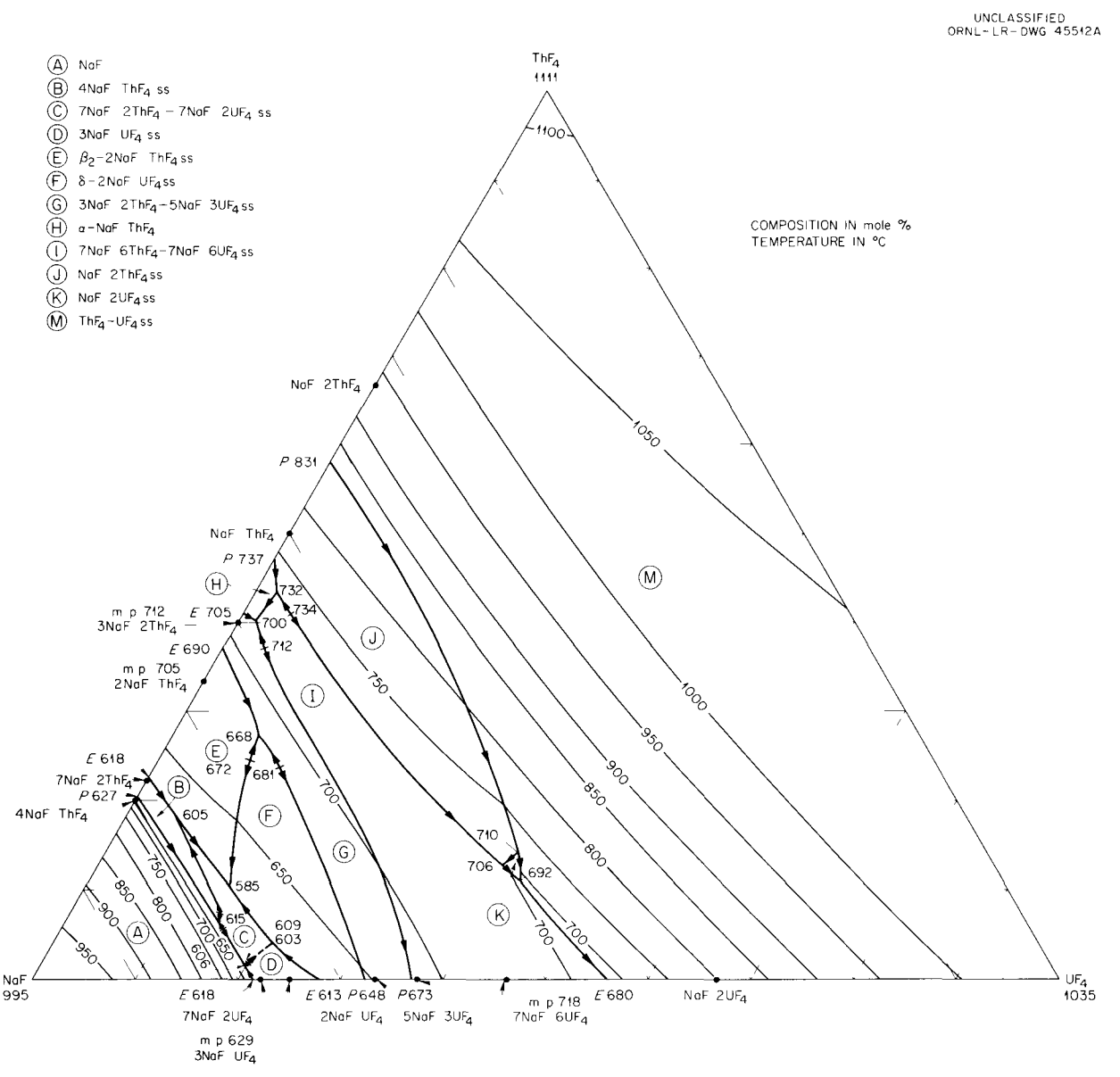

Fig. 1.8. The System NaF-ThF_4-UF_4.

mole % ZrF_4 below 500°C in the molten state. A less advanced investigation of the system LiF-NaF-ThF_4 indicates that the LiF-NaF eutectic may serve as a suitable solvent for the dissolution of fuel elements containing high concentrations of thorium. The eutectic at 504°C (LiF-NaF-ThF_4, 43-33-24 mole %) lies along the composition path between the LiF-NaF eutectic composition and ThF_4, permitting solution of approximately 30 mole % ThF_4 below 600°C.

The System NaF-YF_3

Generalizations about the behavior of the rare-earth fission product fluorides in molten salts are controlled by the facts that (1) the trifluorides LaF_3 and YF_3 represent the two structural types to which all rare-earth trifluorides belong,[19] and

[19] A. Zalkin and D. H. Templeton, *J. Am. Chem. Soc.* 75, 2453 (1953).

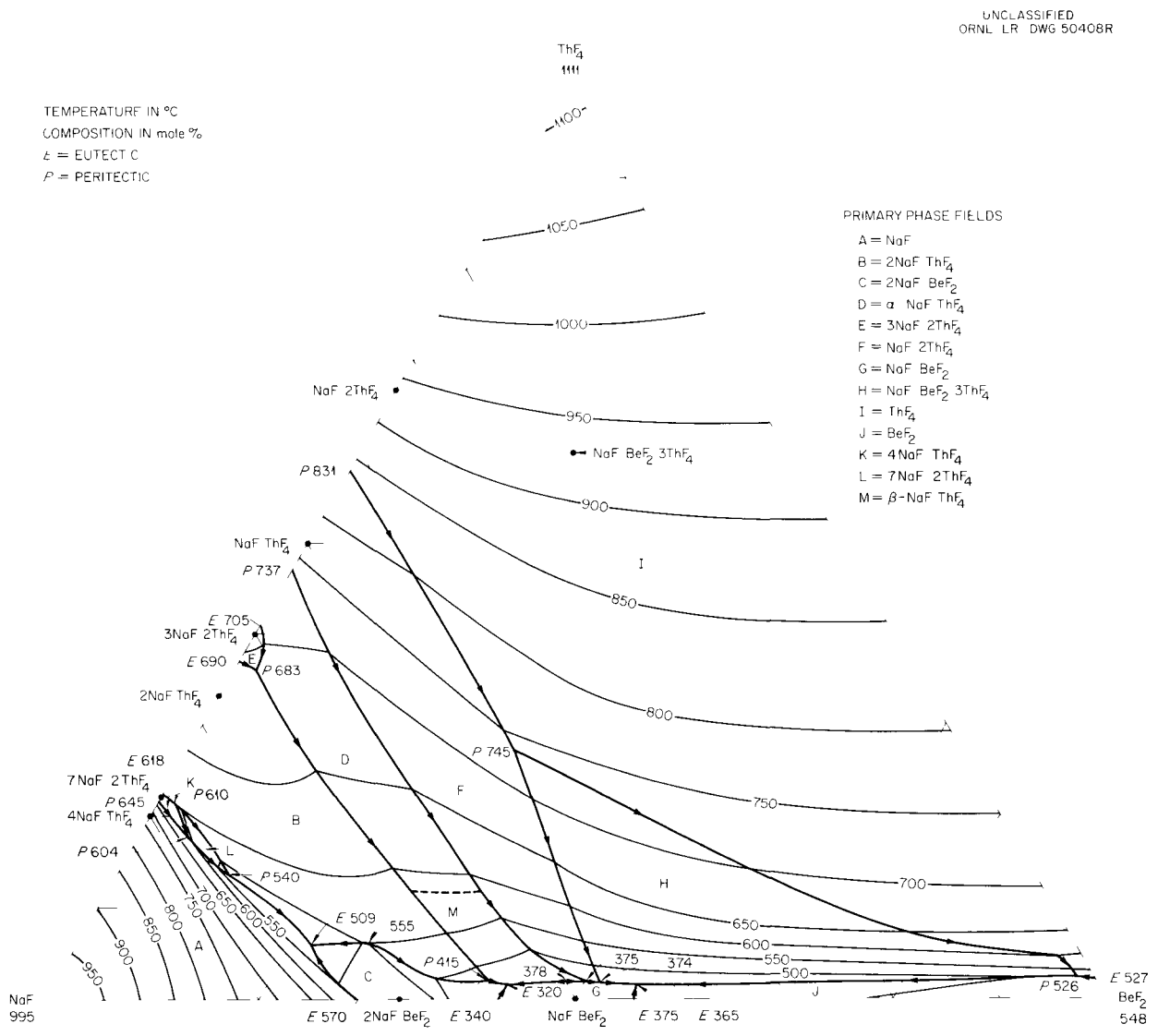

Fig. 1.9. The System NaF-BeF_2-ThF_4.

(2) the binary phase diagrams of rare-earth trifluorides with alkali-metal fluorides are expected to fall into two general types, associated with the relationship between the size of the alkali-metal cation and the size of the trivalent rare-earth cation.[8] Well-defined phase diagrams of the systems containing an alkali-metal fluoride with LaF_3 or YF_3 should, therefore, be of real use in predicting the general behavior of and identity of crystal phases formed by the rare-earth fission product trifluorides in molten-salt reactor fuels and in fuel reprocessing solutions. Credible fluoride-YF_3 systems have been presented,[20,21] but conflicting reports, which we believe incredible, exist concerning the system NaF-YF_3.[21,22]

The equilibrium phase diagram of the system NaF-YF_3 (Fig. 1.11), derived in recent ORNL

[20] R. E. Thoma *et al.*, *J. Phys. Chem.* **65**, 1096 (1961).

[21] E. P. Dergunov, *Doklady Akad. Nauk S.S.S.R.* **60**, 1185 (1948).

[22] F. Hund, *Z. anorg. Chem.* **261**, 106 (1950).

Table 1.2. Invariant Equilibria in the System $NaF-BeF_2-ThF_4$

Solid Phases Present	Composition (mole %)			Invariant Behavior	Temperature (°C)
	NaF	BeF_2	ThF_4		
ThF_4SS, BeF_2, $NaF \cdot BeF_2 \cdot 3ThF_4$	2	96	2	Peritectic	526
$NaF \cdot BeF_2$, BeF_2, $NaF \cdot BeF_2 \cdot 3ThF_4$	43	55	2	Eutectic	365
$NaF \cdot BeF_2$, $NaF \cdot 2ThF_4$, $NaF \cdot BeF_2 \cdot 3ThF_4$	47	51	2	Peritectic	374
$NaF \cdot BeF_2$, $NaF \cdot 2ThF_4$, $NaF \cdot ThF_4$	48	50	2	Peritectic	375
$NaF \cdot BeF_2$, $2NaF \cdot BeF_2$, $NaF \cdot ThF_4$	55	43	2	Eutectic	320
$2NaF \cdot ThF_4$, $2NaF \cdot BeF_2$, $NaF \cdot ThF_4$	57	41	2	Peritectic	415
$2NaF \cdot ThF_4$, $2NaF \cdot BeF_2$, NaF	72	22	6	Eutectic	509
$2NaF \cdot ThF_4$, $7NaF \cdot 2ThF_4$, NaF	76	10	14	Peritectic	540
$2NaF \cdot ThF_4$, $3NaF \cdot 2ThF_4$, $NaF \cdot ThF_4$	62	2	36	Peritectic	683
$NaF \cdot 2ThF_4$, ThF_4SS, $NaF \cdot BeF_2 \cdot 3ThF_4$	42	31	27	Peritectic	745
$2NaF \cdot ThF_4$, $4NaF_4 \cdot ThF_4$, $7NaF \cdot 2ThF_4$	77	1.5	21.5	Peritectic	610
NaF, $4NaF_4 \cdot ThF_4$, $7NaF \cdot 2ThF_4$	77.5	5	17.5	Peritectic	604

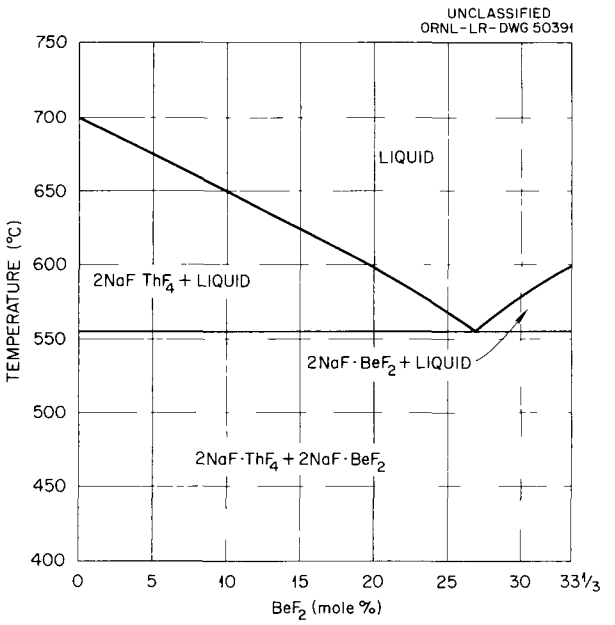

Fig. 1.10. The Composition Section Involving $2NaF \cdot ThF_4 - 2NaF \cdot BeF_2$.

studies, shows the existence of a single intermediate compound, $NaF \cdot YF_3$. Hund[22] reported the polymorphism of $NaF \cdot YF_3$ and showed that the high-temperature form (β-$NaYF_4$) has the fluorite structure. The low-temperature hexagonal form (α-$NaYF_4$) was indexed in the present studies. Its structure is described in the section "Crystal Structure of $NaYF_4$" (this chapter). The system $NaF-YF_3$ contains two eutectics, at 27 and 75 mole % YF_3, and at 640 ± 3 and 956 ± 3°C respectively. The equilibrium inversion temperature of the pure compound, $NaF \cdot YF_3$, occurs at 678 ± 3°C. The inversion in YF_3 is inferred from thermal data,[20] but crystals of the high-temperature form have not been isolated.

The solubility of YF_3 in cubic $NaYF_4$ has already been studied by Hund,[23] who prepared solid solutions containing up to 58 mole % YF_3 in β-$NaYF_4$ by precipitation from aqueous solutions, though he made no study of this phase at high temperatures. Figure 1.11 shows the region of solid solution in detail; the liquidus is seen to exhibit a maximum at 66.5 mole % YF_3. The existence of a compound at this maximum is ruled out by the appearance at 50 mole % YF_3 of a compound having the fluorite structure, with its propensity to form solid solution by addition of

[23] F. Hund, *Z. anorg. u. allgem. Chem.* 263, 102 (1950).

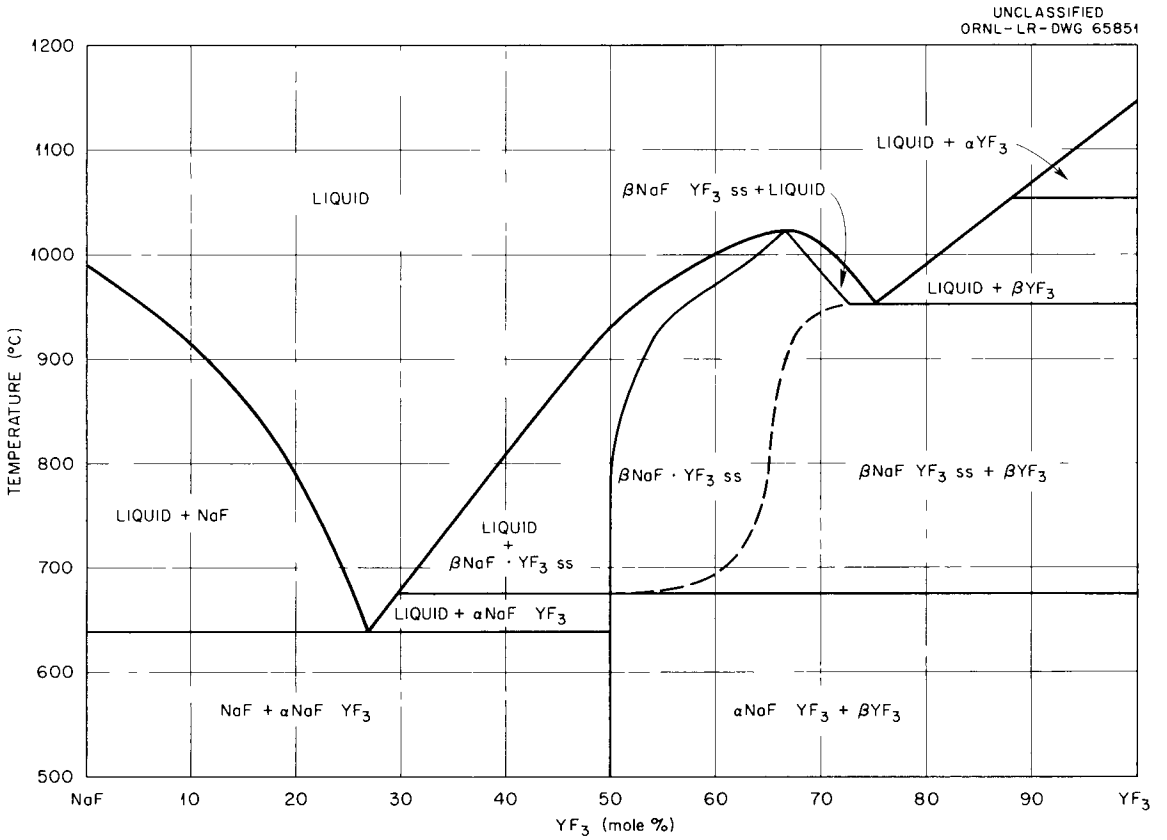

Fig. 1.11. The System NaF-YF_3.

YF_3.[24] Neither of the phases, α-$NaYF_4$ or $LiYF_4$,[20] appears capable of dissolving detectable amounts of YF_3.

Phase Studies on the System CrF_2-CrF_3

Corrosion of chromium-alloy containers by molten fluorides results in the formation of solutions of chromium fluorides. The chromium has generally been found in the divalent state in melts based on BeF_2 or ZrF_4, but in the trivalent state in melts consisting primarily of alkali-metal fluorides;[25] therefore, both CrF_2 and CrF_3 have been used in the study of corrosion by fluoride melts. In the synthesis of these compounds, an intermediate compound, chromium(II,III) fluoride, was encountered.[26] Because of interest in this compound, the CrF_2-CrF_3 system was studied, and preliminary data were reported.[27]

Additional experimental data have been obtained from cooling-curve and thermal-gradient-quenching experiments. Phase transitions observed in these experiments are shown in the equilibrium phase diagram of the system CrF_2-CrF_3 (Fig. 1.12). To prevent disproportionation of CrF_3 into CrF_2 and volatile CrF_5 at the high temperatures, the mixtures were sealed in platinum tubes which were sufficiently strong to withstand the pressures involved.

[24] E. Zintl and A. Ugard, *Z. anorg. u. allgem. Chem.* 240, 150 (1939).

[25] *MSRP Quart. Progr. Rept. Oct. 31, 1958*, ORNL-2626, pp 95–96.

[26] *MSRP Quart. Progr. Rept. Jan. 31, 1959*, ORNL-2684, pp 112–14.

[27] *Reactor Chem. Div. Ann. Progr. Rept. Jan. 31, 1961*, ORNL-3127, pp 4–5.

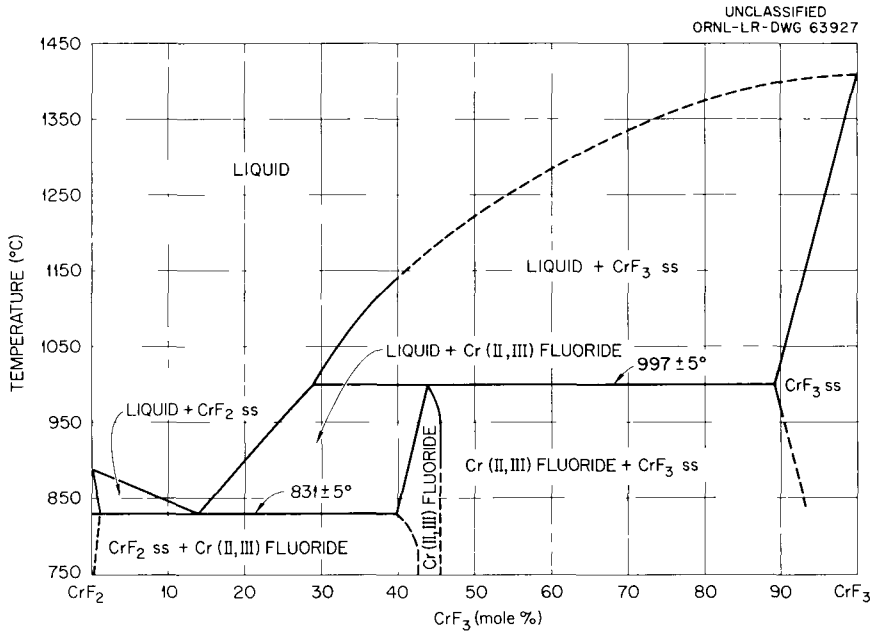

Fig. 1.12. The System CrF_2-CrF_3.

The only compound found in the system, chromium(II,III) fluoride, is a solid solution ranging in composition from $CrF_{2.40}$ to $CrF_{2.45}$. It melts incongruently at 997 ± 5°C. The density, determined pycnometrically at 25°C, is 3.64 g/cm^3. The eutectic at 831 ± 5°C contains 14 mole % CrF_3. Chromium(III) fluoride forms a solid solution containing slightly over 10 mole % CrF_2, which is distinguishable from pure CrF_3 by refractive-index measurements.

CRYSTAL-STRUCTURE INVESTIGATIONS

J. H. Burns D. J. Duchamp[28]

The crystal structures of several fluoride-containing substances were studied by x-ray diffraction. The single-crystal method was employed primarily, but powder diffraction was used when single crystals were not available. For the study of single crystals, use was made of Weissenberg and precession film techniques as well as the single-crystal orienter equipped with a scintillation-counter detector. A complete structure determination was carried out in some cases; in others, unit-cell dimensions, space group, and crystal density were determined.

Crystal Structure of $LiSbF_6$

The crystal structure of $LiSbF_6$ was determined by x-ray diffraction methods employing a single-crystal orienter and a scintillation-counter detector to measure intensities. The unit cell is rhombohedral with $a = 5.43$ A, $\alpha = 56° 58'$; it contains one formula wieght. The space group is $R\bar{3}$. The atoms were placed as follows in the hexagonal pseudo-cell:

$$(0,0,0;\ {}^1/_3,{}^2/_3,{}^2/_3;\ {}^2/_3,{}^1/_3,{}^1/_3) +$$

Sb (a) 0,0,0 ,

Li (b) 0,0,$^1/_2$,

F (f) $\pm(x,y,z;\ \bar{y},x-y,z;\ y-x,\bar{x},z)$;

the structure was described by six parameters: x, y, z, temperature factors for antimony and fluorine, and a scale factor. These parameters were refined by the method of least squares to fit 110 observed intensities, employing the Busing-Levy[29] program

[28] Summer employee; presently attending the Graduate School, California Institute of Technology, Pasadena.

[29] W. R. Busing and H. A. Levy, *A Crystallographic Least Squares Refinement Program for the IBM 704*, ORNL CF-59-4-37 (April 1959).

and the IBM 7090. The final parameters and their standard errors are shown below:

x(F)	0.3186 ± 0.0013
y(F)	0.0540 ± 0.0012
z(F)	−0.0799 ± 0.0004
B(Sb)	0.57 ± 0.02
B(F)	1.20 ± 0.06

The structure of $LiSbF_6$ (Fig. 1.13) is a rhombohedral distortion of the cubic $NaSbF_6$ structure[30] and consists of regular octahedra of fluorine atoms about the antimony and about the lithium atoms at distances of 1.877 ± 0.006 and 2.032 ± 0.006 A respectively.

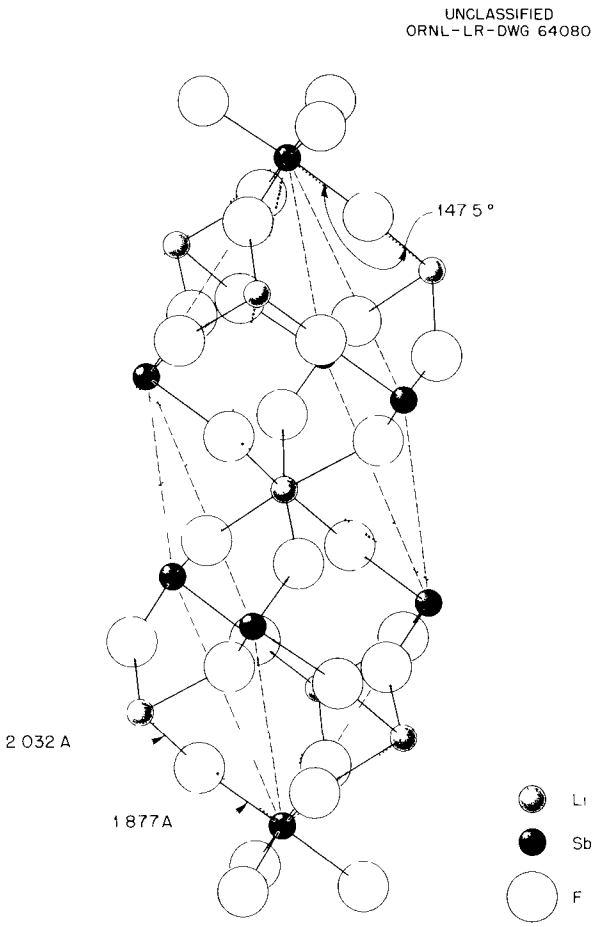

Fig. 1.13. Crystal Structure of $LiSbF_6$.

The location of the relatively light fluorine atoms in a crystal with heavy atoms also present, and hence the accurate determination of the Sb(V)-F bond length, reported here, was obtained because of the use of counter techniques to measure intensities.

Crystal Structure of $NaYF_4$

The low-temperature α-$NaYF_4$ and the high-temperature β-$NaYF_4$ reported by Hund[22] were prepared at this Laboratory and examined by x-ray diffraction. The cubic symmetry of β-$NaYF_4$ (fluorite structure) was confirmed, and α-$NaYF_4$ was determined to be hexagonal. On the basis of the unit-cell dimensions and chemical similarity, the α-$NaYF_4$ was deduced to be isostructural with β_2-$NaLaF_4$. This has been designated the β_2-Na_2ThF_6 structure type by Zachariasen.[31] Unit-cell constants are presented for comparison.

	a	c
β_2-Na_2ThF_6	5.889	3.835
β_2-$NaLaF_4$	6.179	3.827
α-$NaYF_4$	5.954	3.524

The calculated density of α-$NaYF_4$, with $^3/_2$ formula weights per unit cell, is 4.33 g/cm^3, in agreement with the measured value[22] of 4.23. The indexed powder pattern is shown in Table 1.3.

X-Ray Diffraction Study of K_3UF_7 and K_3ThF_7

The structure of green crystals of K_3UF_7 was reported by Zachariasen[32] to be tetragonal (ordered form) and cubic (disordered form) at low and high temperatures respectively. However, anhydrous preparations of K_3UF_7 were reported by Thoma *et al.*[33] to yield blue-green biaxial crystals, which were characterized by a powder pattern of low symmetry.

---

[30] N. Schrewelius, *Z. anorg. u. allgem. Chem.* 238, 241 (1938).

[31] W. H. Zachariasen, *Acta Cryst.* 1, 265 (1948).

[32] W. H. Zacharaisen, *Acta Cryst.* 7, 792 (1954).

[33] R. E. Thoma *et al.*, *J. Am. Ceram. Soc.* 41, 538 (1958).

Table 1.3. Powder Pattern of α-$NaYF_4$

I	d_{obs}	d_{calc}	hkl
64	5.156	5.156	100
63	2.975	2.977	110
47	2 910	2.910	101
8	2.578	2.578	200
21	2.272	2.274	111
68	2.082	2.081	201
6	1.950	1.949	120
5	1.762	1.762	002
20	1.721	1.718	300
42	1.707	1.706	121
5	1.667	1.667	102
4	1.518	1.516	112
7	1.455	1.455	202

Table 1.4. Powder Pattern of K_3UF_7

I	d_{obs}	d_{calc}	hkl
20	7.20	7.22	001
5	6.03		
80	5.44	5.45	011
60	5.15	5.16	110
40	4.85	4.86	101
20	4.19	4.20	111
45	3.59	3.60	021
35	3.29	3.29	200
100	3.15	3.16	121
10	2.95	2.96	112
10	2.817	2.817	211
5	2.715	2.727	022
5	2.675		
5	2.636		
15	2.578	2.580	220
5	2.550	2.553	130
10	2.508	2.517	122
25	2.436	2.432	202
5	2.398	2.407	131
5	2.332	2.333	212

In the present work, single crystals of both the green and the blue-green forms were prepared and examined by x-ray diffraction. The blue-green crystals were found to be orthorhombic, with $a = 6.58$ A, $b = 8.31$ A, and $c = 7.22$ A. The possible space groups are Pnmm and $Pnm2_1$. The powder pattern previously referred to[33] was indexed (Table 1.4) on the basis of this cell, assuring the identity of the single crystals with the previously studied powder.

The green crystals produced a cubic pattern in agreement with that of Zachariasen,[32] but no evidence was found for the tetragonal modification. The cubic diffraction patterns were composed of rather diffuse spots, suggesting that these crystals were poorly formed, perhaps due to quenching from high temperature. The presence of the diffuse cubic pattern superposed on the orthorhombic patterns provides evidence that when the orthorhombic $\rightleftharpoons$ cubic transformation occurs, the orthorhombic a axis becomes the [110] direction in the cube.

Single crystals of K_3ThF_7 were highly twinned, but x-ray patterns indicated that they are isostructural with cubic K_3UF_7.

Structural Studies on Chromium(II,III) Fluoride

Single crystals of chromium(II,III) fluoride (see the section "Phase Studies on the System CrF_2-CrF_3," this chapter) with the composition 60% CrF_2 and 40% CrF_3 were examined by x-ray diffraction. They are monoclinic, with $a = 7.82$ A, $b = 7.57$ A, $c = 7.17$ A, $\beta = 120° 7'$.

The space groups consistent with the systematic absences are $C_{2h}^6 - C2/c$ and $C_s^4 - Cc$. The pycnometric density is 3.64 g/cm^3. There is no stoichiometric ratio CrF_2:CrF_3 in the solid-solution range which will describe a compound such that an integral number of formula weights can occupy this unit cell and yield the observed density. However, an arrangement of 4 formula weights of Cr_2F_5 per unit cell is consistent with the possible space groups and has a calculated density of 3.60.

A structure which would explain both the phase and crystallographic observations is as follows: The Cr^{2+}, Cr^{3+}, and F^- would occupy positions of an "ideal" structure containing four Cr_2F_5 units per cell, yet have a random deficiency of F^- and an equal number of Cr^{3+} replaced by Cr^{2+}. Such an omission solid solution or defect structure would be analogous to that[34] of FeO in which there is a solid-solution range near to, but never attaining, the stoichiometric composition.

[34] E. R. Jette and F. Foote, *J. Chem. Phys.* **1**, 29 (1933).

X-Ray Diffraction Study of $LiRbF_2$ and $LiCsF_2$

The 1:1 compounds in the LiF-RbF and LiF-CsF systems[35] have been studied by single-crystal x-ray diffraction. The compound $LiCsF_2$ is monoclinic, with a = 6.01 A, b = 11.64 A, c = 8.14 A, β = 90° 45′, and has 8 formula weights per cell. The calculated density is 4.15 g/cm^3. Systematic extinctions indicate that the space group is $C2/c$ or Cc; these are indistinguishable by diffraction. A detailed study of atomic positions is in progress.

Since crystals of $LiRbF_2$ are 100% twinned [twinning plane is (001)], reliable data are more difficult to obtain; but the following monoclinic cell dimensions were found: a = 5.83 A, b = 11.16 A, c = 7.86 A, β = 94° 55′. This cell contains 8 formula weights of $LiRbF_2$ with a calculated density of 3.40 g/cm^3.

An obvious feature of the structure of each of these compounds is that one dimension of the unit cell in each case is equal to the cubic dimension of the component alkali fluoride; that is, CsF has a = 6.02 A and RbF has a = 5.64 A. This suggests the presence of chains of Cs-F-Cs-F and Rb-F-Rb-F along a in the corresponding compounds with LiF.

X-Ray Diffraction Study of $6LiF \cdot BeF_2 \cdot ZrF_4$

When the MSRE fuel is allowed to cool slowly, one of the first phases to precipitate is a ternary compound with the stoichiometry $6LiF \cdot BeF_2 \cdot ZrF_4$.[36] Single-crystal specimens of this compound were studied by x-ray diffraction, and it was deduced from the results that the crystals are body-centered tetragonal with a = 6.57 A and c = 18.62 A. The space group is one that is uniquely determined by the Laue symmetry and systematic absences, $D_{4h}^{19} - I4_1/amd$. A density of 3.19 g/cm^3 was calculated for a crystalline fluoride of this stoichiometry by the method of Cantor, which is based on the assumption that the molar volume of the complex compound is the sum of the molar volumes of the components (see the section, "Calculation of Densities of Fluorides," Chap. 5, this report). This value is in good agreement with 3.06 g/cm^3, calculated on the basis of the unit-cell dimensions and the presence of four stoichiometric units of Li_6BeZrF_{12}.

In order to satisfy the space-group requirements, the beryllium and zirconium ions must lie in planes separated by 4.64 A and perpendicular to the c axis. The locations of the other ions will be the subject of further studies.

PREPARATION AND CHARACTERIZATION OF NEW FLUORIDE COMPOUNDS

B. J. Sturm G. M. Hebert

Vanadium Trifluoride

Small quantities of vanadium are expected to be formed in the MSRE from irradiation of the chromium-alloy container: $Cr^{50}(n,\gamma)Cr^{51} \xrightarrow{e^-_K,\gamma} V^{51}$. As its fluoride, VF_3, could possibly form under some unusual conditions of reactor operation, some properties of this compound were studied. The compound was prepared by thermal decomposition of $(NH_4)_3VF_6$.[37,38]

The melting point of VF_3 was determined by the procedure used for CrF_3.[39] The material, contained in a platinum tube, melted at 1406 ± 15°C.[38] Analysis of the compound after melting showed that no chemical change had occurred. Near the melting point VF_3 had a vapor pressure sufficiently high to burst the container and completely volatilize in some tests. The compound forms yellow-green crystals that are biaxial (+), with N_α = 1.536 and N = 1.544. Contrary to published estimated free-energy values[40] indicating reduction to a hypothetical VF_2, VF_3 did not react with either nickel or vanadium at temperatures up to 1250°C.

Oxyfluorides of Zirconium and Uranium

Only limited data are available[41,42] concerning the identity and properties of the solid phases formed on partial hydrolysis of ZrF_4 and UF_4.

[35] C. J. Barton, T. N. McVay, L. M. Bratcher, and W. R. Grimes (unpublished work).

[36] *MSRP Progr. Rept. Feb. 28, 1961*, ORNL-3122, p 110.

[37] B. J. Sturm and C. W. Sheridan, *Preparation of Vanadium Trifluoride by the Thermal Decomposition of Ammonium Hexafluovanadate(III)*, ORNL CF-58-5-95 (May 28, 1958).

[38] B. J. Sturm and C. W. Sheridan, "Vanadium Trifluoride," *Inorganic Synthesis* (in press).

[39] *MSRP Quart. Progr. Rept. Apr. 30, 1960*, ORNL-2973, p 82.

[40] A. Glassner, *The Thermochemical Properties of the Oxides, Fluorides, and Chlorides to 2500°K*, ANL-5750 (1957).

[41] J. L. Williams, *Preparation of Zirconium Tetrafluoride*, Progress Report II, AECD-3335 (1952).

[42] R. W. M. D'Eye *et al.*, *J. Inorg. & Nuclear Chem.* 2, 192 (1956).

Because conditions might be obtained, in molten salt fuels, which could precipitate any or all intermediate solids in the system ZrF_4-UF_4-H_2O, attempts were made to synthesize and characterize the crystalline oxyfluorides in the system.

Zirconium Oxyfluoride. – Crystals of $ZrOF_2$ were prepared by two methods: solid-state reaction of ZrO_2 with ZrF_4 in a sealed tube at 950°C and reaction of ZrO_2 with ammonium bifluoride at low temperatures.[43] Crystals of pure $ZrOF_2$ are colorless, biaxial negative, with $N_\alpha = 1.730$ and $N_\gamma = 1.840$. Pure single crystals of $ZrOF_2$, prepared in these experiments, are being used in crystal-structure studies.

Uranium(IV) Oxyfluoride. – In neither previous[44] nor present investigations were crystals of UOF_2 obtained from reactions of UO_2 and UF_4 at high temperatures. In a series of fusion experiments,[43] unsuccessful attempts were made to substitute U^{4+} into a $ZrOF_2$ host lattice. The reaction products obtained suggested that, of the four compounds ZrF_4, ZrO_2, UF_4, and UO_2, the thermodynamically stable pair is UF_4 and ZrO_2, despite free-energy estimates to the contrary.[40]

Some Chemical Properties of Zirconium Monochloride

Although the published[45] properties of zirconium monochloride[46] suggest its use as a high-temperature lubricating, packing, and sealing material, experiments at this laboratory[47] indicate that the compound is too reactive to be useful for such purposes in the MSRE. The x-ray diffraction pattern obtained on the purchased compound differed somewhat from that published,[45] thus suggesting the presence of impurities.

Zirconium monochloride reacted with water at room temperature and with laboratory air at all temperatures. In room-temperature air the compound slowly gave off acid fumes (presumably HCl) and yielded unidentified solid products. At 800°C it reacted with air to yield ZrO_2 in accordance with the reaction:

$$4ZrCl + 3O_2 \rightarrow 3ZrO_2 + ZrCl_4\uparrow .$$

Below 500°C hydrolysis of $ZrCl_4$ by moisture in the air formed additional ZrO_2, complicating the reaction. At 425°C complete conversion of the ZrCl was obtained in 15 hr. Below 300°C the reaction was slower.

Published[45] free-energy estimates indicate that ZrCl will be oxidized by UF_4. It seems that use of ZrCl should be restricted to situations in which it does not contact air, moisture, or molten fuel.

Alkali-Metal–Alkaline-Earth Fluorides

From correlations of the occurrence of intermediate compounds in binary fluoride systems with relative cation sizes of the components, Thoma[48] suggested that $RbF \cdot SrF_2$, $CsF \cdot CaF_2$, and $CsF \cdot BaF_2$ could be expected to occur as stable compounds. In recent experiments the existence of each of the three compounds has been demonstrated from thermal data and by isolating pure crystals of each compound at its composition. Crystals of $CsF \cdot CaF_2$ and $CsF \cdot BaF_2$ were observed with the polarizing-light microscope to be cubic with refractive indices of 1.450 and 1.476 respectively. Crystals of $RbF \cdot SrF_2$, examined in this study, are biaxial, with $N_\alpha = 1.396$ and $N_\gamma = 1.400$.

[43] *MSRP Quart. Progr. Rept. July 31, 1960*, ORNL-3014, p 80.

[44] J. Wright and J. Warf, *Attempted Preparation of Uranius Oxyfluoride*, Monthly Technical Report, Ames Projects, Feb. 1 to Mar. 10, 1944, CC-1517, p 19.

[45] R. S. Dean, "New Chemical Compound Designed for High Temperature Use," *Ind. Labs.* 10(4), 45–8 (1959).

[46] Commercially available as Zirklor, from Chicago Development Corporation.

[47] B. J. Sturm, *Some Reactions of Zirconium Monochloride*, MSR-60-34 (Nov. 16, 1960).

[48] R. E. Thoma, *Inorganic Chemistry* (in press). Also presented at the annual information meeting, Reactor Chemistry Division, ORNL, May 11–12, 1961.

2. Compatibility of MSRE Components

COMPATIBILITY OF GRAPHITE AND MOLTEN FLUORIDES IN ABSENCE OF RADIATION

F. F. Blankenship S. S. Kirslis

Buoyancy Balance for Studying Graphite Permeation by Fused Salt

A buoyancy balance operable at several atmospheres pressure was constructed for studies of permeation of graphite by fused fluorides as a function of pressure. The method depended on the decreasing buoyancy with increasing permeation of a submerged graphite plummet.

Initial studies, in which a modified analytical balance was used to measure weight changes of graphite in LiF-BeF_2 (68-32 mole %) at 600°C, gave curves for permeation vs pressure similar to mercury porosimeter curves. As expected from the surface tensions, permeation by molten salt was consistently higher than by mercury at a given pressure. However, the ratio of pressures of mercury to salt for the same permeation (presumably occupying all voids accessible by the same minimum pore radius) increased with permeation, whereas the relation $pr = 2\gamma \cos \theta$ implies a constant ratio if the parameters remain constant.

The weighings with the analytical balance had to be made at atmospheric pressure, and were thus uncertain to the extent that molten salt pressurized into the graphite was released when the pressure was relieved. A balance to permit weighing at pressure was constructed, partly to avoid this probably small error but principally to speed up the determinations and to allow observations of equilibration rate. The balance beam was a tungsten wire, $\frac{1}{16}$ in. in diameter and 12 in. long, passing through a small rubber O-ring held in position by a metal gland. The rubber O-ring served both as a fulcrum for the beam and as a seal between a helium-pressurized compartment and the external atmosphere. The graphite plummet was suspended from the internal end of the tungsten beam, and a balance pan was suspended from the external end.

The operation of the balance has been tested at pressures up to 130 psig. It has a sensitivity of 10 mg and a maximum load of 50 g.

Drainage of Coolant Salt from Metal-Graphite Annuli

For molten-salt reactor designs in which the fuel salt is contained in INOR-8 tubes passing through holes in a graphite lattice, the annular spaces between the tubes and the graphite might be filled with coolant salt for better heat transfer. In the event of a reactor shutdown, the coolant salt would be drained, and complete drainage would be desirable. Drainage of 62% LiF–38% BeF_2 salt at 650°C from an INOR-8–graphite annulus $\frac{1}{16}$ in. wide, 3 in. in inside diameter, and 4 in. high was tested and found to be complete. Repeated dunking of the test assembly and examination in air showed no tendency for the salt to be held up in the narrow space. After several hours of exposure to air, the test salt became muddy and was covered by a brown scum. This exposed salt left a film or deposit on some portions of the graphite, but drainage from the annulus was still essentially complete. The conclusion was that a $\frac{1}{16}$-in. annulus is sufficiently wide to allow satisfactory drainage in a simple assembly.

Effect of Cesium Vapor on Graphite

B. J. Sturm

In the MSRE, some of the xenon produced by fission of uranium is expected to diffuse into the graphite moderator and there be converted into cesium by neutron capture. As cesium is known

to intercalate with graphite,[1] it was considered possible that changes in the moderator surface could occur which would permit harmful penetration by the molten fuel. To evaluate this, the behavior of cesium-treated graphite in molten fuel was compared with that of untreated specimens.[2]

Assuming the use of graphite with a D_{Xe} of 10^{-5} cm^2/sec, it was calculated[3] that, in one year of operation of the MSRE at 10 Mw, 80 g of cesium would be deposited in the graphite, nearly all of it near 1.4×10^6 cm^2 of surface, an average of 0.057 g of cesium per 1000 cm^2. Three graphite (AGOT) cylinders weighing 5.4 g each were outgassed and treated with 26½ liters (measured at room temperature) of helium saturated with cesium at 200°C. According to the vapor-pressure data of Kubaschewski and Evans,[4] 0.032 g of cesium was exposed to the graphite; this is about 1.25 g of cesium per 1000 cm^2 of graphite or about 20 times the typical exposure in one year of reactor operation at 10 Mw.

These treated specimens and three similar graphite specimens, that had been merely outgassed, were kept immersed in molten MSRE fuel at 650°C for 41 hr. No wetting was apparent and none of the specimens were changed in appearance by the experiment. Except for a 0.012-g gain in the graphite specimen nearest the cesium inlet, all the tested specimens lost 0.001 to 0.002 g, presumably due to outgassing. Based on these experiments, no significant harm to the MSRE moderator from cesium is expected during one year of operation.

INTERACTION OF FISSIONING MOLTEN FLUORIDE FUEL WITH GRAPHITE

S. S. Kirslis J. E. Savolainen
F. F. Blankenship

None of the BeF_2- or ZrF_4-based fuel mixtures of recent interest as reactor fuels have shown any tendency to wet graphite, or to penetrate graphite except in response to pressure in the manner expected from the pore spectrum of the graphite, as long as the interface is clean. That this nonwetting behavior should not change with fissioning and fuel burnup is a matter of prime importance in the smooth operation of the MSRE. Individually, and apart, the fuel or the graphite is scarcely affected, from a chemical standpoint, by the reactor environment. However, little is known about why some molten salts wet graphite and some do not, and still less is known about changes that might occur at the interface between graphite and an actively operating fluoride fuel.

The contact angle of the fuel miniscus at a vertical blade of graphite had been found to provide a convenient and reliable index of possible changes in wetting. Suitable experimental configurations, involving a vertical graphite blade dipping into a pool of fuel in a graphite boat, also allowed room in the same capsule for compatibility tests on coupons of MSRE core materials. The choice of a boat with a dished inside contour was influenced by the need for a container which could accommodate freeze-thaw cycles without stress. Capsules in previous experiments (47-1, 47-2) had ruptured from freeze-thaw cycles.[5]

Since the fuel and the graphite are chemically inert and thermodynamically compatible with respect to each other in the absence of radiation, rather extreme exposure conditions, limited mainly by the highest metal temperatures consistent with safety, were used in order to accentuate or accelerate the effects of irradiation. To provide a power density of 200 w/cc, the composition of the MSRE fuel, nominally LiF-BeF_2-ZrF_4-ThF_4-UF_4 (70-23-5-1-1 mole %), was adjusted to 1.5 mole % of fully enriched $U^{235}F_4$ rather than the <0.3 mole % estimated for MSRE criticality. At full power of 10 Mw, the MSRE has a burnup rate of 6% per year.

Description of Experiment

As described elsewhere in greater detail,[6] each of four sealed INOR-8 capsules, depicted in Fig. 2.1, contained an R-0025 graphite blade (7.3 g) dipping into a shallow pool of fuel (11.4 g

[1] W. Rudorf, "Graphite Intercalation Compounds," p 224 in *Advances in Organic Chemistry and Radiochemistry*, vol 1 (ed. by H. J. Emeleus and A. G. Sharpe), Academic Press, New York, 1959.

[2] "Effect of Cesium Vapor on Graphite," *MSRP Progr. Rept. Aug. 31, 1961*, ORNL-3215, p 127.

[3] I. Spiewak, "Cesium Distribution in MSRE Graphite," MSR-60-40 (private communication).

[4] O. Kubascheweski and E. Evans, *Metallurgical Thermochemistry*, 2d ed., Wiley, New York, 1956.

[5] "In-Pile Tests," *MSRP Progr. Rept. Feb. 28, 1961*, ORNL-3122, p 100.

[6] F. F. Blankenship *et al.*, "Fuel-Graphite Irradiation Test, ORNL-47-3," ORNL TM-118 (in preparation).

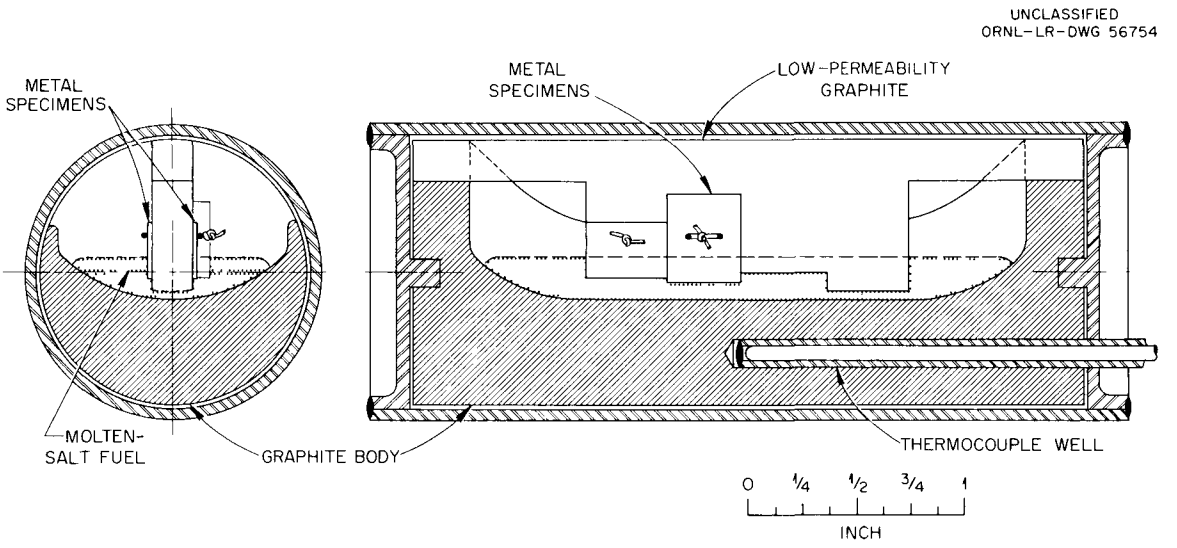

Fig. 2.1. MSRE Graphite–Fuel Capsule for Test ORNL-MTR-47-3.

or 5 cc) held in a graphite boat 3 in. long by 1 ¼ in. wide. Two of the boats were of R-0025 graphite (75 g), a relatively impervious grade, and the other two were of AGOT (66 g) which had been pre-impregnated with 9 g of fuel. The capsules, horizontally aligned in a vertical diamond array, were contained in a sodium bath which served as a heat transfer medium; thermocouple wells, which were affixed through one end of each capsule, measured the graphite temperatures at a point roughly midway between the bottom of the fuel and the capsule wall.

The fuel was purified by treatment at 800°C with HF and with H_2; the graphite was degassed in a vacuum at 2000°C. All subsequent manipulations were carried out in a helium-atmosphere glove box, and several extra capsules were assembled at the same time to provide control specimens.

Control capsules were handled in two ways. One group was subjected to about eight freeze-thaw cycles, each involving a maximum temperature of 900°C, and then opened for checking before the in-pile exposure was started. These revealed that the fuel miniscus had assumed the expected shape and that detectable contamination by oxide had been successfully avoided. However, a thin film of black dust, presumably graphite, had accumulated over portions of the liquid surfaces, and the fuel ingot had cracked into five or six pieces due to contraction around the central graphite blade. Neither of these undesirable manifestations was regarded as important enough to warrant a delay of the experiment.

Another group of control capsules was carried through a heat treatment based on temperature charts obtained from the in-pile capsules during the irradiation exposure. These were used as controls in the postirradiation examination, and they exhibited a frosted or silvery appearance on graphite surfaces near INOR-8 walls; this deposit, which was not found in the short-cycle controls, may have been Cr_3C_2.

The disassembly and initial observations were carried out in hot cells at the Battelle Memorial Institute under the supervision of ORNL Reactor Chemistry personnel, and later the separated pieces were sent to ORNL for further study.

The vapor pressure of the fuel increases by approximately a factor of 10 for each 100° interval between 700 and 1000°C, amounting to about 0.2 torr at 1000°C. At MSRE temperatures the vapor pressure is negligible, and although the control capsules showed no evidence of distillation, a considerable amount of vapor-phase transport (enhanced by the temperature gradient toward the cool walls as well as by the high fuel temperature) did occur in the in-pile capsules. The composition of the vapor seems to be slightly to the BeF_2-rich side of the stoichiometry for Li_2BeF_4, and much lower in quadrivalent cations than the liquid fuel.

To a very good approximation, distillation of the fuel corresponds to the removal of Li_2BeF_4; if an estimated 2.5 g were lost from the liquid fuel in capsules such as No. 15 or 16, leaving 8.9 g of fuel, the LiF-BeF_2-ZrF_4-ThF_4-UF_4 proportions would have been altered from 69.5-23-5-1-1.5 mole % to about 70-19-7.5-1.5-2 mole %. Several effects of the distillation were noted.

The condensation occurred predominantly at cool metal walls, firmly cementing the boats to the capsule walls in a manner that required the walls to be sawed off in strips to open the capsules. The opening operation thus involved some slight mechanical damage to the contents. Enough distilled salt was lost and fuel salt scattered to prevent the obtaining of a satisfactory material balance on either the amount distilled or the amount remaining in the fuel pool. Some condensation occurred in cooler pores of the graphite and caused an uncertainty in the interpretation of the weight changes of the graphite.

A considerable amount of the distilled salt was found in the form of condensed droplets, resembling pearls, that evidently dislodged from the capsule walls and fell onto or among the broken pieces of frozen fuel.

Exposure

The design flux was 2.3×10^{13} neutrons cm^{-2} sec^{-1}. Stainless steel dosimeter wires wrapped on the capsules differed among themselves by a factor of 4 when checked for cobalt activation and averaged a factor of 10 lower than expected for the design value. On the other hand, the ratio of U^{236} to U^{235}, obtained from the spent fuel by use of mass spectrometry, represented slightly less than 10% burnup, corresponding to a flux about 17% greater than the design value; the ratio was uniform for all four capsules. In view of the unexplained discrepancies, the design values of a flux of 2.3×10^{13} and 8.5% burnup have been adopted as the most suitable basis for calculations.

During the four irradiation cycles of three weeks each which the capsules underwent in the reactor (MTR), the fuel underwent about 40 freeze-thaw cycles.

Temperatures

Because of thermal convection in the sodium bath in which the capsules were immersed, the upper capsule, No. 3, operated at higher temperatures than its duplicate, No. 8, which was at the bottom of the diamond array. Capsules 15 and 16 were cooler because of the absence of preimpregnated fuel in the boat. The operating temperatures are given in Table 2.1. The temperatures ran 40 to 45°C higher initially than at the end; almost half of the decrease occurred in the first 70 hr, perhaps due to improved heat conduction as salt-vapor condensate accumulated in the gas gap between the graphite and the capsule wall.

Gas Analyses

The first step in the postirradiation examination was an analysis of the helium cover gas. The helium was present as a result of the final closure,

Table 2.1. Identification of Irradiated Capsules and Time-Averaged Operating Temperatures

Capsule No.	Graphite[a]	Pretreatment	Average Operating Temperature (°C)			
			Fuel Maximum (estimated)	Blade-Fuel[b] (estimated)	Boat-Fuel[b] (estimated)	Thermocouple in Graphite
15 and 16	R-0025	2000°C in vacuum	835	790	730	710
8	AGOT	Preimpregnated with 9 g of fuel	850	810	750	730
3	AGOT	Preimpregnated with 9 g of fuel	945	900	850	825

[a] R-0025 is relatively impervious compared with AGOT.

[b] Interface temperatures. No allowance for films at the fuel interface was made.

by arc welding, in a helium-atmosphere glove box, but the welding electrode was fed with a blanket of argon, and hence there was a small but indefinite amount of argon to be expected in the capsules.

The nominal volume of the gas space in the sealed capsules, not counting about 4.5 cc of voids in the graphite, was about 16 cc; the initial amount of capsule gas, though not known, was estimated as about 17 cc (STP) by assuming an average gas temperature of 50°C at the instant of sealing.

Gas samples were obtained by drilling the end of each capsule in an evacuated chamber which enclosed both the drilling apparatus and the capsule. Before drilling was started, measured leak rates were reduced to acceptably low values. The released gas was transferred by a Toepler pump and an associated manifold into sample bulbs equipped with "break-seals." The transferred gas was divided into four samples (about 100-cc vials) for mass spectrometric analysis, and four smaller samples (about 1.5-cc vials) for gamma-ray spectrometry. A condensed summary of the results from mass spectrometry is given in Table 2.2. As reflected in amounts of gas collected, shown in the second column of Table 2.2, some of the capsules gave samples with much smaller than expected pressures. The difficulty stemmed from a varying combination of lack of sufficient Toepler pump cycles, lack of adequate instrumentation, and lack of information on volumes of various parts of the system, but even after these points were at least partially remedied, there was evidence of a slow rate of gas release from the capsules. Samples of residual gas, accumulated over a period of several hours after the original transfer, were predominantly air from leaks but nevertheless contained 5 to 10% as much capsule gas as the original samples, with the same proportions of constituents. A partial sealing due to the presence of condensed salt vapor may have contributed to the difficulty in transferring the expected total volumes of gas.

Generation of CF_4

The relatively large amounts of CF_4 shown in column 5 of Table 2.2 represent a nonequilibrium condition which had not been fully anticipated; usually, temperatures as high as the 800 to 900°C prevailing in the capsules supply sufficient activation energy to prevent the accumulation of species that are thermodynamically unstable toward reaction by several tens of kilocalories.

The main source of the CF_4 was the graphite-fuel interface. The main sink for CF_4 is the fuel. Most of the CF_4 from the source was probably consumed immediately by the fuel, but some fraction diffused into the graphite and thus was bypassed into a reservoir where it was preserved until it could again come in contact with fuel.

Table 2.2. Off-Gas Compositions from Mass Spectrometry at ORNL and BMI

Capsule	Std cc[a] Sampled	Averaged Values (vol %)						
		Air[b]	He	CF_4	Xe	Kr	CO_2	Ar[c]
15	10	5.84	80.6	9.85	0.012	1.40	0.04	2.29
16	19	22.75	61.45	8.73	0.003	1.14	4.73	1.62
8	7	5.36	76.9	2.32	11.82	1.96	0.11	4.20
3	17	4.57	79.6	0.67	11.43	1.78	0.10	0.96
Control[d]	10	7.38	87	<0.0003			0.17	5.54

[a] Apparent volume of gas transferred from gas release chamber.

[b] Mainly inleakage to the evacuated release chamber while drilling the capsules.

[c] Argon was supplied as a blanket gas for the welding arc used in a helium-atmosphere glove box to seal the capsules.

[d] The control was heated through cycles roughly corresponding to the thermocouple reading vs time for capsules 15 and 16.

The voids in graphite are interconnected and, of course, communicate to the gas space above the boat. In the voids or the gas space, conditions were not favorable for access of CF_4 to a reactive surface. The frequently encountered kinetic inertness of CF_4 in many of its reactions[7] was also a contributing factor. Since a higher concentration of CF_4 was found in the capsules (15 and 16) in which the generation rate was smaller, the consumption rate evidently was the controlling factor as far as the steady-state concentration in the capsule gas was concerned. Several conditions may have diminished the consumption rate: (1) *Films of condensed salt vapor, essentially* Li_2BeF_4, coated the capsule walls. (2) Hotter regions appeared to have been covered by a film resembling a carbon or graphite deposit from the pyrolytic or radiolytic decomposition of CF_4. (3) Even in the control capsules a film of black dust, presumably graphite machining dust, accumulated on the surface of the fuel ingot. In any case the consumption reaction did not proceed rapidly enough to restore equilibrium conditions.

One proposed reaction mechanism which accounts for the faster consumption rate in the capsules with prepermeated boats requires three-phase contact, gas, graphite, and fuel, to allow a heterogenous reaction, and leans on the fact that the reduction of CF_4 even by "unreduced" fuel is thermodynamically favored. Regions of three-phase contact were much more abundant in the prepermeated boats. The fact that the fuel-graphite interface area had a higher temperature in the prepermeated cases was also of importance in accelerating the consumption reaction.

The consumption of CF_4 by dissolution in the fuel and subsequent reaction is probably slow, but even for this mechanism, the area of liquid-gas interface is greater in the prepermeated boats.

The point of concern about the CF_4 generation is the removal of fluoride ions from the fuel; that is, the reduction of the fuel as CF_4 is carried away in the off-gas. Probably this does not occur in a system with submerged graphite, like the MSRE, but if it did, the most readily recognized manifestation of the reduction would be the conversion of UF_4 to UF_3. As the concentration of UF_3 increases, the disproportionation reaction $4UF_3 \rightarrow 3UF_4 + U^0$ leads to the formation of metallic uranium alloys with the container as well as the formation of uranium carbides with the graphite. Although the presence of a measurable amount of reducing power in the fuel from the capsules has not been satisfactorily confirmed, it is instructive to compare the amounts of CF_4 accumulating in the capsules on the basis of the calculated percent conversion of UF_4 to UF_3 in the fuel. This has been done in Table 2.3; no allowance has been made for the anticipated reduction due to the fact that the fissioning process produces a total cation valence requirement greater than can be matched by the four equivalents of fluorides from a gram atom of fissioned uranium.

[7] T. J. Brice, pp 432–33 in *Fluorine Chemistry*, vol I (ed. by J. H. Simons) Academic Press, New York, 1950.

Xenon

In Table 2.4 the amount of xenon found in each capsule is compared with the amount expected for 8.5% burnup of the U^{235}. For the two preimpregnated cases, Nos. 3 and 8, the proper amount was found, but in the other two cases only about 0.1% of the expected yield was found.

No satisfactory explanation can be given, but there is a possibility that the missing xenon was somehow selectively absorbed in some 4 ft of rubber tubing that was used in the gas collecting system. Also an attempt is in progress to analyze the irradiated boats for xenon, but the graphite has been exposed to air several months, so that there is little hope that the graphite analyses will resolve the question. There were no significant differences in the isotopic distribution of the xenon recovered from the various capsules.

Krypton

The behavior of the xenon is even more puzzling in view of the fact that the krypton yields were normal, both in amount and in the proportions of the isotopes.

Physical Properties of Graphite

Dimensions of the graphite boats and blades did not change within the precision with which the measurements were made. Changes greater than 0.1% should have been detectable.

Weight changes on the graphite parts were also not very meaningful, since they represented the effect of distilled salt condensed in the pores, broken and lost graphite, and some sticking salt that was difficult to remove. The blades and

Table 2.3. Calculated Conversion of UF_4 to UF_3 Based on CF_4 Evolution

Capsule	Average vol % CF_4[a]	Total Volume[b] (std cc)	Yield (std cc of CF_4)	Calculated[c] Percent of U^{4+} Reduced
3	0.67	23.5	0.157	0.45
8	2.32	21.1	0.49	1.41
15	9.8	16.5	1.62	8.3
16	8.73	20.5	1.79	9.1

[a]Average of BMI and ORNL mass spectrometer analyses.
[b]Based on krypton analyses and 8.5% burnup.
[c]According to stoichiometry of $4UF_4 + C \rightarrow CF_4 + 4UF_3$, including impregnated UF_4 in calculation.

Table 2.4. Comparison of Xenon Analysis with Theoretical Yield

Capsule	Xe[a] (vol %)	Total Volume[b] (std cc)	Total Xe (std cc)	Theoretical Total Xe[c] (std cc)
3	11.43	23.5	2.69	2.86
8	11.82	21.1	2.52	2.83
15	0.012	16.5	0.0020	1.59
16	0.007	20.5	0.0014	1.61

[a]Average of BMI and ORNL analyses.
[b]Based on krypton analyses.
[c]Based on 8.5% burnup.

unimpregnated boats gained weight, probably as a result of salt-vapor condensation. The preimpregnated boats lost weight by distillation.

The electrical resistance of the graphite parts approximately doubled as a result of the irradiation exposure. Such changes have been attributed to the trapping of conductance electrons in defects induced by radiation.

Rockwell hardness on the R-0025 graphite increased by 10% from 94 to 108 as a result of the exposure. The AGOT boats increased from about 56 to about 80 as a result of preimpregnation with salt, and the readings after radiation were not significantly higher. No differences were found between regions under the salt pool and elsewhere in the same boat.

Wetting Behavior

When the fuel ingot pieces, jostled by the disassembly operations, were fitted into their original positions in the boats, the miniscus was observed to be the same as in the control specimen and to definitely show nonwetting behavior toward graphite; the metal coupons were wetted. The nonwetting behavior is receiving further confirmation from metallography and autoradiography of the graphite, along with analyses of semimicro cores drilled from the graphite. Information from weight changes of the graphite, though uncertain because of complications from distilled salt and mechanical damage in the hot cell, was at least indicative of no pronounced permeation of the graphite by fuel.

Effects on Coupons

Metallographic examinations of coupons on INOR-8, pyrolytic graphite, and molybdenum, which were attached to the blade, have not been completed, but visual observation revealed that the molybdenum had been severely corroded, having lost about one-half of its thickness, while the other specimens appeared unaffected. INOR-8 wires binding the coupons to the blade had become brittle.

Analyses of Fuel

Petrographic and X-Ray Examination. – Except for discoloration, the fuel appeared, under the optical microscope, to have no exceptional features when the composition changes were taken into account. Attempted x-ray examination proved unfruitful because of interference from background gamma radiation. Petrographic observation established that fuel composition had shifted sufficiently so that LiF was the primary phase, and that the main cause of the dark brown discoloration was LiF. The compound Li_2BeF_4, as expected, was also distinguishable in the irradiated fuel; some of the crystals of this compound, ordinarily uncolored, had a faint brownish-purple tint as a result of the radiation. No oxide, no UF_3, and no opaque materials were found. Attempted comparisons of samples from the exterior and interior of the fuel ingot revealed no evidence of segregation.

Chemical Analyses. – Too few samples have been analyzed chemically to provide a meaningful representation of the fuel composition; the preliminary values for the major constituents are plausible only if extensive segregation occurs. Among the corrosion products, chromium analyses are the most consistent, averaging 550 ppm for capsules 15 and 16, and 715 ppm for capsules 3 and 8. Such values, presumably arising from the presence of Cr^{2+}, are well above equilibrium values for a "reduced" fuel. The fuel originally loaded into the capsules analyzed 10 ppm of chromium and 185 ppm of iron. Analyses for iron in the irradiated fuel ranged from 1000 to 2000 ppm; efforts are being made to determine whether such high results represent accidental contamination.

Analyses by Gamma Spectrometry. – Attempts to compare the exterior and interior of the fuel ingot by gamma spectrometry showed that ruthenium was concentrated at the surface, particularly at the gas interface. Cerium-144, barely detectable in surface samples, was prominent in dissolved samples which included interior portions. In all cases, the predominant activity was the mass 95 Zr-Nb decay chain.

Conclusions

Due in part to the difficulties of hot-cell examinations, many aspects of the postexposure examinations have not been satisfactorily culminated, but the main objectives of the experiments have been successfully accomplished. The nonwetting behavior of fissioning fuel toward graphite has been convincingly demonstrated; and the nature of radiation effects, which might arise during MSRE operation, has been disclosed. Only the evolution of CF_4 promises to be a potentially serious problem, and this effect may have been greatly accentuated by the boat-and-pool geometry chosen for the experiment. In any case the gas occupying the voids in graphite exposed to fissioning fuel will contain several percent of CF_4; in reactor operation, however, the graphite is submerged, furnishing a more favorable arrangement for the reaction of CF_4 with the fuel, and the loss of CF_4 to the off-gas in these circumstances may well be insignificant.

3. Fluoride Salt Production

F. A. Doss J. E. Eorgan J. H. Shaffer

Since the inception of the molten-salt reactor concept at ORNL, the Reactor Chemistry Division's fluoride production facility has been maintained in continual operation to support the various fused-salt programs of the Laboratory and the AEC. This facility is utilized to prepare various fluoride mixtures which melt below 800°C and to reduce the impurities of these fluoride melts to very low concentrations. While the method for the production of purified fluoride mixtures has been previously described,[1] a continual effort is expended to improve the production process.

THE PRODUCTION PROCESS

Studies of the corrosion mechanism,

$$M^0 + 2HF \rightleftharpoons MF_2 + H_2 ,$$

showed that chemical equilibrium in fluorides could be achieved by sparging with mixtures of HF and hydrogen at constant partial pressures.[2] Thus, in place of the previously used technique of alternate HF-H_2 treatment, metallic impurities can conceivably be maintained in the reduced state by admixing adequate quantities of hydrogen with HF. As suggested by studies of high-temperature thermocouple research,[3] the presence of hydrogen should also reduce the corrosiveness of the HF-H_2O effluent gas mixture which accompanies the conversion of oxides to fluorides. Since adapting this technique for purifying molten fluoride mixtures, production time cycles have been substantially reduced.

The hydrogen reduction of CrF_2, the impurity most difficult to remove, is exceedingly slow; consequently, about 25% of the production time cycle is devoted to this operation. As a possible alternative method, small-scale experiments were conducted to study the reduction of chromium with a stronger reducing agent. The addition of zirconium metal turnings to a fluoride mixture containing CrF_2 showed that the anticipated reduction of chromium occurred rapidly and almost stoichiometrically. However, during the practical application of this reduction process, fluorides treated with zirconium metal were found to be extremely corrosive toward nickel equipment. Further laboratory studies will be required before the use of this reduction method can be considered in the production process.

For reactor applications, the removal of oxides from molten fluorides is of primary importance. While oxide impurities, in themselves, are probably not detrimental, their presence in the molten-fluoride circuits of the MSRE could result in the deposition of solid oxide particles or scale. The resulting heterogeneous system could alter the heat transfer properties of the reactor components and might also create localized heat sources in the reactor core by the deposition of uranium dioxide. The efficient removal of oxides by the fluoride purification process would increase the "oxide capacity" of these fluoride mixtures for

---

[1] J. E. Eorgan *et al.*, *Reactor Chem. Div. Ann. Progr. Rept. Jan. 31, 1960*, ORNL-2931, p 64.

[2] C. M. Blood, *Solubility and Stability of Structural Metal Difluorides in Molten Fluoride Mixtures*, ORNL CF-61-5-4 (Sept. 21, 1961).

[3] G. W. Keilholtz *et al.*, *Reactor Chem. Div. Ann. Progr. Rept. Jan. 31, 1961*, ORNL-3127, p 133.

inadvertent contamination during reactor operations. Typical laboratory results illustrating the effectiveness of oxide removal from fluoride melts by hydrofluorination in the presence of H_2 are shown in Fig. 3.1.

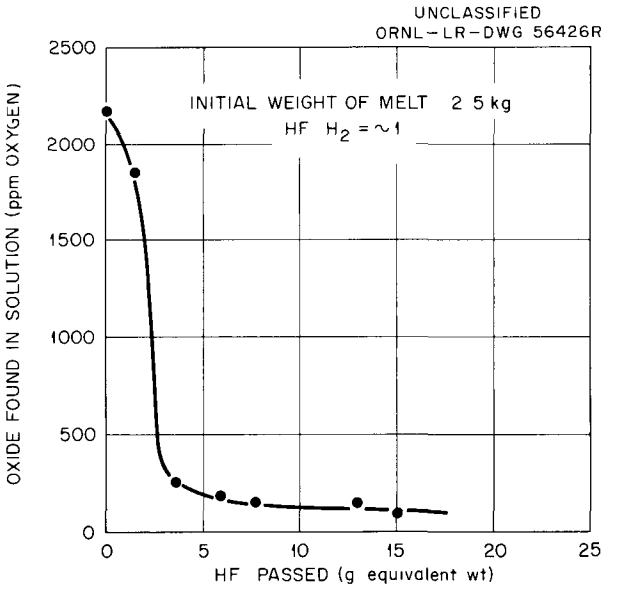

Fig. 3.1. Removal of Oxide from LiF-BeF_2 (63-37 mole %) at 700°C by Treatment with HF-H_2 Mixtures.

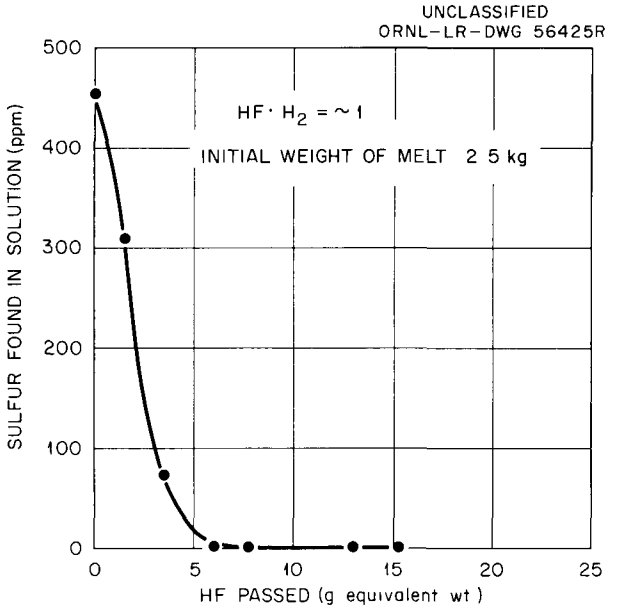

Fig. 3.2. Removal of Sulfur from LiF-BeF_2 (63-37 mole %) by Treatment with HF-H_2 Mixtures at 700°C.

The technique of using HF-H_2 mixtures for fluoride purification has also resulted in an improved method for removing sulfur impurities from fluoride melts. By the previous method of alternate treatment with HF and H_2, sulfates were reduced to sulfides by hydrogen and were subsequently volatilized as H_2S upon hydrofluorination. The present use of HF-H_2 mixtures permits the continual removal of sulfur as H_2S during a single purification step. A typical result shown in Fig. 3.2 demonstrates this operation.

FLUORIDE PRODUCTION OPERATIONS

Approximately 1050 kg of mixtures comprised of LiF, BeF_2, ZrF_4, ThF_4, and UF_4 was prepared for the various experimental engineering tests of the Molten-Salt Reactor Program during 1961. An additional 3700 kg of the mixture NaF-LiF-ZrF_4 (37.5-37.5-25.0 mole %) was prepared for use in the development and demonstration of reactor fuel reprocessing schemes by the Chemical Technology Division. Small batches of various fluoride mixtures were furnished to other groups of the Reactor Chemistry Division, the Chemical Technology Division, and the Battelle Memorial Institute.

In addition to the operation of the fluoride production facility, the following related services are also provided.

Hydrofluorination of the Engineering Test Loop Salt Mixture

A useful application of HF-H_2 mixtures in the fluoride purification process was demonstrated by the in situ oxide cleanup of the fluoride salt mixture used in the current Engineering Test Loop. Since the Loop salt container was fabricated of Inconel, this demonstration illustrated the use of HF-H_2 mixtures to reprocess fluoride mixtures contained in materials which are rapidly corroded by HF alone. Because of relative inexperience with the HF-H_2 gas mixtures with respect to corrosion inhibition, certain control measures were taken: (1) By determining the rate at which water vapor was removed from the system, the minimum HF treatment time necessary to remove essentially all the oxide ion from the molten fluoride could be estimated. The results of this determination are shown in Fig. 3.3. (2) To ascertain the chemical condition of the fluoride mixture during the hydrofluorination treatment,

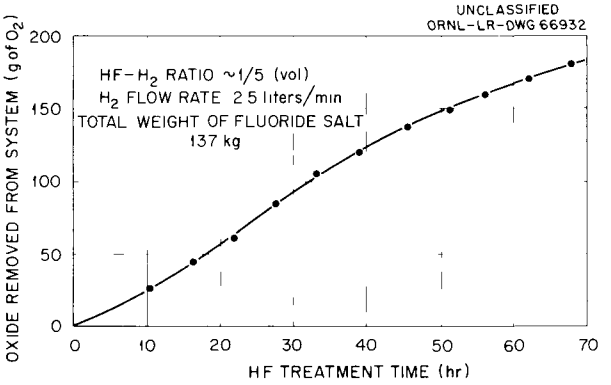

Fig. 3.3. Removal of Oxides from Engineering Test Loop by HF-H_2 Treatment at 1050°F.

salt samples were withdrawn periodically for chemical analysis. The results of these analyses showed that the dissolved oxide ion concentration in the melt diminished from values of 500 ppm (apparent saturation with ZrO_2) to less than 200 ppm during the purification treatment. (3) Since corrosion by mass transfer of metals might occur during conditions of apparent chemical equilibria, metal test specimens exposed to the HF-H_2-salt system were desired. Metallographic examinations[4] of the Inconel dip tubes used for sparging the fluoride melt with the HF-H_2 mixture revealed that they had been only mildly corroded during this operation. The concentrations of structural metals dissolved in the fluoride melt were virtually unaltered by the treatment with the HF-H_2 mixture.

Support of MSRP In-Pile Test Programs

In support of the recent in-pile test of the compatibility of the MSRE fuel with graphite (ORNL-47), a small batch of fluoride fuel mixture, enriched in U^{235}, was prepared in copper tubing. By sectioning this tubing and removing the contained fluorides, an accurate loading of each test capsule with a small quantity of the fluoride mixture was accomplished. In addition to this preparation, graphite boats, which were to contain the salt in the test capsules, were impregnated with the fluoride fuel mixture. This operation was achieved by immersing the boats in the molten fuel mixture under a static helium pressure of 60 psig for 2 hr.

[4]Metallographic examination by C. E. Zachary, Metallurgy Division.

In preparation for the postirradiation examination of this test, four control capsules were subjected to heating and cooling in the absence of radiation but in a pattern which followed the thermal history of the in-pile capsules.

Operations with Liquid Metals

Since the techniques for handling liquid metals are similar to those required for molten fluorides, service operations in this category are also provided. Primarily, these activities are utilized for filling in-pile test assemblies with liquid sodium or with sodium-potassium mixtures. This service was provided for the above-mentioned MSRP irradiation test and for capsules used in irradiation studies in the ORR.

Miscellaneous Service Operations

As an added service, routine operations were provided for assisting various engineering tests which utilize molten fluorides or liquid metals. Primarily, this service consisted of filling or draining operations. In addition, intermediate-scale experimental facilities were provided for various studies with molten-fluoride systems. These facilities have been utilized for assisting in the development of the MSRE fuel sampler-enricher assembly and in attempts to remove oxide films from Zircaloy test specimens by dissolving the films in molten fluorides.

PLANT MODIFICATIONS

Fused-fluoride mixtures are currently produced by a batch process. Each of two units is normally operated according to the following time schedule:

Operation	Time (hr)
Charge and meltdown	12
HF-H_2 treatment	48
H_2 stripping	42
Salt transfer	4
Reactor cooldown for recharging	48
	154

Thus two batches of salt per week are derived from a single-shift, five-day operation.

At the present capacity of approximately 1.3 ft^3/batch, a minimum of 67 weeks of operation would be required to process the fluoride mixtures for the MSRE. From considerations of methods for transporting these purified fluoride mixtures to the reactor, the use of some 50 presently existing shipping containers appeared feasible. Residual salts from previous usage are currently being removed from these containers. The previous capacity of the production facility was limited by the volume of the shipping container; lengthening each vessel by 12 in. will permit utilization of the full capacity of the purification treatment vessels and will increase the production rate to approximately 4.2 ft^3/week. This modification is in progress.

To accelerate the rate of fluoride production, further plant modifications are being considered. An examination of the batch production schedule shows that 60 hr of the 154-hr production cycle is used for cooling the treatment vessel after salt transfer and for melting the starting materials of the next batch. The addition of a separate furnace assembly adjoining each batch facility could be effectively used to charge each treatment vessel with molten starting materials. By proper scheduling, this arrangement would permit continuous operation of each batch facility on a 94-hr production cycle with an increase in production of approximately 64%. A preliminary engineering study to obtain cost estimates for this possible modification is in progress.

4. Chemical Aspects of MSRE Safety

H. F. McDuffie R. Slusher W. L. Marshall
M. J. Kelly D. R. Cuneo B. J. Sturm

Safety aspects of the molten-salt reactor make it important to know the short- and long-term effects of a spill of molten reactor fuel or of reactor coolant into the water-sand mixture at the bottom of the containment shell. Since this shell is designed to withstand a maximum pressure of 5 atm (approximately equivalent to the vapor pressure of H_2O at 150°C), the maximum temperature of interest, when considering long-term effects, would be 150°C. Solubilities of reactor coolant (Li_2BeF_4) and fuel mixture (LiF-BeF_2-ZrF_4-ThF_4-UF_4, 70-23-5-1-1 mole %) in water have been explored at 25°C and at higher temperatures. The sudden injection of molten salt into water has also been studied to determine the short-term pressure and temperature effects and the nature of the frozen salt produced by the contact with water.

Consideration was given to another safety problem – iodine volatilization from the MSRE fuel – both under normal operating conditions and in the case of an accidental spill in the presence of air.

SOLUBILITY OF MSRE FUEL AND COOLANT SALTS IN WATER

Experimental

Solid Li_2BeF_4 and MSRE fuel mixture were obtained from the fluoride production facility (see Chap. 3, this report). The Li_2BeF_4 contained approximately 2 wt % excess LiF. These solids were ground to powders in a glove box and were added separately to flasks containing water. The mixtures were stirred at room temperature (approximately 25 ± 2°C) and at controlled temperatures up to 90°C. Samples of solution phases were analyzed for the various components.[1]

Dissolution of Li_2BeF_4 in H_2O

The concentrations of Li, Be, and F found in solution, when excess Li_2BeF_4 solid was mixed with H_2O at 25°C, are given in Fig. 4.1 as a function of time. Based on the data for lithium and beryllium, it appears that equilibrium was attained at least within six days and perhaps sooner. The changes in the compositions of the solutions (revealing a higher ratio of beryllium to lithium than that in the original solid) require the appearance of some solid which is richer in lithium than the starting material and which is presumably LiF. The data suggest that an invariant point may have been established.

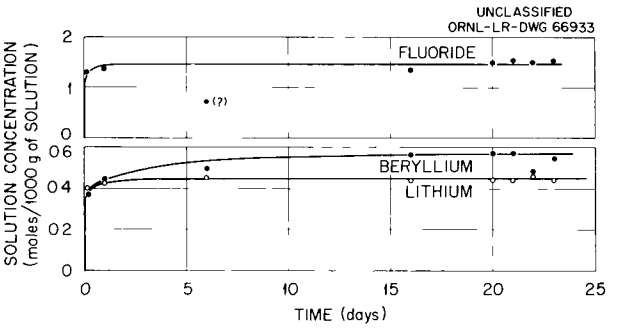

Fig. 4.1. Effect of Time on Dissolution of Li_2BeF_4 in H_2O at 25°C.

[1] Analyses performed by the Analytical Chemistry Division.

The concentrations of Li, Be, and F found in solution are given in Fig. 4.2 as a function of

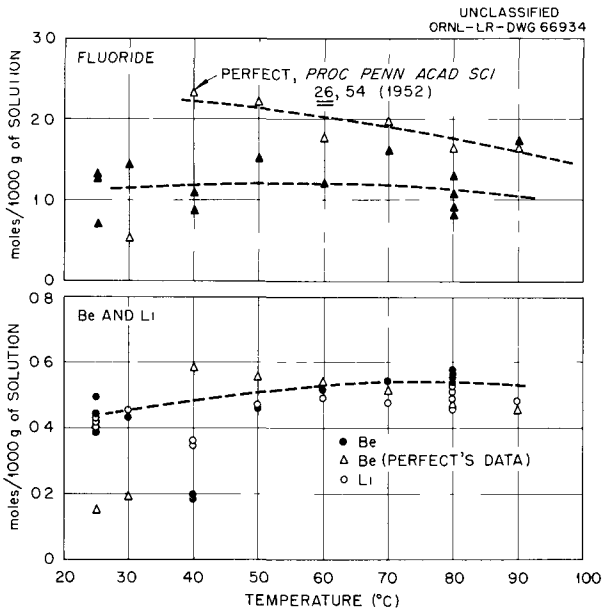

Fig. 4.2. Effect of Temperature on Dissolution of Li_2BeF_4 in H_2O.

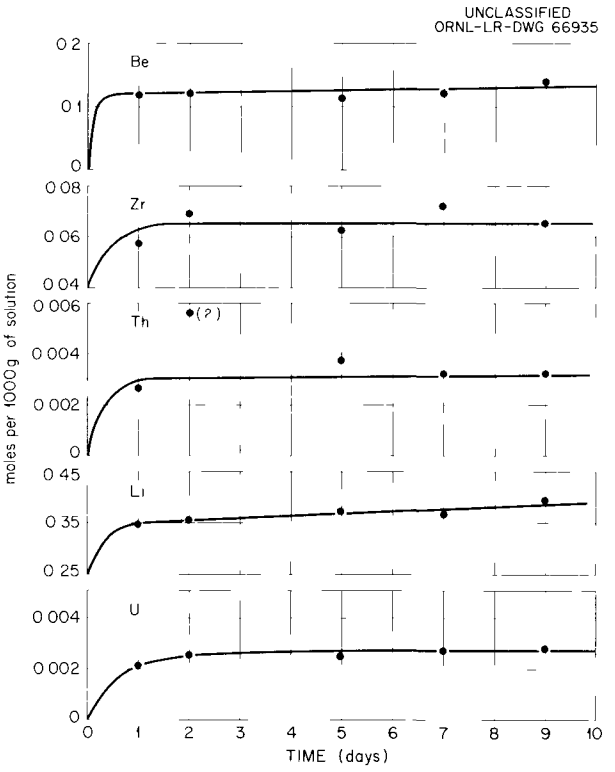

Fig. 4.3. Effect of Time on Dissolution of MSRE Solid Fuel in H_2O at 25°C.

temperature. Mixtures of liquid and Li_2BeF_4 solid were equilibrated 4 hr to three days before sampling the solution phases for analyses. Also included are the data obtained at 25°C (from Fig. 4.1).

Dissolution of MSRE Fuel Mixture

The analytical results from the run with fuel mixture at 25°C as a function of time are shown in Fig. 4.3. As with the reactor coolant, equilibrium appeared to be attained within six days. Nevertheless, a consistent increase in concentration of lithium and uranium was noted. In this experiment it was presumed that tetravalent uranium from the solid phases had been converted to the hexavalent state in the solution phase[2] by the action of oxygen from the air.

In Fig. 4.4 are the analytical results for solution concentrations of U, Li, Th, Zr, and Be as a function of temperature. The time of equilibration at each temperature before sampling was one day. Also included is one value for uranium obtained previously.[3] The analytical results from samples taken upon stepwise lowering of the temperature of the solution-solid mixture consistently gave higher values for the solution concentrations of the various components. It is believed that equilibrium was not reached on cooling.

In view of the appreciable uranium concentration found in solution under these conditions, it has been recommended that neutron poisons be present in any water which could mix with the fuel in the event of a reactor accident.

[2]H. C. Nikolaef and Yu. A. Luk'yanchef, *Atomnaya Energ.* 11, 67 (1961).

[3]R. F. Apple, Analytical Chemistry Division.

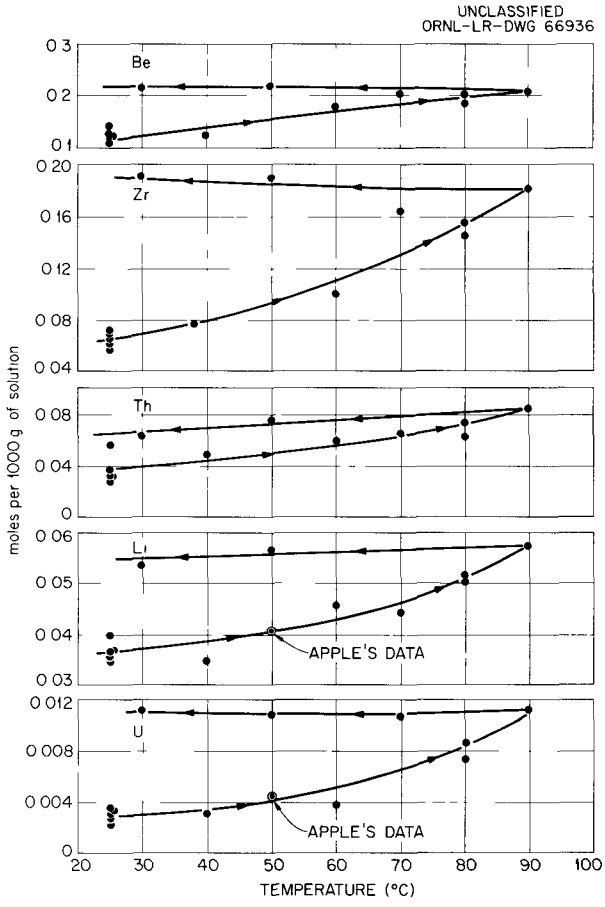

Fig. 4.4. Effect of Temperature on Dissolution of MSRE Solid Fuel in H_2O.

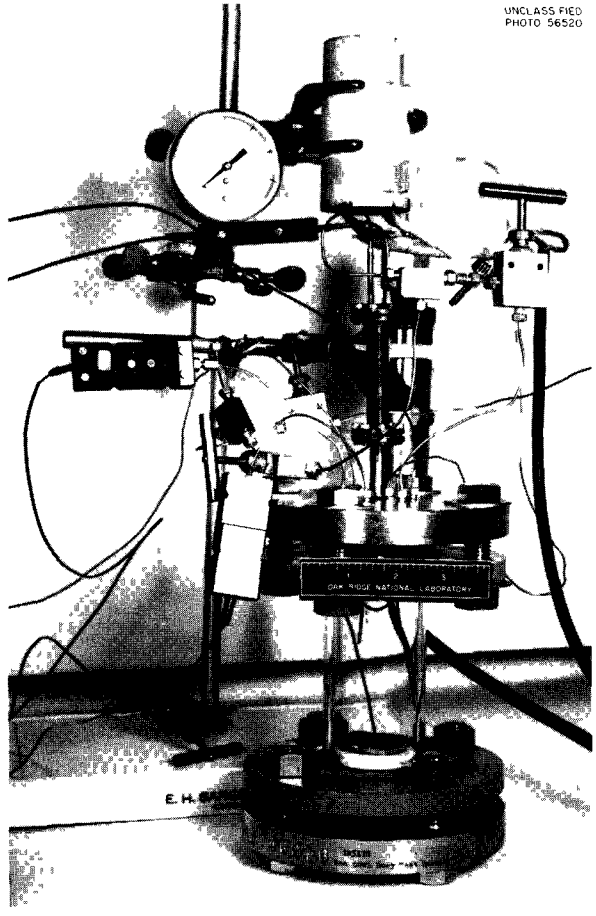

Fig. 4.5. Salt Jet Apparatus.

INTERACTION OF MOLTEN FLUORIDES WITH WATER

The apparatus of Fig. 4.5 was constructed to observe the effect, on a laboratory scale, of injecting molten salt into water. Fuel salt is loaded into the upper chamber ($\frac{1}{2}$-in.-diam, 3-in.-long flanged Hastelloy tube). The small furnace mounted around the containment vessel is brought to the desired temperature. The molten fuel salt is then jetted by helium pressure into water contained in the inverted nickel cone in the lower assembly, or water chamber (2-in.-diam, 6-in.-long Pyrex pipe). Pressure buildup and temperatures at selected points may be followed as a function of time by means of a high-speed potentiometric recorder. Data from a test experiment are shown in Fig. 4.6.

Empirical tests were considered desirable, since the rate of heat released by the salt under these conditions was impractical to calculate. If a large burst of superheated steam were released into the reactor vessel, a safe pressure might be exceeded despite the fact that for the total quantities of heat involved the equilibrium heat balance would result in a safe pressure in the vessel. Tests are being conducted with various ratios of salt to water and of volume heated to total heat available.

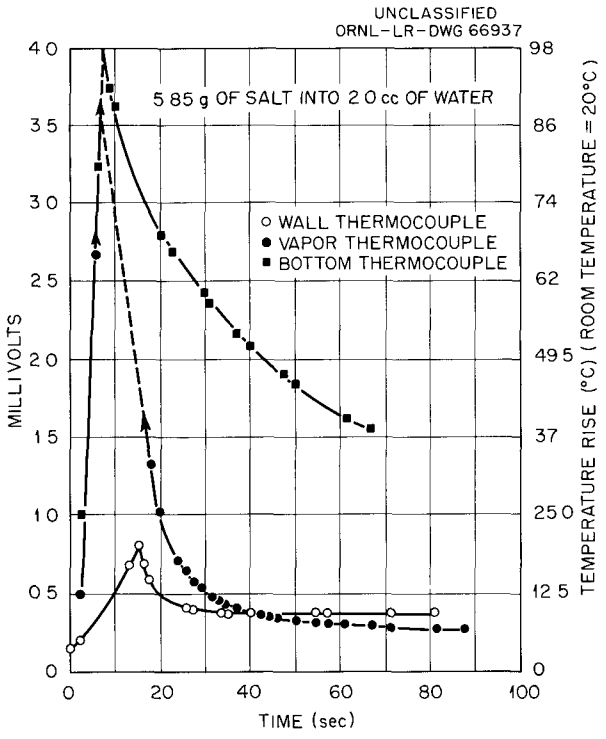

Fig. 4.6. Temperature Rise in Water Chamber with the Introduction of Molten Salt.

VOLATILIZATION OF IODINE FROM THE MSRE

If much fission-produced iodine is volatilized from the molten-salt reactor, it, being very radioactive, must be kept from contaminating the atmosphere. This would require removing the iodine from the inert-gas stream swept through the reactor; various methods for this have been reported.[4] No volatile iodine was found in the Aircraft Reactor Experiment,[5] but the test may not have been sufficiently exhaustive.

Since the molten fuel is in equilibrium with the chromium alloy INOR-8, there will be some U^{3+} present. This U^{3+} can reduce elemental iodine to iodide. Accordingly, any iodine volatilized into the reactor gas stream is expected to be in the form, not of free iodine, but rather of an iodide, probably BeI_2 or BeIF.[6,7] Even in the worst situation, in which BeIF might be formed, the volatility of iodide would not be serious. Assuming the applicability of Raoult's law, a 1% burnup of a fuel containing 1 mole % UF_4 would result in a pressure of approximately 10^{-6} mm Hg at reactor temperature (662°C).[8]

A different problem would be the accidental release of molten fuel into the air. Sufficient oxygen would then be available to oxidize both the U^{3+} and the I^-; therefore free iodine might be volatilized.

---

[4] L. Silverman *et al.*, *Iodine Collection Studies*, TID-7593, pp 322–43 (1961).

[5] W. B. Cottrell *et al.*, *Disassembly and Post-operative Examination of the Aircraft Reactor Experiment*, ORNL-1868, p 39 (1959).

[6] F. F. Blankenship, B. J. Sturm, and R. F. Newton, *Predictions Concerning Volatilization of Free Iodine from the MSRE*, ORNL MSR-60-4 (Sept. 29, 1960).

[7] *MSRP Progr. Rept. Aug. 31, 1961*, ORNL-3215, pp 126–27.

[8] B. J. Sturm, *Calculated Vapor Pressure of Iodide from MSRE Fuel*, ORNL MSR-60-6 (Oct. 11, 1960).

5. Physical Chemistry of Molten-Salt Systems

FREEZING-POINT DEPRESSIONS IN SODIUM FLUORIDE AND LITHIUM FLUORIDE

S. Cantor W. T. Ward
G. D. Robbins[1]

This study is part of a comprehensive investigation which seeks to relate the effects of structural parameters of the components, such as radius, charge, and polarizability, to the thermodynamic properties of fused fluoride solutions. The approach used in this study has been to investigate a conveniently determined thermodynamic property of a solvent, in which type and concentration of solute can be systematically altered, and then to relate variations in this property to structural parameters of the pure solutes. The object of the researches described here was to measure the depressions of freezing points in two solvents, NaF and LiF, and correlate the derived thermodynamic information with the structure of the solutes. Studies dealing with the effects of divalent and tetravalent fluoride solutes on NaF have been previously reported.[2,3]

Trivalent Fluorides in NaF

When several trivalent fluorides, in concentrations up to about 15 mole %, were dissolved in NaF, the freezing-point lowerings were all greater than would be consistent with ideal-solution behavior. For the same solute concentrations, the smaller the radius of the solute cation, the lower the freezing point of NaF. Most of the results are shown in Fig. 5.1. The curves converge in the lower solute-concentration range.

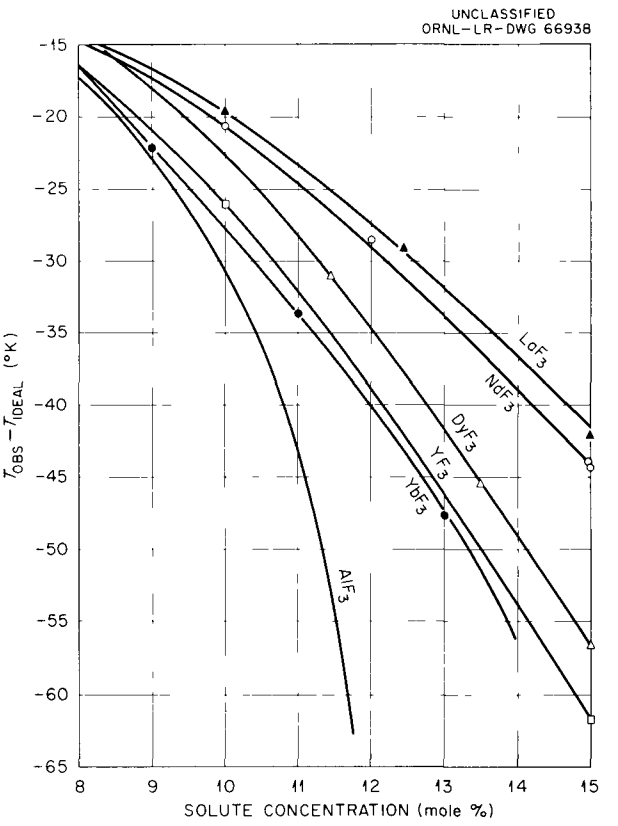

Fig. 5.1. Deviation from Ideal Freezing-Point Depressions by Trivalent Metal Fluorides in NaF.

The curve for AlF_3 was derived from the data of Grjotheim.[4] Although some lists of ionic radii show Y^{3+} smaller than Yb^{3+}, the radius of the Yb^{3+} ion is probably less than that of Y^{3+} in an environment of fluoride ions, since in the isostructural trifluoride crystals, YF_3 has the larger

[1] Summer employee, 1961, now at University of North Carolina, Chapel Hill.

[2] S. Cantor, *J. Phys. Chem.* 65, 2208 (1961).

[3] S. Cantor, *Reactor Chem. Div. Ann. Progr. Rept. Jan. 31, 1961*, ORNL-3127, p 20.

[4] K. Grjotheim, *Norske Videnskas Selskabs Skrifter* No. 5 (1956).

cell volume.[5] As yet a quantitative relationship has not been discovered between the partial molal free energy of mixing of NaF with trivalent fluoride solutes and *simple* functions of the ionic radii or interionic distances of these solutes.

Alkali Fluorides in NaF

Solutions of LiF in NaF are ideal up to concentrations of about 11 mole % LiF and show negative deviations from ideality at higher concentrations. However (see Fig. 5.2), positive deviations from ideality are observed at all concentrations when CsF is the solute. Freezing-point curves for solutions of KF and of RbF in NaF show positive deviations from ideality above 7 mole % of solute and are virtually identical to near 20 mole %; solutions of RbF show larger deviations than those of KF at the highest concentration.

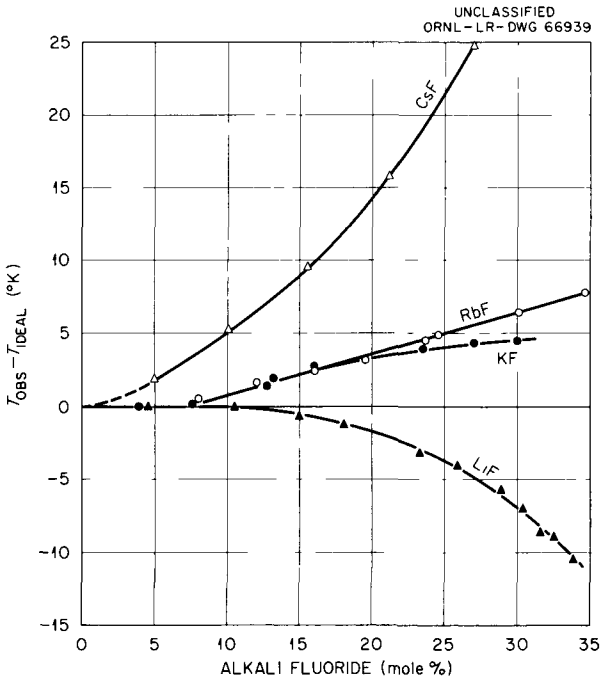

Fig. 5.2. Deviation from Ideal Freezing-Point Depressions by Alkali Fluorides in NaF.

Simple theoretical models[6,7] consider purely coulombic forces and predict negative deviations from ideality for the mixtures; in addition to these, another type of interaction must be considered to rationalize the data of Fig. 5.2. Lumsden[8] and Blander[9] have recently shown that London dispersion forces between next-nearest neighbors may be significant in ionic melts. These London forces qualitatively help to explain the positive deviations, since when an alkali fluoride with a large polarizable cation is dissolved in an alkali fluoride with a small nonpolarizable cation the net change in dispersion energy will be positive. In the solutions under study these positive dispersion ion energies will fall in the order CsF > RbF > KF, which happens to be the order observed for partial molal free energies of mixing of NaF with CsF, RbF, and KF as solutes.

Although a more detailed understanding of the NaF liquidus curves may be possible from considerations of the interatomic forces, the results may also be correlated empirically in terms of ion size and charge effects. The greater the *difference* between Na^+ and the solute cation in their charge-to-size ratios, the greater the deviation from ideality; where the charge-to-size ratio of the solute cation is less than that of Na^+, the deviations are positive; where greater, the deviations are negative. This empirical rule is consistent with the results obtained with all uni-, di-, and trivalent fluoride solutes that were dissolved in NaF. Tetravalent fluoride solutes follow the rule only partially. As shown in a previous report,[3] they cause the largest negative deviations from ideality, but within the family the expected order is reversed; the freezing-point lowering follows the order $ThF_4 > UF_4 > HfF_4 = ZrF_4$.

Alkali Fluorides in LiF

Simple theory[6,7] predicts that the alkali fluoride solutes would cause the LiF freezing-point curve to display negative deviations from ideality, and

[5] A. Zalkin and D. H. Templeton, *J. Am. Chem. Soc.* 75, 2453 (1953).

[6] T. Førland, *On the Properties of Some Mixtures of Fused Salts*, N. T. H. Trykk, Trondheim, Norway (1958).

[7] M. Blander, *J. Chem. Phys.* 34, 697 (1961).

[8] J. Lumsden, *Discussions Faraday Soc.* No. 32 (1961).

[9] M. Blander, to be published in *Journal of Chemical Physics*.

that these deviations would be greater for CsF solutes than for RbF solutes and so on. However, interactions involving changes in London dispersion forces, as discussed in the previous section, might be important in altering the expected order.

The results, shown in Fig. 5.3, are as expected, except for CsF. The smaller negative deviation in the case of CsF solute is most probably a consequence of the change of its next-nearest-neighbor London dispersion energy.

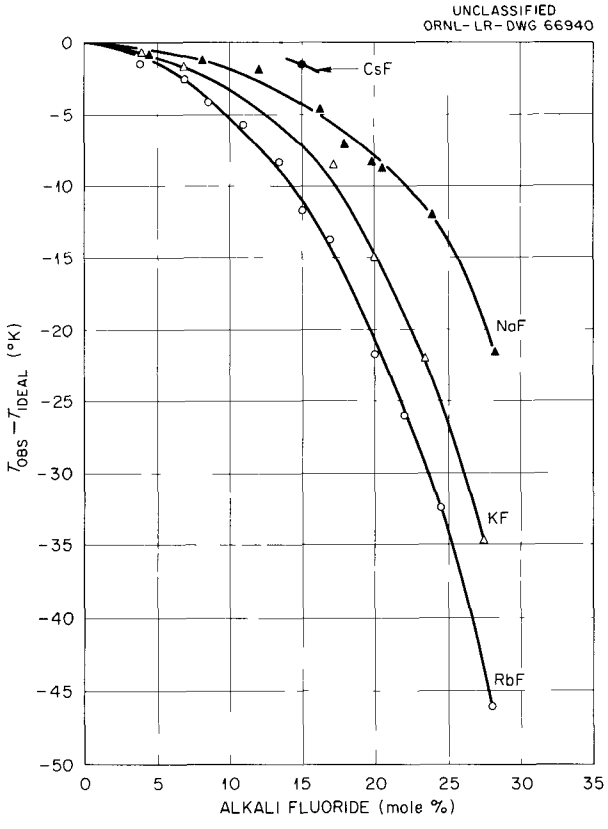

Fig. 5.3. Deviation from Ideal Freezing-Point Depressions by Alkali Fluorides in LiF.

The relative roles of coulombic and London dispersion forces help to explain why the deviations are negative in LiF while in NaF the same compounds result in positive deviations. The coulombic forces, which are roughly proportional to the difference of the cation radii of the solution components, are considerably greater in LiF than in NaF because the ionic radius of Li^+ is smaller than that of Na^+ by 0.3 A. Since Li^+ and Na^+ are both relatively small unpolarizable cations, the London-force interactions for solutions containing KF, RbF, or CsF are about the same when the solvent is LiF or NaF. Apparently the coulombic-force contribution is sufficiently greater in LiF to result in negative deviations.

NaF-LiF Liquidus

Measurements of the liquidus temperatures for the system LiF-NaF were extended to cover the entire concentration range. These measurements, which were of the precision of ±1°C, permitted the evaluation of partial molal excess free energies of mixing for each component to a precision of ±8 cal. These free energies (see Fig. 5.4) were found to be (1) negative in sign, (2) asymmetric with composition, and (3) otherwise inconsistent with regular solution behavior. Properties (2) and (3) are in disagreement with a recent theory of thermodynamic properties of ionic melts.[8]

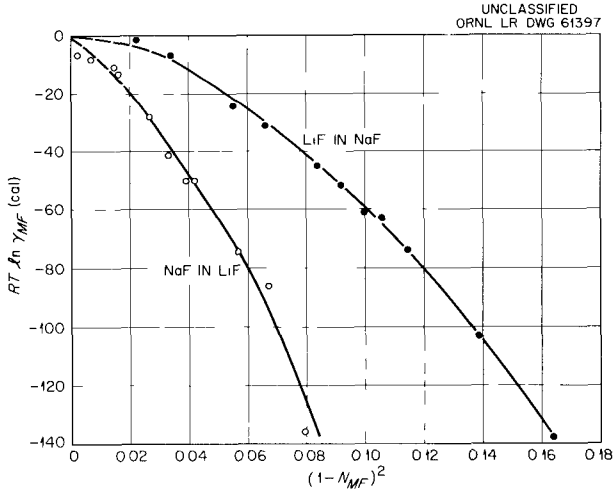

Fig. 5.4. Asymmetry in the Partial Molal Excess Free Energy of Mixing in the LiF-NaF System.

An empirical equation of the form $\Delta F^E = n_1 N_2 (a + bN_1)$ was used to rationalize the data. (ΔF^E = total excess free energy of mixing, n_1 is the number of moles of LiF, N_1 and N_2 are the mole fractions of LiF and NaF respectively, and a and b are constants with the dimensions of calories.) The excess partial molal free energies of mixing

of LiF and NaF respectively are then given by the equations

$$\frac{\partial \Delta F^E}{\partial n_1} = aN_2^2 + 2bN_1N_2^2 ; \qquad (1)$$

$$\frac{\partial \Delta F^E}{\partial n_2} = aN_1^2 + bN_1^2(N_1 - N_2) . \qquad (2)$$

The observed asymmetry in the partial free energies is accounted for in the second term in each of the above equations. The constants, a b, were evaluated when the experimental partial free energies and mole fractions were substituted in Eq. (1) ($a = -820$ cal, $b = -310$ cal). These constants were then used to calculate the free energies of NaF from Eq. (2). Up to concentrations of 50 mole % LiF the calculated values agreed within ±8 cal with the experimentally derived partial molal free energies of mixing. At higher concentrations of LiF (from 50 to 60 mole %) the calculated values diverged markedly from the experimental quantities.

The constant a is believed to reflect changes, on mixing, of coulombic and London dispersion forces between the cations, and the polarizability of the anion. The asymmetry constant b is believed to reflect changes in the interactions of third-nearest neighbors.

CALCULATION OF DENSITIES OF FLUORIDES

S. Cantor

Calculation of the Density of Solid Complex Metallic Fluorides

Densities obtained by Archimedean and dilatometric techniques are most frequently used to determine the number of molecules per unit cell in an x-ray structure analysis. However, these densities may include effects of porosity and impurities. For the solid complex metallic fluorides, an attempt was made to predict densities which would be just as useful as measured densities for deducing the "ideal" or x-ray density.

From a theoretical standpoint, metallic fluorides are relatively simple solids in which the cohesive forces are primarily coulombic and in which the ions are essentially close-packed. Therefore the density of the more complex fluorides may be estimated by assuming that the molar volume is an additive function of simpler volumes which also are ionically bonded and close-packed. The simpler volumes chosen are those of the component fluorides. For instance the estimated molar volume of K_2ThF_6 is the sum of two KF and one ThF_4 molar volumes.

The x-ray data on complex fluorides,[10-15] in which one of the simpler components was an alkali fluoride, were used to test the method of prediction. From a total of 45 compounds the average deviation between x-ray density and calculated density was 5.5%. The molar volumes of the simpler fluorides used in the calculations came from x-ray data.[16-21]

This method has been applied to compounds currently under investigation and whose unit-cell volume has been determined. Table 5.1 shows how closely the estimated densities compare with some possible densities. It is clear that the estimates facilitated the choice of the number of molecules per unit cell.

Estimation of Densities of Molten Fluorides

The purpose of this study was to develop a more useful means of estimating densities of fluoride mixtures, especially those which may be important as circulating fluids in nuclear reactors. Cohen

---

[10] W. H. Zachariasen, *J. Am. Chem. Soc.* **70**, 2147 (1948).

[11] K. Knox, *Acta Cryst.* **14**, 583 (1961).

[12] L. A. Harris, G. D. White, and R. E. Thoma, *J. Phys. Chem.* **63**, 1974 (1959).

[13] L. A. Harris, *Acta Cryst.* **13**, 502 (1960).

[14] P. A. Agron and R. D. Ellison, *J. Phys. Chem.* **63**, 2076 (1959).

[15] F. Hund, *Z. anorg. Chem.* **261**, 106 (1950).

[16] R. G. Wyckoff, *Crystal Structures*, vol 1, Interscience, New York (1948).

[17] E. S. Makarov, *Crystal Chemistry of Simple Compounds of Uranium, Thorium, Plutonium, and Neptunium*, Consultants Bureau (1959).

[18] A. Zalkin and D. H. Templeton, *J. Am. Chem. Soc.* **75**, 2453 (1953).

[19] R. D. Burbank and F. N. Bensey, Jr., *The Crystal Structure of ZrF_4*, K-1280 (Oct. 31, 1956); R. D. Burbank, *The Crystal Structure of UF_4*, K-769 (June 6, 1951).

[20] W. H. Baur, *Acta Cryst.* **11**, 488 (1951).

[21] K. H. Jack and R. Maitland, *Proc. Chem. Soc.* 1957, p 232.

Table 5.1. Densities of Compounds Whose Structures Are Under Investigation

Compound	Density (g/cc)		Molecules per Unit Cell[a]	Deviation (%)
	Calculated	X-Ray		
$LiRbF_2$	3.56	3.40	4	+4.71
		2.55	3	
		4.25	5	
$LiCsF_2$	4.19	4.15	8	+0.95
		3.11	6	
		5.19	10	
Li_6BeZrF_{12}	3.19	3.06	8	+4.25
		2.28	6	
		3.81	10	
α-$NaYF_4$	4.31	4.33	1½	−0.46
		2.88	1	
		5.77	2	
Orthorhombic K_3UF_7	3.80	4.11	2	−7.54
		2.05	1	
		6.16	3	

[a]Number of molecules per unit cell assumed in determining the x-ray densities shown.

and Jones[22] first developed a method of estimation after measurements had been made on 15 mixtures. When applied to the larger body of data now available[23–27] (see Table 5.2), their predicted densities varied greatly from the measured values (e.g., for MSRE fuel, of nominal composition, 70-23-5-1-1 mole % LiF-BeF_2-ZrF_4-ThF_4-UF_4, the predicted values are 15% higher than those observed[27]). A method for estimating densities of fluoride systems has recently been developed[28] by assuming additivity of ionic volumes and assuming that the volume contributions of polyvalent fluorides are due solely to their fluoride ions. When this method was tested against all the measured (or interpolated) values at 800°C, relatively good agreement was obtained, the average deviation being about 4%. However, for most mixtures that were reported to have low concentrations of UF_4 (the most important mixtures as far as reactor fuels are concerned), the calculated values are 6% lower.

For many fused-salt mixtures, the molar volumes of the mixture are, to a very good approximation, a linear function of mole fraction and molar volume of the pure components; that is,

$$V_{\text{mixture}} = N_1 V_1 + N_2 V_2 \cdots + N_m V_n , \quad (3)$$

where V is volume, N is mole fraction, and the subscript numbers refer to components. Recent publication[29] of the molar volumes of liquid UF_4 and ThF_4 facilitate testing whether Eq. (3) is

[22]S. I. Cohen and T. N. Jones, *A Summary of Density Measurements on Molten Fluoride Mixtures and a Correlation for Predicting Densities of Fluoride Mixtures*, ORNL-1702 (July 19, 1954).

[23]B. C. Blanke *et al.*, Mound Laboratory MLM-1076 (April 1956).

[24]B. C. Blanke *et al.*, Mound Laboratory MLM-1086 (December 1956).

[25]B. C. Blanke, Mound Laboratory CF 55-11-14, p 22 (1955).

[26]S. I. Cohen *et al.*, *A Physical Property Summary for ANP Fluoride Mixtures*, ORNL-2150 (Aug. 23, 1956).

[27]S. S. Kirslis, *MSR Progr. Rept. Aug. 1, 1960, to Feb. 28, 1961*, ORNL-3122, p 122.

[28]P. B. Bien, S. Cantor, and F. F. Blankenship, *Reactor Chem. Div. Ann. Progr. Rept. Jan. 31, 1961*, ORNL-3127, p 24.

[29]A. D. Kirshenbaum and J. A. Cahill, *J. Inorg. & Nuclear Chem.* 19, 65 (1961).

Table 5.2. Density Data of Fluoride Mixtures

Components	No. of Mixtures Measured	Stated Precision of Measurement	Reference No.
LiF, BeF_2, UF_4	15 binary 43 ternary	1%	24
NaF, BeF_2, UF_4	13 binary 70 ternary	0.32%	23
LiF, NaF, BeF_2, UF_4	4 ternary 1 quarternary	Unstated	25
LiF, NaF, KF, RbF, UF_4, ZrF_4	4 binary 6 ternary 5 quaternary	5%	26
LiF-BeF_2-ZrF_4-UF_4-ThF_4, 70-23-5-1-1 mole %	1 quinary	~0.4%	27

a good representation of the data. The molar volumes of the liquid alkali fluorides[30] are known over a long temperature range, but the molar volume of BeF_2 has been measured at only 800°C.[31] The values of $V_{mixture}$ were computed for 600 and 800°C by Eq. (3) for all mixtures listed in Table 5.2 that did not contain ZrF_4. The molar volumes of the liquid alkali fluorides, UF_4, and ThF_4 were obtained by extrapolation, and the molar volume of BeF_2 at 600°C was estimated from the 800°C value by assuming that the cubic coefficient of expansion was 0.0045 cc/°C (the approximate average for the measured cubic coefficient of expansion for mixtures containing BeF_2). The average deviation of the calculated molar volumes from the experimental values was 3%. However, for those mixtures which had UF_4 concentrations of 1 to 8 mole %, the average deviation was 5%. The molar volume of liquid ZrF_4 was calculated by using the measured molar volume of the 50-50 mole % NaF-ZrF_4 mixture as the left-hand side of Eq. (3) and solving for V_{ZrF_4}, which when used for mixtures containing ZrF_4, gave an average deviation of 3.5%.

To decrease the percentage deviations – that is, to effect a better fit of Eq. (3) to the experimental values – some of the molar volumes of the pure components were changed. These empirical or pseudo molar volumes are listed in Table 5.3. Using these volumes the average deviation of the calculated from the observed molar volumes is 2%. Only for 12 mixtures are the deviations greater than 3%, and none is higher than 8%.

Table 5.3. Empirical Molar Volumes of Fluorides

	Molar Volume (cc/mole)	
	At 600°C	At 800°C
LiF	14.0	14.7
NaF	19.37[a]	20.43[a]
KF	27.95[a]	29.87[a]
RbF	33.84[a]	36.06[a]
BeF_2	23.6	24.4
ZrF_4	46	49
ThF_4	47.8[a]	49.0[a]
UF_4 present as 1–8 mole %	58	60
UF_4 present as 8–100 mole %	48	50

[a]Volumes extrapolated from literature values.

[30]F. M. Jaeger, *Z. anorg. u. allgem. Chem.* **101**, 177–78 (1917).

[31]J. D. MacKenzie, *J. Chem. Phys.* **32**, 1150 (1960).

It is obvious that any estimation of density is based on the assumption that the measured values are accurate for the *compositions as listed*. The difficulty in preventing the removal of some of the UF_4 from solution by precipitation of UO_2 may very well be the reason that it is necessary to have two empirical molar volumes of UF_4 to get a good agreement of calculated and "observed" values. In the absence of more information on the purity of the mixtures, it is probable that the experimental densities are in error by much more than the precisions stated in Table 5.2, with the exception of the 5% assigned by Cohen *et al.*[26] Nonetheless, the true densities of fluoride mixtures containing any concentration of the components of Table 5.2 can be safely estimated (probably to within 3%) by substituting the values of Table 5.3 in Eq. (3).

MOLAR ENTHALPIES OF MIXING IN THE LIQUID LiF-KF SYSTEM

R. A. Gilbert[32]

Kleppa *et al.*[33] have recently shown experimentally that the enthalpies of mixing in molten binary alkali nitrate systems are all negative and that the molar mixing enthalpy (ΔH^M) increases in regular fashion with increasing difference in size between the participating cations. His maximum ΔH^M (approximately -700 cal/mole) therefore appeared in the $LiNO_3$-$RbNO_3$ system (the system $LiNO_3$-$CsNO_3$ was not measured). Unfortunately, limitations in his calorimeter would not permit Kleppa to extend his measurements to temperatures required to study molten alkali halides. Blander,[34] however, has predicted that the enthalpies of mixing should be considerably greater in the halide systems; they might, accordingly, be determinable with good precision, even though necessarily as the difference of two large numbers, with the Bunsen ice calorimeter.

Samples of pure KF, LiF, and mixtures of these were sealed in capsules of Nichrome V which were machined from a single bar and adjusted to identical weights. The salt transfers and the sealing by welding were accomplished in inert-atmosphere boxes. The pressure of high-purity helium in the capsules after sealing was 1 atm. The sample capsules and an identical capsule filled only with helium were individually heated to 874.0°C and then dropped into the calorimeter. From the data thus obtained the enthalpy changes from this temperature to 0°C were determined for the mixture and the pure compounds.

The measured enthalpy values for the mixtures were compared with calculated values based on the enthalpies of the pure components and on the assumption that there were no heat effects on mixing; the differences, which were negative in each case, are shown in Table 5.4, as are the enthalpies of mixing. The latter are also plotted in Fig. 5.5 versus mole fraction LiF.

[32] Chemistry Division.

[33] O. J. Kleppa, *J. Phys. Chem.* **64**, 1937 (1960); O. J. Kleppa and L. S. Hersh, *J. Chem. Phys.* **34**, 351 (1961).

[34] M. Blander, private communication, 1961.

Table 5.4. Molar Enthalpies of Mixing of LiF and KF at 874.0°C

Composition X_{LiF}	ΔH (cal)			Total Moles	ΔH^M (cal/mole)
	Measured	Calculated[a]	Difference		
0.193	3420	3551	−131	0.1921	−682
0.385	3937	4187	−250	0.2280	−1096
0.593	4404	4705	−302	0.2600	−1162
0.747	5682	5993	−312	0.3340	−934

[a] From the values for pure compounds: $\Delta H_{LiF} = -17{,}700$ cal/mole [T. B. Douglas and J. L. Dever, *J. Am. Chem. Soc.* **76**, 4826 (1954) give −17,630 cal/mole, a difference of +0.4%]; $\Delta H_{KF} = -18{,}680$ cal/mole [V. S. Lyaehenko, *Metallurg.(U.S.S.R.)***10**, 85 (1935) gives −18,330 cal/mole, a difference of +1.9%].

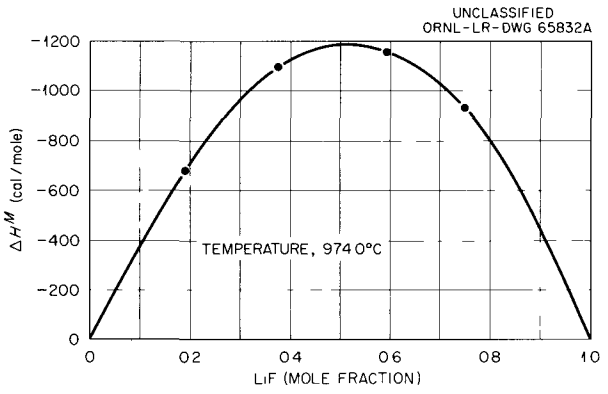

Fig. 5.5. Molar Enthalpies of Mixing in Liquid LiF-KF Mixtures.

It appears that enthalpies of mixing in these systems are sufficiently large for determination by this procedure. An analysis of the data, as suggested by Kleppa, by plotting $\Delta H^M/X(1 - X)$ against X, where X is the mole fraction of one component, can be attempted, but additional data will be required before a satisfactory estimate can be made of the difference in the limiting heats of solution.

BEHAVIOR OF SOME TRANSITION-METAL FLUORIDES IN MOLTEN FLUORIDE MIXTURES

C. M. Blood
F. F. Blankenship
W. R. Grimes
G. M. Watson

For reactions such as

$$NiF_2 + H_2 \rightleftharpoons 2HF + Ni \qquad (A)$$

at elevated temperature with H_2 and HF as gases, with the NiF_2 in unsaturated solution in a molten fluoride mixture, and with crystalline nickel present in large excess, the true equilibrium constant, K_a, and an experimentally determinable equilibrium constant, K_N, are given by

$$K_a = \frac{f_{HF}^2}{(f_{H_2})(a_{NiF_2})} = \frac{f_{HF}^2}{(f_{H_2})(N_{NiF_2})(\gamma_{NiF_2})} \qquad (4)$$

and

$$K_N = \frac{p_{HF}^2}{(p_{H_2})(N_{NiF_2})} , \qquad (5)$$

where f, a, p, N, and γ indicate, respectively, fugacity, activity, partial pressure, mole fraction, and activity coefficient, and where, given a consistent choice of reference states,

$$-\Delta F^0 = RT \ln K_a . \qquad (6)$$

Careful measurements of K_N for this reaction in several molten mixtures of NaF with ZrF_4 and in a single LiF-BeF_2 mixture have been performed.[35] Equilibration at elevated temperature was accomplished, in nickel equipment, by continuous sparging of a melt for many days with a mixture of HF and H_2 of known concentration. Concentrations of these gases were determined periodically on both inlet and outlet streams. Samples of the melt were drawn periodically through sintered copper filters, and the NiF_2 concentration of the melt was determined by chemical analysis. The system was considered at equilibrium when the NiF_2 content remained constant for three successive days at constant temperature and inlet-gas composition. Between experiments the NiF_2 concentration was adjusted as required by addition of this compound, by reduction of excess NiF_2 by increasing the H_2 concentration of the gas stream, or by reaction of the HF-H_2 mixture with the container. Equilibrium concentrations were routinely established by approach from the NiF_2-rich and NiF_2-deficient directions.

Careful measurements of K_N for the reaction in each solvent studied showed the values to vary with temperature and with the solvent composition but to be independent of NiF_2 concentration within each system. A typical plot of K_N vs N_{NiF_2} is shown as Fig. 5.6.[35] This constancy of K_N with N_{NiF_2} has been demonstrated in several solvent systems to be valid over the entire concentration range studied – that is, from less than 5% to more than 95% of the solubility at saturation. From inspection of Eqs. (4) and (5), and remembering that (at high temperatures and low partial pressures) pressure and fugacity are equivalent for these gases, it is clear that the activity coefficient γ_{NiF_2} is independent of NiF_2 concentration in all these solutions.

[35] C. M. Blood, *Solubility and Stability of Structural Metal Difluorides in Molten Fluoride Mixtures*, ORNL CF-61-5-4 (Sept. 21, 1961).

UNCLASSIFIED
ORNL-LR-DWG 58532

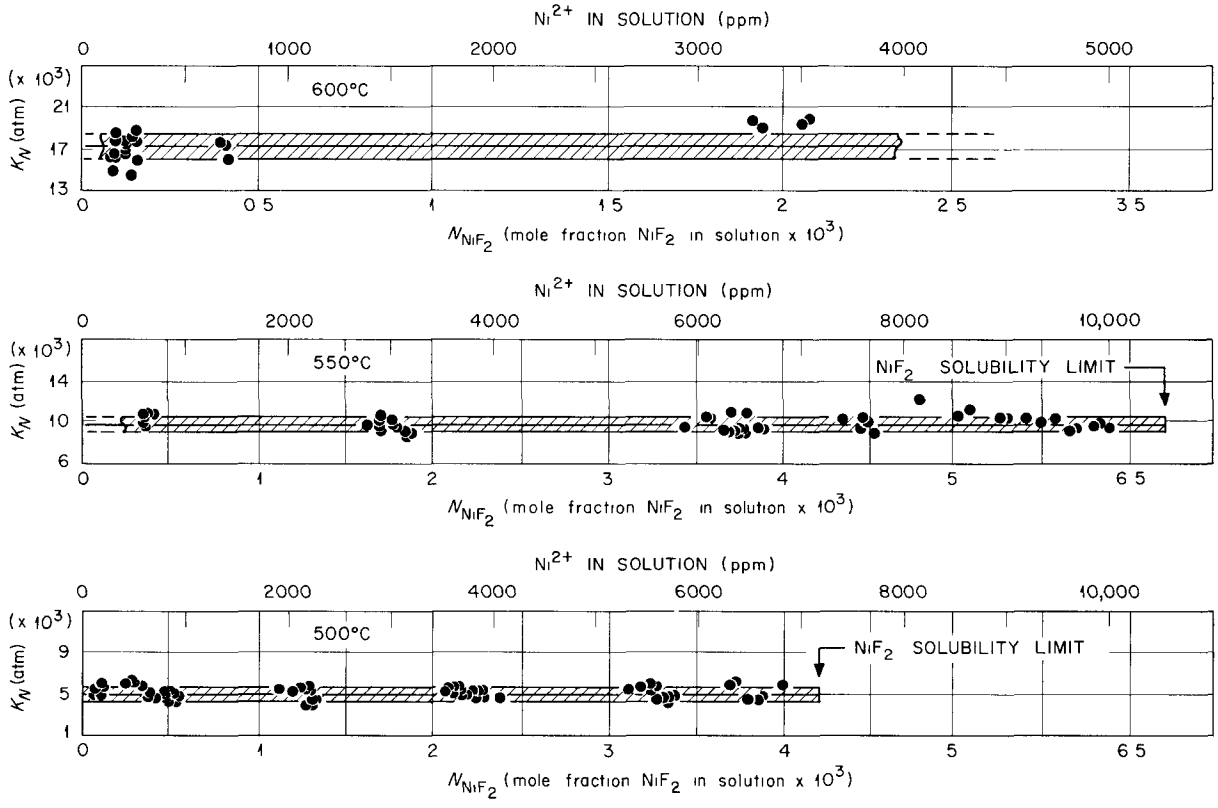

Fig. 5.6. Equilibrium Quotients for the Reduction by Hydrogen of NiF_2 in LiF-BeF_2 (62 mole % LiF).

Among the solvents studied, the LiF-BeF_2 mixture with 62 mole % BeF_2 is unique in that pure NiF_2 is the phase in equilibrium with its saturated solutions. Accordingly, for that solvent system activity coefficients with crystalline solid as reference state, $\gamma_{NiF_{2(c)}}$, are immediately available from solubility data. Clearly, in saturated solutions within this system at any given temperature

$$\gamma_{NiF_{2(c)}} = 1/N^{*}_{NiF_2}, \qquad (7)$$

where $N^{*}_{NiF_2}$ is the concentration (in mole fraction) of the saturated solution at that temperature. Since the activity coefficient has been shown (Fig. 5.6) to be independent of NiF_2 concentration, the $\gamma_{NiF_{2(c)}}$ values from Eq. (7) may be taken as valid for the unsaturated solutions.

Combination of appropriate values of $\gamma_{NiF_{2(c)}}$ with values of K_N in the LiF-BeF_2 system determines $K_{a(c)}$ and $\Delta F^0_{(c)}$ for the reaction

$$NiF_{2(c)} + H_{2(g)} \rightleftharpoons 2HF_{(g)} + Ni_{(c)} \qquad (B)$$

for each temperature for which data are available. These data and the calculated $K_{a(c)}$ and $\Delta F^0_{(c)}$ values are shown in Table 5.5. Insertion of appropriate values of $\Delta F^0_{(c)}$ with pertinent thermodynamic data (either available or capable of reliable estimation) into the equation

$$\frac{\Delta(F^0_T - H^0_0)}{T} = \frac{1}{T}\left[\Delta(H^0_{298} - H^0_0) + \int_{298}^{T} \Delta C_p\, dT\right] - \left[S^0_{298} + \int_{298}^{T} \frac{\Delta C_p}{T}\, dT\right] \qquad (8)$$

yields values of 26.304, 26.251, and 26.271 kcal/mole for ΔH_0^0 for reaction (*B*) at 773, 823, and 873°K. The mean value is 26.275 ± 0.02 kcal/mole. This leads to a value of 26.777 as $\Delta H_{298.16}^0$ for reaction (*B*). Further, and obvious, third-law treatment of the system permits evaluation of $\Delta F_{(c)}^0$ at other temperatures and permits calculation of $\Delta F_{(l)}^0$ and $K_{a(l)}$ values for the reaction

$$NiF_{2(l)} + H_{2(g)} \rightleftharpoons 2HF_{(g)} + Ni_{(c)} \qquad (C)$$

with supercooled liquid NiF_2 as the reference state. Typical values for these thermochemical quantities are shown in Table 5.6. It is then possible to obtain activity coefficients, typical

Table 5.5. Solubility of NiF_2 and Equilibrium Constants for $NiF_2 + H_2 \rightleftharpoons 2HF + Ni$ in $LiF\text{-}BeF_2$ (62 mole % BeF_2)

Temperature (°K)	Solubility[a] of NiF_2 (N_{NiF_2})	$\gamma_{NiF_{2(c)}}$	K_N (atm)	$K_{a(c)}$ (atm)	$\Delta F_{(c)}^0$ (kcal)
	$\times 10^{-3}$		$\times 10^3$		
748	3.49	288			
773	4.23	240	5.04	21.32	-4.699
798	5.15	194			
823	6.18	160	9.90	61.18	-6.727
848	7.33	136			
873	8.59	120	17.3	148.61	-8.675

[a]Values correspond to enthalpy of solution of 9.7 kcal/mole.

Table 5.6. Thermochemical Functions for $NiF_2 + H_{2(g)} \rightleftharpoons 2HF_{(g)} + Ni_{(c)}$

Temperature (°K)	$NiF_{2(c)}$		$NiF_{2(l)}$	
	$\frac{-\Delta(F^0 - H_{298.16}^0)^{(a)}}{T}$ (cal/°K)	ΔF^0 (kcal)	$\frac{-\Delta(F^0 - H_{298.16}^0)^{(b)}}{T}$ (cal/°K)	ΔF^0 (kcal)
298.16	41.377	14.440	40.511	1.600
633	40.949	0.856	38.235	-10.524
773	40.757	-4.728	37.128	-15.021
823	40.680	-6.703	36.750	-16.567
873	40.605	-8.671	36.504	-18.189
1073	40.289	-16.453	35.056	-23.936

[a]$\Delta H_{298.16}^0 = 26.777$ kcal for reaction with $NiF_{2(c)}$.

[b]$\Delta H_{298.16}^0 = 13.679$ kcal for reaction with $NiF_{2(l)}$.

values for which are shown in Table 5.7, for all solvents and all temperatures for which K_N values are available.

The thermochemical data obtained in this study differ appreciably from those derived from the earlier data of Jellinek and Rudat[36] who determined equilibrium partial pressures of H_2 and HF for this reaction with both NiF_2 and nickel as crystalline solids and whose work forms the basis for most of the published estimates[37] of the thermochemical functions for NiF_2. Their data, for example, over the temperature interval 573 to 773°K give 2.099 atm for $K_{a(c)}$ at 773°K and extrapolate to 6.35 and 17.2 atm at 823 and 873°K respectively. These data lead to a value 28.2 kcal/mole for $\Delta H^0_{298.16}$ and to free-energy values about 3.5 kcal less negative than those obtained in this study. It should be noted that the Jellinek and Rudat K_a values in combination with the present observation of constancy of γ_{NiF_2} with N_{NiF_2} lead to predicted solubilities for NiF_2 about tenfold less than experimentally determined in this study and to values considerably in excess of unity for $\gamma_{NiF_{2(l)}}$.

The constancy of activity coefficients with NiF_2 concentration merely indicates that the solutions (even when nearly saturated) are so dilute that the ionic associations within the solvent are not appreciably modified by NiF_2 additions. Crystalline solid NiF_2 clearly is a poor reference state from which to assess properties of such solutions. The variation of $\gamma_{(l)}$ with solvent composition in the NaF-ZrF_4 mixtures suggests that all these solvents are less effective fluoride donors than is (hypothetical) liquid NiF_2 at these temperatures; the discrepancy diminishes as alkali (donor) fluoride concentration is increased and as associations of fluoride ions with the zirconium ions are weakened by increasing temperature. Presumably, $\gamma_{(l)}$ would increase to a maximum and then decrease as the NaF concentration is further increased in this system. It is not possible from the data at a single composition in the LiF-BeF_2 solvent system to specify whether the solvent is a more or a less effective donor than liquid NiF_2.

A similar, though considerably less extensive, study of the behavior of FeF_2 and CrF_2 has been

[36] K. Jellinek and A. Rudat, *Z. anorg. u. allgem. Chem.* **175**, 281 (1928).

[37] See, for example, L. Brewer *et al.*, Paper 6 in *The Chemistry and Metallurgy of Miscellaneous Materials: Thermodynamics*, ed. by L. L. Quill, McGraw-Hill, New York, 1950.

Table 5.7. Activity Coefficients for NiF_2 in Molten Fluorides

Solvent (mole %)	Temperature (°C)	K_N (atm)	$\gamma_{NiF_{2(c)}}$	$\gamma_{NiF_2(l)}$
		$\times 10^3$		
LiF-BeF_2 (62% LiF)	500	5.04	240	0.29
	550	9.90	160	0.39
	600	17.3	120	0.48
NaF-ZrF_4 (60% NaF)	575	19.2	200	0.64
	600	25.9	175	0.72
	625	37.2	166	0.91
NaF-ZrF_4 (53% NaF)	550	7.57	125	0.30
	575	11.0	115	0.36
	600	15.3	103	0.43
	625	21.9	98	0.54
NaF-ZrF_4 (43% NaF)	600	4.55	31	0.13

performed.[35] Although the data are not sufficient to permit so rigorous a treatment, the behavior of these materials, which is qualitatively quite similar to that of NiF_2, suggests very similar conclusions.

THEORY OF MOLTEN SALTS

M. Blander R. C. Bansal[39]
D. L. Manning[38] J. Braunstein[39]
R. M. Lindgren[39]

Reciprocal Systems

A continuation of experimental and theoretical studies of molten-salt systems containing at least two *cations* (A^+ and B^+) and two *anions*[40] (C^- and D^-) was made at concentrations of two of the ions (A^+ and C^-) which were low enough so that their most important associated species were AC, AC_2^-, and A_2C^+ for which the thermodynamic association constants K_1, K_2, and K_{12} could be evaluated.

Association Constants in the System $AgNO_3$-NaBr-$NaNO_3$ and Their Comparison with the Quasi Lattice Theory.[41] – The thermodynamic association constants K_1, K_2, and K_{12} for the formation of AgBr, $AgBr_2^-$, and Ag_2Br^+ evaluated from electromotive-force measurements in $AgNO_3$-NaBr-$NaNO_3$ mixtures at 402, 438, 460, and 500°C are given in Table 5.8. Comparison of these constants with the relations derived from the calculations based on the quasi-lattice model[42]

$$K_1 = Z(\beta_1 - 1) , \qquad (9)$$

$$K_1 K_2 = \frac{Z(Z-1)}{2!}(\beta_1\beta_2 - 2\beta_1 + 1) , \qquad (10)$$

$$K_1 K_{12} = \frac{Z(Z-1)}{2!}(\beta_1\beta_{12} - 2\beta_1 + 1) , \qquad (11)$$

where $\beta_i = \exp(-\Delta A_i/kT)$ and Z is a coordination number, led to the values of the "specific Helmholtz free energy," ΔA_i, listed in Table 5.8 for $Z = 4$, 5, and 6, which should cover all reasonable values of Z. Within the estimated error in the measurements, the values of ΔA_i do not vary with temperature. This is further confirmation of the theoretical prediction that for associations in which the change of the internal degrees of freedom of the ions involved in the association process is small, Eqs. (9–11) with constant values of ΔA_i and for any reasonable value of Z lead to a prediction of the temperature coefficients of K_1, K_2, and K_{12}.[43–45]

A comparison of the values of ΔA_i (for $Z = 5$) for the associations of Ag^+ and Cl^- and of Ag^+ and Br^- in the two molten solvents $NaNO_3$ and KNO_3 is made in Table 5.9. It is believed likely that a major contribution to the differences between the two solvents is from a "reciprocal Coulomb effect." In the two-dimensional representation in Fig. 5.7 it can be seen that the major change which takes place upon the formation of an AC ion pair is the interchange of nearest-neighbor BC and AD pairs to form AC and BD. Using reasonable values for the ionic radii[46,47] and assuming nearest-neighbor interactions, the values of $RT \ln [K_{1(KNO_3)}/K_{1(NaNO_3)}]$ in column 5 of Table 5.9 were calculated. The relative magnitudes are in the same direction as the measured differences. Although the effect of long-range interactions cannot be assessed easily in terms of a realistic three-dimensional model, calculations of the "reciprocal Coulomb effect" for the infinite one-dimensional chains

$$\ldots \text{BDBDBCBDBD} \ldots + \text{BDBDADBDBD} \ldots \rightleftharpoons \text{BDBDBDBDBD} + \text{BDBDACBDBD} ,$$

[38] Analytical Chemistry Division.

[39] University of Maine, Orono.

[40] A. R. Alvarez-Funes *et al.*, *Reactor Chem. Div. Ann. Progr. Rept. Jan. 31, 1961*, ORNL-3127, p 17.

[41] D. L. Manning *et al.*, to be published in *Journal of the American Chemical Society* (1962). Work done at Oak Ridge National Laboratory and the University of Maine.

[42] M. Blander, *J. Chem. Phys.* 34, 432 (1961).

[43] D. G. Hill, J. Braunstein, and M. Blander, *J. Phys. Chem.* 64, 1038 (1960).

[44] D. G. Hill and M. Blander, *J. Phys. Chem.* 65, 1866 (1961).

[45] A. R. Alvarez-Funes, J. Braunstein, and M. Blander, to be published in *Journal of the American Chemical Society* (1962).

[46] J. A. A. Ketelaar, *Chemical Constitution*, p 28, Elsevier, New York, 1958.

[47] O. J. Kleppa and L. S. Hersh, *J. Chem. Phys.* 35, 765 (1961).

Table 5.8. Values of K_1, K_2, and K_{12} and Derived Values of the "Specific-Bond Free Energy" for Associations of Ag^+ and Br^- in $NaNO_3$

	Temperature (°C)			
	402	438	460	500
K_1	633 ± 5%	500 ± 3%	430 ± 3%	325 ± 4%
K_2	246 ± 20%	180 ± 10%	151 ± 10%	103 ± 20%
K_{12}	280 ± 25%[a]	200 ± 15%	167 ± 15%	120 ± 20%
		$Z = 4$		
ΔA_1	6.79[b]	6.82	6.83	6.74
ΔA_2	6.9	6.8	6.7	6.5
ΔA_{12}	7.0	6.9	6.9	6.7
		$Z = 5$		
ΔA_1	6.51	6.52	6.50	6.43
ΔA_2	6.5	6.4	6.3	6.1
ΔA_{12}	6.6	6.5	6.5	6.3
		$Z = 6$		
ΔA_1	6.27	6.26	6.24	6.16
ΔA_2	6.2	6.1	6.0	5.8
ΔA_{12}	6.3	6.2	6.1	6.0

[a] Calculated from scattered data.
[b] Values of ΔA_i are in kcal/mole.

using a method of calculation described previously,[48] led to the estimated values of $RT \ln [K_{1(KNO_3)}/K_{1(NaNO_3)}]$ listed in column 6 of Table 5.9. These indicate that the long-range interactions are in a direction such as to bring the measured and estimated values closer together. Although this is no proof, it does indicate that at least part of the solvent effect is probably coulombic.

Association Constants of Ag^+ and CN^- in Molten Equimolar $NaNO_3$-KNO_3 Mixtures.[49] – These measurements were undertaken to see what influence changes of internal (including rotational) degrees of freedom of ions involved in the association process would have on the temperature coefficients of the association constants. Because of the very strong associations of Ag^+ and CN^-, measurements down to extremely low concentrations of Ag^+ and CN^- (5×10^{-7} mole fraction) were required, necessitating modifications of

[48] M. Blander, *J. Chem. Phys.* 34, 697 (1961).
[49] D. L. Manning and M. Blander, in preparation.

Table 5.9. Comparison of Average Values of ΔA_1 for the Formation of AgCl and AgBr Ion Pairs in $NaNO_3$ and KNO_3

Ion Pair	Solvent	ΔA_1 for $Z = 5$	$\Delta A_{1(NaNO_3)} - \Delta A_{1(KNO_3)} \simeq RT \ln K_{1(KNO_3)}/K_{1(NaNO_3)}$		
			Measured	Coulombic Calculation	
				Nearest Neighbor	Infinite Chain
Ag^+Cl^-	$NaNO_3$	-4.8_3[a]	1.0_5	2.5_8	1.7_8
	KNO_3	-5.8_8			
Ag^+Br^-	$NaNO_3$	-6.5_0	0.6_4	1.4_1	0.9_7
	KNO_3	-7.1_4			

[a] All values in kcal/mole.

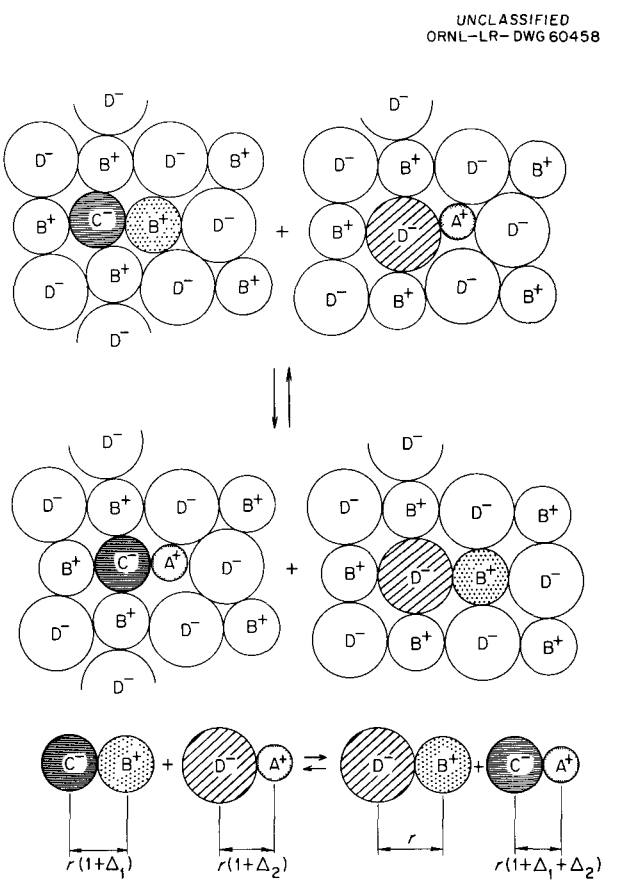

Fig. 5.7. Two-Dimensional Representation of the Reciprocal Coulomb Effect.

previous techniques. The evaluated association constants are listed in Table 5.10, and indicate that associations of Ag^+ and CN^- are the strongest which have been measured in molten salts. The entropies of ion-pair formation $[d(RT \ln K_1)/dT]$ for associations involving the diatomic CN^- (and the polyatomic SO_4^{2-} previously measured[50]) are more positive than for the association of Ag^+ with the monatomic ions Cl^- and Br^- and are larger than the "configurational" contribution to the entropy of association calculated from the quasi-lattice model.

Association of Cadmium Ion with Bromide or Iodide Ions in Molten Equimolar $NaNO_3$-KNO_3 (ref 51) and with Bromide Ions in $LiNO_3$-KNO_3 Mixtures. – Electromotive-force measurements were made in concentration cells with silver–solid silver halide electrodes [Ag/AgX(sat), NaX-KX, $NaNO_3$-KNO_3 | $NaNO_3$-KNO_3, $Cd(NO_3)_2$, NaX-KX, AgX(sat)/Ag] and were used to evaluate the thermodynamic association constants for the formation of CdX^+ and CdX_2 given in Table 5.11. Although the quasi-lattice model applies strictly to systems containing only monovalent ions,

[50] W. J. Watt and M. Blander, *J. Phys. Chem.* **64**, 729 (1961).

[51] J. Braunstein and R. M. Lindgren, to be published in *Journal of the American Chemical Society* (1962). Work done at Oak Ridge National Laboratory and the University of Maine.

Table 5.10. Values of K_1, K_2, and K_{12} and Derived Values on the "Specific-Bond Free Energies" for the Associations of Ag^+ and CN^- in Equimolar $NaNO_3$-KNO_3 Mixtures

	Temperature (°C)		
	246	286	326
K_1	230,000 ± 7%	220,000 ± 7%	190,000 ± 7%
K_2	140,000 ± 20%	105,000 ± 35%	(50,000) ± 50%
K_{12}	80,000 ± 15%	60,000 ± 20%	(36,000) ± 50%
	Z = 4		
$-\Delta A_1$	11.3[a]	12.1	12.8
$-\Delta A_2$	11.8	12.4	(12.4)
$-\Delta A_{12}$	11.2	11.8	(12.0)
	Z = 5		
$-\Delta A_1$	11.1	11.9	12.6
$-\Delta A_2$	11.5	12.1	(12.1)
$-\Delta A_{12}$	10.9	11.5	(11.7)
	Z = 6		
$-\Delta A_1$	10.9	11.7	12.3
$-\Delta A_2$	11.3	11.8	(11.8)
$-\Delta A_{12}$	10.7	11.2	(11.4)

[a] Values of ΔA_i are in kcal/mole.

Table 5.11. Successive Association Constants[a] and Specific Helmholtz Free Energies of Formation[b] of Cadmium Ion–Halide Ion Associations in Molten Equimolar $NaNO_3$-KNO_3 Mixtures

Temperature (°C)	Bromide				Iodide			
	K_1	$-\Delta A_1$	K_2	$-\Delta A_2$	K_1	$-\Delta A_1$	K_2	$-\Delta A_2$
240	1520	5.6_7	680	5.7_3	5330	6.9_4	2200	6.9_4
290					3130	7.0_3	1300	7.0_3
300	990	5.8_3	450	5.9_3				

[a] [moles/mole (Na, K)NO_3]$^{-1}$. The estimated uncertainties are ±5% for K_1 and ±10% for K_2. The association constants on the molality scale are 0.0933 multiplied by the above values.

[b] kcal/mole. The estimated uncertainties are ±0.06 for ΔA_1 and ±0.10 for ΔA_2.

these values of the association constants were compared with Eqs. (9) and (10) derived from the quasi-lattice theory; values of ΔA_1 and ΔA_2 for $Z = 6$ are given in Table 5.11. For the associations with iodide the variations of ΔA_i with temperature are smaller than the experimental uncertainty, and for associations with the bromide the variations of ΔA_i with temperature are only slightly larger than the experimental uncertainty. This indicates that the results of the quasi-lattice model may be useful for predicting the temperature coefficients of the association constants of singly charged ions with multiply charged ions as well as with other singly charged ions.

Thermodynamic association constants were determined potentiometrically for the formation of $CdBr^+$ and $CdBr_2$ at 240°C in five molten mixtures of lithium nitrate and potassium nitrate containing between 26 and 80 mole % lithium nitrate (N_{LiNO_3}); at 170°C the association constants were measured in equimolar lithium nitrate–potassium nitrate. The negative specific Helmholtz free energy of association, $-\Delta A$, increased linearly with the mole fraction of lithium nitrate at 240°C according to the equation $-\Delta A$ (kcal/mole) = 5.80 + $1.05N_{LiNO_3}$ (with an assumed quasi-lattice coordination number of 6) and was the same, within the experimental error, for the stepwise formation of $CdBr^+$ and of $CdBr_2$. The value of ΔA was independent of temperature (-6.30 ± 0.05) in the equimolar mixture and was, surprisingly, 0.5 kcal/mole more negative than ΔA for the formation of $CdBr^+$ determined in equimolar sodium nitrate–potassium nitrate.

Binary Systems with a Common Anion

Excess Free Energies and Heats of Mixing in Certain Molten Salt Mixtures. – Reiss, Katz, and Kleppa[52] have shown that the results of a perturbation theory which is related to conformal solution theory[53] are consistent with certain features of experimental measurements on the heats of mixing of molten alkali nitrates.[54] The calculations were based on the perturbation of the cation radii of a "test salt" and led to a simple expression for the second-order terms. The higher order terms were too complicated to state.

By the choice of particular relative values of the two perturbation parameters, we have simplified the higher terms and obtained the relation for the excess free energy (including terms to the fourth order)

$$\frac{\Delta F^E}{kT} = X_1 X_2 P\delta^2 + X_1 X_2 (X_1 - X_2) Q\delta^3 + [X_1 X_2 R + X_1 X_2 (X_1 - X_2)^2 S]\delta^4 + \ldots , \quad (12)$$

where X_i is the mole fraction of component i; P, Q, R, and S are related to the configurational integral; and $\delta = (\lambda_1 - \lambda_2)/(\lambda_1 + \lambda_2)$, where λ_i is the sum of the radii of the cation and anion of salt i. Similar forms can be obtained for the other excess thermodynamic quantities. Although the parameters P, Q, R, and S have not been evaluated, the third- and fourth-order terms and P, Q, and S have been empirically shown to be important,[53] and P, Q, R, and S can be easily evaluated in terms of a crude one-dimensional model.[47] Although the Reiss theory has been derived for hard sphere ions interacting according to a generalized form of the coulomb potential, Eq. (12) can be derived for more general pair potential functions.

Van der Waals Energy Changes in the Mixing of Molten Salts.[55] – Deviations from ideal-solution behavior of mixtures of $AgNO_3$ (ref 56) or $TlNO_3$ (ref 57) with alkali nitrates have indicated that in addition to the solution effects present in mixtures of alkali nitrates, the energy change due to another type of interaction needs to be postulated to rationalize the observed heats of mixing. Although van der Waals interactions (or London dispersion interactions) are often considered to be of short range, the estimated values in column 2 of Table 5.12 of the contribution of the change of these interactions between *next-nearest-neighbor* cations are relatively large. When these are

[52] H. Reiss, J. Katz, and O. J. Kleppa, *J. Chem. Phys.* 36, 144 (1962).

[53] H. C. Longuet-Higgins, *Proc. Roy. Soc.* A205, 247 (1951).

[54] O. J. Kleppa, *J. Chem. Phys.* 34, 351 (1961).

[55] M. Blander, to be published in *Journal of Chemical Physics* (1962).

[56] O. J. Kleppa and L. S. Hersh, *J. Chem. Phys.* 35, 175 (1961).

[57] O. J. Kleppa and L. S. Hersh, *J. Chem. Phys.* 36, 544 (1962).

Table 5.12. Calculated Values of ΔU_T Compared with $4\Delta H^M_{0.5}$

All values are in kcal/mole

Mixture	$\Delta U_{++}^{B\text{-}Ag} - \Delta U_{++}^{B\text{-}Na}$	U_c	ΔU_T	$4\Delta H^M_{0.5}$
$(Li\text{–}Ag)NO_3$	+0.84	−0.38	+0.46	+0.65
$(Na\text{–}Ag)NO_3$	+0.67	−0.00	+0.67	+0.59
$(K\text{–}Ag)NO_3$	+0.22	−0.53	−0.31	−0.45
$(Rb\text{–}Ag)NO_3$	−0.01	−1.00	−1.01	−1.19
	$\Delta U_{++}^{B\text{-}Tl} - \Delta U_{++}^{B\text{-}Rb}$			
$(Li\text{–}Tl)NO_3$	+1.28	−2.27	−0.99	−0.880
$(Na\text{–}Tl)NO_3$	+1.08	−0.72	+0.36	+0.256
$(K\text{–}Tl)NO_3$	+0.58	−0.03	+0.55	+0.440
$(Rb\text{–}Tl)NO_3$	+0.31	−0.01	+0.30	+0.232

added to the values in column 3, which are estimated for the mixtures indicated if $AgNO_3$ and $TlNO_3$ behaved as alkali nitrates, the resultant quantities given in column 4 are, within the expected error of the calculations, in correspondence with measured values of the heats of mixing given in column 5. This suggests that the method of calculation used may be useful for predictions in real systems. The postulated effect should be important not only in mixtures containing Ag^+ and Tl^+ but more generally in a large class of other mixtures containing, for example, Cs^+, Rb^+, K^+, Ba^{2+}, Sr^{2+}, Ca^{2+}, or other polarizable ions (cations or anions).

Part II

Aqueous Reactor Programs

6. Chemistry of Pressurized-Water Reactor Systems[1]

C. F. Baes, Jr. T. H. Handley[2]

There are two important unsolved problems associated with the water chemistry of pressurizer-water reactor primary systems: (1) the transport and deposition of corrosion products (crud), which foul heat transfer surfaces and impair the operating reliability of mechanical systems exposed to primary water; (2) the transport and deposition of long-lived activities (originating from the activation of corrosion products in the reactor flux), which cause a long-term buildup of radiation levels throughout the primary system. In undertaking a study of the water chemistry of the ORR pressurized water loop, during the past year, the primary objective was to gain an increased knowledge of the nature and behavior of water-borne activity and crud in the hope that new methods for their control would be suggested.

Results obtained thus far provide strong evidence that a large part of the low-level longer-lived water-borne activity during normal loop operation (principally Mn^{54}, Fe^{59}, Co^{58}, and Co^{60}) is present as dissolved ionic material. Thus, tests in which cooled water samples were passed through a series of decreasing-porosity Millipore filters showed a lower limit to crud particle size of about 0.5 μ, virtually all remaining water-borne activity passing through a 0.01-μ filter. This "nonfilterable" activity was absorbed reversibly by cellulose backing pads used in some filtration tests. Such activity, when absorbed on chromatographic paper, was found in electromigration tests to move toward the cathode with a velocity expected for simple cations. Finally, when the same specific activity was assumed for the dissolved material as was found for the filterable crud, the resulting concentration of ionic material, calculated on the assumption that all the nonfilterable activity is present as simple ions, was in reasonable agreement with the ion concentration indicated from observed loop-water conductivity.

Other results suggest, further, that the dissolved activity exchanges at an appreciable rate with the crud activity. This crud was found from electron micrographs to be crystalline in appearance and from x-ray diffraction patterns to exhibit the structure of magnetite, often found to be a principal constituent of PWR crud. The apparent lower limit to particle size suggests that recrystallization occurs, which of course would result in activity exchange. Finally, the previous assumption of equal specific activities for the dissolved material and the crud is consistent with such exchange.

Since magnetite (Fe_3O_4) is the stable oxide of iron in such systems and is a principal constituent of crud, it is a possible high-temperature filter, ion exchange medium. If, as suggested here, this constituent both supplies and exchanges with the ionic material in the high-temperature water, the introduction of a bed of nonactivated magnetite into a PWR coolant system might well accumulate, by the same process which now contributes to the transport of activity, the dissolved activity without otherwise disturbing the chemical or nuclear behavior of the system. Accordingly, tests are in progress to examine the suitability of magnetite as such a purification medium.

---

[1] Summary of a contribution to the *Maritime Reactor Program Ann. Progr. Rept. Nov. 30, 1961*, ORNL-3238, pp 43–50.

[2] Analytical Chemistry Division.

7. Phase Equilibria in Aqueous Systems at Elevated Temperatures

Knowledge of phase equilibria in aqueous systems at elevated temperatures, in addition to being of fundamental interest, has had important applications in the selection and modification of the fuel composition of the HRE-2. Aqueous homogeneous reactor-fuel solutions for use at power-producing temperatures originally contained only H_2O and UO_2SO_4; developments in technology and changes in goals led to the introduction of $CuSO_4$ as a catalyst, the switch from H_2O to D_2O as the base solvent, the addition of D_2SO_4 to permit operation with lower uranium concentrations, and, finally, the accumulation of substantial concentrations of $NiSO_4$ as a consequence of the corrosion of stainless steel. Each of these changes compounded the complexity of the phase equilibrium relationships which needed to be known for the fuel system. Development of breeder blankets has also been an important goal of the aqueous reactor program, and, toward that end, studies have been made of systems involving thorium. The desire for reactor systems which would operate at much higher temperatures leads to an interest in the properties of aqueous systems near and above their critical temperatures. The results of phase equilibrium studies, while originally and primarily oriented toward aqueous reactor systems, may ultimately be useful in connection with the general problem of water purification.

SOLID-LIQUID AND LIQUID-LIQUID EQUILIBRIA

W. L. Marshall
J. S. Gill
E. V. Jones
Ruth Slusher

Solubility and Nature of the UO_3 Hydrates in the System UO_3-SO_3-H_2O, 150 to 300°C

In a previous investigation[1] the solubilities of UO_3 hydrates were determined in solutions of SO_3 and H_2O at temperatures between 150 and 290°C and at concentrations of SO_3 from 10^{-3} to 1.0 *m*. In this current investigation further solubilities were obtained. Particular attention was directed to the various hydrates of UO_3 and the region of temperature and concentration of SO_3 at which each one was stable. The overall work is incorporated into a paper which will appear shortly.[2]

Saturation molal ratios, $m_{UO_3}:m_{SO_3}$, obtained by extrapolation of the previous data from 290 to 300°C were approximately 10% higher than those of the new data. In the present study of the system UO_3-SO_3-H_2O, most solution-solid mixtures were rocked at 300°C for a minimum of 16 hr. Previously, although experimental data were reproducible after 15 min at one temperature, an entire run – at several temperatures – was usually finished in 10 hr. In the earlier investigation at temperatures up to 290°C, UO_3 monohydrate was stated to be the solid phase. The stable phase at 300°C in the most recent investigation was identified as the hemihydrate, $UO_3 \cdot \frac{1}{2}H_2O$, by the use of an accepted x-ray diffraction pattern for this solid.[3]

The results given in Fig. 7.1 show that the stable solid phase at 150°C is α-$UO_3 \cdot H_2O$, at 225°C is presumably β-$UO_3 \cdot H_2O$, and at 300°C is $UO_3 \cdot \frac{1}{2}H_2O$. If at any temperature a metastable solid is present but is converting to the stable solid, the observed solubility should be that for the metastable solid, which has the higher solubility. The previous data at 270 and 290°C and

[1] W. L. Marshall, *Anal. Chem.* **27**, 1923 (1955).

[2] W. L. Marshall and J. S. Gill, "Aqueous Systems at High Temperature. III. Investigations on the System UO_3-CuO-NiO-SO_3-H_2O at 300°C," in press, *Journal of Inorganic and Nuclear Chemistry.*

[3] J. K. Dawson *et al.*, *J. Chem. Soc.* **1956**, p 3531.

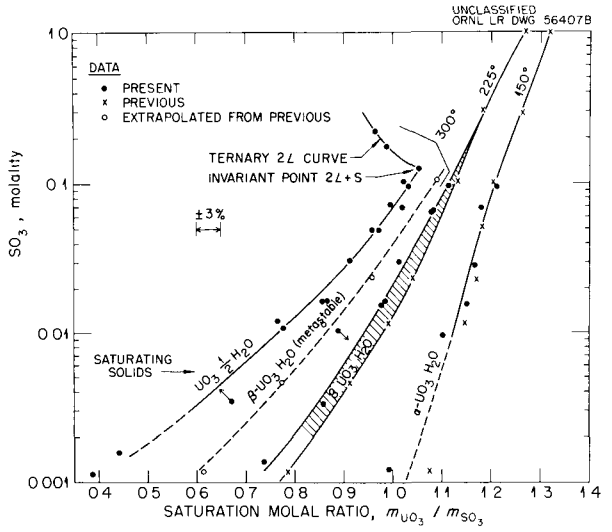

Fig. 7.1. Saturation Molal Ratios at 150, 225, and 300°C for the Solubility of UO_3 Hydrates in H_2SO_4-H_2O Solutions.

extrapolations to 300°C from these data (Fig. 7.1) should represent the solubility of metastable β-$UO_3 \cdot H_2O$. In Fig. 7.1, even the previous results at 225°C may represent the solubility of metastable α-$UO_3 \cdot H_2O$, while the present data at 225°C show the solubility of stable β-$UO_3 \cdot H_2O$. Two curves at this temperature are drawn, although there is at most only a 5% difference in molal ratio between the two sets of data. Low heats of transition among the three solid hydrates of UO_3 may be expected, and therefore it appears that metastability by one or the other could easily occur in the above range of temperature.

Further Investigations[2] on the System UO_3-CuO-NiO-SO_3-H_2O at 300, 325, and 350°C

In the five-component system, UO_3-CuO-NiO-SO_3-H_2O, the compositions of solutions saturated simultaneously with the three solid phases, $UO_3 \cdot \frac{1}{2}H_2O$, $CuO \cdot 3UO_3$, and $NiO \cdot 3UO_3$, were determined at 300, 325, and 350°C. In these solutions the $UO_3 : SO_3$ molal ratio at 300°C increased from 0.55 to 0.95 as the SO_3 concentration was increased from 0.002 *m* to 0.06 *m*; the $CuO : SO_3$ and $NiO : SO_3$ molal ratios were 0.009 ± 0.003 and 0.024 ± 0.004, respectively, over this SO_3 concentration range. When the temperature was raised, the $UO_3 : SO_3$ ratio was decreased; at 0.01 *m* SO_3 the ratios were 0.75, 0.72, and 0.69 at 300, 325, and 350°C respectively. At 350°C and approximately 0.016 *m* SO_3 an isothermal invariant point was found at which the three solids were simultaneously in equilibrium with two liquid phases; the light liquid phase had a $UO_3 : SO_3$ molal ratio of 0.75; the $CuO : SO_3$ and $NiO : SO_3$ molal ratios were very low.

Compilation of Solubilities in H_2O at High Temperature[4]

Figure 7.2 is a compilation of the majority of solubilities for systems of stoichiometric salts in H_2O (two components) above 200°C. It does not include investigations at ORNL or investigations by geochemists of solubilities in the range of parts per million to several weight percent. It is evident that very little information exists above 374°C. With sufficient study above this temperature, regions of stability might be defined for solutions containing UO_3 and other components. Fuel compositions could then be specified which would be stable from 25°C to temperatures considerably above 374°C.

Critical Phenomena and Liquid-Liquid Immiscibility in the Systems UO_3-CuO-SO_3-D_2O, UO_3-NiO-SO_3-D_2O, and UO_3-CuO-NiO-SO_3-D_2O, 280 to 410°C

The ultimate purpose for the determination of the temperatures of liquid-liquid immiscibility in D_2O systems containing UO_3, CuO, NiO, and SO_3 components is to define limits of stability of aqueous homogeneous reactor fuels over a very wide range of composition.

Previously, temperatures at which second liquid phases or critical phenomena were observed were reported for the systems UO_3-SO_3-H_2O,[5] UO_3-SO_3-D_2O, CuO-SO_3-D_2O, and UO_3-CuO-SO_3-D_2O; $m_{UO_3}/m_{SO_3} = 1.0$.[6] Temperatures of immiscibility and critical temperatures were plotted against $m_{\text{metal oxide}} : m_{SO_3}$, the saturation molal ratio, or the sum of these ratios at various selected concentrations of SO_3. The molalities of SO_3 were varied from 0.01 to 1.0.

[4] W. L. Marshall, "Aqueous Solubility Equilibria, 200 to 374°C," presented at the 135th National Meeting of the American Chemical Society, Boston, Mass. (April 1959).

[5] W. L. Marshall and G. M. Hebert, *Reactor Chem. Div. Ann. Progr. Rept. Jan. 31, 1960*, ORNL-2931, pp 100–103.

[6] W. L. Marshall, E. V. Jones, and F. J. Smith, *Reactor Chem. Div. Ann. Progr. Rept. Jan. 31, 1961*, ORNL-3127, pp 39–41.

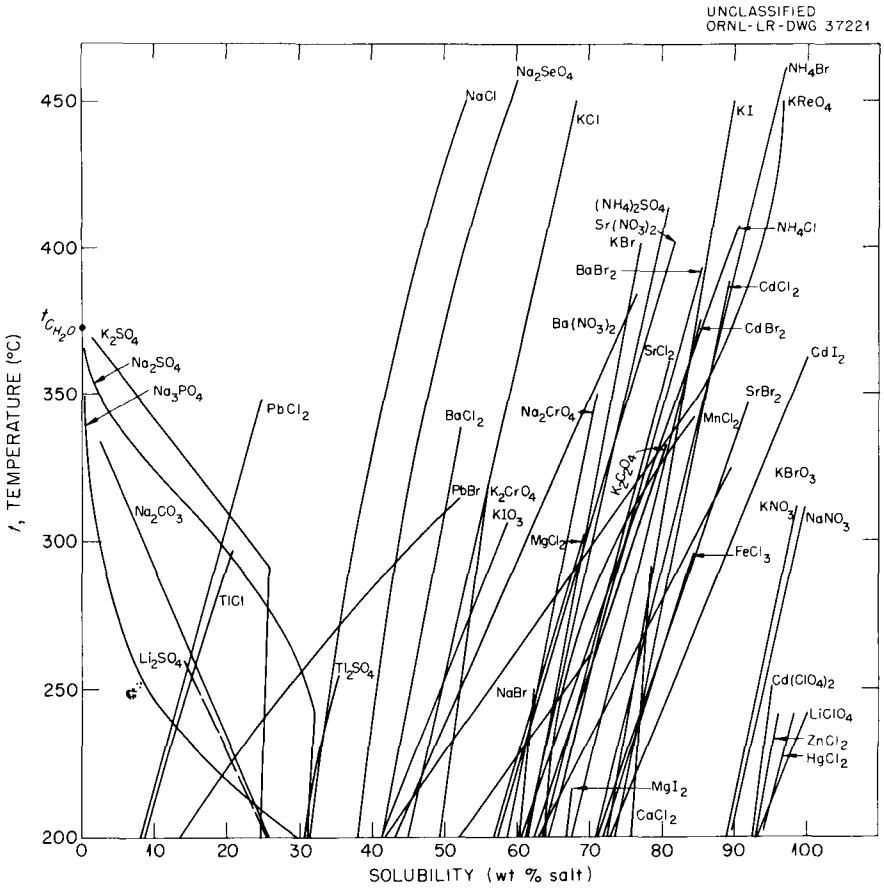

Fig. 7.2. Compilation of the Majority of Salt Solubilities in Two-Component H_2O Systems Above 200°C (Exclusive of ORNL Data and of Salts Showing Very Low Solubilities).

These investigations have been extended to the system UO_3-CuO-SO_3-D_2O at $m_{CuO} : m_{UO_3} = 0.333$, to the system UO_3-NiO-SO_3-D_2O at $m_{NiO} : m_{UO_3} = 1$ and 0.333, and finally to the system UO_3-CuO-NiO-SO_3-D_2O. In the study on the five-component system, values of $m_{CuO} : m_{UO_3}$ and $m_{NiO} : m_{UO_3}$ were held constant at 0.25. All experiments were carried out by the synthetic method described elsewhere.[7]

The results for the various systems are shown in Figs. 7.3–7.6, plotted as the summation of the molal ratios, $\Sigma(m_{\text{metal oxide}} : m_{SO_3})$, against either the observed critical temperature or the temperature of liquid-liquid immiscibility. The curves for each system are similar and also correspond to the curves presented previously for the other systems.[5,6] In all cases large concentrations of metal-oxide components were observed in the supercritical fluids.

The systems which contained an NiO component gave results which were not as precise as those from systems not containing NiO. These variations may be related to the fact that the system NiO-SO_3-H_2O was not found to show a region of liquid-liquid immiscibility under saturation vapor

[7] C. J. Barton, G. M. Hebert, and W. L. Marshall, "Aqueous Systems at High Temperature. II. Liquid-Liquid Immiscibility Above 300°C in the System UO_3-SO_3-N_2O_5-H_2O," in press, *Journal of Inorganic and Nuclear Chemistry.*

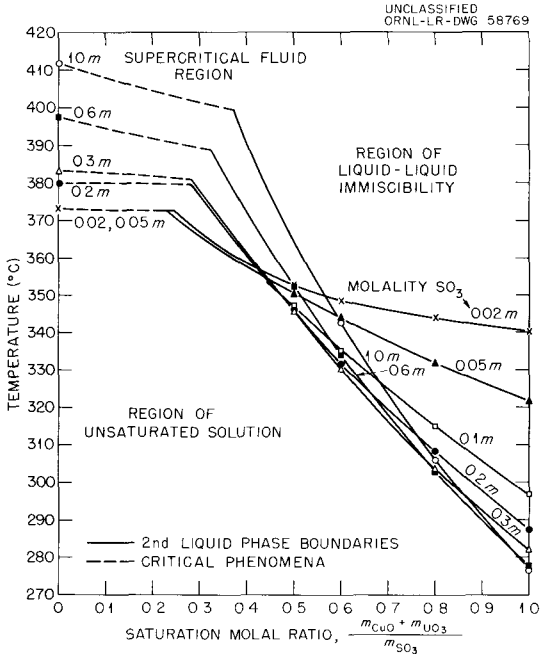

Fig. 7.3. Temperatures of Liquid-Liquid Immiscibility in the System UO_3-CuO-SO_3-D_2O; $m_{CuO} : m_{UO_3} = 0.333$.

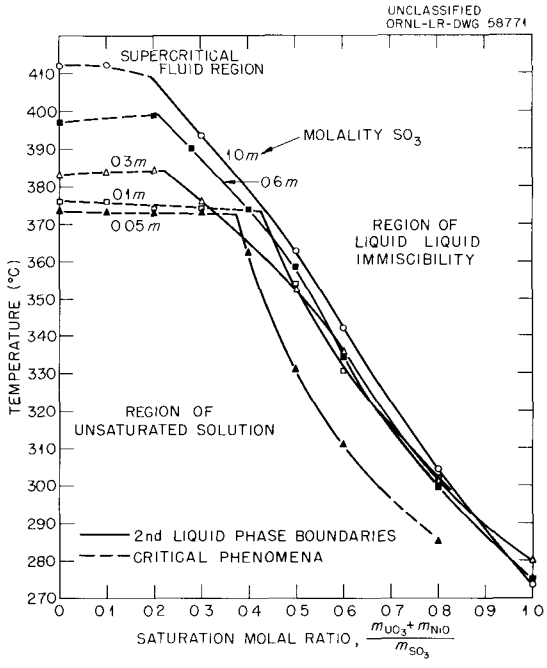

Fig. 7.5. Critical Phenomena and Temperatures of Liquid-Liquid Immiscibility in the System UO_3-NiO-SO_3-D_2O; $m_{NiO} : m_{UO_3} = 0.333$.

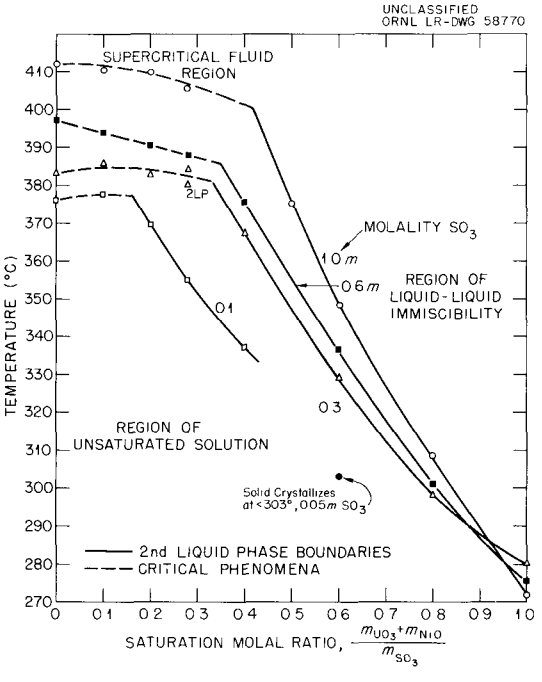

Fig. 7.4. Critical Phenomena and Temperatures of Liquid-Liquid Immiscibility in the System UO_3-NiO-SO_3-D_2O; $m_{NiO} : m_{UO_3} = 1.00$.

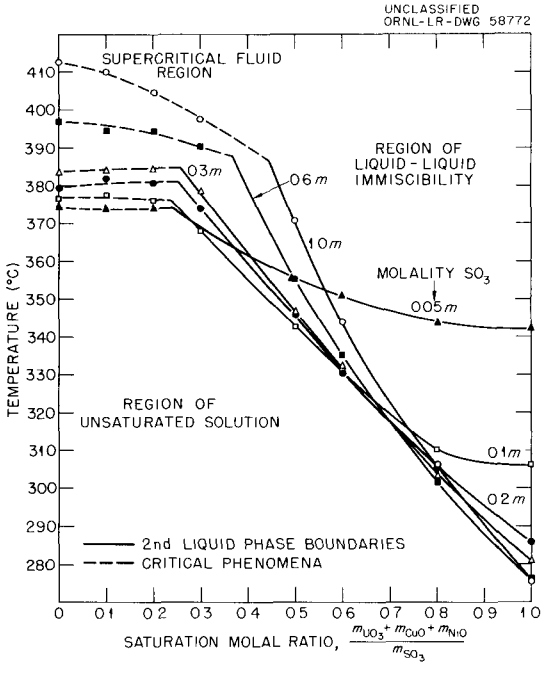

Fig. 7.6. Critical Phenomena and Temperatures of Liquid-Liquid Immiscibility in the System UO_3-CuO-NiO-SO_3-D_2O; $m_{CuO} : m_{UO_3} = m_{NiO} : m_{UO_3} = 0.250$.

pressures.[8] Furthermore, variations in composition were found in other investigations of systems containing an NiO component.[9]

Effect of Hydrostatic Pressure on Liquid-Liquid Immiscibility Temperatures of Stoichiometric UO_2SO_4-H_2O Solutions and of a UO_3-SO_3-D_2O Solution

In a study of the effect of pressure on liquid-liquid immiscibility it was desirable to make direct visual observations of the occurrence of two-liquid-phase formation as well as quantitative measurements of pressure and temperature. In order to make visual observations a high-pressure metal-to-glass connection unit was developed. By means of this connection unit, H_2O solutions of UO_3 and SO_3 could be subjected to known hydrostatic pressures at selected temperatures, and the effect of pressure on liquid-liquid immiscibility could be determined.

Some results are given in Figs. 7.7 and 7.8 for several stoichiometric UO_2SO_4-H_2O solutions and for a D_2O solution 0.6 *m* in UO_3 and 1.0 *m* in SO_3. These easily reproducible results are the first obtained by the visual method. The changes in immiscibility temperature with pressure, $\Delta t/\Delta p$, are given on the figures and are within the limits estimated previously.[10] They are in agreement with expectations that pressure effects on liquid-liquid immiscibility in these systems would be relatively large.

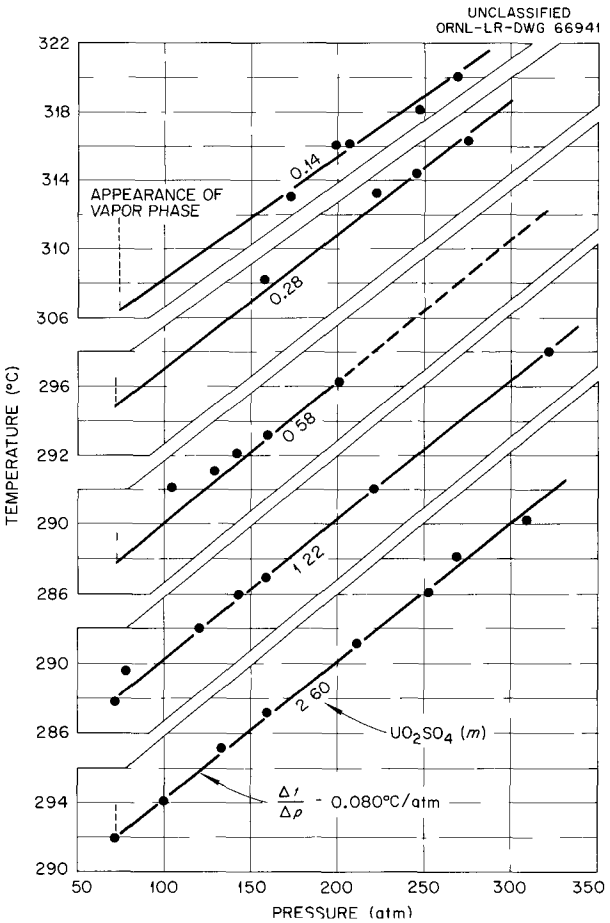

Fig. 7.7. Effect of Pressure on the Temperature of Liquid-Liquid Immiscibility of UO_2SO_4-H_2O Solutions.

Phase Equilibria in the System NiO-SO_3-H_2O and Its D_2O Analog from 10^{-4} to 2 *m* SO_3, 150 to 400°C

Previous studies of solubilities of $NiSO_4 \cdot H_2O$ and its D_2O analog in aqueous solutions of H_2SO_4 (ref 11) were extended at 300, 325, and 350°C

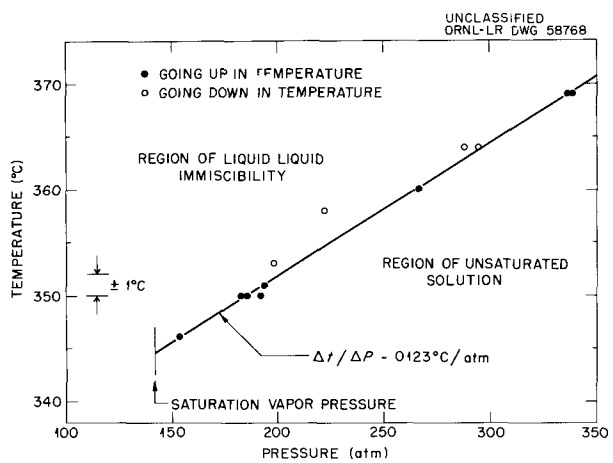

Fig. 7.8. Effect of Hydrostatic Pressure on the Temperature of Liquid-Liquid Immiscibility of a D_2O Solution 0.6 *m* in UO_3 and 1.0 *m* in SO_3.

[8] W. L. Marshall and F. J. Smith, *Reactor Chem. Div. Ann. Progr. Rept. Jan. 31, 1961*, ORNL-3127, p 37.

[9] E. V. Jones and W. L. Marshall, "Aqueous Systems at High Temperature. V. Distribution of CuO and NiO Components in the System UO_3-SO_3-H_2O and Its D_2O Analog, 300–350°C," in press, *Journal of Inorganic and Nuclear Chemistry*.

[10] W. L. Marshall and J. S. Gill, *HRP Quart. Progr. Rept. Jan. 31, 1960*, ORNL-2920, pp 70–71.

[11] W. L. Marshall, J. S. Gill, and R. Slusher, *HRP Quart. Progr. Rept. July 31, 1958*, ORNL-2561, pp 308–11.

over a range of concentrations of acid. The nature of the nickel oxysulfates stable at very low concentrations of SO_3 was further investigated. All work was combined with previous results and will appear elsewhere.[12] A summary is presented here.

All solubility data for the system $NiO\text{-}SO_3\text{-}H_2O$ are plotted in Fig. 7.9 as the saturation molal ratio, $m_{NiO} : m_{SO_3}$, defined as R_{Ni} and equal to the number of moles of NiO component present for each mole of SO_3 component, against the logarithm of the SO_3 molality. The concentration of the NiO component at saturation is obtained by multiplying R_{Ni} by the selected molality of SO_3. Values of R_{Ni} lower than those along a curve at constant temperature represent unsaturated solutions.

Regions of Stability of Solid Phases. – The solids, $NiSO_4 \cdot H_2O$ and $Ni(OH)_2$, specified as stable phases in Fig. 7.9, were identified by comparison of x-ray diffraction patterns of the solids removed from the pressure vessels after a run with known patterns for these compounds. Powder-pattern x-ray diffraction data were obtained for other solids, I, II, III, and IV, but

[12] W. L. Marshall, J. S. Gill, and R. Slusher, "Aqueous Systems at High Temperature. VI. Investigations on the System $NiO\text{-}SO_3\text{-}H_2O$ and Its D_2O Analog from 10^{-4} to 2 molal SO_3, 150–400°C," in press, *Journal of Inorganic and Nuclear Chemistry*.

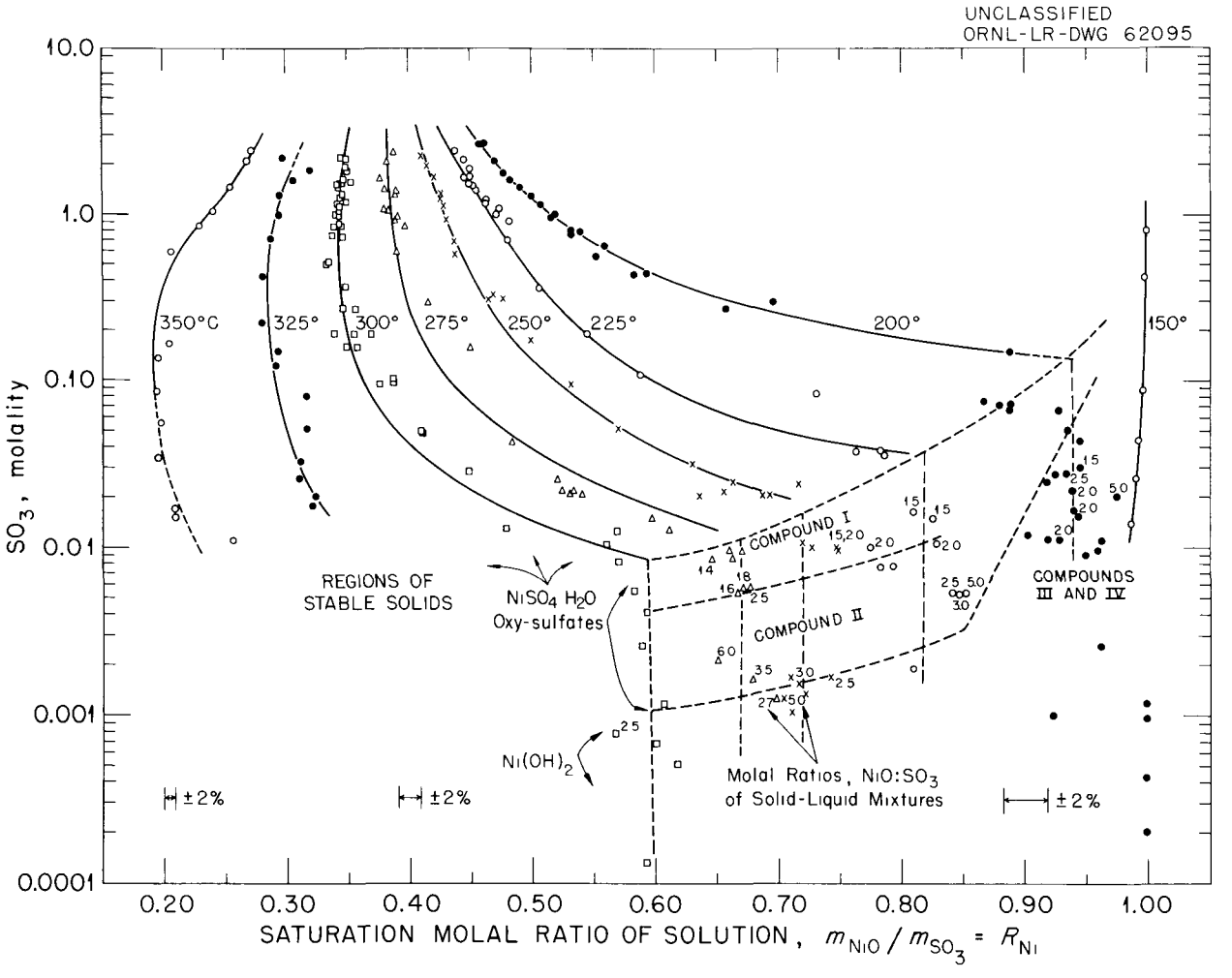

Fig. 7.9. The System $NiO\text{-}SO_3\text{-}H_2O$, 150–350°C.

could not be matched with any published values for nickel compounds.

From an examination of relative solution-composition groupings (see Fig. 7.9) for various experimental runs as well as the x-ray diffraction data, with respect to initial composition of mixtures, two oxysulfates were favored having a molal ratio, $NiO:SO_3$, near 1.5 for solid I and near 2.5 for solid II. For the 150°C data the solid phases observed ranged from solid I for the two highest concentrations through III, IV, and $Ni(OH)_2$ for the others.

Although the solution phases appeared to be saturated in less than 2 hr at constant temperature, metastable nickel oxysulfates or $Ni(OH)_2$ may have been incompletely converted to stable oxysulfates or $Ni(OH)_2$, thus resulting in low precision of the solubility data. The extreme dilution of the liquid phases and the fact that the solids, other than $NiSO_4 \cdot H_2O$, were not visibly crystalline made the collection of precise data difficult.

Solubility of $NiSO_4 \cdot H_2O$ in H_2SO_4-H_2O. – If the compositions of liquid phases over which $NiSO_4 \cdot H_2O$ is a stable solid are expressed in terms of $NiSO_4$, H_2SO_4, and H_2O as the components, the solubilities of $NiSO_4 \cdot H_2O$ may be plotted against the concentration of excess H_2SO_4. Plots of the solubility of $NiSO_4 \cdot H_2O$ against the concentration of excess H_2SO_4 are shown in Fig. 7.10 and define solubility curves at various temperatures between 200 and 350°C. These solubilities were treated by a computer technique involving a method of least squares and are expressed by an empirical equation. This equation is given in Table 7.1, together with the values for the coefficients, the number of observations, and the standard error of fit, at the different temperatures. The experimental precision of the data can be compared with the calculated curves in Fig. 7.10.

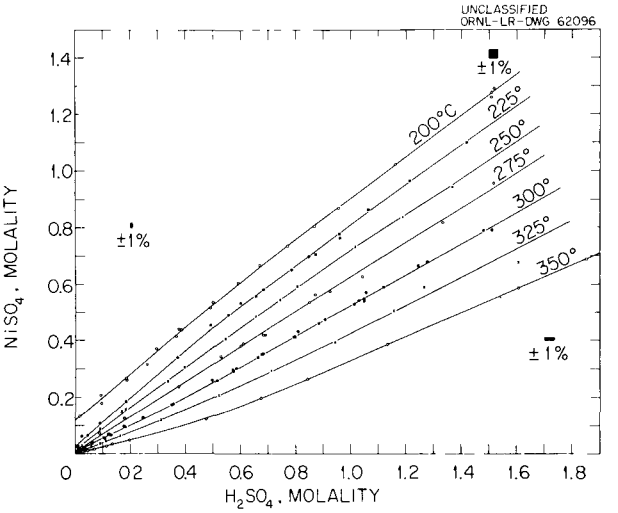

Fig. 7.10. Solubility of $NiSO_4 \cdot H_2O$ in H_2SO_4-H_2O Solutions, 200–350°C.

Table 7.1. Equation and Coefficients for the Solubility of $NiSO_4 \cdot H_2O$ in H_2SO_4-H_2O Solution, 200 to 350°C

Applicable for ranges of data shown in Fig. 7.10

$$m_{NiSO_4} = a_0 + a_1(m_{H_2SO_4}) + a_2(m_{H_2SO_4})^2 + a_3(m_{H_2SO_4})^3$$

T (°C)	$a_0 \times 10^3$	$a_1 \times 10$	$a_2 \times 10^2$	$a_3 \times 10^2$	Standard Error of Fit (molal units)	Number of Observations
200	+116.5	+8.513	−5.518	0	0.0100	21
225	+29.18	+8.680	−8.272	0	0.0106	21
250	+15.53	+7.647	−6.027	0	0.00519	17
275	+8.497	+6.113	+0.3607	0	0.00946	21
300	+4.109	+5.040	+1.773	0	0.00634	43
325	+1.181	+3.934	−0.7614	+3.899	0.00233	14
350	+2.085	+1.892	+18.61	−4.766	0.00222	15

Solubility of $NiSO_4 \cdot D_2O$ in D_2SO_4-D_2O. – Experimental solubilities of $NiSO_4 \cdot D_2O$ in D_2SO_4-D_2O solutions as a function of the concentration were similarly expressed by an empirical equation and the coefficients given in Table 7.2.

The marked effect of sulfuric acid on the solubility of the monohydrate, both in H_2O and in D_2O, may be due in part to general ionic effect and in part to formation of HSO_4^- (as in Ag_2SO_4).[13] A larger effect (by about 5 to 15%, depending upon concentration of excess acid and temperature) found in D_2O may indicate that the second ionization constant of the acid is smaller (by roughly the same amount) in D_2O than in H_2O. To the best of our knowledge, reported solubilities of stoichiometric salts at low temperature are always lower in D_2O than in H_2O due to the effect of solvent. The interaction of these two effects – reactant and solvent – may be observed in this study by comparison of the hypothetical solubility in water, represented by the coefficient a_0 (Tables 7.1 and 7.2). At constant temperature this coefficient for the H_2O system is always larger than for the D_2O system. Thus, as the concentration of excess sulfuric acid approaches zero, there is a crossover in the curves, and the solubility in H_2O solution becomes greater than in D_2O solution.

[13] M. H. Lietzke and R. W. Stoughton, *J. Phys. Chem.* 63, 1188 (1959).

Solubility of ThO_2 in Solutions of HNO_3-H_2O at 150 and 200°C

Thorium nitrate solutions have always been of interest as possible breeding blankets for aqueous homogeneous reactors. The report of a method for effectively removing protactinium from aqueous $Th(NO_3)_4$ solutions[14] made it possible to visualize a blanket solution which would generate very little power. Such a solution could be maintained at a lower temperature than the fuel solution. Consequently, the solubilities of ThO_2 in HNO_3-H_2O were determined at 150 and 200°C to supplement the information previously reported[15] for temperatures of 200 and 300°C.

Solubilities of ThO_2 determined after the longest intervals of time at the respective equilibration temperatures are shown in Fig. 7.11. The current values at 200°C are in good agreement with those obtained previously by using ThO_2 fired at 650°C (ORNL Pilot Plant batch No. DT-58-650). The earlier values at 300°C with the same ThO_2 product are included in Fig. 7.11. Comparison of results with the previous values suggested a moderately fast rate of dissolution of refractory ThO_2 in HNO_3-H_2O solution at 150 as well as at 200 and 300°C.

[14] M. J. Kelly, G. L. Johnson, and D. R. Cuneo, *Reactor Chem. Div. Ann. Progr. Rept. Jan. 31, 1961*, ORNL-3127, pp 56–58.

[15] R. Slusher and W. L. Marshall, *Reactor Chem. Div. Ann. Progr. Rept. Jan. 31, 1961*, ORNL-3127, p 47.

Table 7.2. Equation and Coefficients for the Solubility of $NiSO_4 \cdot D_2O$ in D_2SO_4-D_2O Solution, 200 to 350°C

Applicable for D_2SO_4 molalities up to 0.25 at 200°, 0.3 at 250°, 1.0 at 300°, 1.0 at 325°, and 0.65 at 350°C

$$m_{NiSO_4} = a_0 + a_1(m_{D_2SO_4}) + a_2(m_{D_2SO_4})^2$$

T (°C)	$a_0 \times 10^3$	$a_1 \times 10$	$a_2 \times 10^2$	Standard Error of Fit (molal units)	Number of Observations
200	+87.12	+8.208	0	0.00293	3
250	+4.956	+9.337	−33.18	0.00236	12
300	+3.276	+5.989	−2.682	0.00374	31
325	+0.1908	+4.469	+2.552	0.00161	7
350	+0.9858	+2.442	+15.96	0.000476	6

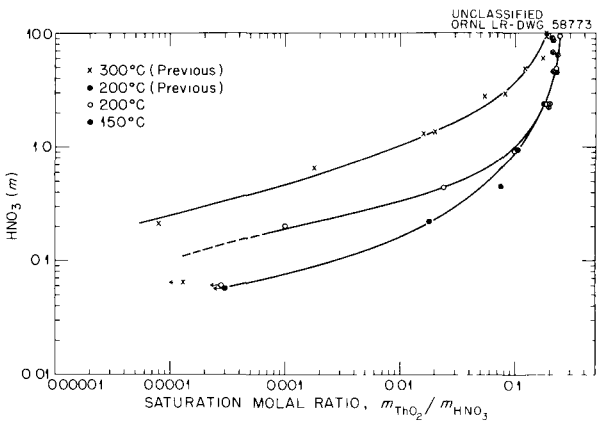

Fig. 7.11. Solubility of ThO_2 in HNO_3-H_2O Solutions at 150, 200, and 300°C.

High-Pressure Vessel Incorporating a Teflon Gasket for Use to 500°C and 1000 bars

A vessel with Teflon as a gasketing material was designed for equilibrating liquid-solid mixtures at extremes of temperature and pressure. Details of its construction and use are presented elsewhere.[16] A diagram of the vessel is shown in Fig. 7.12.

GAS-LIQUID EQUILIBRIA

Gas Solubility Studies

L. O. Gilpatrick H. H. Stone

Studies on gas solubility in aqueous systems have both applied and fundamental aspects. They provide data of direct interest to chemical and reactor operations and to design activities. From a fundamental point of view, the effect of concentrations of inorganic species on solubility has been studied only slightly, particularly in conjunction with changes in the temperature. The experimental procedures and some previous data have been reported elsewhere.[17–19]

Table 7.3 shows the solubility of H_2 in H_2O and of D_2 in D_2O from 260 to 300°C. Data from 25 to 250°C have previously been reported.[18]

The D_2-D_2O data, in the form moles of D_2 per mole of D_2O at 1 atm of deuterium overpressure, were fitted by an Oracle code to an empirical equation of the form $\ln s = a/T + b + cT$, where s is in moles of D_2 per mole of D_2O, and T is in degrees Kelvin. Values of $a = 2013.9$, $b = -23.17$, and $c = 0.01803$ were obtained; the equation describes the experimental data to within 4% from 0 to 300°C.

Table 7.4 shows the depression of the solubility of hydrogen by 0.1 *M* $K_2Cr_2O_7$ and the difference observed between [0.1 *M* $Cu(ClO_4)_2$, 1 *M* $HClO_4$] and [1 *M* $HClO_4$] solution. Since the differences are moles of H_2 per mole of H_2O, this depression represents a real loss in solubility and is essentially the same for both solutes. This loss in solubility is surprisingly large for such small solute concentrations. Table 7.4 also contains values for the effect of 1 *M* $HClO_4$ on the solubility of hydrogen in water. Here the hydrogen ion seems to decrease the solubility below 55°C and to enhance the solubility above this temperature, although the precision of the data is such that only the trend is evident.

[16] J. S. Gill and W. L. Marshall, *Rev. Sci. Instr.* 32, 1060 (1961).

[17] L. O. Gilpatrick and H. H. Stone, *HRP Quart. Progr. Rept. Nov. 30, 1960*, ORNL-3061, pp 47–48.

[18] L. O. Gilpatrick and H. H. Stone, *Reactor Chem. Div. Ann. Progr. Rept. Jan. 31, 1961*, ORNL-3127, pp 60–61.

[19] L. O. Gilpatrick and H. H. Stone, *HRP Progr. Rept. Dec. 31–May 31, 1961*, ORNL-3167, pp 49–50.

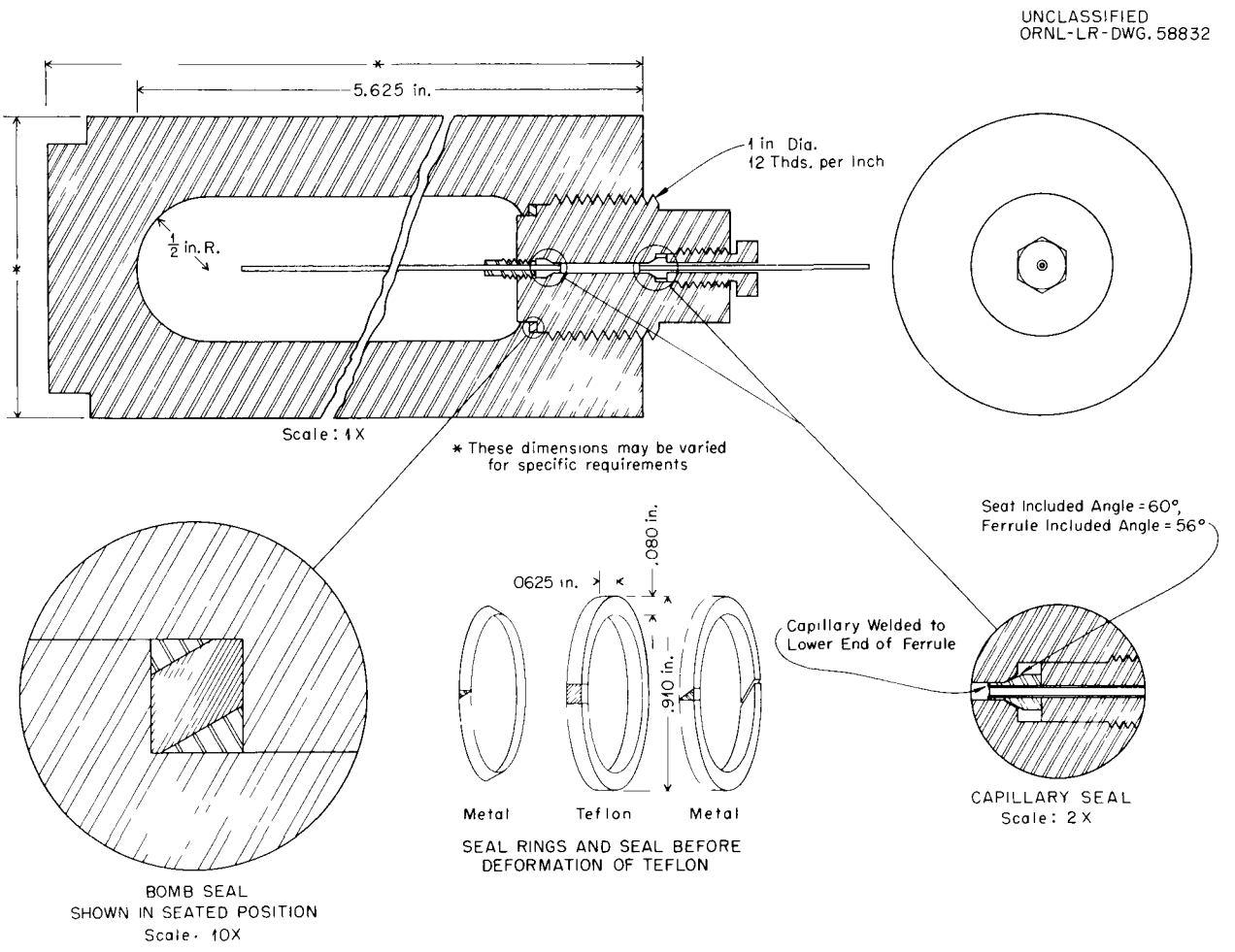

Fig. 7.12. High-Pressure Vessel Incorporating Teflon Gasket for Use to 500°C and 1000 atm.

Table 7.3. Solubility of H_2 in H_2O and of D_2 in D_2O

Temperature (°C)	H_2-H_2O System		Standard Deviation (%)	D_2-D_2O System		Standard Deviation (%)
	Number of Samples	Solubility (std cc g^{-1} atm^{-1})		Number of Samples	Solubility (std cc g^{-1} atm^{-1})	
		$\times 10^{-2}$			$\times 10^{-2}$	
260	9	6.706	2.13	2	6.070	0.60
270	5	7.514	0.76	3	6.864	0.20
280	7	8.552	1.90	7	7.19	3.50
290	6	9.632	0.98	5	8.945	2.33
300	5	11.142	0.33	2	10.718	0.33

Table 7.4. Depression of Hydrogen Solubility in Various Solutions

Temperature (°C)		Depression of Solubility [(moles of H_2) (mole of H_2O)$^{-1}$ (atm of H_2)$^{-1}$]		
		0.1 *M* $Cu(ClO_4)_2$	0.1 *M* $K_2Cr_2O_7$	1.0 *M* $HClO_4$
		$\times 10^{-5}$	$\times 10^{-5}$	$\times 10^{-5}$
0			-0.119 ± 0.04	
20				-0.072 ± 0.02
25		-0.112 ± 0.01		-0.058 ± 0.01
30				-0.035 ± 0.02
40		-0.086 ± 0.01	-0.071 ± 0.03	-0.028 ± 0.02
50		-0.088 ± 0.02		-0.016 ± 0.02
60		-0.088 ± 0.02	-0.073 ± 0.02	$+0.007 \pm 0.02$
70		-0.082 ± 0.02		$+0.021 \pm 0.02$
80		-0.085 ± 0.02	-0.082 ± 0.02	$+0.028 \pm 0.01$
90		-0.091 ± 0.03		$+0.028 \pm 0.03$
100		-0.080 ± 0.02	-0.081 ± 0.03	$+0.044 \pm 0.02$
110		-0.082 ± 0.03		$+0.054 \pm 0.03$
120		-0.094 ± 0.01	-0.110 ± 0.04	$+0.042 \pm 0.03$
	Average	-0.089 ± 0.02	-0.089 ± 0.03	

8. Physical Chemistry of Aqueous Solutions

HYDROLYSIS OF URANIUM AND THORIUM COMPOUNDS IN AQUEOUS SOLUTIONS

C. F. Baes, Jr. N. J. Meyer[1]

A program of high-temperature acidity measurements, reported previously,[2,3] has been continued during the past year. Its purpose has been to gain an increased fundamental knowledge of the hydrolytic and ion-association behavior of selected metal cations in high-temperature aqueous systems. Such knowledge should contribute significantly to the interpretation and, ultimately, to an understanding of the chemical and thermodynamic behavior of a variety of high-temperature aqueous systems.

Thus far the hydrolysis of uranium(VI) and thorium(IV) has been studied, using the glass-electrode concentration cell described previously,[2] in measurements at 94°C.

Thorium(IV) Hydrolysis Measurements at 94°C

Thorium(IV) hydrolysis is being measured in 1 *M* sodium perchlorate at 94°C. A comparison of the results obtained thus far at this temperature with the results of others[4] at 25°C in the same medium is shown in Fig. 8.1. It is seen that hydrolysis of Th^{4+} increases markedly with temperature. In general, a given value of the hydroxyl number $\bar{n}$ (the average number of bound OH^- ions per Th^{4+} ion) occurs about one pH unit lower at

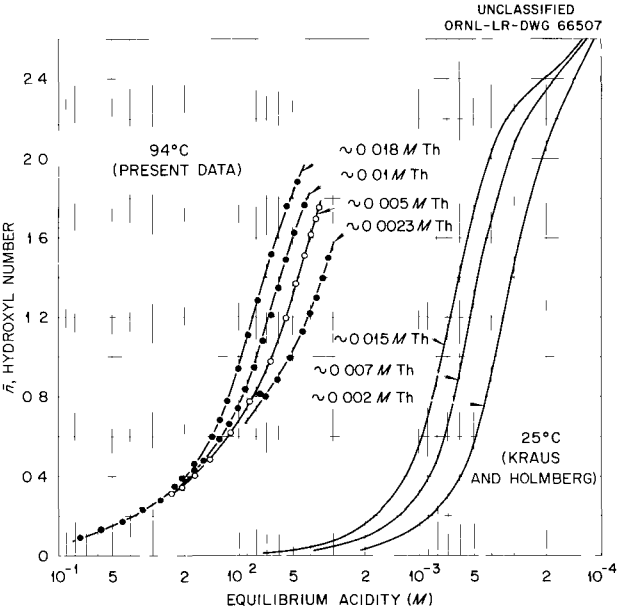

Fig. 8.1. Hydrolysis of Thorium(IV) in 1 *M* Sodium Perchlorate Solution.

94° than at 25°C. In the hydrolysis of stoichiometric $Th(ClO_4)_4$ solutions at the two temperatures the comparative results were as follows:

$Th(ClO_4)_4$ Molarity (in 1 *M* $NaClO_4$)	25°C[a]		94°C	
	$\bar{n}$	pH	$\bar{n}$	pH
0.011	0.45	3.35	~1.5	2.5
0.005	0.22	2.96	1.1	2.2
0.002	0.11	2.66	0.7	1.9

[a]Estimated from Kraus and Holmberg's results (ref 4).

Hydrolytic precipitation occurs at $\bar{n}$ values greater than 1.5 to 2 at 94°C, compared with 2.5 to 2.8 at 25°C.

---

[1]ORINS summer participant, 1961. Professor of Chemistry, Bowling Green State University, Bowling Green, Ohio.

[2]C. F. Baes, Jr., *Reactor Chem. Div. Ann. Progr. Rept. Jan. 31, 1960*, ORNL-2931, p 130.

[3]C. F. Baes, Jr., and N. J. Meyer, *Reactor Chem. Div. Ann. Progr. Rept. Jan. 31, 1961*, ORNL-3127, pp 64–65.

[4]K. A. Kraus and R. W. Holmberg, *J. Phys. Chem.* 58, 325 (1954).

At $\bar{n}$ values > 0.7, the dependence of $\bar{n}$ on acidity and on thorium concentration at 94°C is similar to that at 25°C (Fig. 8.1), indicating a hydrolysis mechanism in which the polynuclear products $Th_x(OH)_y^{(4x-y)+}$ are formed. Hietanen,[5] from her results in the same medium at 25°C, has suggested a "*core-links*" *mechanism in which the products* are $Th^{4+}:OH^- = 2:3, 3:6, 4:9, \ldots, x:(3x-3)$. This, however, is inconsistent at low $\bar{n}$ values (<0.3) with the detailed results of Kraus and Holmberg,[4] who propose the formation of 1:2, 2:2, and possibly 1:1 and 2:3 species in the early stages of hydrolysis. Since the formation of the initial 1:1, 1:2, and 2:2 species, which are not members of the sequence $x:(3x-3)$, could seriously affect the validity of the core-links treatment proposed by Hietanen,[5] it is significant that the present results at 94°C suggest the formation of mononuclear initial species which are even more stable than at 25°C. This is indicated in Fig. 8.1 by the convergence of the curves at different thorium concentrations to a single curve as $\bar{n}$ decreases at 94°C. A similar increase in stability of a mononuclear uranium(VI) hydrolysis product with increasing temperature has been reported previously.[3]

At the high acidity (>0.01 *M*) of initial thorium(IV) hydrolysis at 94°C, the glass-electrode measurements were found less precise than previously. Accordingly, an attempt is being made to check and extend them with the hydrogen electrode before a detailed interpretation of these results is made. The results of preliminary tests of the concentration cell

$$H_2 \,|\, Pt \,|\, \text{test solution} \,||\, \text{reference solution} \,|\, Pt \,|\, H_2$$

at 94°C are quite promising. With both electrodes exposed to a common hydrogen atmosphere and with agitation of both cell solutions, response to changes in acidity were rapid and were independent of the hydrogen pressure.

Uranium(VI) Hydrolysis Behavior[6]

The study of uranium(VI) hydrolysis in 0.3 *m* nitrate solutions at 94 and 25°C reported in part previously[3] has been completed. The three hydrolysis reactions listed in Table 8.1, leading to species in which $UO_2^{2+}:OH^- = 1:1$, 2:2, and 3:5, are proposed to account for the data. The corresponding equilibrium quotients which are listed were first estimated by hand calculation, and then final values were obtained by use of a FORTRAN nonlinear least-squares computer program.[7] The differences between observed values

[5] S. Hietanen, *Acta Chem. Scand.* 8, 1626 (1954).

[6] Presented at the 140th Annual Meeting of the American Chemical Society, Chicago, September 1961. Paper submitted for publication in the *Journal of Inorganic Chemistry*.

[7] "Hydrolysis Constant Program," consisting of the "General Least Squares Program" of W. R. Busing and H. A. Levy and a subroutine "Calculation of Hydroxyl Number" by R. M. Rush.

Table 8.1. Uranium(VI) Hydrolysis at 25 and 94°C in 0.5 *m* KNO_3

Reaction	Equilibrium Quotient		ΔH^a (kcal)	$\Delta F_{25°C}{}^a$ (kcal)	$\Delta S_{25°C}{}^a$ (cal/°K)
	25°C	94°C			
(1) $UO_2^{2+} + H_2O \rightleftharpoons UO_2OH^+ + H^+$	$Q_{11} = (2 \pm 1) \times 10^{-6}$	$(6.5 \pm 1) \times 10^{-5}$	11 ± 2	7.8 ± 0.5	11 ± 5
(2) $2UO_2^{2+} + 2H_2O \rightleftharpoons (UO_2)_2(OH)_2^{2+} + 2H^+$	$Q_{22} = (1.2 \pm 0.1) \times 10^{-6}$	$(3.1 \pm 0.2) \times 10^{-5}$	10.2 ± 0.5	8.08 ± 0.05	7.1 ± 2
(3) $3UO_2^{2+} + 5H_2O \rightleftharpoons (UO_2)_3(OH)_5^{+} + 5H^+$	$Q_{35} = (6 \pm 1) \times 10^{-17}$	$(1.8 \pm 0.5) \times 10^{-13}$	25.1 ± 1.5	22.1 ± 0.1	10 ± 5

[a] These values were determined directly from the equilibrium quotients (uncorrected to $I = 0$, ΔH assumed constant) and so are not standard thermodynamic quantities.

of the hydroxyl number $\bar{n}$ (the formal number of OH^- ions per UO_2^{2+} ion) and values calculated from these quotients agree within experimental error, the standard deviations being ~0.005 in $\bar{n}$ at each temperature.

This scheme of hydrolysis products (1:1, 2:2, 3:5) differs from a core-links scheme previously proposed by Ahrland, Hietanen, and Sillen[8] (2:2, 3:4, 4:6, 5:8, etc.) to account for Ahrland's data in perchlorate solutions,[9] but it is essentially consistent with an earlier study by Sutton,[10] who proposed the sequence 2:2, 3:4, 3:5, 3:6, 3:7, 3:8. Recently others at this Laboratory,[11] from ultracentrifuge and emf measurements of uranium(VI) hydrolysis in chloride solutions at 25°C, have found a scheme similar to the present one, with the interesting difference that the additional species $(UO_3)_3(OH)_4^{2+}$ was found. Accordingly, this 3:4 species, also in Sutton's sequence, was assumed in testing the present data by the computer code, with the result that the fit of calculated to observed $\bar{n}$ values was not significantly improved and the corresponding formation quotient Q_{34} value was virtually zero.

Thus it appears that the mechanism of hydrolysis is influenced by the medium. In nitrate and perchlorate (from a computer-code test of Ahrland's data[9] by Rush *et al.*[11]) the hydrolysis products are evidently the 1:1, 2:2, and 3:5 species. In chloride (and perhaps in sulfate, from the appearance of recent results of Peterson[12]) they are probably 1:1, 2:2, 3:4, and 3:5. The neutral and anionic trimeric products also proposed by Sutton have not been confirmed, because later workers have encountered precipitation of UO_3 at lower $\bar{n}$ values than Sutton was able to reach.

[8] S. Ahrland, S. Heitanen, and L. G. Sillen, *Acta Chem. Scand.* 8, 1907 (1954).

[9] S. Ahrland, *Acta Chem. Scand.* 3, 374 (1949).

[10] J. Sutton, *J. Chem. Soc.* 1949, suppl 2, p S-275.

[11] R. M. Rush, J. S. Johnson, and K. A. Kraus, "Hydrolysis of U(VI); Ultracentrifugation and Acidity Measurements in Chloride Solutions," paper presented at the 140th Annual Meeting of the American Chemical Society, Chicago, September 1961. Paper submitted for publication in the *Journal of Inorganic Chemistry*.

[12] A. Peterson, *Acta Chem. Scand.* 15, 101 (1961).

[13] W. L. Marshall and R. Slusher, *Reactor Chem. Div. Ann. Progr. Rept. Jan. 31, 1961*, ORNL-3127, p 47.

Hydrolysis of Uranium(VI) and the Solubility Behavior of $UO_3(s)$ in HNO_3 at Elevated Temperatures

The uranium(VI) hydrolysis results should provide an increased understanding of the observed solubility behavior of uranium trioxide in nitric acid at elevated temperatures.[13] Interpretation of high-temperature phase behavior in terms of ionic species and equilibria in solution has, from the outset, been a primary objective in this program of hydrolysis measurements. In terms of the hydrolysis reactions shown in Table 8.1, the following dissolution equilibria may be written for uranium:

$$UO_3(s) + 2H^+ \rightleftharpoons UO_2^{2+} + H_2O, \quad Q^s_{10} = C_{10}/[H^+]^2,$$

$$UO_3(s) + H^+ \rightleftharpoons UO_2OH^+, \quad Q^s_{11} = C_{11}/[H^+],$$

$$2UO_3(s) + 2H^+ \rightleftharpoons (UO_2)_2(OH)_2^{2+}, \quad Q^s_{22} = C_{22}/[H^+]^2,$$

$$3UO_3(s) + H^+ + 2H_2O \rightleftharpoons (UO_2)_3(OH)_5^+, \quad Q^s_{35} = C_{35}/[H^+].$$

The quotients Q^s_{xy} are related to Q_{xy} in Table 8.1 as follows:

$$Q_{11} = Q^s_{11}/Q^s_{10},$$

$$Q_{22} = Q^s_{22}/(Q^s_{10})^2,$$

$$Q_{35} = Q^s_{35}/(Q^s_{10})^3.$$

From these it is seen that the concentration of monovalent cations should vary directly as the first power of the acidity and that of divalent cations as the second power of the acidity. Thus it is to be expected that at low total nitrate concentrations (lower acidity) the predominant cations will be H^+, UO_2OH^+, and $(UO_2)_3(OH)_5^+$, while at high total nitrate concentrations (higher acidity) the predominant cations will be UO_2^{2+} and $(UO_2)_2(OH)_2^{2+}$. Assuming that the above equilibria are the only important ones in the dissolution of UO_3 in nitric acid solutions (i.e., neglecting nitric acid association and UO_2^{2+}–NO_3^- association), then it may be shown that

$$\frac{M_U}{M_{NO_3}} = \frac{Q^s_{11} + 3Q^s_{35} + (Q^s_{10} + 2Q^s_{22})[H^+]}{1 + Q^s_{11} + Q^s_{35} + (2Q^s_{10} + 2Q^s_{22})[H^+]}. \quad (1)$$

At present it can be said only that the observed phase behavior is in qualitative agreement with this relation, the principal consistency being that the observed ratio of uranium to nitrate (M_U/M_{NO_3}) is found to be nearly constant in dilute saturated solutions, wherein the above relation reduces to

$$\frac{M_U}{M_{NO_3}} = \frac{Q_{11}^s + 3Q_{35}^s}{1 + Q_{11}^s + Q_{35}^s} . \qquad (2)$$

Since Q_{11}^s and Q_{35}^s are formally independent of ionic strength, this ratio is expected to be constant. A more quantitative comparison of Eq. (1) with the solubility data is now in progress. If successful, this analysis not only will provide a better understanding of the phase behavior in this system but also should extend the temperature dependence of Q_{11}, Q_{22}, and Q_{35} (Table 8.1) to temperatures higher than 94°C.

OSMOTIC BEHAVIOR OF AQUEOUS ELECTROLYTES AT 140°C

B. A. Soldano

As a continuation of a general program of investigating the osmotic behavior of aqueous electrolytes at elevated temperatures,[14-16] representative salt solutions were studied as a function of concentration at 140.3°C. Design details of the equipment and its modification for the present work are recorded elsewhere.[15,16] In brief, a magnetic balance is operated in a vapor chamber 20 in. in diameter. This arrangement permits the weighing, in situ, of aqueous solutions contained in 16 titanium dishes. The total weight of each dish plus solution approximates 11 g. The design allows all transfers of dishes, variations in vapor pressure, etc., to be performed without exposing the internal system to outside conditions. In principle, therefore, the accuracy in determining the osmotic coefficients is essentially controlled by the accuracy of weighing at elevated pressures, temperatures, and variable humidities.

The experimental part of this study was concerned with the osmotic behavior of a variety of aqueous salt solutions over a concentration range from 9.8 m to approximately the limit of solubility. In addition, comparisons with previous work[15,16] at 25, 100, and 121°C were made.

Experimental

Duplicate solutions of seven salts were simultaneously equilibrated with a pair of sodium chloride solutions and a 200-ml reservoir of sodium chloride solution.

From an operational standpoint, the use of an air thermostat at ~140°C placed a considerable strain on the present heating output of the system. The resultant temperature excursions, although minute, reduced the overall precision of the data to approximately 1%. There is, however, reason to believe that an increase in the power output of the present system should improve its long-term stability. Furthermore, since the balance system operates with greater sensitivity at higher temperatures, it is not unreasonable to anticipate precisions better than 0.5% at temperatures above 140°C.

Results

In the absence of available reference standard data at temperatures above 100°C, the experimental data are presented, Table 8.2, as isopiestic ratios relative to NaCl.

The isopiestic ratio at fixed water activity is defined as

$$R = \gamma m_{std}/\gamma m , \qquad (1)$$

where γ is the idealized number of ions formed per mole of salt in the assumed standard state (i.e., $\gamma = 3$ for Na_2SO_4) and m is the molality of the solute. The experimental ratios (Table 8.2) for the 1-1 electrolytes at 140.3°C were smoothed by reading values at rounded concentrations from large-scale graphs representing isopiestic ratios R vs molality. For comparison with 25, 100, and 121.1°C values, osmotic coefficients for 140.3°C were calculated, Eq. (2), on the basis of estimated ϕ_{NaCl} values obtained by extrapolation of Smith's[17] boiling-point data for NaCl: $\phi_{NaCl} \times R = \phi_i$.

[14] B. A. Soldano *et al.*, pp 224–35 in *The Structure of Electrolytic Solutions*, Wiley, New York, 1958.

[15] C. S. Patterson, L. O. Gilpatrick, and B. A. Soldano, *J. Chem. Soc.* 1960, pp 2730–34.

[16] B. A. Soldano and C. S. Patterson, "The Osmotic Behavior of Aqueous Salt Solutions at Elevated Temperatures, Part II," to be published in the *Journal of the Chemical Society*.

[17] R. P. Smith, *J. Am. Chem. Soc.* 61, 500 (1939); R. P. Smith and D. S. Hirtle, *J. Am. Chem. Soc.* 61, 1123 (1939).

Table 8.2. Isopiestic Ratios at 140.3°C

Molality of Each Salt	ϕ_{NaCl} (estd)	Isopiestic Ratio, R, Eq. (1), with NaCl as Standard					
		LiCl	KCl	CsCl	$BaCl_2$	$MgSO_4$	UO_2SO_4
0.70	0.914				0.820		
0.75	0.915	1.049	0.969		0.787		
0.80	0.917				0.760		
1.00	0.923	1.046	0.962	0.929	0.815		
1.25	0.934	1.050	0.958	0.935			
1.50	0.945	1.058	0.955	0.934			
1.75	0.957	1.067	0.952	0.934			
2.00	0.967	1.067	0.949	0.935			
2.16[a]	0.977					0.437	
2.20[a]	0.980					0.442	0.402
2.50	0.998	1.095	0.945	0.925		0.462	0.412
3.0	1.026	1.115	0.941	0.910		0.480	0.427
3.5	1.051	1.140	0.939	0.913		0.490	0.440
4.0	1.075	1.166	0.937			0.502	0.450
4.5						0.513	0.460
5.0		1.240	0.934			0.524	0.468
5.5		1.282	0.933			0.533	0.476
6.0		1.31	0.932			0.542	0.483
6.5			0.9315			0.551	0.490
7.0			0.931			0.560	0.497
7.5						0.568	0.504
8.0			0.935				0.510
9.0							0.523
10.0							0.536
11.0							0.548
12.0							0.560

[a]Experimental values. Others at rounded concentrations.

These estimated values are reasonably consistent with the comprehensive, excellent, primary standard NaCl data for temperatures of ~100 to 260°C, presently being obtained by deNordwall and Gluekauf.[18] The calculated values of ϕ are shown in Figs. 8.2–8.4.

Figure 8.5 shows the temperature dependence of ϕ at an arbitrarily chosen concentration of 2.4 m. No new trends in the temperature dependence are introduced for the chloride salts by the 140°C data. The two sulfates, however, show a marked decrease in the rate of decrease of ϕ with increasing temperature. Uranyl sulfate appears to have a minimum ϕ at about 130°C, and magnesium sulfate appears to be approaching a minimum at a temperature above 140°C. The lithium chloride curve continues to decrease almost linearly with increasing temperature. This is not surprising if it is recalled that the lithium ion is a very strong stabilizer of the ice structure of water. If, therefore, the major temperature features of the behavior of salts in the range of 0 to ~140°C are connected with the structural properties of water, it should be expected that the lithium ion would be one of the very last ions to reverse this washing out of the structural features in aqueous solutions. This interpretation is consistent with the results of the energy-density measurements of Gibson,[19]

[18]H. J. deNordwall, private communication.

[19]R. E. Gibson and A. Loeffler, *Ann. N.Y. Acad. Sci.* 51, 727 (1949).

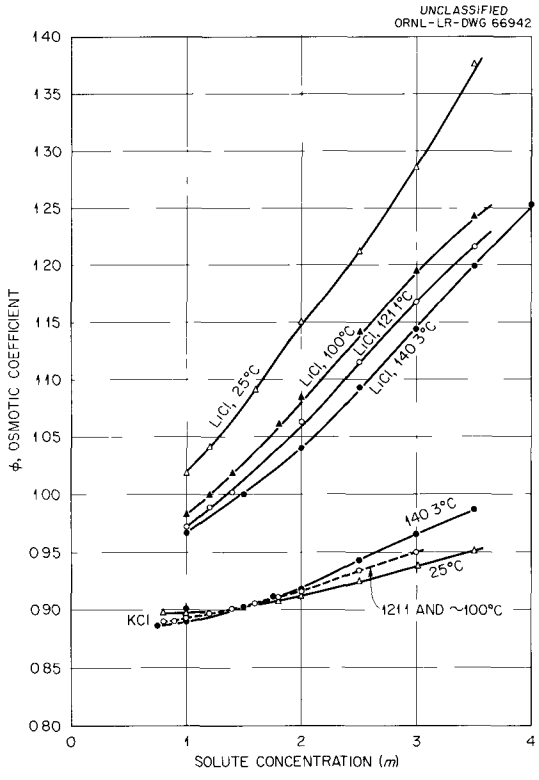

Fig. 8.2. Smoothed Values of ϕ as a Function of Molality for LiCl and KCl.

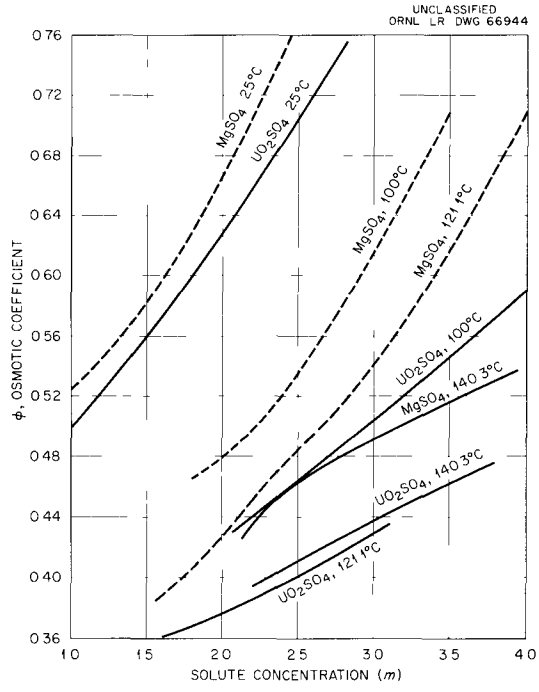

Fig. 8.4. Smoothed Values of ϕ as a Function of Molality for $MgSO_4$ and UO_2SO_4.

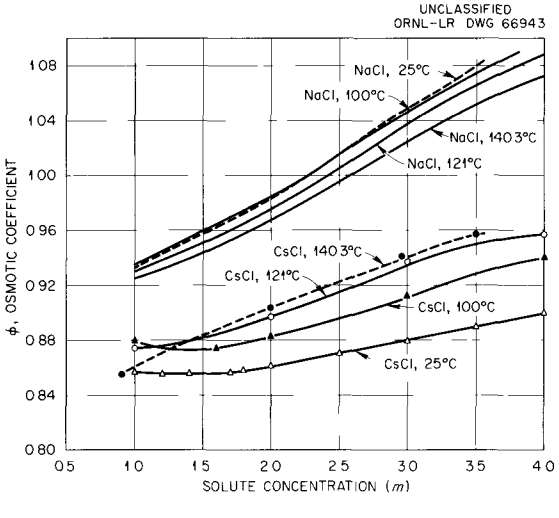

Fig. 8.3. Smoothed Values of ϕ as a Function of Molality for NaCl and CsCl.

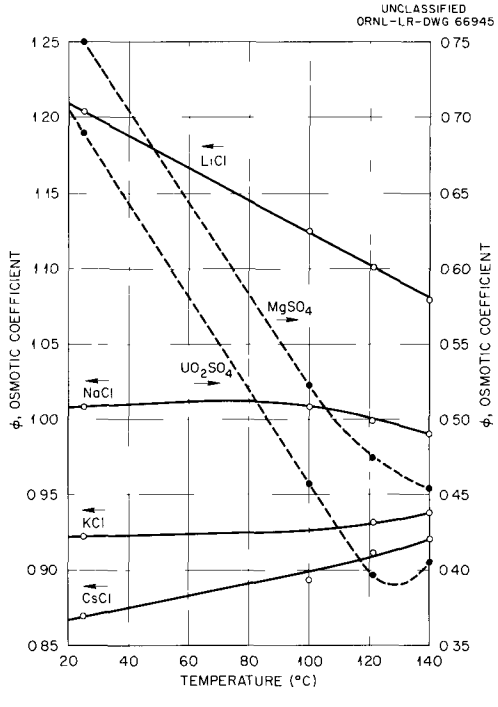

Fig. 8.5. Temperature Dependence of ϕ at 2.4 m.

who noted that the structural features of water appeared to be eliminated at about 150°C. This general pattern tends to indicate that beyond ~140°C, water is a more nearly ideal solvent and that salt effects in solutions above this temperature will not have a close relationship with the ice-making and -breaking features of water. Conversely, the linear relationship previously noted in osmotic ratios as a function of temperature[16] may be due primarily to the effect of temperature on the structural characteristics of the solvent water.

[20] Consultant.

[21] Temporary employee, 1960, Institut für Physikalische Chemie und Elektrochemie, Karlsruhe Technische Hochschule, Karlsruhe, Germany.

[22] E. U. Franck, J. E. Savolainen, and W. L. Marshall, *Rev. Sci. Instr.* 33, 115–17 (1962).

ELECTRICAL-CONDUCTANCE MEASUREMENTS FROM 25 TO 800°C AND AT PRESSURES UP TO 4000 BARS

A. H. Quist
H. R. Jolley[20]
E. U. Franck[21]
J. E. Savolainen
W. L. Marshall

A detailed paper appears elsewhere[22] describing the construction of an electrical-conductance cell for use at extremes of temperature and pressure; Fig. 8.6 illustrates its construction. By use of

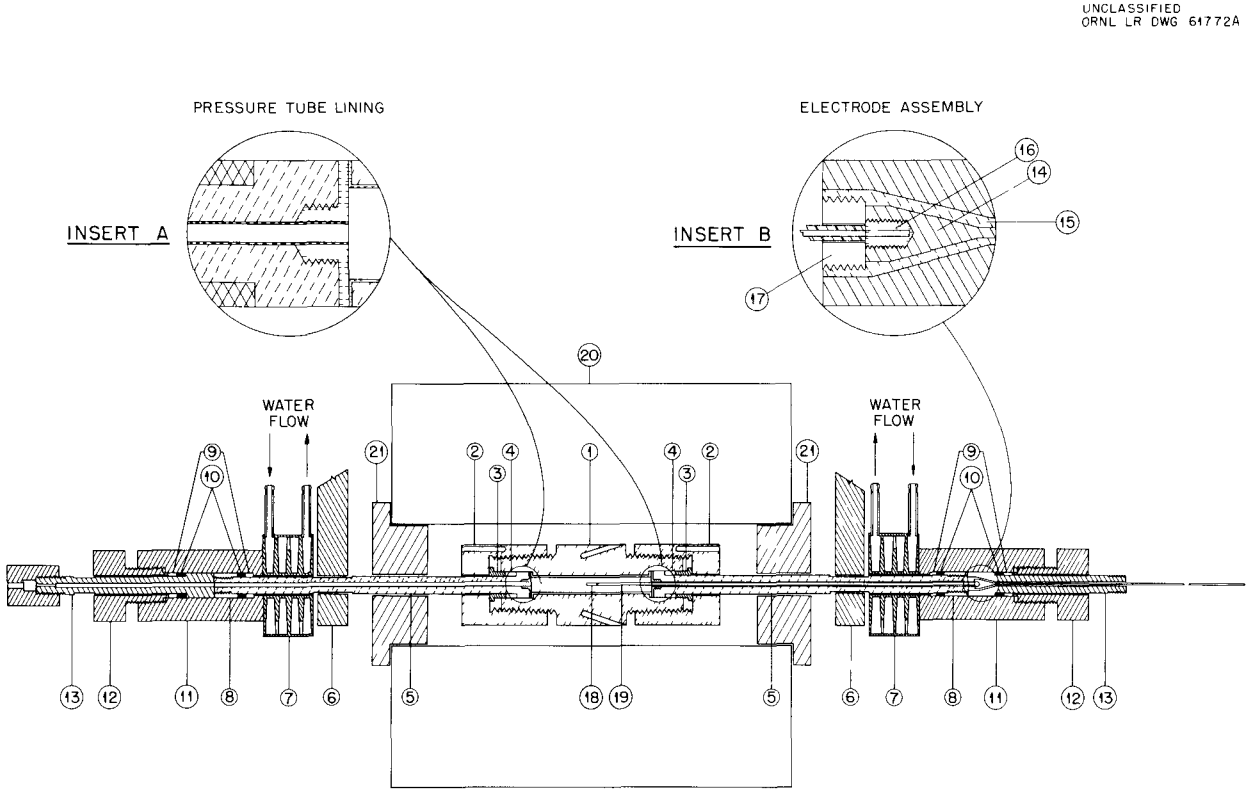

1	Main body (constructed from Udimet alloy)	13	Upper and lower closing pistons
2	Caps (Udimet alloy)	14	Stainless steel cone
3	Tungsten carbide retaining rings	15	Liner reinforced Bakelite
4	Copper packing rings	16	Threaded platinum tip
5	Pressure tubes	17	Teflon plug
6	Stainless steel clamps	18	Pt-Ir cylinder (electrode)
7	Copper cooling jackets	19	Nonporous, sintered Al_2O_3 insulating tube
8, 9	Metal rings (Udimet)	20	Furnace
10	Neoprene packing ring	21	Split, ceramic plugs
11, 12	Closure seals and plugs		

Fig. 8.6. Conductance Cell Assembly.

this cell, measurements of the electrical conductivity of dilute aqueous solutions of inorganic compounds up to temperatures of 800°C and pressures of 60,000 psi were continued. In order to make corrections for the effects of electrode polarization, the apparatus was modified so that conductivity measurements could be made at several frequencies over the range 500 to 20,000 cps to permit extrapolation to an infinite frequency.

Some of the results of measurements on solutions of potassium sulfate are shown in Figs. 8.7–8.9. Figure 8.7 permits a comparison of the effect of pressure on the specific conductivities of 0.005 *m* solution of potassium sulfate and sulfuric acid near room temperature. Exploratory measurements with sulfuric acid at higher temperatures did not give acceptably reproducible values of conductivity. The presence of corrosion products in the solutions remaining after a run is believed to account for the irreproducible results, and modifications of the equipment and measuring procedures are necessary to reduce these effects. The changes include construction of a separator unit incorporating a floating piston to isolate parts of

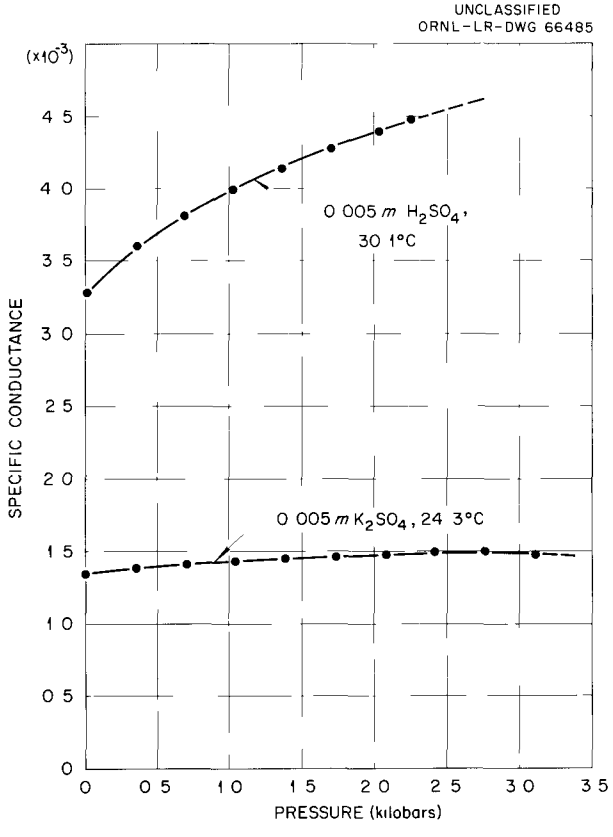

Fig. 8.7. Comparative Effect of Pressure on the Specific Conductance of H_2SO_4 and K_2SO_4 Solutions.

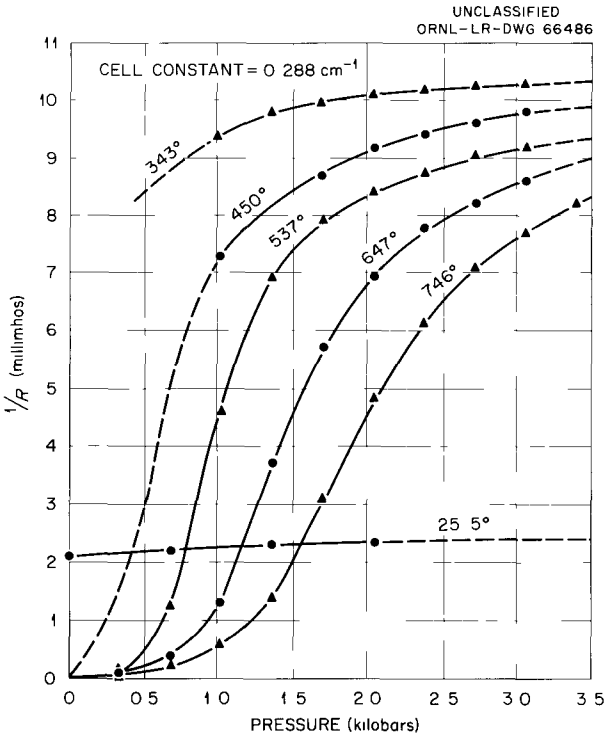

Fig. 8.8. Relative Effect of Pressure on the Conductance of a 0.00218 *m* K_2SO_4 Solution, 25–750°C.

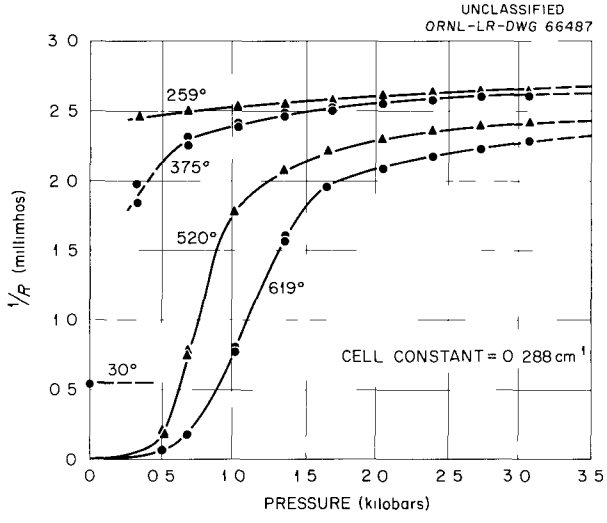

Fig. 8.9. Relative Effect of Pressure on the Conductance of a 0.0005 *m* K_2SO_4 Solution, 25–619°C.

the high-pressure assembly from corrosive solutions, and retention of the solutions in the conductivity cell for minimum lengths of time.

A systematic determination of the specific conductivities of pure water at the various temperatures and pressures is in progress. Completion of these measurements will permit the accurate calculation of equivalent conductance for the various solutes under investigation.

REACTIONS OF AQUEOUS THORIUM NITRATE SOLUTIONS WITH HYDROGEN PEROXIDE[23]

M. J. Kelly D. R. Cuneo G. L. Johnson[24]

Reactions of thorium ion with hydrogen peroxide have been studied since similar thorium ion–deuterium peroxide reactions would occur in a solution blanket for breeder-type reactors.

The interaction between the thorium ion and the peroxide may not be simple since Th^{4+} is susceptible to complexing by anions and undergoes extensive hydrolysis (see "Hydrolysis of Uranium and Thorium Compounds in Aqueous Solutions," this chapter). The principal reported[25,26] hydrolytic species is $Th(OH)_2^{2+}$ (or ThO^{2+}). Kraus and Holmberg confirmed the existence of the former in later work[27] and also established evidence for $Th_2(OH)_4^{6+}$.

Chainlike complexes of formula $Th(^{O}_{OH}Th)_n^{4+n}$ have been reported by Lundgren and Sillen,[28] Lundgren,[29] and Dorby *et al.*[30] in the crystal structures of thorium hydroxide and basic thorium chromate. Hietanen[31] has reported an equilibrium constant equal to $10^{-7.50}$ for successive steps ($n = 0, 1, 2, 3, \ldots$) for

$$Th[(OH)_3Th]_n^{4+n} + Th^{4+} + 3H_2O = Th[(OH)_3Th]_{n+1}^{5+n} + 3H^+ .$$

Such chain species have been proposed to predominate in the latter stages of hydrolysis in solution.

Kraus[32] and Kilpatrick[33] have pointed out that other anions in solution will compete with water and OH^- for positions in the coordination sphere of the metal ion, thus destroying the bridges and reducing the degree of polymerization. These conclusions, by others, strengthen observations by Hamaker[34,35] that the relatively insoluble peroxy compounds show stoichiometry which is dependent on the anions present and the acidity of the solution.

The decomposition studies utilized equipment and techniques previously described.[36] The solutions were prepared from Baker and Adamson cp nitric acid, Mallinckrodt analytical reagent-grade 30% hydrogen peroxide, and Baker and Adamson reagent-grade thorium nitrate (crystal). The thorium content of each solution was determined by ignition to ThO_2. Total acidity was determined by the method of Day *et al.*[37] Iron and copper values were calculated on the basis of additions of previously analyzed stock solutions.

A chosen quantity of 30% H_2O_2 was added to the sample solution, after which successive samples were withdrawn and titrated for peroxide. These data allowed determination of the rate of disappearance of the peroxide.

---

[23]Paper presented December 1961, Combined Regional Meeting, American Chemical Society, New Orleans.

[24]Research participant, Duke University.

[25]E. Chauvenet and J. Tounet, *Bull. soc. chim. France* 47(4), 701 (1930).

[26]E. Chauvenet and Souteyrand-Franck, *Bull. soc. chim. France* 47(4), 1128 (1930).

[27]K. A. Kraus and R. W. Holmberg, *J. Phys. Chem.* 58, 325 (1954).

[28]G. Lundgren and T. G. Sillen, *Arkiv Kemi* 1, 277 (1949).

[29]G. Lundgren, *Arkiv Kemi* 2, 535 (1953).

[30]A. Dorby, S. Guinand, and A. Mathiew-Sicaud, *J. chim. phys.* 50, 501 (1953).

[31]S. Hietanen, *Acta Chem. Scand.* 8, 1626 (1954).

[32]K. A. Kraus *et al.*, paper No. P/731, *Proc. Intern. Conf. Peaceful Uses Atomic Energy, Geneva, 1955* 7, 245 (1956).

[33]M. Kilpatrick, "Polynuclear Complexes Formed in the Hydrolysis of Metal Ions," p 76 in *Proceedings of the Symposium on Coordination Chemistry*, Copenhagen, August 1953.

[34]J. W. Hamaker and C. W. Koch, "A Study of Thorium Peroxides," sec 7.2, part 1, *Production and Separation of U^{233}, Collected Papers*, TID-5223 (1952).

[35]J. W. Hamaker and C. W. Koch, "A Study of Thorium Peroxide Sulfate," sec 7.3, part 1, *Production and Separation of U^{233}, Collected Papers*, TID-5223 (1952).

[36]M. J. Kelly *et al.*, *HRP Quart. Progr. Rept. Oct. 30, 1960*, ORNL-3061, pp 43–44.

[37]H. O. Day, Jr., *et al.*, *Anal. Chem.* 26, 611 (1954).

The solid thorium peroxide nitrate was prepared by adding an excess of 30% H_2O_2 to boiling thorium nitrate solution, filtering the rapidly formed slurry, and washing the residue with boiling water and then with acetone. The flocculent residue was then vacuum-dried for several days at room temperature. The thorium content was determined by ignition, the peroxide by titration with $Ce(SO_4)_2$, the nitrate by Nitron reagent, and the water by difference.

The stoichiometry of thorium peroxynitrate prepared in solution was studied by varying, over a wide range, the concentration of peroxide in several solutions 0.1 *M* in $Th(NO_3)_4$. A reaction time of 24 hr at room temperature produced a solid phase which was easily centrifuged. The supernatant fluid from each solution was analyzed by previously described methods for peroxide, thorium, and hydrogen ion; the composition of the solid phase was determined by difference.

Thorium concentration appeared to have little effect on the decomposition rate; the effects observed could be due to impurities in the thorium nitrate. The catalytic effect of ferric ion is shown in Fig. 8.10. It is seen to be negligible when compared with iron catalysis in other systems, one example being uranyl peroxide in uranyl nitrate solutions.[38] Figure 8.11 shows the catalytic effect of cupric ion in the presence of ferric ion. This effect continued to increase with increasing cupric ion concentration. This is contrary to data reported for uranium solutions,[39] where no further enhancement of rate was observed above 30 ppm of added cupric ion. The effect of temperature on peroxide decomposition in the thorium system was previously reported[40] and has been confirmed as corresponding to an activation energy of about 22 kcal/mole.

Results of analysis of the thorium peroxynitrate, prepared at the boiling point, are shown in Table 8.3. Other preparations prepared at room temperature, both from stoichiometric solutions and those with added acid, gave similar results, perhaps because the precipitate washing process removes excess acid and peroxide while the solid material may still undergo change. It has not been possible to prepare a crystalline solid suitable for x-ray analysis. It may be surmised that water

[38] M. J. Kelly *et al.*, *HRP Quart. Progr. Rept. Apr. 30, 1960*, ORNL-2947, p 50.

[39] M. J. Kelly *et al.*, *HRP Quart Progr. Rept. Apr. 30, 1960*, ORNL-2947, p 52.

[40] M. J. Kelly *et al.*, *Reactor Chem. Div. Ann. Progr. Rept. Jan. 31, 1961*, ORNL-3127, p 57.

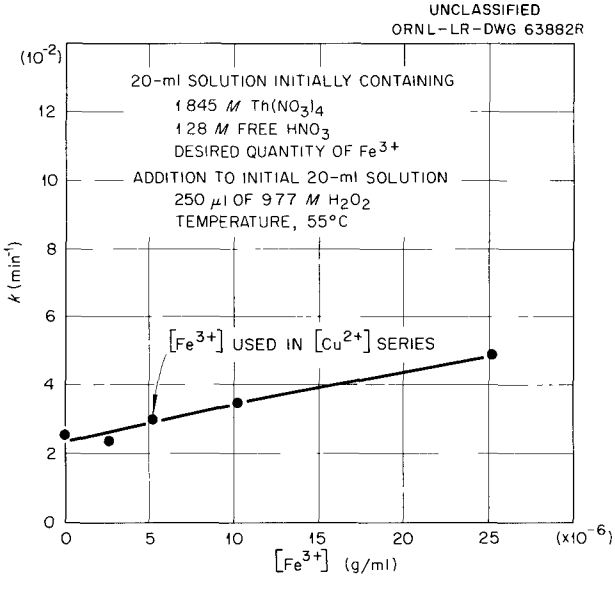

Fig. 8.10. Catalytic Effect of Ferric Ion.

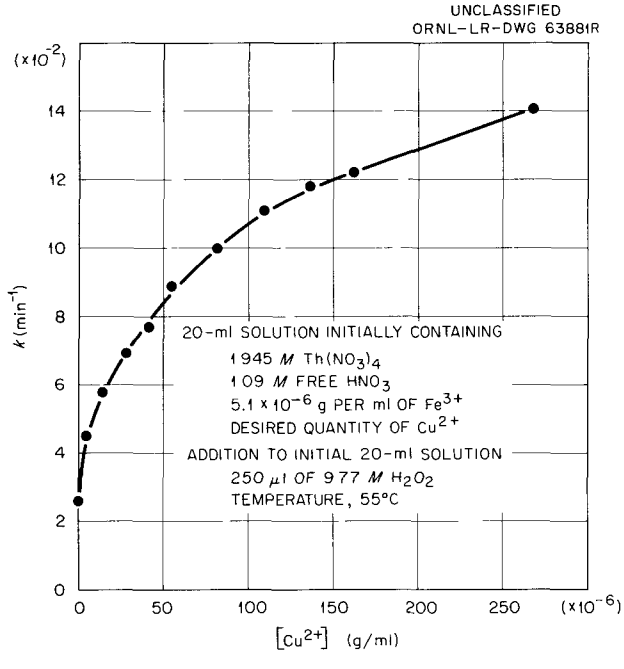

Fig. 8.11. Catalytic Effect of Copper with Ferric Ion Present.

Table 8.3. Results of Analysis of Thorium Peroxynitrate Prepared at the Boiling Point

	Solids Analysis	Solution Analysis	Theoretical[a]
Th^{4+}	1	1	1
O_2^{2-}	1.65	1.73 ± 0.1	1.67
NO_3^-	0.65		0.67
H_2O[b]	1.68		1.67
H^+ (formed)		3.4 ± 0.1	3.33

[a] $Th_6(OO)_{10}(NO_3)_4 \cdot 10H_2O$.

[b] H_2O by difference.

molecules form a hydration sheath that precludes crystal formation. The analytical data are in agreement with the formula

$$Th_6(OO)_{10}(NO_3)_4 \cdot 10H_2O .$$

There are some physical indications that the chain length decreases with added free acid. For instance, a crystallike solid appears in a relatively clear liquid at higher acid concentrations as opposed to a milky slurry, very slow to settle, at lower acid concentrations. The end molecules of the chain structure are believed to be anions from the original system. (Some work has been done with the SO_4^{2-} and Cl^- anions as well as the NO_3^-.)

Data from the solution system tend to confirm results from the solids analysis. Figure 8.12

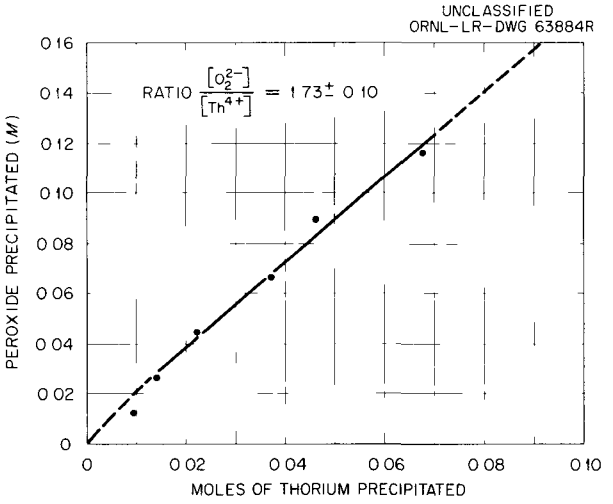

Fig. 8.12. Peroxide vs Thorium Precipitated.

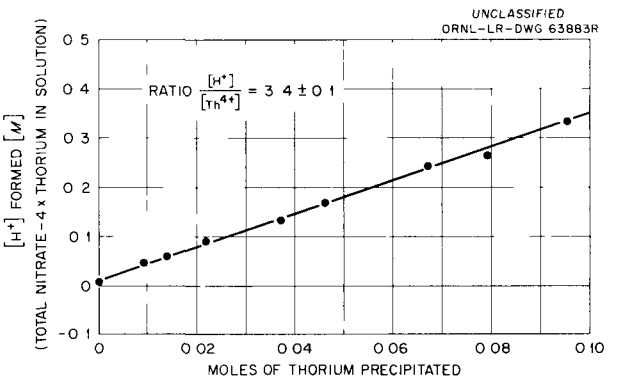

Fig. 8.13. Hydrogen Ion Formed vs Thorium Ion Removed.

shows the ratio of peroxide removed from solution to thorium removed from solution over a wide range of peroxide additions. It is seen that this ratio, 1.73 ± 0.1, is the same as that determined from the solids analysis.

Figure 8.13, which shows the H^+ formed vs the Th^{4+} removed from solution, gives a value for $[H^+]/[Th^{4+}]$ of 3.4 ± 0.1. This is compatible with the calculated value for the proposed structure.

From these studies it was found that the rate of decomposition of thorium peroxynitrate is little affected by iron, normally an excellent catalyst, at solution concentrations acceptable for thorium breeder blanket use. This surprising result, coupled with the catalytic behavior found for the cupric ion, indicates that the mechanism of decomposition is not the same as that found for uranyl solutions.

REACTIONS AND SOLUBILITY OF PROTACTINIUM IN AQUEOUS SOLUTION

M. J. Kelly

C. J. Barton
J. E. Strain[41]
D. R. Cuneo
G. L. Johnson[42]

Stability of Protactinium in Thorium Nitrate–Nitric Acid Solutions at 21 to 200°C

A practical method for removing protactinium from thorium nitrate–nitric acid solutions was reported in the previous annual report.[43] A con-

[41] Analytical Chemistry Division.

[42] Research participant, Duke University.

[43] M. J. Kelly *et al.*, *Reactor Chem. Div. Ann. Progr. Rept. Jan 31, 1961*, ORNL-3127, pp 56–58.

current engineering study by Lindsey[44] indicated that a thorium nitrate solution blanket would be economically attractive for breeding if cheap N^{15} were available and the protactinium formed could be kept below ~50 ppm by continuous removal.

These results encouraged a preliminary investigation to provide data on the stability of protactinium in thorium nitrate–nitric acid solutions at temperatures to 200°C.

Six experiments were performed in which thorium nitrate–nitric acid solutions containing Pa^{231} and Pa^{233} tracer were heated in a stainless steel bomb (8-ml capacity). The apparatus was enclosed in a negative-pressure glove box for safety. The solution samples were passed through a sintered stainless steel filter disk, maintained at approximately the same temperature as the bomb, to remove suspended material.

In the first four experiments the bomb and filter unit were immersed in a solid heat-conductivity medium (sand for experiment No. 1 and aluminum powder for Nos. 2, 3, and 4) contained in a beaker heated by a hot plate. This resulted in a large vertical temperature gradient and therefore considerable uncertainty regarding the solution temperature. The most significant observations from these four experiments [containing 2 *M* $Th(NO_3)_4$ and 3 *M* HNO_3 plus Pa^{231}] were: (a) when the solution was heated to a temperature (above 200°C) where thorium precipitated, almost all the protactinium was also precipitated (experiment 1); (b) a fraction of the protactinium originally in solution in the first two experiments was lost regardless of temperature, probably to the walls of the stainless steel bomb; (c) after the walls of the bomb became saturated with protactinium, solution containing 109 ppm of Pa^{231} showed no change in protactinium concentration at room temperature or when heated to 130 to 155°C for about 90 hr (experiment 3); (d) in the fourth experiment a solution containing 2.5 *M* $Th(NO_3)_4$ and 0.5 *M* HNO_3 with an initial concentration of 23.7 ppm of protactinium showed a loss of about 5% of the protactinium when heated for 82 hr at 140 to 160°C.

The fifth experiment was started by using the powdered-aluminum heating bath, which was then changed to a mercury bath to obtain uniformity of temperature. The initial solution contained 2.5 *M* $Th(NO_3)_4$, 0.5 *M* HNO_3, and 104 ppm of protactinium. The solution stood in the 8-ml bomb for 19 hr at room temperature in contact with several lengths of Zircaloy-2 rod; some of these had been heated quite hot with a burner in air, and the remainder were used as received. The bomb was then heated in the powdered-aluminum bath for 55 hr at approximately 125°C, during which time the protactinium concentration dropped to 92 ppm. The heating bath was then changed to mercury, and the protactinium concentration dropped to 73 ppm after a short heating period at 181°C; further heating at this temperature for 18 hr resulted in a protactinium concentration of 67 ppm. When the temperature was raised to 200°C for 3 hr, the protactinium concentration dropped sharply to 29 ppm.

In experiment 6 the bomb and filter unit was heated by a tubular furnace with a negligible temperature. Short lengths of Zircaloy-2 rod, half of which had been deliberately oxidized (as above), were placed in the solution to determine the effect of this material on protactinium solution stability. There was no significant change in the initial protactinium content of the solution (81 ppm) on standing for 25 hr at 24°C, but 5 hr heating at 175°C resulted in a drop to 30 ppm. Subsequent samples taken during further heating for 48 hr at temperatures ranging from 175 to 210°C gave erratic protactinium concentration values ranging from 7 to 33 ppm, but analysis of the final solution, sampled after cooling to room temperature, gave a protactinium concentration of 27 ppm, indicating that there was probably little change in the protactinium concentration in solution after the initial drop, in spite of the large temperature fluctuation and long heating period. The initial and final solutions (experiment 6) were analyzed for thorium and total nitrate content, with the following results:

Solution Component	Initial Solution Concentration (*M*)	Final Solution Concentration (*M*)
Thorium	2.10	2.06
Total NO_3	8.64	8.40
Free acid (calculated)	0.24	0.16

The free-acid concentration was only 50% of the intended initial value, which may account for the

[44] E. E. Lindsey, *Thorium Nitrate as a Breeder Blanket*, ORNL CF-60-8-150 (Aug. 8, 1960).

sharp drop in protactinium concentration when the solution was heated to 175°C.

The Zircaloy specimens were rinsed in 1:1 HNO_3, removed from the bomb, dried, and counted individually to determine the amount of adherent protactinium. There was no significant difference between oxidized and unoxidized specimens. The total protactinium found on the Zircaloy rods represented only 18% of the amount lost from solution.

One may conclude from these experiments that protactinium is sufficiently stable in thorium nitrate–nitric acid solutions (especially with higher acid concentration; in 0.5 *M* HNO_3, the steady-state concentration of protactinium is seen to be some 67 ppm at 181°C as opposed to 30 ppm at 175°C in 0.24 *M* HNO_3) in contact with stainless steel and Zircaloy-2 to permit the protactinium to be available for removal by continuous processing of a fraction of the blanket solution if the blanket temperature does not exceed the temperature of thorium instability.

Protactinium Solubility in Specific Aqueous Systems

Removal of tracer protactinium from thorium nitrate–nitric acid solutions has been previously demonstrated.[43] To verify these results with measurable quantities of protactinium, a solution containing 2 *M* $Th(NO_3)_4$, 3 *M* HNO_3, and 109 ppm of Pa^{231} previously heated at 130 to 155°C for 90 hr, and then cooled to room temperature, was prepared. A 500-μl portion of this solution was added to 200 μl of 30% H_2O_2, stirred, and centrifuged. The supernatant fluid was sampled and analyzed. A concentration of 2.94 μg of Pa^{231} per milliliter was found; 96% of the protactinium had been removed from the solution with the precipitate. Agreement with previous tracer work was excellent.

A 500-μl portion of this same solution, together with 2 ml of 2 *M* $Th(NO_3)_4$–3 *M* HNO_3 and 5 ml of diisobutyl carbinol in xylene, was placed in a 30-ml separatory funnel, shaken for 7 min, and sampled the following day. Seventy-five percent of the Pa^{231} had been extracted into the organic phase, indicating that the protactinium was in true solution.

Protactinium, precipitated as the hydroxide, was found to be soluble in 1.95 *M* HNO_3 to the extent of 8.21 ± 0.9 μg/ml, in good agreement with the results of Thompson.[45] No precipitation of protactinium peroxide was observed upon the addition of 1 ml of 30% peroxide to 4.5 ml of this solution. Conversely, the precipitate formed by the addition of peroxide to a sulfuric acid solution of protactinium was found to be soluble in 1.95 *M* HNO_3 to the extent of only 2.29 ± 0.75 μg/ml.

[45] R. C. Thompson, "Solubility of Protactinium in Common Acids," sec 6.7, part 1, *Production and Separation of U^{233}, Collected Papers*, TID-5223 (1952).

9. Chemical Aspects of Corrosion of Zircaloy-2

EXAMINATION OF HRE-2 CORROSION SPECIMENS

G. H. Jenks J. E. Baker
M. D. Silverman

Examination of corrosion specimens which had been exposed in various locations in the HRE-2, and for various operating periods, is continuing in the postirradiation examination facility and other remote-examination services at this Laboratory. Several groups of these specimens were removed prior to run 20. The results of examinations of one group were reported in detail[1] in 1961; the results of examinations of others had been reported previously.[2,3] Another group of specimens, mainly those removed after completion of reactor operation, is under examination. All specimens were removed from the reactor by the Reactor Operations Group.

A summary of the latest examinations of specimens removed prior to run 20, showing specimen materials and locations, exposure schedules, and examinations performed, is given in Table 9.1.

With a few exceptions, the results were in near agreement with predictions from in-pile loop tests, indicating comparable corrosion behavior between the in-pile loop and the reactor, or were explicable in terms of poor quality of material, as determined in out-of-radiation tests. The areas of agreement and the exceptions for the principal materials examined are summarized below.

Scale Deposits. – In-pile loop results had shown that most of the scale formed by corrosion in the core or elsehwere is transported to and deposited on surfaces outside the core.[4] The behavior in the HRT was apparently similar. During run 17, there was extensive corrosion in the core and overheating of a core specimen array associated with uranium deposition during power operation; however, examination of specimens recovered from the core indicated that only thin films were on the undamaged surfaces. Specimens exposed at very low fission power densities in the core outlet retained large amounts of scale, which ranged in weight from 3 mg/cm^2 nearest the core to about 25 mg/cm^2 farthest from the core. Specimens from the blanket array which were in contact with solution generating appreciable fission power densities retained little scale (< 1 mg/cm^2). Other specimens recovered from various parts of the circulating systems showed considerable scale deposits, 5 to 10 mg of oxide per cm^2.

Type 347 Stainless Steel. – Average corrosion rates of about 2.5 mpy (based on 890 hr of exposure) for annealed blanket specimens were within the range expected from in-pile loop results. Welded specimens of this material were corroded at about 5 mpy. The core-outlet specimens showed some acceleration of corrosion over that expected during out-of-pile exposures or during exposure at comparably low power densities in in-pile loops (3–5 mg/cm^2 weight losses compared with 1 mg/cm^2 or less[5] for no radiation effect). The specimens exposed in the core and blanket circulating lines showed no acceleration of corrosion over that expected in the absence of radiation.

---

[1] J. E. Baker *et al.*, *HRT Corrosion Samples – Additional Data on Specimens Removed Prior to Run No. 20*, ORNL CF-61-2-95 (Feb. 2, 1961).

[2] A. R. Olsen, *HRE-2 Corrosion Specimens – Blanket Region of Pressure Vessel (Loading No. 1) – Weight Data and Scale Analysis*, ORNL CF-58-10-83 (Oct. 31, 1958).

[3] G. H. Jenks *et al.*, *Examinations of Specimens and Scales Taken from the HRT Following Runs 13 and 14*, ORNL CF-58-9-37 (Sept. 11, 1958).

[4] G. H. Jenks *et al.*, *HRP Quart. Progr. Rept. July 31, 1957*, ORNL-2379, p 103.

[5] G. H. Jenks and J. E. Baker, *In-Pile Loop Corrosion Experiments with Uranyl Sulfate Solutions at 235 and 250°C*, ORNL-3131 (in preparation).

Table 9.1. Summary of Exposure History and Examination of Some HRT Specimens Removed Prior to Run 20

Specimens Examined	Exposure History						Examinations			
	Installed After Run:	Removed After Run:	Approximate Reactor Energy (Mwhr)		Approximate Total Exposure at 250°C or Higher (hr)	Fission Power Density Near Specimen (w/ml)	Visual	Specimen Weight Changes	Scale Weight	Scale Analyses
			Core	Blanket						
Core loading No. 1 (core outlet)[a]	16	17	1504	922	890	0.01–0.10	X	X	X	X
Core loading No. 1 (core)[a]	16	17	1504	922	890	5–6	X			
Blanket loading No. 2[b]	16	17	1504	922	890	0.4–0.5	X	X	X	X
Solution-circulating-line arrays										
No. 103 (pump outlet – core side)[c]	*d*	7	0	0	1333					
	7	13	49	0	737		X	X	X	X
No. 103-A (pump outlet – core side)[c]	13	19	2997	1805	2898		X	X	X	X[e]
No. 203 (pump outlet – blanket side)[c]	*d*	7	0	0	1333					
	7	19	3039	1812	3635		X	X	X	X[e]
No. 125 (pump surge – core side)[f]	*d*	19	3039	1812	4968		X			
No. 125 (pump surge – blanket side)[f]	*d*	19	3039	1812	4968		X			

[a] Twenty-four tensile and impact specimens of various stainless steels and of zirconium and titanium alloys.

[b] Twenty-four tensile and impact specimens of various stainless steels, of Incoloy, and of zirconium and titanium alloys.

[c] Eight coupons, two each of Ti-75A, Zircaloy-2, 347 SS, and 309 SCb.

[d] Before shakedown run.

[e] Scale scraped from titanium holder was analyzed. Scale from coupons not analyzed.

[f] Four coupons: Haynes Stellite No. 12, Haynes Stellite No. 19, Graphitar No. 14, Al_2O_3. One beam-type stress specimen: 347 SS.

It is noteworthy that the low corrosion rates for type 347 stainless steel specimens from the circulating system showed that the high initial rate of steel corrosion in run 13 (about 20 mpy overall rate in the core system, based on the amount of nickel in solution)[6] was not uniform over the surfaces of the high-pressure system and that, therefore, some surfaces, at presently unknown locations, corroded at greater rates than the average.

Zircaloy-2. – Corrosion rates of 3 to 4 mpy (based on 890 hr of exposure) for specimens in the blanket array and negligible rates for the core outlet and circulating line specimens were within the range of expected values.[7]

Titanium Alloy. – Corrosion rates of a few tenths mil per year or less for all specimens for which weight data were obtained were as expected.[8]

AUTOCLAVE TESTS OF ZIRCALOY-2 CORROSION

G. H. Jenks H. C. Savage
R. J. Davis T. H. Mauney

An in-pile autoclave experiment was designed primarily to provide information on the radiation corrosion of Zircaloy-2 by a uranyl sulfate fuel solution at temperatures to 360°C. A leak caused termination of the in-pile exposure before any 360°C operation. However, data of interest were obtained, and they are summarized here. These include: out-of-pile corrosion at 360°C, out-of-pile sorption of uranium on specimen surfaces, and in-pile recombination of radiolytic gases.

The source of the leak was shown to be a loosening of the autoclave closure, probably from yielding of materials (bronze and Zircaloy-2) due to differential thermal expansion in the screw arrangement by which pressure was applied to effect the initial closure. A duplicate experiment leaked during in-pile exposure, before 360°C was reached, because of failure of a platinum capillary tube. The cause of the tube failure was not established.

The autoclave was fabricated of Zircaloy-2 and contained five Zircaloy-2 corrosion test specimens. The autoclave was charged with a solution of 0.08 *m* UO_2SO_4, 0.02 *m* $CuSO_4$, and 0.24 *m* D_2SO_4 in D_2O and with oxygen gas under pressure. The excess acid was required[9] to maintain the chemical stability of the solution at 360°C.

Before in-pile operation, the autoclave was operated at 360°C for 350 hr out-of-pile to obtain corrosion data for comparison with that observed under irradiation. After 124 hr at 360°C, the autoclave was opened and the amount of uranium sorption in the surface film on the test specimens was determined by alpha counting.

The in-pile tests completed were concerned with a determination of the activity of the copper catalyst for recombination of radiolytic gases. Recombination rates at temperatures of 230, 250, and 280°C were obtained.

Out-of-Pile Corrosion

The average overall penetration of the Zircaloy-2 during 350 hr at 360°C was 0.07 to 0.08 mil. For the last 300 hr, the corrosion rate was about 1.3 mpy, based on oxygen uptake; this is in line with an extrapolation of rates for Zircaloy-2 in a previous autoclave experiment[10] with uranyl sulfate solution at 290°C. However, it is considerably below the 8 mpy obtained on Zircaloy-2 weld metal with a similar solution in a pump-loop test.[11]

Uranium Sorption on Specimen Surfaces

After 124 hr of out-of-pile operation at 360°C, the quantity of uranium sorbed on the water-washed Zircaloy-2 specimen surfaces averaged 0.24 $\mu g/cm^2$. Values for the ten surfaces (two sides of five specimens) ranged between 0.19 and 0.29 $\mu g/cm^2$. These values are low compared

[6] J. R. Engel *et al.*, *Summary of HRE-2 Run No. 13*, ORNL CF-58-10-115 (Oct. 29, 1958).

[7] G. H. Jenks, *Review and Correlation of In-Pile Zircaloy-2 Corrosion Data and a Model for the Effect of Irradiation*, ORNL-3039 (July 6, 1961).

[8] G. H. Jenks and J. E. Baker, *In-Pile Loop Investigation of Corrosion of Zircaloy-2 and Other Reactor Materials in 0.04 m UO_2SO_4 at 280°C*, ORNL-2962 (In press).

[9] W. L. Marshall *et al.*, *HRP Progr. Rept. Nov. 30, 1960*, ORNL-3061, p 53.

[10] G. H. Jenks, *Effect of Radiation on the Corrosion of Zircaloy-2*, ORNL CF-57-9-11, p 14 (Sept. 30, 1957).

[11] J. C. Griess, *HRP Progr. Rept. May 31, 1961*, ORNL-3167, p 62.

with a few tens of micrograms per square centimeter previously found[12,13] on specimens irradiated in solutions containing about one-tenth as much excess acid as that in this test. Correlations of the in-pile corrosion data[7] and out-of-pile tests of uranium sorption on hydrous zirconia[14] also indicate marked reduction of uranium sorption with increased excess-acid concentration.

[12]G. H. Jenks *et al.*, *HRP Quart. Progr. Rept. Jan. 31, 1958*, ORNL-2493, p 125.

[13]G. H. Jenks *et al.*, *HRP Quart. Progr. Rept. Apr. 30, 1959*, ORNL-2743, p 162.

[14]R. J. Davis *et al.*, unpublished work.

Rates of Recombination of Radiolytic Gases

Recombination-rate constants as a function of temperature for the copper-catalyzed recombination of radiolytic gas were estimated by analyses of the rate of pressure increase following initiation of irradiation. The values obtained at 230, 250, and 280°C are shown in Fig. 9.1. The analysis does not require a knowledge of G_{D_2}, but does include the solubility of D_2. Values used for D_2 solubility were 0.454, 0.377, and 0.283 psi cc^{-1} liter (volumes at STP) at 230, 250, and 280°C respectively.

The values in Fig. 9.1 are lower by about one-third to one-half than those predicted for uranyl

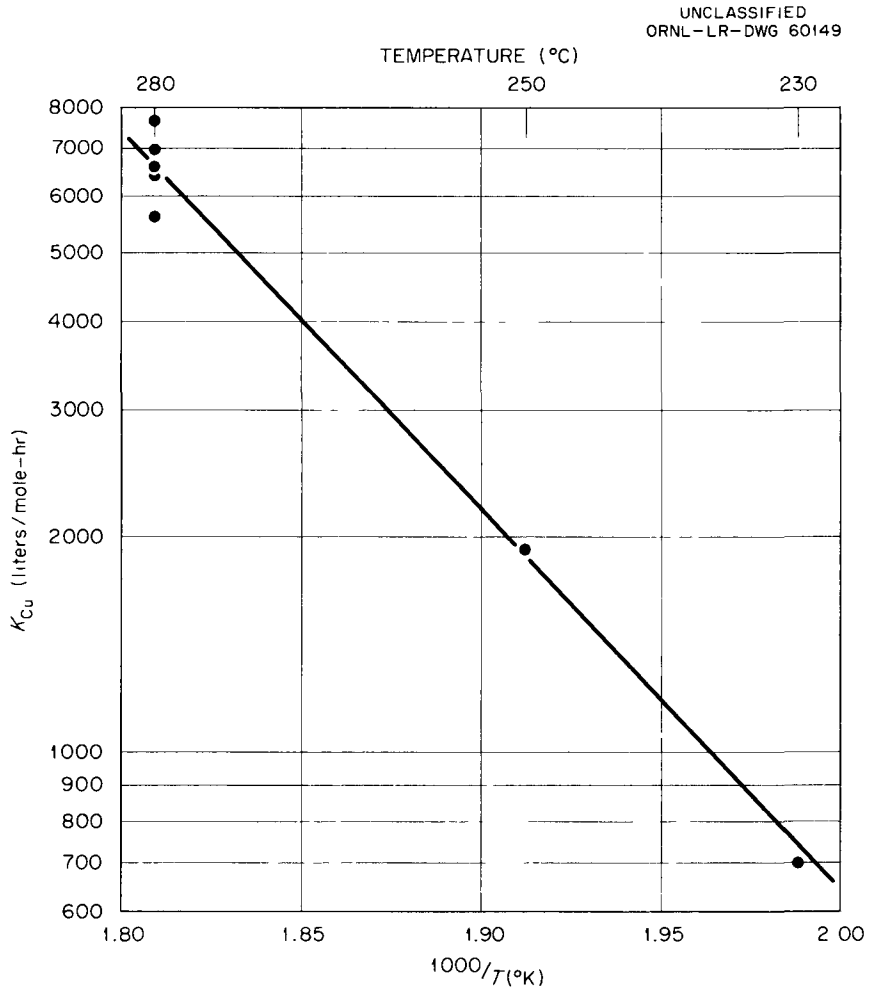

Fig. 9.1. Values of K_{Cu} in 0.08 *m* UO_2SO_4, 0.02 *m* $CuSO_4$, 0.24 *m* Excess D_2SO_4, in D_2O Solution.

sulfate solutions (D_2O solvent) with lower acid concentrations.[15-18] Thus it appears that the results are in agreement with rates obtained in other tests, which indicate a decrease in K_{Cu} with increased excess-acid concentrations.[18,19]

OXIDE GROWTH AND CAPACITANCE ON PREIRRADIATED ZIRCALOY-2

R. J. Davis G. H. Jenks

Fission fragments or reactor radiations greatly increase the rate of corrosion of Zircaloy-2 in aqueous solutions. One mechanism for the radiation effect which is considered possible is that radiation damage in the metal leads to an increased reaction rate through an increase in the metal reactivity or through the formation of oxide with poor protective qualities.[7] In a study of the effects of damage in the metal, growth rate and protective qualities of oxide formed on preirradiated Zircaloy-2 will be investigated. The qualities of the oxide will be gaged by capacitance measurements.[20]

The $3\frac{1}{2}$-in.-long, $\frac{3}{16}$-in.-diam specimens to be used will be machined, mechanically polished, and irradiated in an inert environment. They will then be oxidized, with unirradiated controls, in 300°C steam plus oxygen. Periodically the specimens will be removed for weight-gain and capacitance measurements. Variations in the penetration-time behavior and capacitance-penetration behavior are expected to give good clues to the mechanism of radiation corrosion.

The vacuum system for evacuating the irradiation capsules and filling them with helium has been built. The steam-oxygen furnace, which oxidizes up to four specimens at a time, has been built and tested. Specimens can be heated in the furnace to 300 ± 5°C in 30 sec, which will enable meaningful exposure for 5 min or longer. A microbalance has been set up and is apparently capable of measuring specimen weight changes to a few micrograms. A General Radio Company No. 1750-A impedance bridge, a Hewlett-Packard model 200 CD wide-range oscillator, an oscilloscope, and an appropriate cell have been set up for the capacitance measurements. All of the equipment has been tested.

Preliminary experiments with unirradiated specimens are planned to demonstrate possible effects of exposure schedule on subsequent corrosion and/or capacitance values and of the capacitance measurements on subsequent corrosion. The first exposures will be of freshly machined and abraded specimens to reactor irradiation in a helium atmosphere.

SORPTION ON HYDROUS ZIRCONIA IN UO_2SO_4 SOLUTION AT ELEVATED TEMPERATURES

R. J. Davis G. H. Jenks
S. H. Wheeler

Investigation of the sorption of uranium and other solutes on hydrous zirconia in uranyl sulfate solutions continued, with the immediate objective of characterizing uranium and sulfate sorption with respect to oxide surface area, concentrations of UO_2SO_4 and excess acid, and temperatures in the range 100 to 300°C. A more distant objective was the determination of the effects on sorption of other solution additives, such as lithium, copper, and nickel sulfates. The work was discontinued before the latter objective was reached. The status of the work directed toward the first objective is summarized here. The results of previous investigations of some features of the sorption have been reported.[21,22]

[15] R. J. Davis *et al.*, *Autoclave Studies of Radiation Corrosion of Zircaloy-2 in UO_2SO_4 Solution* (in press).

[16] M. J. Kelly *et al.*, *The Effectiveness of Cupric Ion as a Homogeneous Catalyst in the UO_3-HNO_3-H_2O Systems for the Recombination of Hydrogen and Oxygen Produced by Radiolytic Decomposition*, ORNL CF-59-9-15 (Sept. 3, 1959).

[17] G. H. Jenks and J. E. Baker, *Apparent Copper Rate Constants in In-Pile Loop Experiment L-2-22*, ORNL CF-60-3-88 (Mar. 23, 1960).

[18] M. J. Kelly *et al.*, *HRP Progr. Rept. Oct. 31, 1959*, ORNL-2879, p 94.

[19] H. F. McDuffie *et al.*, *The Radiation Chemistry of Homogeneous Reactor Systems. III. Homogeneous Catalysis of the Hydrogen-Oxygen Reaction*, ORNL CF-54-1-122 (Jan. 26, 1954).

[20] J. N. Wanklyn and D. R. Silvester, *J. Electrochem. Soc.* 105, 647 (1958).

[21] G. H. Jenks *et al.*, *Reactor Chem. Div. Ann. Progr. Rept. Jan. 31, 1961*, ORNL-3127, pp 90–93.

[22] G. H. Jenks *et al.*, *HRP Quart. Progr. Rept. Aug. 1 to Nov. 30, 1960*, ORNL-3061, pp 69–73.

With D_2O solutions of uranyl sulfate plus D_2SO_4, 110 experiments were performed. Uranyl sulfate and D_2SO_4 initial concentrations were varied respectively from 0.02 to 0.17 *M* and from 0.02 to 0.2 *M*. Exposure temperatures were 100, 200, 250, 280, and 300°C, and the exposure time was 3 hr in each case.[21,22] The methods were similar to those previously reported for experiments with light-water solutions.[23] The zirconia was the same as that used previously, hydrous oxide from City Chemical Company which was preheated for 2 hr at 100°C in air before storage in capped bottles. The three batches of this material, designated AF oxide, contained 36 to 44% H_2O and 1.4 to 2% SO_3. Previous work indicated that the sulfate is present as H_2SO_4 and as alkali-metal and alkaline-earth sulfates and that these materials are mobile during high-temperature exposure.[24] The surface area before use was 275 to 383 m^2 per g of ZrO_2 by nitrogen adsorption.

Surface Areas After Solution Exposure

Surface areas of the residual oxides were measured by nitrogen adsorption. The primary purpose of these measurements was to provide a possible basis for correlation of the uranium and other sorption data. The experimental spread of the data was quite large, but general correlations between surface area and temperature of exposure and between surface area and sulfate ion concentration were noted. The areas ranged from 545 to 100 m^2 per g of ZrO_2, with the lowest values produced by solutions of high sulfate concentration, and the highest at the two lowest temperatures in solutions in which the final concentrations of excess acid were near or below zero. Other variables, such as the excess-acid concentration and differences in the kinetics of the surface area changes, probably influenced the relative areas also.

Several analyses for zirconium in solution after 250°C exposures showed a regular increase in dissolved zirconium with increasing sulfate concentration, which suggests that the final surface areas are inversely related to the amounts of zirconium dissolved.

Total Sulfate Sorption

The total amount of sulfate sorbed was evaluated as the sum of that sorbed from solution, as shown by analysis before and after equilibration, plus that initially in the zirconium oxide. For low excess-acid concentrations, which varied with temperature, the amounts of sulfate sorbed at all temperatures fell within the same range, mostly between 0.004 and 0.007 millimole/m^2 at sulfate concentrations ranging from 0.02 to 0.33 *M*. Marked increases in sulfate sorption above these values, due to increased acid sorption, occurred at final acid concentrations greater than about 0.01 *M* at 100°, 0.03 to 0.06 *M* at 200°, or 0.05 to 0.07 *M* at 250°, but did not occur at concentrations up to 0.15 *M* at 280 or 300°C. The sorption at these higher acidities did not exceed 0.028 millimole/m^2. The results of analyses for zirconium in final solutions, mentioned in the preceding paragraph, indicated that the increases were not a result of dissolution of ZrO_2.

The sorption of 0.006 millimole/m^2 corresponds to about 4×10^{14} ions/cm^2, about that estimated for sulfate monolayer formation, with an average area of 23 A^2 per sulfate ion. Thus it is concluded that sulfate adsorption in the low-acid solution may be explained as monolayer or near-monolayer formation. Some form of multilayer adsorption probably occurred in the solutions of higher acidities.

Uranium Sorption

With solutions initially containing 0.02 *M* acid and $\geq$0.08 *M* uranium, sorption of uranium did not change appreciably in the temperature range 100 to 300°C. However, at 0.17 *M* UO_2SO_4 the 250°C data scattered appreciably, and at 280 and 300°C marked increases in uranium sorption occurred. It is believed that these changes are related to the formation of the concentrated second liquid phase near these temperatures and solution concentrations. This is borne out by the fact that at higher initial acidities (0.06 to 0.2 *M*), which raise the temperature of second-liquid-phase formation, the uranium sorption showed no irregularities of the types observed at the lower acidity. The sorption increased with increasing

[23] J. C. Banter and S. H. Wheeler, *Adsorption of Uranium on Hydrous Zirconium Oxide from Uranyl Sulfate Solution at Elevated Temperatures*, ORNL CF-61-3-94 (Mar. 1, 1961).

[24] Gerald Goldstein, *Sorption of Uranium on Zirconium Oxide*, ORNL-3177 (Aug. 28, 1961).

uranium concentration, as reported previously[21-24] for H_2O solutions at 250 to 300°C. The amounts sorbed from the solutions with 0.02 *M* initial acid were also in rough agreement with those found in the studies with water solutions.

At higher initial acidities (0.06 to 0.2 *M*) the uranium sorption was lower in most cases by factors of about 2 to 3 or more. There were no definite correlations between amounts sorbed and initial excess acid in this range of acidities. Comparisons of bands drawn to encompass the data show that there was little effect of temperature on the sorption in the range 100 to 300°C.

The final acidities were generally much lower than the initial ones. Preliminary considerations have indicated a correlation between uranium sorbed and the estimated final hydrogen ion concentration at the temperature of exposure. More accurate estimates of the hydrogen ion concentration, as well as the concentrations of other species at temperature, appear worthwhile as a basis for correlation of the results with respect to solution composition and for evaluation of the adsorption mechanisms.

ELECTROCHEMICAL STUDIES OF ZIRCALOY-2 CORROSION

A. L. Bacarella

It has previously been demonstrated[25] that electrochemical measurements could be performed on a corroding specimen at high temperatures (200 to 300°C) and pressures (1000 to 2000 psi). In view of this success it was considered of interest to extend the program and measure other electrochemical parameters. Potentiostatic (constant potential) and galvanostatic transient techniques are employed to obtain these data. It is true that the same information is obtained from the potentiostatic measurements as from the previously performed galvanostatic measurements. However, potentiostatic experiments are much easier to interpret, and in some cases (as used here) easier to perform.

A Zircaloy-2 electrode was chemically polished (100 cc H_2O, 100 cc HNO_3, 16 cc 4% HF) and then passivated at 293°C in oxygenated 0.05 *M* H_2SO_4. The electrode was exposed for 13 days at these conditions, after which corrosion currents were measured potentiostatically as a function of potential (−1.400 to +0.300 v vs Pt) and temperature (150 to 300°C) in the same oxygenated aqueous acid solution.

The measurements were carried out in a titanium reaction cell designed to contain approximately 50 cc of aqueous acid at 300°C and 2000 psi. The reaction cell contained five ports, four at the top and one at the bottom. Solution entered through the bottom port and exited from one of the top ports. The other three ports contained a titanium thermocouple well, the platinum reference electrode, and the Zircaloy-2 test electrode. Teflon cones were used to insulate these electrodes from the reaction cell and to provide a pressure seal. At the temperatures used it was necessary to air-cool the Teflon cones to maintain the pressure seals. This was accomplished with two titanium-tube extensions which were air-cooled at a rate such that the temperature at the Teflon seal positions was about 30°C and independent of the temperature of the reaction cell.

Potentiostatic measurements require the reference potential to be independent of any temperature or solution composition changes in the reaction cell. To effect this the platinum reference electrode was situated entirely in the air-cooled titanium-tube extension of the reaction cell. The temperature at the platinum reference position was therefore constant, and, thus, the potential also. The results of these measurements are shown in Figs. 9.2 and 9.3.

These results can be interpreted according to Eq. (1):[26]

$$J_p = (J_a - J_c) = K_a' \exp -\left[\frac{\Delta H_a^{\circ\ddagger} - (\alpha\lambda)_a FE}{RT}\right] - K_c' \exp -\left[\frac{\Delta H_c^{\circ\ddagger} + (\alpha\lambda)_c FE}{RT}\right]. \quad (1)$$

Here J_p is the net current, J_a and J_c are the anodic and cathodic partial process currents, the K's contain the potential- and temperature-independent portions of the specific rate constants of the

[25] A. L. Bacarella, *J. Electrochem. Soc.* **108**, 331 (1961).

[26] This equation assumes only one anodic and one cathodic partial process both under activation control.

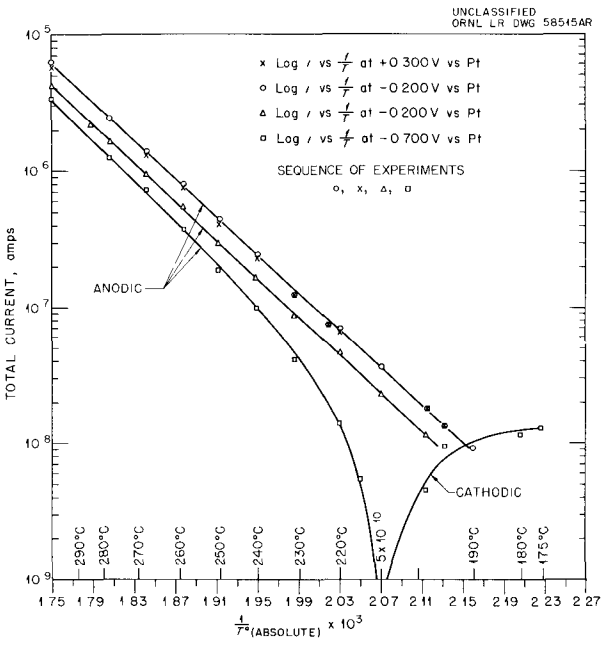

Fig. 9.2. Logarithm of Current vs Reciprocal of Temperature for Passivated Zircaloy-2 in Oxygenated 0.05 *m* H_2SO_4 at Various Fixed Potentials.

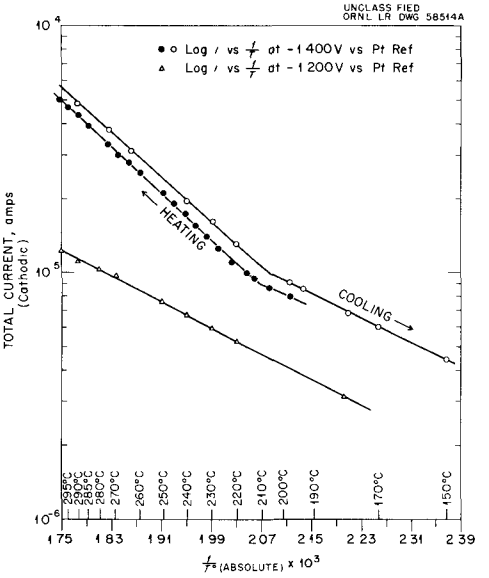

Fig. 9.3. Logarithm of Current vs Reciprocal of Temperature for Passivated Zircaloy-2 in Oxygenated 0.05 *m* H_2SO_4 at Various Fixed Potentials.

partial process and the concentration of the reactants, and $\Delta H_a^{\circ\ddagger}$ and $\Delta H_c^{\circ\ddagger}$ are the (standard) enthalpies of activation of the anodic and cathodic partial processes respectively. The $(\alpha\lambda)$'s and E have the usual meaning: $(\alpha\lambda)$ is the electrochemical transfer coefficient for the anodic and cathodic reaction, and E is the measured potential.

The interpretation of the results reported here is considered tentative, because a visual examination of the specimen reveals small areas of nonuniform corrosion.

In Figs. 9.2 and 9.3 the measured currents are plotted as a function of the reciprocal of temperature for the various chosen constant potentials. The general interpretation of these data, based on the relationship shown in Eq. (1), is the following: At the more anodic potentials (E more positive) the contribution of the cathodic current becomes negligible; similarly, at the more cathodic potentials (E more negative) the contribution of the anodic current to the measured net current is negligible. At intermediate potentials, −0.700 v vs Pt (Fig. 9.2), for example, the contribution of the cathodic current to the measured net current is negligible from 300 to 240°C, but at lower temperatures the cathodic current becomes more and more significant, and at 212°C the anodic and the cathodic current are equal and $J_p = 5 \times 10^{-10}$ amp, or nearly zero (this also implies that $E = E_0$, the open-circuit potential). At potentials between −0.700 to −1.200 v vs Pt, the measured net current is a complicated function of temperature and is probably explained by contributions from several factors entering into Eq. (1).

From the data in Figs. 9.2 and 9.3 it was found that the activation energy for the anodic partial process (oxidation of zirconium) is 31.1 kcal/mole and is independent of potential and temperature in the range studied. The activation energy for the cathodic partial process (reduction of oxygen) is, however, a function of potential and temperature, 10.8 kcal/mole at −1.400 v vs Pt between 220 and 300°C, changing to 5.4 kcal/mole at temperatures below 220°C. At −1.200 v vs Pt the activation energy is 5.4 kcal/mole over the entire temperature range.

When the data are presented as in Table 9.2, it is seen that at positively increasing potentials (series 1 to 2 and 3 to 4) a steady-state rate,

Table 9.2. Current as a Function of Time and Potential for Zircaloy-2 in Oxygenated 0.05 *M* H_2SO_4 at 298°C in the Passive State

Measurement Series	Time of Measurement (After 13 Days Prior Exposure) (hr)	Potential vs Pt (v)	*I*, Steady-State Total Current (amp)
			$\times 10^{-6}$
1	0	−0.933	6.0[a]
2	0 to 192	−0.200	Initially 25; decreases to 6.0[b]
3	216 to 336		No measurements[c]
3	336	−1.025	6.0[a]
4	336 to 358	+0.300	Initially 35; decreases to 6.0[b]
5	358 to 360.5	−0.200	4.3
6	360.5 to 363.5	−0.700	3.4
7	366	−1.035	1.8[a]
8	376	−1.023	4.9[a]

[a]These are open-circuit results; total current was obtained from small current polarizability, with

$$\Sigma(\alpha\lambda) = 1/2, \quad I = RT/F[\Sigma(\alpha\lambda)], \quad \text{and} \quad (\Delta E/\Delta I)_{I\to 0}.$$

[b]Steady-state current.

[c]Temperature during this period was 24°C.

6.0×10^{-6} amp, independent of potential is obtained. Subsequent measurements at negatively increasing potentials (series 5 to 7, 8) indicate corrosion currents less than the steady-state value. It is proposed that these results are not for steady-state conditions, and that given sufficient time at these potentials the rate should increase to the same steady-state value. That this is so is indicated by the results at open circuit, (7) and (8), which show an increase in corrosion current with time.

It is suggested that the model proposed by Vetter[27] for film formation on passive iron can explain these results.

The essential factors proposed by Vetter for film formation on passive iron are: (1) inside the oxide there is a field which pulls the ions through the film, (2) the ionic current changes with the field intensity, (3) these ions comprise the corrosion current and may enter into film formation or solution, (4) a potential difference at the oxide-solution interface is established through the equilibrium $O^{2-} + 2H^+ \rightleftharpoons H_2O$, (5) the ionic current through oxide-solution interface is determined by the potential difference at this interface.

The results are explained on the basis of this model as follows: At the potentials −0.200 v vs Pt and +0.300 v vs Pt the field strength in the oxide is increased and, consequently, the ionic current is increased (see factor 2 above). However, the ionic current across the oxide-solution interface is unchanged (factors 4 and 5). Consequently, since the ionic current through the oxide is greater than the current from oxide to solution, the excess goes into film formation. As the film thickness increases, the field strength and, therefore, the ionic current through the oxide decrease until steady state is again established, whereby the ionic current through the oxide is equal to the ionic current across the

[27]K. J. Vetter, *Z. Elektrochem.* 62, 642 (1958).

oxide-solution interface. Since the potential established at the oxide-solution interface via the $O^{2-} + 2H^{+} \rightleftharpoons H_2O$ equilibrium is a function of the temperature and pH (both constant), and since the current into the solution phase is controlled by this potential, the steady-state rate is a constant and is independent of total potential. The thickness of the oxide is, however, a function of this potential.

For measurements after that at +0.300 v vs Pt (series 5–8, Table 9.2), at less positive potentials, the field strength in the oxide is decreased and the ionic current through the film is less than the current from oxide to solution. Consequently, the net current is not at steady state; thus the film thickness decreases and the field strength increases until steady state is again established.

These conclusions will receive further testing, particularly those relating to film dissolution. A most important test will, however, involve the rate and potential dependence on pH *through* the equilibrium $O^{2-} + 2H^{+} \rightleftharpoons H_2O$.

10. Corrosion by Solutions

J. C. Griess
J. L. English
L. L. Fairchild
D. N. Hess
T. H. Mauney
H. C. Savage
P. D. Neumann
J. G. Rainwater[1]
L. Rice
J. F. Winesette

CORROSION STUDIES FOR THE AQUEOUS HOMOGENEOUS REACTOR PROGRAM

Stress-Corrosion Cracking of Type 347 Stainless Steel in Uranyl Sulfate Solutions

During the past year a program to study the effects of several variables on the stress-corrosion cracking behavior of type 347 stainless steel in simulated chloride-containing aqueous fuel solution (0.04 *m* UO_2SO_4, 0.02 *m* H_2SO_4, and 0.005 *m* $CuSO_4$) was completed. Part of the data was reported previously.[2-6] The following paragraphs summarize the major results derived from the entire investigation.

Stressed specimens from two different heats of type 347 stainless steel exhibited failure rates of 48 and 85%, respectively, in an air-aerated and boiling solution containing 50 ppm of chloride, 0.04 *m* UO_2SO_4, 0.02 *m* H_2SO_4, and 0.005 *m* $CuSO_4$. The difference in observed failure rates appeared to be related to minor variations in chemical composition and/or metallurgical condition in the two heats.

The cracking frequency of both heats of steel was independent of chloride concentration between 25 and 500 ppm in the boiling solution; no cracking occurred at chloride levels of 10 ppm or less. If cracking was observed, it generally took place during the first 500 hr. Cracks were transcrystalline in nature.

The susceptibility to cracking was markedly decreased, but not completely eliminated, by removal of oxygen from the solution. Increasing the dissolved-oxygen content increased the cracking frequency.

Cracking in the chloride-containing uranyl sulfate solution was observed at temperatures as low as 50°C (122°F), although the cracking frequency was low.

Addition of mercuric chloride to the boiling uranyl sulfate–chloride solution greatly increased cracking frequency and reduced the time required for crack initiation. However, when only mercuric chloride was added to the uranyl sulfate solution, cracking did not occur. Other additives such as zinc, arsenic, antimony, and platinum salts had no effect on cracking behavior.

Sodium dichromate (~ 100 ppm) effectively prevented cracking in the boiling uranyl sulfate–chloride solution. As expected, precipitation of chloride ion from solution as silver chloride produced the same effect.

The data indicated that uranyl ion concentration up to about 0.40 *m* enhanced the ability of the solution to produce cracks, but no cracking was experienced in boiling uranyl sulfate–chloride solutions when the uranyl sulfate concentration was 0.40 *m* or greater.

---

[1] Summer research participant from the University of Arkansas.

[2] J. C. Griess *et al.*, *HRP Quart. Progr. Rept. Apr. 30, 1957*, ORNL-2331, pp 90–91.

[3] J. C. Griess *et al.*, *HRP Quart. Progr. Rept. Oct. 31, 1957*, ORNL-2432, pp 82–83.

[4] J. C. Griess *et al.*, *HRP Quart. Progr. Rept. Jan. 31, 1958*, ORNL-2493, p 92.

[5] J. C. Griess *et al.*, *HRP Progr. Rept. Apr. 30 and July 31, 1958*, ORNL-2561, pp 119–20.

[6] J. C. Griess *et al.*, *HRP Quart. Progr. Rept. Jan. 31, 1959*, ORNL-2696, pp 89–90.

Residual stresses in specimens due to cold work were of sufficient magnitude to promote cracking in the absence of an applied stress. Annealing of the specimens eliminated cracking.

Substantial reduction in cracking frequency was realized by exposure of specimens to the chloride-free fuel solution prior to immersion in the same solution containing 50 ppm of chloride. Pre-exposure times of 5 to 500 hr were equally effective, as were pretreatment temperatures of 100 to 300°C. Similar results were obtained whether the specimens were pretreated before or after stressing.

Corrosion Behavior of QMV Beryllium in Heavy Water at Elevated Temperatures

Autoclave tests were initiated to examine the corrosion behavior of hot-pressed QMV beryllium and that of beryllium oxide in heavy water at elevated temperatures. The tests were conducted to determine whether unclad beryllium or beryllium oxide could be used as a reflector material in a replacement HRE-2 core assembly.

The sintered and hot-pressed QMV beryllium specimens were representative of the quality of metal used for the reflector in the MTR and were obtained from the Brush Beryllium Corporation. The beryllium oxide, a commercial grade designated as UOX material, was procured from the same source. Tests of 60 to 120 days in degassed and in oxygenated heavy water at 250 and 300°C were conducted. The oxygenated tests were run by pressurizing the autoclaves with 10 psi of oxygen at room temperature. The following specimens were exposed in each of the four environments: three beryllium coupons, two beryllium oxide wafers, and single beryllium-to-beryllium, beryllium–to–Zircaloy-2, and beryllium–to–type 347 stainless steel couples.

The results of the investigation thus far are summarized in the following paragraphs.

There was no apparent difference in corrosion behavior in degassed water at 250 and 300°C after 120 days; specimens exposed at both temperatures developed a thin, tenacious film, which could not be completely removed by standard descaling techniques, and exhibited small weight gains. Some pitting was observed; pits ranged up to 1.6 mils deep at 250°C and up to 3.6 mils at 300°C.

In the presence of oxygen, thicker films were found on specimens both at 250 and 300°C; defilmed corrosion rates (not all scale removed) for 120 days were 0.2 mpy or less. Some pitting attack was experienced at both temperatures; the intensity of the attack was the same in both cases (2.4 mils maximum depth).

The coupling of beryllium to beryllium in degassed water at 250 and 300°C produced no adverse effects after 90 days. All specimens showed slight weight gains and shallow pitting attack (3.0 mils or less in depth). When oxygen was present, defilmed corrosion rates between 0.2 and 0.5 mpy were obtained. Pitting was slightly more intense on contact surfaces (up to 4.1 mils) than on other surfaces.

At 250 and 300°C in degassed water, the coupling of Zircaloy-2 to beryllium produced no major effect on either member of the couple. The beryllium specimens showed small weight increases and some shallow pitting (2.4 mils or less) on contact surfaces. However, in the presence of oxygen, attack on the beryllium members was pronounced. At 250°C, the defilmed rate was 1.1 mpy after 120 days; at 300°C, the rate was lower, 0.5 mpy. Pits up to 4.0 and 6.4 mils in depth were measured on contact faces at 250 and 300°C respectively.

Beryllium coupled with type 347 stainless steel in degassed water at both temperatures underwent little attack after 60 days. Specimens exhibited slight weight gains and mild pitting on contact surfaces. The addition of oxygen to the system resulted in near-catastrophic attack on the beryllium members of the couples, particularly at 250°C. The attack assumed the form of massive pits, approximately 100 to 125 mils in depth, over all surfaces. Heavy tubercles of white corrosion product were much in evidence.

Beryllium oxide corroded at rates of 1.0 and 1.2 mpy in degassed water at 250 and 300°C respectively. In the presence of oxygen, a rate of 1.5 mpy was obtained at both temperatures. The corrosion was uniform on all specimens, and attack rates decreased with time during the 120-day test period.

Corrosion in the Steam Generator of the HRE-2

Corrosion assemblies which were exposed in the steam generators of the HRE-2 for nearly three and one-half years were removed after the

final shutdown of the reactor in May 1961. These specimens were examined for evidence of corrosion damage, and a report of the findings has been prepared.[7]

Three stainless steel alloys, three carbon steel alloys, and two titanium alloys were fabricated into simple-beam-type corrosion test assemblies. One member of each assembly was stressed to approximately 70% of its annealed yield stress for testing. Two simulated tube-to-tube-sheet joints were also fabricated from type 347 stainless steel for inclusion in the study.

The weight-loss determinations and metallographic examinations of these materials indicated that the stainless steels (types 347, 309 SCb, and Croloy 16-1) and titanium alloys 55A and 75A were not corroded significantly (<0.1 mpy) in the steam generators. The carbon steel alloys (A212 grade B, A105 grade 2, and A106 grade B) showed average corrosion rates of approximately 0.3 mpy, with only scattered light pitting and crevice corrosion.

The minor damage observed on these test specimens indicates that many more years of useful service life could have been expected from the steam generators of the HRE-2.

These results show that carbon steel components can give satisfactory service in homogeneous reactor steam generators, provided that good water-treatment practices, including the use of an oxygen scavenger such as hydrazine,[8] are carried out. The absence of stress-corrosion cracking of the austenitic stainless steels indicates that chloride levels of 1 ppm or less, as maintained in the boiler water, and the elimination of oxygen from the system will effectively prevent cracking in high-temperature boiler water.

EFFECT OF HEAT FLUX ON THE CORROSION OF ALUMINUM BY WATER

High Flux Isotope Reactor Tests

The testing program for determining the adequacy of aluminum cladding for fuel elements to be used in the High Flux Isotope Reactor (HFIR) was completed, and the experimental procedure and the results were presented in detail in a series of reports.[9]

The effect of very high heat fluxes on the corrosion of types 1100 and 6061 aluminum alloys was determined under a range of conditions bracketing those that will exist during operation of the HFIR. At heat fluxes between 1×10^6 and 2×10^6 Btu hr^{-1} ft^{-2} and with coolant temperatures and velocities in the range 131 to 250°F and 31 to 51 fps, respectively, a layer of boehmite (α-$Al_2O_3 \cdot H_2O$), which has a low thermal conductivity, formed on the water-cooled aluminum surfaces. With constant conditions, the oxide accumulated at a constant rate during ten-day tests. The rate at which the boehmite formed on the surface (and consequently the rate at which the aluminum temperature increased) was a function of the temperature at the specimen-water interface and the pH of the coolant. The lower the temperature and the lower the pH (in the range 5.0 to 6.5 with HNO_3), the lower the rate of corrosion-product formation. Within the ranges 300 to 900 psi and 31 to 51 fps, pressure and flow rate were without effect. When only relatively thin films formed, the boehmite was nearly transparent and adhered tightly to the aluminum. On the other hand, when the films were relatively thick (2 to 3 mils), some of the oxide spontaneously spalled from the surface.

In those cases where the pH of the coolant was 5.0 or 5.3, corrosion penetration was uniform and, even under the most severe conditions, did not exceed 1.5 mils in ten days. Where the rate of oxide formation was high and oxide spalled from the surface, localized attack of the aluminum in the form of subsurface voids extending several mils into the metal was always observed.

From the experimental data, fluid-film heat transfer coefficients were calculated and the thermal conductivity of the corrosion product was estimated. The fluid-film heat transfer coeffi-

[7] P. D. Neumann, *Examination of HRE-2 Steam Generator Corrosion Assemblies*, ORNL TM-105 (to be issued).

[8] P. D. Neumann, *Water Treatment in Aqueous Homogeneous Reactors, Experience in HRE-2*, ORNL CF-61-1-19 (Jan. 26, 1961).

[9] J. C. Griess, H. C. Savage, *et al.*, *Effect of Heat Flux on the Corrosion of Aluminum by Water. Part I. Experimental Equipment and Preliminary Test Results*, ORNL-2939 (Apr. 29, 1960); *Part II. Influence of Water Temperature, Velocity, and pH on Corrosion Product Formation*, ORNL-3056 (Feb. 10, 1961); *Part III. Final Report on Tests Relative to the High Flux Isotope Reactor*, ORNL-3230 (Dec. 5, 1961).

cients were in good agreement with those determined by others[10] under similar conditions, and a value of 1.3 ± 0.2 Btu hr^{-1} ft^{-2} $(°F)^{-1}$ ft was obtained as the thermal conductivity of the corrosion-product film.

Although 1100 and 6061 aluminum demonstrated identical corrosion behavior, 6061 aluminum was the preferred alloy because of its better mechanical properties at reactor operating temperatures. The results obtained from this study indicate that 6061 aluminum will be a satisfactory cladding material for the HFIR fuel plates, provided the pH of the coolant is maintained at 5.0 or even 5.3 with nitric acid. Corrosion damage, *per se*, does not appear to be a problem, and although somewhat excessive temperatures are probable at the hot spots, the great majority of the fuel plates will operate at reasonable temperatures.

Advanced Test Reactor Tests

The Advanced Test Reactor (ATR) is a high-performance reactor to be built by the AEC in Idaho. The reactor has many features similar to those of the HFIR, including fuel elements composed of thin uranium-bearing plates, which will produce heat fluxes as high as 1.5×10^6 Btu hr^{-1} ft^{-2}. Present estimates indicate fuel-element surface temperatures as high as 180 to 195°C at the start of a 17-day reactor cycle. As with the HFIR, economic considerations make aluminum the most desirable cladding material, provided adequate corrosion resistance can be demonstrated. Although aluminum appears to be suitable for use in the HFIR, its use in the ATR is problematical because of the higher temperature (180 to 195°C vs 173°C) and longer fuel cycle (17 days vs 10 to 15 days) in the ATR than in the HFIR. Thus it is necessary to determine the corrosion behavior of certain commercially available aluminum alloys under conditions approximating those that will exist during operation of the ATR. Such a program has been started, and the results obtained to date are summarized below. The test equipment and the procedures were the same as those used in the HFIR program. However, to expedite the acquisition of data a second test facility, including a type 347 stainless steel pump loop, power supply, and necessary instrumentation, was constructed.

Preliminary tests conducted in the old loop yielded results similar to those expected from an extrapolation of the HFIR data; that is, at the higher surface temperatures higher rates of oxide formation were observed. However, at the higher temperatures the rates of temperature increase were essentially parabolic, rather than linear as observed in most of the HFIR tests. When the corrosion-product films became 2 to 3 mils thick, spallation of the oxide occurred on both 6061 and X8001 aluminum, the only two alloys examined. When the conditions were the same, the rates of oxide accumulation on the two alloys were essentially the same. One important difference between the two alloys, however, was that, whenever oxide spalled spontaneously from 6061 specimens, localized attack of the underlying metal was found, whereas with X8001 specimens, only very uniform corrosion was observed.

Under identical conditions, tests conducted in the newly constructed loop consistently showed significantly lower rates of oxide accumulation than were observed in the old loop, even though no difference could be detected in the composition of the coolant. This fact is illustrated in Fig. 10.1, where the temperature of an X8001 aluminum specimen from each loop is plotted against the exposure time. In both cases the operating conditions were the same, and the temperature plotted is the average temperature determined by two thermocouples attached to the outside of each specimen at the axial midpoint.

Visual examination of the test specimens at the end of the two runs showed that the specimens from the old loop had a smooth, adherent black film, whereas those from the new loop were also smooth and adherent but brownish. The appearances of the specimens from each of the two loops were always the same. When metallographic sections of the specimens were prepared, a thin deposit overlying the boehmite film was always found on the specimens from the new loop, but never on the specimens from the old loop. Figure 10.2 shows photomicrographs of transverse sections taken from the specimens used to conduct the tests, the results of which are shown in Fig. 10.1. The additional phase on the surface from the new loop, although thin, is clearly visible in

[10] W. R. Gambill and R. D. Bundy, *HFIR Heat-Transfer Studies of Turbulent Water Flow in Thin Rectangular Channels*, ORNL-3079 (June 5, 1961).

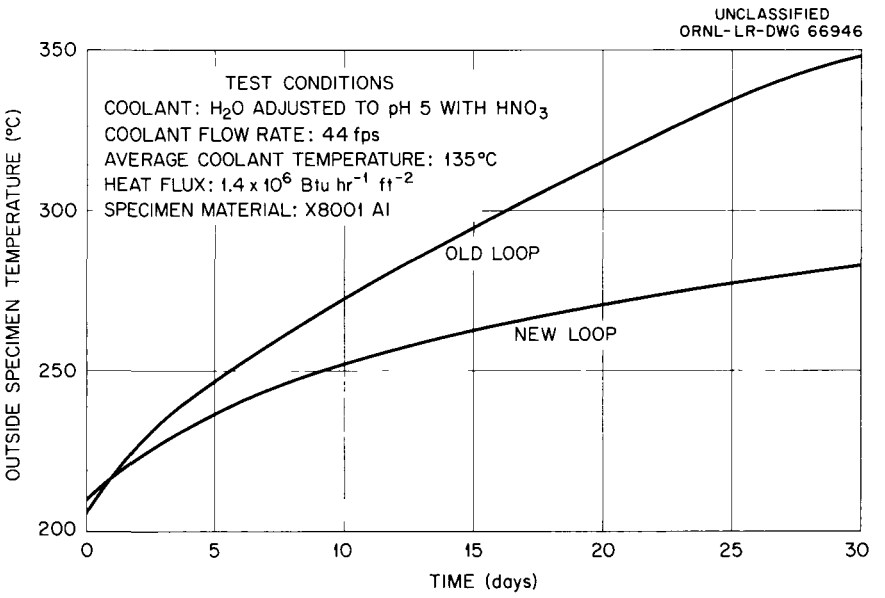

Fig. 10.1. Temperatures Observed at the Axial Midpoint on Test Specimens Exposed in the Old and New Test Loops.

the bottom photomicrograph. Note that the magnification on the photomicrograph of the specimen from the new loop is three times that on the one from the old loop. The bright particles entrapped in the boehmite in the bottom photo are intermetallic compounds which are present in the alloy and are not corroded in test. The metallographic section used for the upper photo was etched with 1% HF, which dissolved the intermetallic phase, leaving only holes in the boehmite.

Although the material on the surface of the boehmite has not been identified, it appears to be rich in iron. Since the deposit was associated only with the new loop, which had not been run at high temperature, it seemed possible that some component removed by the water from the new stainless steel surface was deposited on the boehmite and that this film was responsible for the lower rate of oxide formation in the new loop.

To investigate the above possibility the new loop without an aluminum specimen was operated for four days with deionized water containing 2 to 4 ppm oxygen at 275°C to develop a thin corrosion-product film on all stainless steel surfaces, and a bed of new, type 347 stainless steel turnings was placed in the old loop. Then standard tests with X8001 specimens were started under conditions nearly identical to those referred to in Fig. 10.1. The average temperatures measured on the outside of the specimens are shown in Fig. 10.3. (Note that the scale on the graph has been expanded over that in Fig. 10.1.) Although the tests were not run as long as were those shown in Fig. 10.1, it can be noted that the above experimental procedure resulted in a reversal in behavior of the two loops; that is, the rate of oxide accumulation on the specimen exposed in the old loop with the large surface area of new stainless steel was less than that in the new loop after pretreatment.

The specimens have not yet been fully examined, but the surface films on both specimens were dark, as has been the case with all X8001 specimens exposed in the old loop. There was no trace of the brownish surface deposit, characteristic of the specimens exposed in the new loop, on either specimen.

Although it is too early to draw definite conclusions, it appears that a large surface area of new stainless steel exposed to the water used to cool the aluminum produced a beneficial effect by reducing the rate at which oxide formed on the surface of the aluminum and, presumably, by reducing the corrosion rate.

Future tests will be concerned with the verification of the above results and, in general, with a

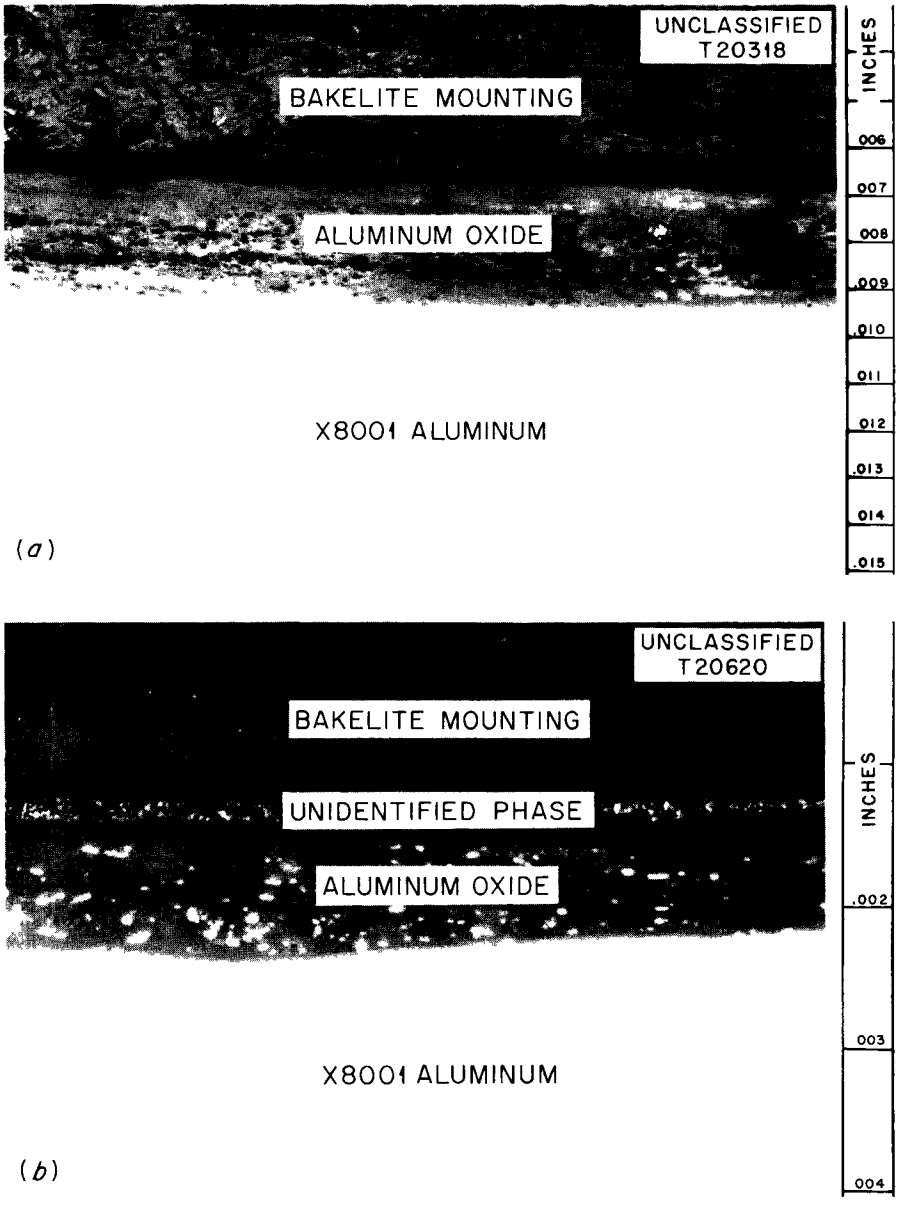

Fig. 10.2. (*a*) **Transverse Section from X8001 Aluminum Specimen Exposed in the Old Loop; 250X;** (*b*) **Section from Specimen Exposed in New Loop; 750X; Note Presence of Additional Phase on Aluminum Oxide.**

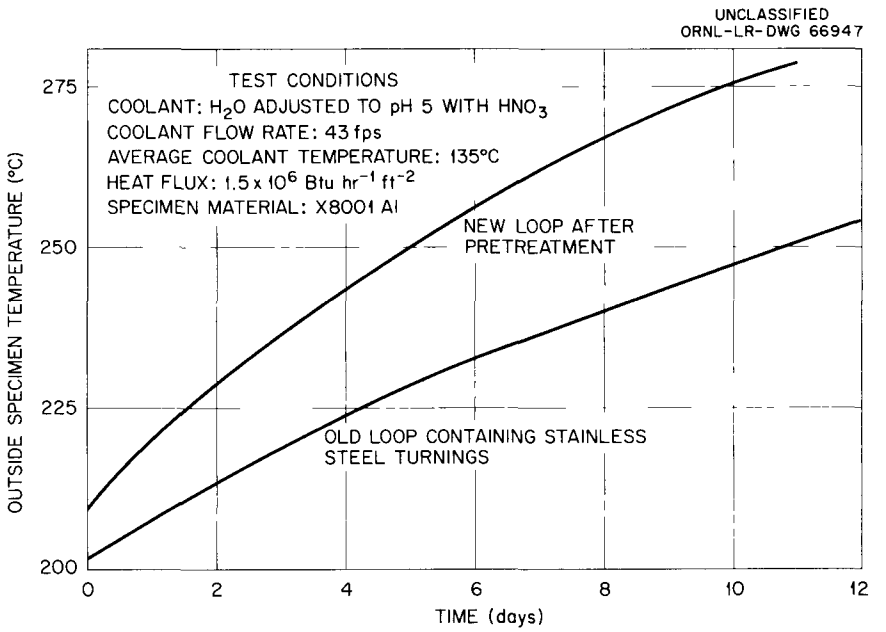

Fig. 10.3. Temperatures Observed at the Axial Midpoint on Test Specimens Exposed in the Old and New Test Loops.

search for practical means by which oxide accumulation rates, and thereby fuel-element temperature, can be minimized.

SERVICE CORROSION

Corrosion Tests in Support of Power Reactor Fuel Element Processing

These tests support the development programs concerned with the aqueous processing of spent power reactor fuel elements and with the treatment and storage of radioactive waste solutions originating from such processes. The corrosion resistance of many metals and alloys potentially suitable for containers for various dissolution processes or for storage of waste solutions has been determined under conditions simulating those that would exist in different processing plants.

During the past year, tests have been carried out in support of the following aqueous processes which are either developed or under development by the Chemical Technology Division: Thorex, Sulfex, Darex, Perflex, Zirflex, and various modifications and combinations of these processes. Tests in simulated waste solutions that would be stored as such, and experiments to determine the corrosion resistance of materials possibly suitable for equipment used in the evaporation and calcination of certain waste solutions have been conducted. Also, tests have been run in gaseous hydrogen chloride and carbon tetrachloride to determine the corrosion resistance of several alloys that might find use in the Zircex process.

The testing program is an integral part of the development work on the various processes, and as such the pertinent results obtained from the corrosion tests are included in the reports issued by the Chemical Technology Division.[11]

Corrosion Studies for the Transuranium Processing Facility

Exploratory corrosion tests have been started to evaluate the behavior of various potential materials for use in the fabrication of process equipment for the transuranium processing facility, the major function of which will be the processing of irradiated High Flux Isotope Reactor

[11] R. E. Blanco, *Chemical Development Section B Monthly Progress Report*, ORNL CF-61-2-61 (January 1961); ORNL CF-61-3-50 (February 1961); ORNL CF-61-4-108 (March 1961). *Chemical Development Section B Quarterly Progress Report*, ORNL TM-1 (April–June 1961); ORNL TM-81 (July–September 1961).

target rods for recovery of Pu, Am, Cm, Bk, Cf, and Es. The separation of these elements from the rare earths and partially from each other will be made in solutions containing high concentrations of chloride ions.

A literature survey was made to select materials that offered promise of suitable corrosion resistance to high-chloride-containing solutions. Corrosion tests were then carried out with these materials in simulated process solutions. Table 10.1 lists the more important results obtained. Specimens were exposed in the solution, at the interface, and in the vapor above the solution. The reported rates were the highest values

Table 10.1. Summary of Corrosion Test Data for Transuranium Processing Facility

Material	Medium	Temperature (°C)	Time (hr)	Corrosion Rate[a]
Hastelloy C	3 *M* $HCl-O_2$	43	336	13
Zirconium			336	<0.1
Hastelloy C	3 *M* HCl–1 *M* HNO_3-O_2	43	336	1
Hastelloy C	8 *M* HNO_3-O_2	43	1008	3
Haynes 21			336	0.1
Haynes 25			336	0.1
Zirconium			336	nil
Tantalum	6 *M* HCl (no O_2)	105	168	nil
Zircaloy-2			96	0.1
Zirconium			72	<0.1
Hastelloy B	6 *M* $HCl-H_2O_2$	105	96	7[b]
Molybdenum			96	[c]
Zircaloy-2			96	1[b]
Zirconium			96	1
Niobium	6 *M* $HCl-O_2$	112	400	1
Zirconium		105	336	<0.1
Haynes 25	6 *M* HCl–8 *M* HNO_3 (no O_2)	105	96	3
Tantalum			168	nil
Titanium-55A			72	3
Zircaloy-2			24	14
Zirconium			24	165
Chlorimet-2	10 *M* LiCl–0.1 *M* $HCl-O_2$	128	168	5
Hastelloy A			168	3
Hastelloy B			168	3
Tantalum			24	nil
Hastelloy B	10 *M* LiCl–0.1 *M* $HCl-H_2O_2$	128	48	44
Tantalum			120	nil
Niobium	10 *M* LiCl–0.5 *M* HCl_2-O_2	128	400	0.3

[a] Mils of penetration per month of exposure, calculated from weight losses of specimens.

[b] Flowing system.

[c] Specimens completely disintegrated.

observed, regardless of specimen position; usually the highest rates were obtained on the specimens exposed in the solution.

Tantalum was the most resistant material tested; corrosion rates were negligible in all environments. Zircaloy-2 and zirconium were nearly completely resistant in either nitric or hydrochloric acid solutions but were unsatisfactory in mixtures of the two acids. Hastelloys B and C looked promising in certain of the solutions, as did niobium.

Numerous other alloys were tested in the environments shown in Table 10.1; however, all corroded at rates too high to permit serious consideration. Even in less corrosive solutions such as the neutralized lithium chloride–aluminum nitrate systems, conventional materials such as the austenitic stainless steels exhibited either low corrosion rates with extensive pitting or high corrosion rates with no pitting.

A joint effort with Chemical Technology Division personnel is in progress to examine the effect of high alpha radiation levels in solution on the corrosion behavior of prospective container materials such as Hastelloy B, Hastelloy C, tantalum, commercial-grade titanium, and Zircaloy-2. Preliminary results have been reported.[12]

Corrosion Studies in the Oak Ridge Research Reactor

In a continuation of the service furnished to the ORR, some long-term corrosion tests were completed. A group of aluminum alloy test specimens was removed from the reactor core for evaluation after an 8712-hr exposure. During this period the reactor was at power for 6630 hr and produced a total of 120,217 Mwhr. No significant corrosion was observed on any of the aluminum alloys (1100, 3003, 5052, 5154, and 6061). Corrosion rates were all below 0.1 mpy.

Similarly, aluminum test specimens exposed in the core cooling-water strainer for 10,600 hr revealed no change in corrosion behavior from that observed after shorter exposures. Corrosion rates of less than 0.1 mpy were measured on all aluminum alloys (1100, 3003, 5154, 6061) at this location.

Another group of aluminum specimens (1100, 3003, 5154, 6061) was removed from the secondary cooling water for the pool heat exchanger after 13,440 hr. As in tests for shorter periods, corrosion rates of less than 0.1 mpy were observed.

In view of the results obtained during the past year and those previously reported,[13] it is concluded that the structural material in the ORR should give many years of service free from major corrosion problems, provided current water-treatment practices are continued.

Acceptance Tests

Considerable effort was expended in conducting various material acceptance tests for a number of ORNL and Y-12 programs. Approximately 475 boiling 65% HNO_3 tests (ASTM:A262-55T) were run on austenitic stainless steels. Nearly 75% of these were for the High-Radiation-Level Examination Laboratory (HRLEL). In addition, 510 electrolytic oxalic acid tests (ASTM:A262-55T) were made; the majority of these were on type 304L stainless steel for the HRLEL.

Miscellany

Short corrosion tests on materials used in specific applications were conducted for various divisions and projects. These included a determination of the corrosion of the stainless steel cladding on UO_2 fuel rods and the leaching of uranium by high-temperature water from defective rods; a demonstration of the susceptibility of the type 304 stainless steel pipe used in the NS "Savannah" to stress-corrosion cracking in aqueous environments containing low concentrations of chloride ions; tests to show the beneficial effect of a proprietary surface coating in minimizing corrosion of the EGCR pressure vessel in marine atmospheres during shipment; and static and dynamic tests with several materials for specific applications in the High Flux Isotope Reactor.

[12] R. D. Baybarz, *Corrosion of Metals Exposed to Chloride Solutions Containing High Alpha*, ORNL TM-100 (to be issued).

[13] P. D. Neumann, *Corrosion of Aluminum Alloys in the ORR*, ORNL-3151 (May 18, 1961).

11. Surface Chemistry of Thoria in Dilute Aqueous Electrolytic Solutions

C. H. Secoy F. H. Sweeton H. F. Holmes

IONIC ADSORPTION EQUILIBRIA

A method for determining the adsorption equilibrium between ThO_2 and electrolytic solutions has been studied. The general approach has been to determine the amount of electrolyte lost from an electrolytic solution equilibrated with specially prepared ThO_2. The composition of the equilibrated solution has been followed by acidity measurements supplemented by electrolytic conductivity measurements. The tests so far have been confined to nitric acid at room temperature.

The adsorption cell used to equilibrate the solid and the solution is shown in Fig. 11.1. The Millipore filter is mounted as shown on top of a Teflon supporting disk having tiny radial and circumferential grooves so arranged that the filtrate can flow out the bottom fitting. This arrangement lets the filtrate out with a minimum of holdup volume and supports the filter adequately, even with 1 atm of pressure across it. The filtration pressure is supplied by purified compressed air admitted through an alternate plug in the top of the cell.

Two pH cells were used. The first had a polystyrene body holding the glass electrode and a glass attachment which could form a flat liquid junction with the saturated KCl solution of the calomel electrode. The second cell consisted of a Teflon block with machined fittings sealing the glass and calomel electrodes in a stream of the solution flowing through the block.

The first of two conductance cells was constructed of machined Teflon and platinum parts clamped together to form a cell with a volume of about 0.4 ml and a cell constant of about 2.6 cm^{-1}. The second cell was constructed of Pyrex with thin sealed-in platinum electrodes. Its volume was about 0.2 ml, and its cell constant was about 50 cm^{-1}.

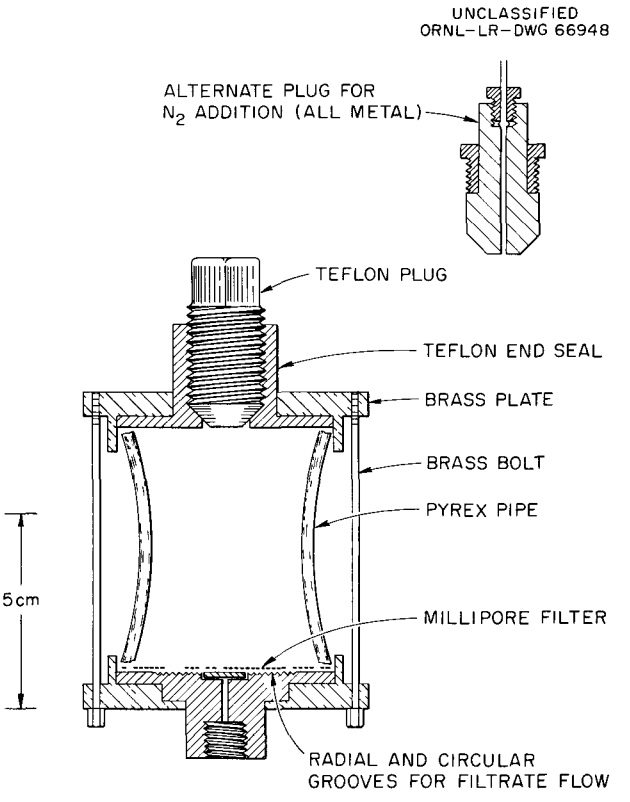

Fig. 11.1. Adsorption Cell.

The ThO_2 used had been prepared[1] by chemically breaking up particles of ThO_2 prepared from

[1] F. H. Sweeton and C. H. Secoy, *Reactor Chem. Div. Ann. Progr. Rept. Jan. 31, 1961*, ORNL-3127, pp 70–71.

the oxalate. The particles in the sample were between 2000 and 3000 A in effective diameter. The specific surface area, as measured by nitrogen adsorption, was 6.87 m^2/g. This sample, amounting to 7 g, was used in its entirety in each of the tests; a total of about 6.3% of it was lost in the course of the whole series.

In the first runs the solid and the solution in the adsorption cell were mixed by mounting the cell on a 60-rpm motor-driven shaft in such a way that the cell rotated end-over-end. In each case the sample was treated twice with dilute KOH (1 to 10 mM) in the adsorption cell to free the ThO_2 of adsorbed CO_2. Then, after the solid was washed with several batches of distilled water to remove the KOH, known amounts of nitric acid and water were added. The slurry was mixed for at least 20 min and then a sample of filtrate was transferred through glass and Teflon tubing to the Teflon conductance cell and the polystyrene pH cell. Additional values were determined by repeating with more water and acid.

The results of runs 2A and 2B can be seen in Fig. 11.2. The equilibrium concentration of HNO_3 in solution was taken as equal to the antilog of the negative pH reading. The fraction of coverage was obtained by dividing the equivalents of acid adsorbed by the total absorbable, assuming that complete adsorption would amount to 21.3×10^{-6} moles/m^2 (ref 2). The chronological sequence of the plotted points is indicated by the arrows on the lines connecting the points. The large increments in pH represent additions of both acid and water; the points close together were obtained after adding water alone or just further mixing.

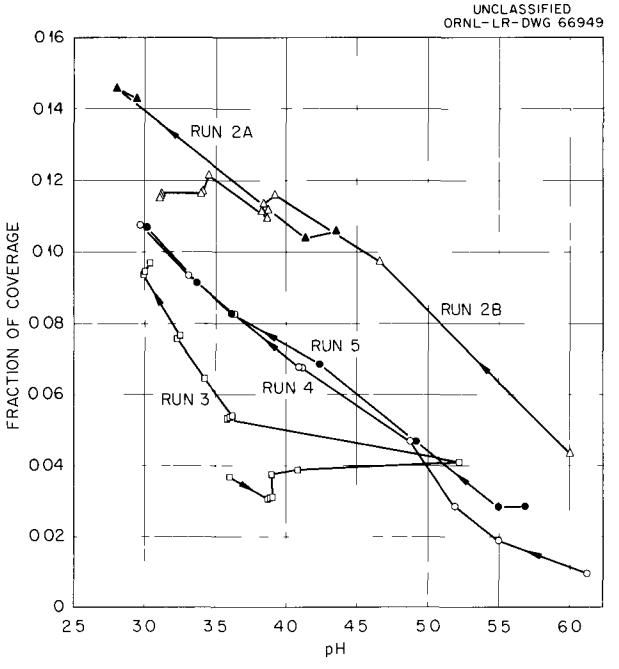

Fig. 11.2. Adsorption of HNO_3 on ThO_2.

Two main changes in technique were introduced with run 3 to see whether the apparent adsorption would change. The ThO_2 was purified outside the adsorption cell while in the form of a filter cake, and a commercial paint shaker was used to mix the slurry. The shaker was used for only 2 to 10 min at a time, since it was very effective. At this same time the glass conductivity cell and the Teflon pH cell were incidentally substituted for the previously used cells.

The data of run 3 differed greatly from the previous data, as is evident from the figure. The primary effect was a great decrease in apparent adsorption. Also, the first part of the new curve was more erratic, while the last part was more self-consistent. Visual observations indicated that the paint shaker greatly improved the mixing. However, cleaning the ThO_2 surface while the ThO_2 was outside the adsorption cell was not satisfactory, because the method was too slow and required more care to prevent CO_2 contamination.

Runs 4 and 5 utilized the paint shaker as in run 3 and the ThO_2-cleaning methods of runs 2A and 2B. As can be seen in the figure, the data for these last two runs fell between those of the earlier one. The new data form two curves which are much smoother; in the region of 3 to 5 pH units these two curves are mutually consistent to within 0.005 unit on the fractional coverage scale and to within 10% of their own values. Likely explanations can be made of why the data from the earlier runs differ from these last two. The apparent adsorption of runs 2A and 2B could have been high because the mixing was inadequate for complete removal of the alkali during the washing steps. The apparently low adsorption data of run 3 might have been caused by CO_2 contamination of the treated ThO_2 filter cake, which had been held for about a month before the adsorption tests were made.

[2]This is compatible with the absorbability of four monovalent groups on one face of the ThO_2 face-centered unit cell.

The last two runs appear to indicate a reasonably self-consistent method for the desired study of ionic adsorption on ThO_2. This consistency having been achieved, the next step is to look further into the adequacy of ThO_2 samples for such adsorption tests. It is necessary that the adsorption measured be related to the outside surface of the particle and not to any internal surface.[1]

Work is in progress to prepare ThO_2 samples which are expected to have little or no internal surface. The first such effort is with arc-fused ThO_2. A sample of the fused material has been obtained by hand separation of pieces in a partially crushed sample of mixed fused and unfused ThO_2. The selected material is being crushed in a ball mill[3] with steel balls, and the product after separation of iron impurities is being classified by elutriation methods.

HEAT OF WETTING OF THORIUM OXIDE

Work on the adiabatic calorimeter[4] for use with aqueous systems up to 250°C is continuing. Several important modifications have been made in the original design. The creep strength of copper, which had been neglected in the initial design calculations, is such that it will be impossible to construct a copper calorimeter vessel which would have the desired thermal characteristics. Accordingly, the calorimeter vessel is to be fabricated from Inconel X. The exterior will be given a thick plating of copper, which will be covered by a thin, highly reflecting gold plate. The interior of the calorimeter vessel will be covered with a nonporous platinum coating obtained by the vapor-phase decomposition of platinum chlorocarbonyl. The material used in the reference block to provide thermal damping will be a potting compound, Silastic RTV501, rather than the originally intended material, Teflon. The thermal properties of Silastic RTV501 are, for all practical purposes, as good as those of Teflon. The use of this potting compound in place of Teflon will make construction of the reference block more economical and less difficult. Samples of Silastic RTV501 have been tested for thermal stability at 250°C, and construction of the reference block is in progress.

The electrical calibration console has been constructed and is in use with the room-temperature calorimeter. The power source for the electrical calibration is four 6-v lead storage batteries in parallel. The voltage drops across the standard resistor and the calorimeter heater are measured with a Leeds and Northrup type K-3 potentiometer and an electronic null detector. Heating current can be varied with a Dekastat variable resistor in series with the voltage source. The duration of the heating cycle is measured with a six-digit electronic counter having an accuracy of ±2 counts in the last digit. This counter has been checked against the NBS standard frequency broadcast. Its trigger circuit is connected across the calorimeter heater and the voltage source; the counter is activated by the positive pulse and is stopped by the negative pulse. This arrangement provides exact synchronization of the counter and the calorimeter heater. At present this counter is used on a range which gives a time interval measurement accurate to ±0.002 sec. The calibration console has given trouble-free service since its initial use.

One of the most important changes in the adiabatic calorimeter has been the decision to return to the use of glass sample bulbs. The most important heat effect in using an evacuated sample container in an aqueous system at 250°C is the comparatively large quantity of heat required to vaporize enough water to fill the void space in the sample container. This effect will be compensated by the use of a flexible metal bellows to break the sample bulb and exactly compensate for the previously determined void volume in the sample bulb. In effect, this will amount to a constant-volume experiment. The convenience of glass sample bulbs and the ability to compensate for the heat of vaporization of water prompted the decision.

Work on the remaining phases of the adiabatic calorimeter is continuing. With the exception of the control system for the oil bath, all of the required instrumentation is on hand. Figure 11.3, a section view of the assembled calorimeter bomb, shows all of the important parts, with the exception of the vacuum valve and the hydraulic line to the metal bellows. The thermocouple junctions

[3]The cooperation of R. A. McNees of the Metallurgy Division in providing the ball-milling service is gratefully acknowledged.

[4]H. F. Holmes and C. H. Secoy, *Reactor Chem. Div. Ann. Progr. Rept. Jan. 31, 1961*, ORNL-3127, pp 72–73.

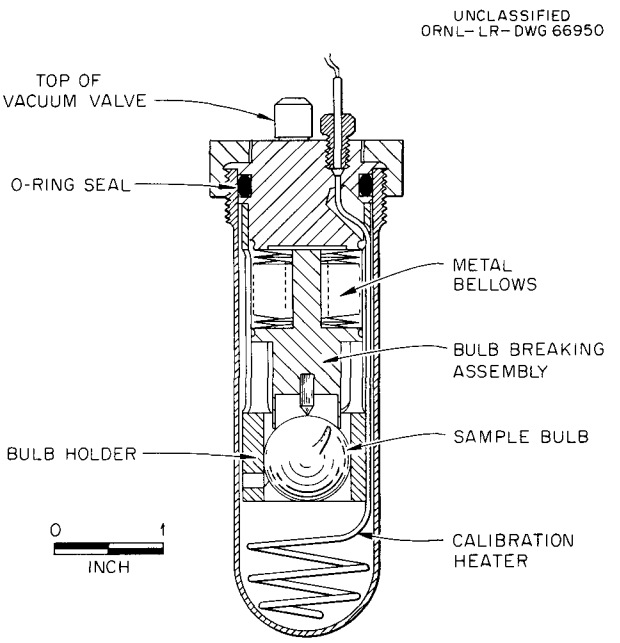

Fig. 11.3. Section View of Assembled Calorimeter Bomb.

will be attached to the outside of the calorimeter as an integral part of the mechanical support. Figure 11.4 is a block diagram showing the relationship of the instrumentation required for the adiabatic calorimeter.

Several preliminary measurements of the heat of wetting of thorium oxide in water at 25°C have been made with a relatively simple calorimeter. The basic part of this calorimeter is a 265-ml Dewar flask connected to a brass plate. This is suspended inside a jacket by nylon rods. This entire assembly is immersed in a thermostatic water bath. The calorimeter contains a stirrer, a cooling coil, a heater well, a thermometer well, and a sample holder capable of holding five sample bulbs. The sample bulbs are broken against the bottom of the stirrer, which is driven by a synchronous motor.

The temperature-sensing device is a 100-ohm thermistor enclosed in a glass probe. The thermistor is used as a three-lead resistance thermometer in conjunction with a Leeds and Northrup type G-2 Mueller bridge. The unbalance potential of the bridge is amplified by a Keithley model 149 dc amplifier. The output of this amplifier is fed to a zero-center strip-chart recorder operating at a chart speed of 30 in./hr. In normal use the amplifier is operated at a gain such that full scale on the recorder is approximately 2×10^{-3} degree. This results in a sensitivity of approximately 20 microdegrees, which could be increased by one order of magnitude before the thermal noise of the electrical circuit would become objectionable. However, the present calorimeter is not capable of such extreme sensitivity. The electrical calibration has been covered in a previous paragraph, as all of the instruments necessary for the operation of this calorimeter have been available from *the instruments required for the adiabatic calorimeter.*

Three samples of thorium oxide were prepared by the oxalate precipitation process and subsequent thermal decomposition (ORNL lot No. DT-37-100). The samples were fired for 4 hr at 650, 1000, and 1400°C. Surface areas corresponding to the different firing temperatures were 14.7, 5.64, and 0.99 m^2/g, as determined by the BET nitrogen-adsorption method. Water used for the wetting process was prepared by passing distilled water through a mixed-bed ion exchange column. This water had a pH of approximately 6.9 and an electrical conductivity of 4.5×10^{-7} ohm^{-1} cm^{-1} or less.

Samples were prepared by evacuating at a pressure of 1×10^{-5} mm Hg or less for 24 hr at temperatures of 200, 300, 400, and 500°C. The samples were contained in thin-walled glass sample bulbs and were sealed off under vacuum. The sample bulbs were blown from 5-mm-OD Pyrex tubing and had a wall thickness of 0.003 to 0.006 in. and a diameter of 2 cm. They were shaped by being blown in a hemispherical graphite mold. Void volumes in the bulbs were determined by weighing in air and in water.

The correction for the heat of bulb breaking was determined by breaking empty sample bulbs in the calorimeter. The mean obtained by breaking six evacuated sample bulbs was 0.554 joule with a standard deviation of 0.035 joule. In contrast, the value obtained by breaking three sample bulbs which had been sealed at atmospheric pressure was 0.123 joule with a standard deviation of 0.034 joule. The value obtained for the evacuated bulbs agrees within the experimental uncertainty with the value obtained by Makrides and Hackerman.[5] The difference between evacuated and non-

[5] A. C. Makrides and N. Hackerman, *J. Phys. Chem.* 63, 594 (1959).

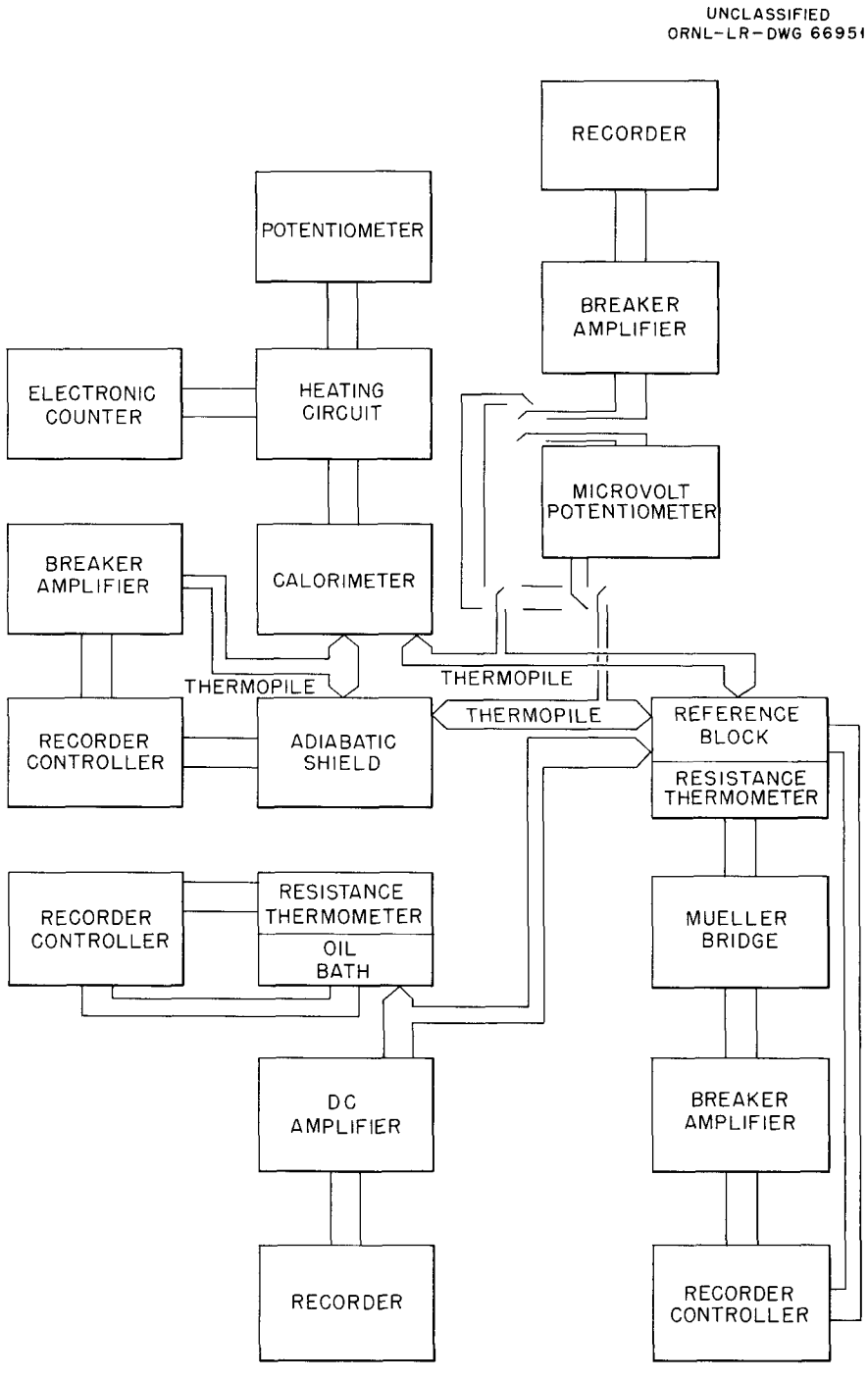

Fig. 11.4. Block Diagram of Instrumentation for the Adiabatic Calorimeter.

evacuated bulbs has been noted by others.[6] The uncertainty associated with this correction is annoying; it amounts to only about 0.1% in the case of the higher-surface-area samples, but can be as high as 2% in the case of the low-surface-area samples. It was also found necessary to apply a small correction for the heat produced by manipulating the sample holder during the bulb-breaking process.

Results of the measurements to date are summarized in Table 11.1. The absolute values of the results are probably correct to ±30%. This large uncertainty is due to the uncertainty in the absolute value of the surface area.[7] Relative values are probably consistent to a few percent.

Although the precision of the results leaves little to be desired, the accuracy of the calorimetric measurements is probably no better than 4 or 5%. Although this is comparable with the calorimetric accuracy of the majority of reported measurements of heats of wetting, it is not sufficient to enable accurate determination of temperature coefficients, heats of ionic adsorption, and heat of wetting as a function of surface coverage. As a partial check on the calorimetric results, the heat of solution of barium chloride in water to give a 0.01 *m* solution was determined. The mean of three measurements was 3112 cal/mole with a standard deviation of 79 cal/mole. Criss and Cobble[8] have reported a value of 3037 ± 19 cal/mole for this same reaction. The heat of solution of barium chloride also provided a check on the thermal characteristics of the calorimeter. From the shape of the time-temperature curves it is believed that the most objectionable feature of the present calorimetric apparatus is the slow rate of attaining thermal equilibrium after a reaction period. It will be necessary to reduce this in order to investigate the possibility of a slow heat evolution in the wetting process. An increase in the rate of attaining thermal equilibrium should also result in more accurate calorimetric measurements. Present work is directed toward reducing the time necessary to attain thermal equilibrium and toward completion of the study of the effect of pretreatment on the heat of wetting of thorium oxide.

[6] F. E. Bartell and R. M. Suggitt, *J. Phys. Chem.* **58**, 36 (1954).

[7] P. H. Emmett, *J. Phys. Chem.* **63**, 449 (1959).

[8] C. M. Criss and J. W. Cobble, *J. Am. Chem. Soc.* **83**, 3223 (1961).

Table 11.1. Heat of Wetting of Thorium Oxide in Water at 25°C

Firing Temperature (°C)	Surface Area (m^2/g)	Heat of Wetting ($ergs/cm^2$) at Specified Outgassing Temperature			
		200°C	300°C	400°C	500°C
650	14.7	718, 716	795, 801, 796	928	
1000	5.64	711, 720	809, 790	989	950, 949
1400	0.99	698, 688	782, 743	867	805, 832

Part III

Heterogeneous Systems Studies

E. L. Compere
J. M. Baker
W. J. Leonard*
R. A. Lorenz
R. E. McDonald*
T. H. Mauney
H. C. Savage
S. A. Reed
D. M. Richardson
A. J. Shor
J. F. Winesette
L. F. Woo

*Metallurgy Division.

12. Investigation of the Compatibility of Coated Fuel Particles and Coated Matrices with Liquid Coolants

An investigation of the compatibility of coated fuel particles and coated matrices with liquid coolants has been initiated. The study was prompted by the encouraging results of investigations related to gas-cooled reactor systems, which have demonstrated that fissionable materials such as UO_2 and UC_2 may be given coatings which protect them from reaction with the environment and, moreover, retain the fission products for reasonably long periods. Such coated fuel particles incorporated into a graphite or ceramic fuel element which could be cooled by conventional liquid coolants (such as pressurized water, organic liquids, molten salts, or liquid metals) might offer several important advantages over metal-clad fuels; examples are improved heat transfer, lower maintenance costs, and more economical fuel reprocessing.

The initial phase of the investigation is the out-of-pile evaluation of unclad graphite matrices in which are incorporated spherical particles of Al_2O_3-coated UO_2 or pyrolytic-carbon-coated UC_2 from commercial vendors. Comparison tests are being conducted with unfueled matrix materials.

One lot of 150-μ spherical UC_2 particles coated with $\sim$70 μ of pyrolytically deposited carbon was procured from National Carbon Company (NCC), and a batch of $\sim$200-μ spherical UO_2 particles coated with $\sim$40 μ of Al_2O_3 was purchased from Nuclear Materials and Equipment Corporation (NUMEC). Both types were obtained for incorporation in graphite matrices. They were examined for surface contamination by alpha assay, for coating integrity by leaching in nitric acid and thermal cycling, and for uniformity of coating thickness by microscopic examination after cross-sectioning. Results of the examinations are shown in Table 12.1. Both materials are regarded as satisfactory.

Major work during the period was directed toward modification of existing equipment and procurement of new equipment and materials for initiating the test programs.

Table 12.1. General Information on As-Received Coated Particles

	Al_2O_3-Coated Spherical UO_2	Pyrolytic-Carbon-Coated Spherical UC_2
Supplier	NUMEC	NCC
Lot No.	915	NCC-201
Visual appearance	Gray, surface knobby	Dull, smooth
Nature of coating	Translucent, continuous	Duplex, uniform
Nominal coating thickness, μ	40	70
Nominal core-particle size, μ	200	150

Table 12.1 (continued)

	Al_2O_3-Coated Spherical UO_2	Pyrolytic-Carbon-Coated Spherical UC_2
Surface contamination, alpha counts/min per g of particles	None detected	6
Uranium removed by HNO_3 leach, mg of U per g of particles[a]		
A. New particles	None detected	0.17
B. After thermal treatment	None detected[b]	0.0008[c]

[a]Leached 8 hr in 1:1 HNO_3 at 95°C.
[b]Heated at 650°C for 48 hr.
[c]Thermal cycled between 1800°C and room temperature, three times.

Coupon and rod-type specimens were fabricated of standard grades of nuclear graphite, AGOT, TSX, CEQ, ATJ, and special grades (TS-148, TS-160, FE-3, FE-4)[1] of matrix graphites suitable for supporting coated fuel particles. Each special grade was baked at 1400, 2000, and 2800°C. Similar fueled specimens as well as unfueled controls are being prepared by Speer Carbon Company.

PRESSURIZED WATER AND ORGANIC COOLANTS

The above specimens are to be exposed in a pump loop capable of long-term operation at 360°C with pressurized water. The effects of coolant flow velocity, operating temperature, cover gas, and grain orientation in the graphite on matrix integrity and particle stability will be determined. Similar tests will be performed in a second pump loop with organic moderator-coolants at temperatures up to ~700°F. Santowax R (Monsanto Chemical Company) has been chosen as the first organic coolant to be tested. The effects of fouling the graphite due to thermal and/or chemical polymerization of the organic liquids will also be considered. The effects of heat flux will be tested in both coolants in separate dynamic experiments using rod-type samples with electrical resistance heating.

The use of electrical resistance heating for making such tests was successfully demonstrated with a ¼-in.-diam rod of spectrographically pure graphite placed axially in a stream of deoxygenated water flowing at 0.2 fps in a forced-flow test loop. The rod, with an effective surface area of 0.05 ft^2, was heated to estimated surface temperatures of 300 to 370°C at bulk coolant temperatures of 250 to 305°C; calculated heat fluxes were 135,000 to 236,000 Btu hr^{-1} ft^{-2}.

MOLTEN FLUORIDE SALT COOLANTS

Graphite or carbon matrix elements containing dispersed, coated fuel particles are attractive for use in high-performance power reactors cooled by molten fluoride salt. The excellent compatibility of fueled molten fluoride salt and 100% graphite has been reported in connection with the Molten-Salt Reactor Experiment.[2]

Further compatibility studies are in progress at 500 to 1000°C with barren fluoride melts. Various grades of graphite and carbon matrix materials,

[1]National Carbon Company designations.

[2]R. J. Sheil, R. B. Evans, and G. M. Watson, *Molten Salt-Graphite Compatibility Test. Results of Physical and Chemical Measurements*, ORNL CF-59-8-133 (Aug. 31, 1959).

α-Al_2O_3 and pyrolytic-carbon coating materials, alumina-coated UO_2 spheres, pyrolytic-carbon-coated UC_2 spheres, and fueled compacts of these materials will be tested. Cover gas will be hydrogen, helium, or vacuum.

Sapphire (Al_2O_3) spheres (1000-μ diam) were exposed at 800°C for 1 hr to a water-contaminated NaF-KF mixture of nominally eutectic composition in a nickel crucible under vacuum in a torch-fired furnace. An initial rapid reaction and gassing were observed. After posttest dissolution of the frozen salt in methanol, it was found that about 20% of each sapphire single-crystal microsphere had been etched off.

A similar test was made with LiF-NaF eutectic salt, believed free of water. In a test for 1 hr at 800°C, and also after 1 hr at 900°C, no dimensional change was found in the sapphire microsphere specimens.

13. Hydriding of Zirconium-Base Alloys

OUT-OF-PILE TESTING IN TOROIDS

The toroid test program concerned with the variables associated with hydriding of zirconium alloys during exposure to circulating aqueous slurries of ThO_2 and Th-U oxides[1] was completed, and a final report of the investigation is in process.[2]

It was concluded that the rate and extent of hydriding of zirconium and zirconium-base alloys during exposure to circulating aqueous thoria and thoria-urania slurries at 200, 280, and 330°C were primarily dependent upon the type and overpressure of the gaseous atmosphere. Thus hydriding did not occur, even in toroids under oxidizing atmospheres, and did not occur in the presence of dissolved hydrogen or oxygen when the specimens were continuously immersed in slurry in a dynamic loop, for example. The alternate fluid and gas exposure caused by the slug flow in a toroid was important in promoting hydriding.

Other significant factors were temperature, flow velocity, exposure time, slurry type, and hydrogen pressure. The temperature effect seemed to be maximum at about 280°C, less hydriding being observed at 330°C and none at 200°C. The rate and severity of hydride formation increased with flow velocity, exposure time, and hydrogen pressure. Also, increased U/Th ratio drastically increased hydriding; Zircaloy-2 exposed to a slurry containing an oxide with U/Th = 0.13 under 100 psi D_2 pressure hydrided catastrophically in 300 hr at 280°C.

Reaction of hydrogen with the alloys was initiated at localized areas of bare metal which had resulted from erosion of surface film by the slurry. Hydriding progressed due to intergranular diffusion of hydrogen. Depending on conditions, the gaseous hydrogen as well as hydrogen from corrosion could participate in the hydride formation.

Of the conventional alloys, coarse-grained Zircaloy-2 was most susceptible to hydriding. Fine-grained Zircaloy-2 and Zircaloy-3 were moderately hydrided. Only localized areas of zirconium hydride needles were observed in Zircaloy-4 and pure zirconium. Experimental binary alloys of zirconium with palladium (1 and 0.1%) were grossly hydrided; similar alloys with platinum were only moderately hydrided. The alloy Zr–15% Nb was not detectably hydrided, although it was severely eroded under hydrogen atmosphere.

---

[1] E. L. Compere *et al.*, *Reactor Chem. Div. Ann. Progr. Rept. Jan. 31, 1961*, ORNL-3127, pp 103–5.

[2] S. A. Reed *et al.*, *Hydriding of Zirconium-Base Alloys During Exposure to Circulating Aqueous Thoria and Thoria-Urania Slurries* (to be published as an ORNL report).

14. Thoria Pellet Test Program

A test program was continued in cooperation with the Metallurgy and Chemical Technology Divisions to evaluate experimental preparations of pellets and sol-gel fragments of thoria. These materials are being considered for potential application as blanket materials in a two-region breeder reactor.[1] Standardized attrition tests with ball mills, spouted beds, and autoclaves[2] were employed to determine the relative integrity of 88 different experimental batches of ThO_2 pellets and of 27 samples of thoria sol-gel fragments.

Data obtained during routine testing of the various samples have been reported in detail to the groups concerned with preparation of the materials, and results of many of the test series have been reported in HRP progress reports;[3] consequently they will not be reported here. However, following is a brief summary of test data obtained with one batch of pellets, designated code P-82, which have displayed a high degree of resistance to attrition and which consequently have been tested more extensively out-of-pile as well as in-pile.[4]

Techniques of fabrication of code P-82 pellets, which were developed by the Ceramics Group of the Metallurgy Division, have been reported previously.[5] Physical properties of the pellets are shown in Table 14.1, and results of routine laboratory attrition tests are presented in Table 14.2.

In addition to the routine evaluation tests, a series of laboratory fluidized-bed tests was conducted at room temperature in 1- and 2-in.-ID glass columns with water as the fluidizing medium.

Table 14.1. Physical Properties of Code P-82 ThO_2 Pellets

Right Cylinders with Hemispherical Ends
0.219-in. Diam × 0.205-in. Length
Calcined at 1650°C for 2 hr

Surface area (BET, krypton)	0.011 m^2/g
Average pore radius (Hg intrusion, 760–770 mm)	0.964 μ
Pore volume (Hg intrusion)	0.0055 cc/g or 5.1 vol %
Density (Hg immersion)	9.49 g/cc

Table 14.2. Attrition Rates of Code P-82 ThO_2 Pellets in Various Accelerated Tests

Test	Average Weight Loss Rate (%/hr)
Spouted bed (10 pellets); superficial velocity, 0.37 fps; two 1-hr exposures:	
Before autoclaving	0.27
After autoclaving in water	
at 260°C	0.49
at 350°C	0.51
Ball mill (10 pellets); 3.75-in.-ID rubber-lined mill, 150 rpm; twenty 1-hr exposures	1.12

[1] I. Spiewak *et al.*, *HRP Quart. Progr. Rept. Apr. 30, 1960*, ORNL-2947, p 32.

[2] E. L. Compere *et al.*, *Reactor Chem. Div. Ann. Progr. Rept. Jan. 31, 1961*, ORNL-3127, p 96.

[3] E. L. Compere *et al.*, *HRP Progr. Rept. Dec. 1, 1960, to May 31, 1961*, ORNL-3167, p 84.

[4] J. P. McBride *et al.*, *HRP Progr. Rept. Dec. 1, 1960, to May 31, 1961*, ORNL-3167, p 73.

[5] R. A. McNees *et al.*, *HRP Progr. Rept. Aug. 1 to Nov. 30, 1960*, ORNL-3061, p 101.

Fluidization might well serve as one means of mixing the pellets, either continuously or intermittently in a blanket system. Further, small fluidized beds could be used for in-pile testing of pellets to determine the combined effects of agitation and irradiation. Test data are presented in Figs. 14.1 and 14.2. Tests were limited by the availability of pellets.

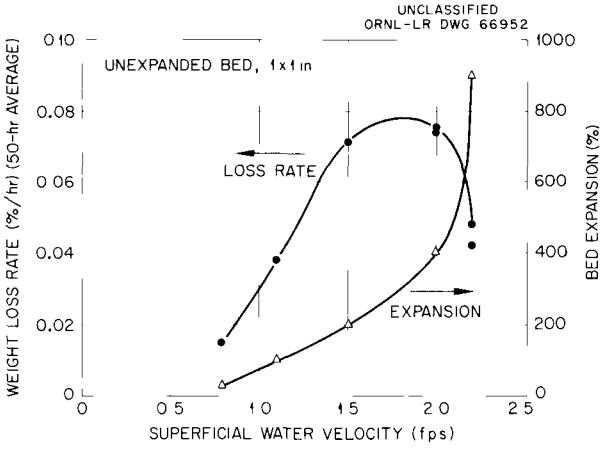

Fig. 14.1. Pellet Weight Loss Rates and Fluidized Bed Expansions at Various Superficial Velocities.

At a bed expansion of 30%, all pellets were being uniformly agitated, and each pellet contacted its neighbors almost continuously. Between impacts, acceleration of pellets by water to maximum velocities did not appear to be fully developed. As superficial flow velocity was increased, bed expansion increased, and pellets collided more violently. At a bed expansion of 900%, pellets contacted one another only intermittently except when occasional gluts were formed in the columns. Higher velocities would have resulted in bed elutriation. Bed expansions of 30, 100, 200, 400, and 900% were used (Fig. 14.1).

Attrition rates of pellets increased with superficial water velocity up to 200% bed expansion, apparently due to increasing violence of collisions. As the velocity was increased, however, the increase in bed expansion resulted in less frequent collisions, and the drag of the water on the pellet limited the maximum velocity. Consequently an inhibiting effect on attrition rate resulted, and the rate at 400% bed expansion was not much higher

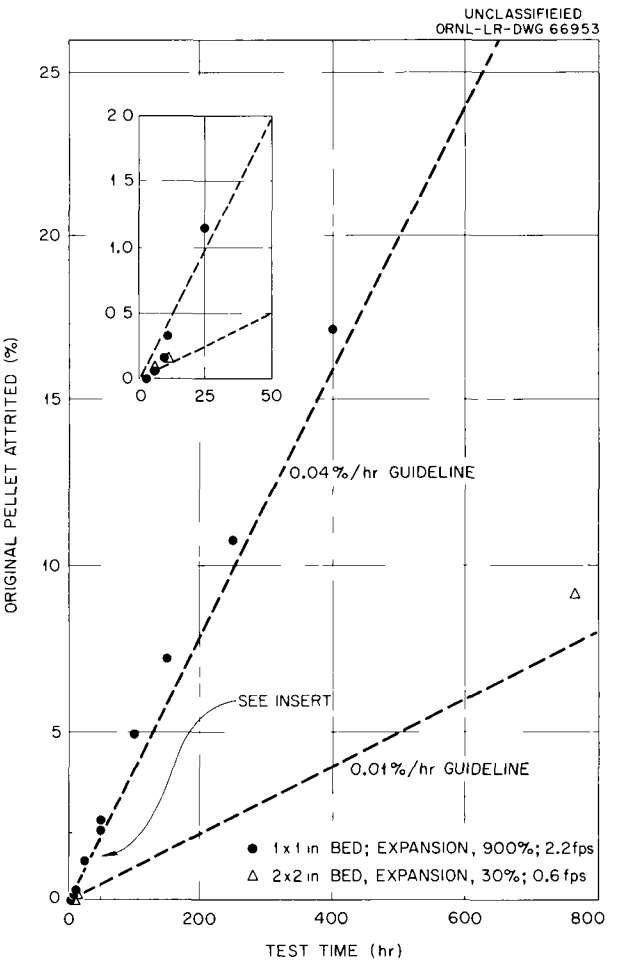

Fig. 14.2. Attrition of P-82 Pellets in Fluidized Bed Tests as a Function of Time.

than the rate at 200%. Further increase in flow velocity to a bed expansion of 900% resulted in a decrease in attrition rate, in accordance with the above.

Doubling the bed diameter and height had little effect on the wear rate of the pellets, the controlling factor being flow velocity and resultant bed expansion.

In two extreme cases, long-term tests (760 hr) were carried out (Fig. 14.2). A 2 × 2 in. bed expanded 30% (flow velocity 0.6 fps) gave an average wear rate at 760 hr which agreed with those observed at 6 and 12 hr (slightly above 0.01%/hr). A bed expansion of 900%, developed in a 1 × 1 in. bed at 2.2 fps, gave a generally constant wear rate, somewhat above 0.04%/hr, over the 760-hr period. Thus wear rates appear to be linear with time.

In the operation of fluidized-bed blankets of reactors, a bed expansion of 30% could be of interest for continuous or semicontinuous operation at minimum attrition.

A thermal-convection test of 2500 hr was performed in a loop which contained a static bed of randomly packed pellets heated to 260°C, through which oxygenated water circulated in an upward direction at a superficial velocity of 0.4 fps. A schematic diagram of the test loop and the average temperature distribution in the system are shown in Fig. 14.3.

While the pellets were not detectably affected as a result of exposure in the loop test, as evidenced by weight change or by physical examinations, it was found that a thorium-decay product, the Ra^{228} daughter, had been preferentially leached from the pellet bed and had been deposited on the loop piping, apparently as a function of the temperatures across the system.

At the completion of the test, the loop was disassembled and was examined for residual thorium activity with a gamma spectrometer. Residual thorium activity and Ra^{228} activity, each expressed as the ratio of activity to the activity of one thoria pellet (0.8 g ThO_2), are shown in Table 14.3. Areas A through E in the table are indicated in Fig. 14.3 by shading. Each area corresponds to a 12-in. length of pipe. It will be noted that, with the exception of the pellet bed container, the distribution of residual activity in the system followed the temperature profile of the loop, with activity levels highest in the coolest portions of the system and lowest in the hottest sections, indicating preferential deposition of material downstream from the heated areas.

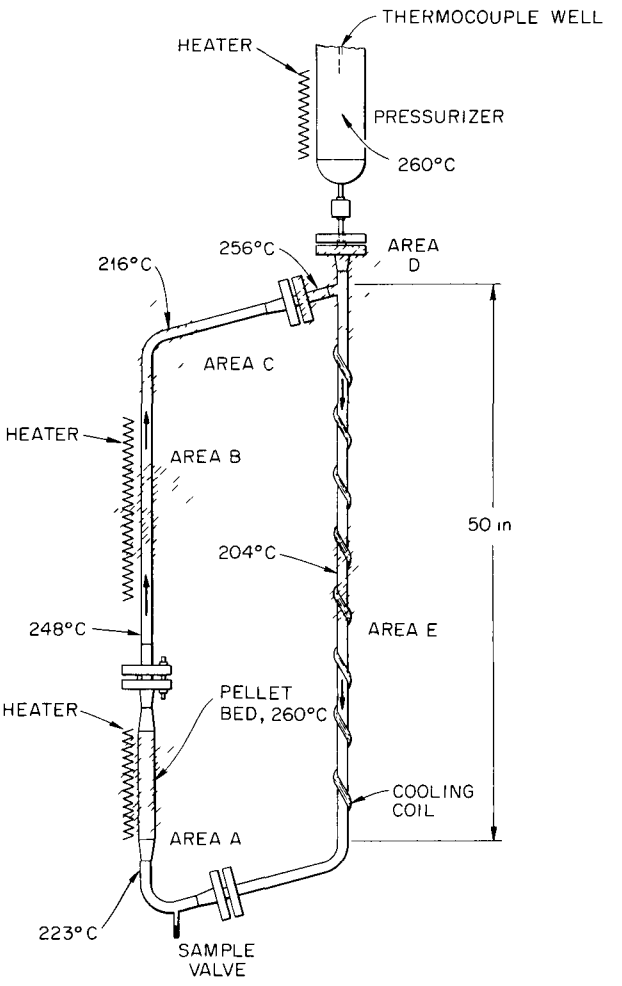

Fig. 14.3. Thermal Convection Loop Used for Testing Code P-82 Pellets.

Table 14.3. Distribution of Residual Thorium and Ra^{228} Activities in Thermal-Convection-Loop Piping

Area	Approximate Temperature (°C)	Thorium Activity[a]	Ra^{228} Activity[a]
A (bed)	260	10	60–70
B (heater)	255	None detected	None detected
C (heater outlet)	261	<1	2
D (cooler top)	256	1	10
E (cooler center)	204	1	15

[a]Ratio of activity to the activity of one ThO_2 pellet.

15. Examination of In-Pile Slurry Loop

During the past year the examination of materials from the first irradiated in-pile slurry loop experiment, L-2-27S, has been largely completed. Satisfactory operation of the loop in-pile for 2220 hr after 895 hr of preirradiation slurry circulation has been reported.[1-4] Prior to insertion in the reactor, the circulating slurry contained 980 g of Th per liter at 280°C (1350 g of Th per kg of D_2O), with an enriched-uranium/thorium ratio of 0.004, and 0.019 *m* palladium. The circulating concentration was reduced during operation by removal of six samples and subsequently by six terminal samples.

LOOP CUTUP OBSERVATIONS

After irradiation was completed and the loop was drained, it was transferred to the post-irradiation examination facility for cutup, examination of components, and removal of corrosion specimens. Virtually all regions of the loop have been examined to some extent for evidence of slurry caking or localized erosion, with particular emphasis on the irradiated regions. No erosion or deposition of slurry was found. Sections of core piping, coupons, and coupon holders were carefully inspected. No nonrinsable solids were found, and no evidence of localized attack was seen. Coupon surfaces were covered by corrosion films which appeared perhaps less polished than those developed in unirradiated regions.

Visual examination of the internal parts of the circulating pump, including the scroll, impeller, and Al_2O_3 bearings, showed no undue wear on surfaces exposed to turbulent slurry flow. No deposition or caking of slurry was observed. The pump appeared to have been in excellent condition and capable of continued operation for an indefinite period.

The sintered-metal filter tube had broken loose at the rigidly attached end, and quantities of slurry were found in the filter annulus and in the pressurizer. The loss of solids through the cracked filter is believed to have occurred shortly after shipment of the loop to the X-10 area, and before the loop had been irradiated long. This view is supported by changes in concentration of samples of circulating slurry during this part of the run, and by the examination of material recovered from the filter annulus and pressurizer. Surface area, particle size, crystallite size, and fission- and neutron-activation-product activity of the material recovered from these regions showed levels characteristic of samples withdrawn near the beginning of the irradiation.

SLURRY FILTRATION

The availability in circulating slurry systems of clean water free of solids is important in the operation of both the slurry loop experiment and large-scale slurry systems. Consequently the development of the slurry filtration system used in the experiment is of general interest.

A thorough visual and metallographic examination of the sintered stainless steel filter has been

---

[1] E. L. Compere, H. C. Savage, *et al.*, *Reactor Chem. Div. Ann. Progr. Rept. Jan. 31, 1961*, ORNL-3127, pp 105–10.

[2] E. L. Compere, H. C. Savage, *et al.*, *HRP Progr. Rept. Dec. 1, 1960, to May 31, 1961*, ORNL-3167, pp 92–97.

[3] H. C. Savage *et al.*, *In-Pile Loop Irradiation of Aqueous Thoria-Urania Slurry at Elevated Temperatures. Design and In-Pile Operation of Loop L-2-27S*, ORNL-3222 (in press).

[4] E. L. Compere, H. C. Savage, *et al.*, *Trans. Am. Nuclear Soc.* 4(1), 57 (1961).

made.[5] Two types of deposits were noted on the filter: granular material on the filter walls and in some interstices, presumably ThO_2; and a film deposit (corrosion product) on the stainless steel grains. The deposit varied greatly from one region to another. Pressure-drop flow tests across the filter tube removed from the loop showed easy flow through the filter; thus reduction in flow rate through the pressurizer circuit observed in the loop experiment was not a result of filter plugging. It is attributed to near blockage of the pressurizer outlet line, which contained a 50-mil-ID capillary section, by slurry that leaked through the cracked filter tube.

MATERIAL BALANCE

Complete recovery of slurry solids from the slurry holdup tank enabled an accurate material balance of slurry solids. The slurry holdup tank received all slurry drained from the loop, including sample purges and slurry discharged at the termination of the experiment. Weights of material actually recovered in samples and weights of material recovered during cutup from the pressurizer and filter annulus were determined separately. The material balance obtained is shown in Table 15.1.

Caking Implications. – The high recovery shown in Table 15.1 implies very strongly that no appreciable loss of solids by deposition or caking remains undetected. Since no cakes have been found, it is inferred that no noteworthy solids deposition occurred in the experiment.

CORROSION

Corrosion specimens of Zircaloy-2, type 347 stainless steel, and titanium alloys 45A and 110AT were exposed at three flux levels and at two velocities, 8 and 22 fps. Each specimen holder contained an identical array of coupons.

Observations of the specimens and adjacent internal surfaces of the loop piping with stereo-optics did not show any marked accumulations of solids. Besides the normal oxide coloration, a number of specimens showed lighter shaded

[5] E. J. Manthos and E. H. Lee, *Metallographic Examination of a Sintered 347 SS Filter from In-Pile Slurry Loop L-2-27S*, ORNL Metallography Report No. 411 (Nov. 30, 1961).

Table 15.1. Slurry-Solids Material Balance

	Input (g)	Recovery (g)	
Y-12			
DT-22 thoria-urania	1395.4		
Catalyst solids	167.3		
Corrosion products	5	Samples	451.1
Y-12 subtotals	1567.7		451.1
Net transferred to X-10	1116.6		
X-10			
Catalyst solids	6.6	Filter assembly	86
Corrosion products	7	Pressurizer	268
Tracer solids (just before shutdown)	9.0	Samples	293.5
		Slurry holdup tank	481
Totals	1590.3		1579.6

regions, which might have been very thin deposits of thoria solids. Several Zircaloy-2 specimens showed markings having the appearance of stringer-corrosion striations across the length of the specimens. These markings were present in the specimens originally, their visibility apparently being somewhat enhanced as a result of the in-pile exposure.

Table 15.2 shows the weight-change data obtained. The flow of the slurry was from the lower

Table 15.2. Weight Changes of Corrosion Coupons from In-Pile Slurry Loop

Specimen	Position	Weight Removed by Scrubbing (mg)		Weight Removed by Defilming (mg)		Weight Change of Scrubbed (or Scrubbed and Defilmed) Specimens (mg)	
		8 fps	22 fps	8 fps	22 fps	8 fps	22 fps
Zircaloy-2							
Unirradiated	1	5.4	3.6			+1.2	−26.1
	4	5.9	4.2			+0.7	−28.5
	5	4.2	3.4	0.4	4.8	+0.3	−29.3
	8	5.0	3.7			+0.8	−50.4
Low flux[a]	1	3.7	3.1			+3.7	−17.8
	4	4.0	2.3			+4.0	+1.5
	5	4.0	1.7	0.7	1.2	+3.0	+0.8
	8	5.0	2.4			+3.9	+3.1
High flux[b]	1	2.3				−3.5	
	4	4.7				+5.0	
	5	3.8		0.9	0.4	+3.9	
	8						
1 mpy ≈ 9 mg metal lost or 3 mg oxygen pickup in 3115 hr of slurry circulation							
Titanium-110AT							
Unirradiated	2	33.4	4.1			+7.8	−17.6
Low flux[a]	2	3.8	2.2			−0.4	−7.9
High flux[b]	2	1.4				−1.0	
Titanium-45A							
Unirradiated	7	26.3	3.6			+5.5	−14.5
Low flux[a]	7	4.3	4.7			+0.5	+0.5
High flux[b]	7	3.3				+0.7	
1 mpy ≈ 7 mg metal lost or 4 mg oxygen pickup in 3115 hr of slurry circulation							
347 Stainless Steel							
Unirradiated	3	3.8	5.8			+1.3	−39.5
	6	4.8	2.1	0.7	2.8	−1.9	−36.9
Low flux[a]	3	2.2	1.6			+0.5	−10.1
	6	1.8	2.5	25.6	75.0	−25.1	−80.0
High flux[b]	3	3.4				+0.3	
	6	4.2		153.6	129.0	−153.1	
1 mpy ≈ 12 mg metal lost or 2 mg oxygen pickup (net with CrO_3 loss) in 3115 hr of slurry circulation							

[a] At core-rear position ($\sim 10^{12}$ *nv*).
[b] At core-front position ($\sim 10^{13}$ *nv*).

to the higher position number. The total area of the ¼- by ⅝- by 1/16-in. coupons was 2.7 cm^2, and the exposed wetted area was 1.6 cm^2. Weight change data were not obtained for specimens in the high-flux 22-fps holder, as the specimens were slightly damaged during recovery.

Corrosion of Zircaloy-2 was not great, and little or no radiation effect is revealed. At low velocities, slight weight gains were predominant; at high velocities, particularly in the unirradiated region, weight losses amounting to as much as 5.5 mpy were noted. It is concluded that under the conditions of the experiment no enhancement of corrosion by radiation was revealed. However, data from the high-flux 22-fps position to support this conclusion were not available.

No substantial radiation effect is seen for the titanium alloys. Corrosion was most severe in the unirradiated 22-fps holder, similar to the case of Zircaloy-2.

Stainless steel appears to exhibit both a substantial effect of irradiation and a substantial effect of velocity. Whether the effects are simply additive or are synergistic is not resolved, since data from the high-flux 22-fps holder is not complete. However, the major portion of the corrosion products was removed by defilming in the majority of cases. The amount of film removed from the high-flux 22-fps specimen is slightly lower than that from the 8-fps high-flux specimen. Assuming that the film value is representative of corrosion, the radiation effect does not appear to have been increased at the higher velocity. The maximum observed corrosion rate corresponded to about 13 mpy.

The generalized corrosion rate of the stainless steel in the loop main stream, as indicated by the rate of decrease of O_2 pressure and the rate of accumulation of iron in the slurry, was 0.4 mpy.[6]

RADIOCHEMICAL CONSIDERATIONS

The radiochemical examination of terminal and other slurry samples enabled calculation of fission dose, burnup, and average flux and observation of the distribution of fission and activation products. The calculation of total fissions was based on Zr^{95} and Ce^{144}. Cesium-137 was regarded as a less reliable nuclide for this purpose, since it partitioned between solid and liquid phases in an inadequately defined way. As shown in Table 15.3, 7×10^{16} fissions per gram of slurry solids resulted during the 1839 hr of net irradiation exposure developed during the 2220-hr in-pile period.

A conversion of 4.0×10^{17} atoms of Th per gram of solids was calculated from Pa^{233} counting, during the exposure of 1.6×10^{19} *nvt*. An apparent effective thorium cross section of 10.9 barns is estimated from these data.

Table 15.3. Radiochemical Data from In-Pile Slurry Loop L-2-27S

(Irradiated 1839 hr)

Fissions per gram of solids	7×10^{16}
Burnup	0.9% of orig. U^{235} or 0.003% of metal atoms
Average flux	2.4×10^{12}
nvt	1.6×10^{19}
Distribution of fission products, *K* (solids/liquid)	
Cs^{137}	~1
Zr^{95}	$>10^5$
Ce^{144}	10^4
Pa^{233}	10^4

EFFECTS ON SLURRY PARTICLES

The effects of irradiation and circulation on the properties of the slurry particles developed progressively as the experiment continued.[7] As is shown in Fig. 15.1, particle size continued to degrade throughout most of the run. The original average particle diameter was 1.7 μ; the final diameter was 0.3 μ. As much as 25% by weight

[6] E. L. Compere *et al.*, *HRP Progr. Rept. Aug. 1 to Nov. 30, 1960*, ORNL-3061, p 90.

[7] E. L. Compere, A. J. Shor, L. F. Woo, and H. C. Savage, "Irradiation Effects on Thoria-Urania Slurries," paper 27 in *Nuclear Reactor Chemistry, Second Conference, Gatlinburg, Tenn., Oct. 10–12, 1961*, TID-7622 (in press).

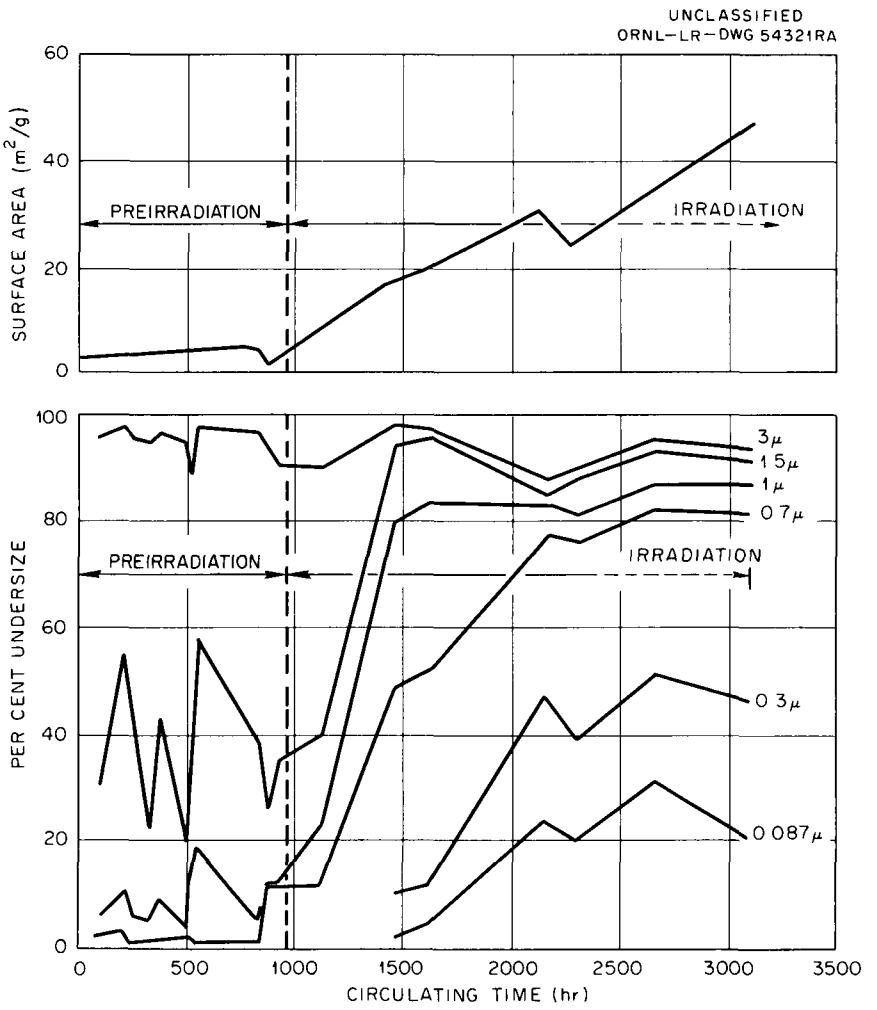

Fig. 15.1. Effect of Irradiation and Circulation on Slurry Particle-Size Distribution and Surface Area.

of the material was reduced to below 0.087 μ (870 A). A regular increase in surface area, from 2–4 m^2/g to over 40 m^2/g, occurred as irradiation continued.

Crystallite size was determined on four-month-cooled samples by x-ray line broadening techniques. These data are compared with the corresponding surface-area measurements in Fig. 15.2. An inverse relationship is indicated, similar to that suggested[8] for thoria preparations fired at different temperatures. However, surface areas of irradiated material consistently ran above the maximum theoretical value (sphere or cube) for a given crystallite size.

Automatic techniques[9] of pore-volume determination[10] recently developed at the Oak Ridge Gaseous Diffusion Plant were applied[11] to samples from the experiment.

Distribution of pore volume as a function of pore radius is shown in Fig. 15.3. The pore-area distribution calculated from these data is presented in Fig. 15.4. It may first be noted that the

[8] V. D. Allred, S. R. Buxton, and J. P. McBride, *J. Phys. Chem.* 61, 117–20 (1957).

[9] P. G. Dake, E. A. Woy, and H. A. Kermicle, *Routine Automatic N Adsorption-Desorption Measurements*, paper 48, Fifth Conference on Analytical Chemistry in Nuclear Reactor Technology, Gatlinburg, Tenn., Oct. 10–12, 1961.

[10] E. P. Barrett, L. G. Joyner, and P. P. Halenda, *J. Am. Chem. Soc.* 73, 373–80 (1951).

[11] A computer code developed by Barton Roberts of the Reactor Chemistry Division was used.

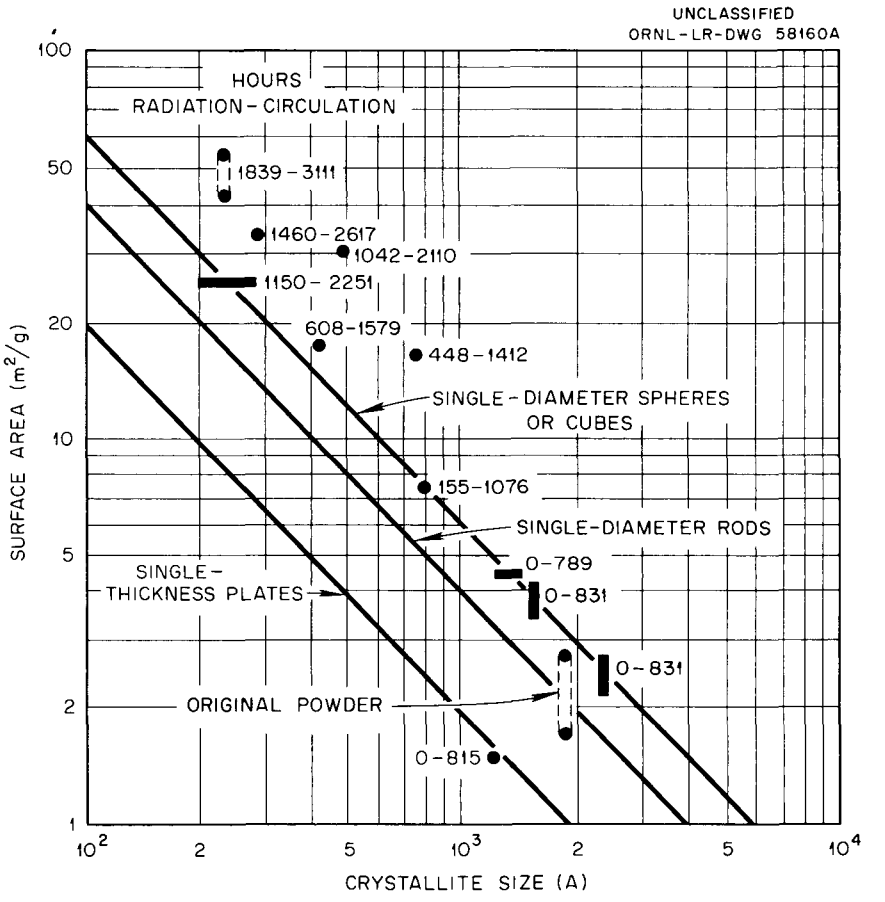

Fig. 15.2. Effect of Irradiation on Properties of Slurry Particles in In-Pile Loop Experiment.

integrated pore and surface areas agree reasonably well with BET monolayer determination. The lower curve is for the original thoria-urania powder; the intermediate curve is for the mixture of this powder with the low-fired thoria-supported palladium catalyst, after 831 hr of circulation, and the upper curve is for the fully irradiated slurry. More than half the area of the irradiated material is associated with pores of radius below 45 A; a substantial fraction is associated with pores of radius below 10 A.

The possibility of evaporation[12] of thoria by fission fragments in aqueous systems has been noted by Sowden,[13] who reported evaporation of 5000 or more atoms per fission. In the case of the loop experiment, it has been estimated that all fission fragments escape the original particle and about 10% of them enter another particle. Assuming that all energy below 116 kev directly results in knockons,[14] and using 6.9 ev as the energy of evaporation of thoria, then about 3500 thorium atoms per fission might be evaporated. In the course of the experiment about 10% of the thorium atoms in the slurry would have been evaporated. In the flocculated slurry system these

[12] F. C. Lapteva and B. V. Ershler, *Atomnaya Energ.* 4, 63–66, (1956).

[13] R. G. Sowden, B. R. Harder, and A. E. Truswell (AERE, Harwell, England), and H. S. G. Slooten (N. V. KEMA, Arnhem, The Netherlands), "Irradiation Experiments with Aqueous Suspensions of PuO_2 and ThO_2-UO_2," paper 26 in *Nuclear Reactor Chemistry, Second Conference, Gatlinburg, Tenn., Oct. 10–12, 1961*, TID-7622 (in press).

[14] G. J. Dienes and G. H. Vineyard, *Radiation Effects in Solids*, p 9, Interscience, New York, 1957.

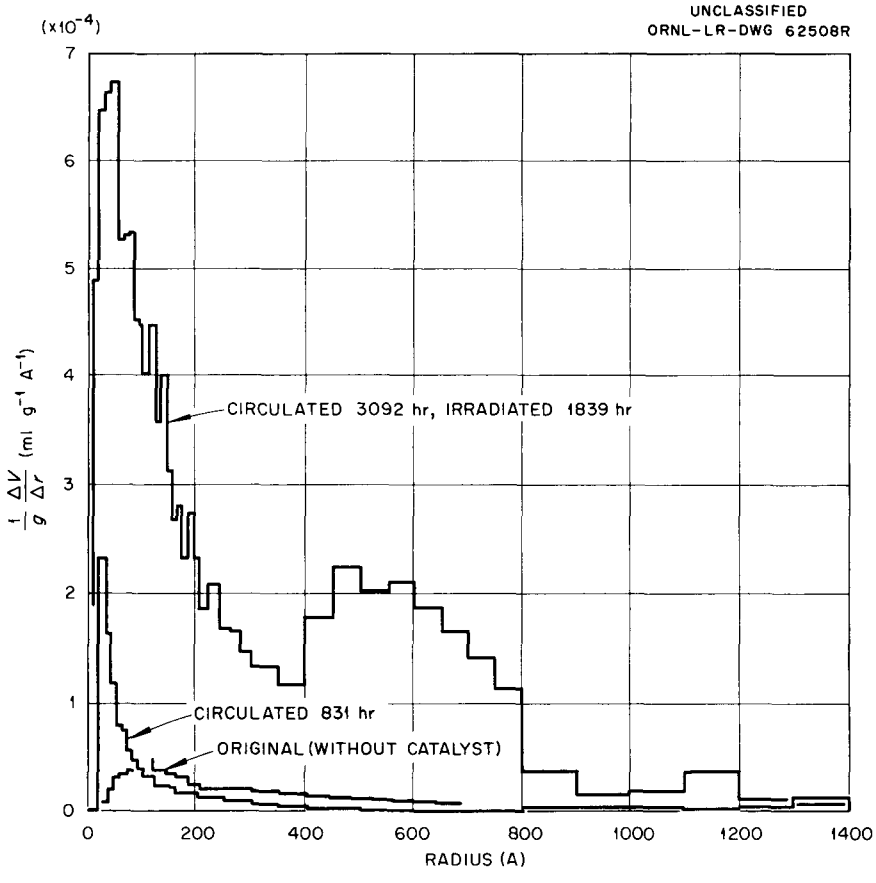

Fig. 15.3. Distribution of Pore Volume as a Function of Pore Radius.

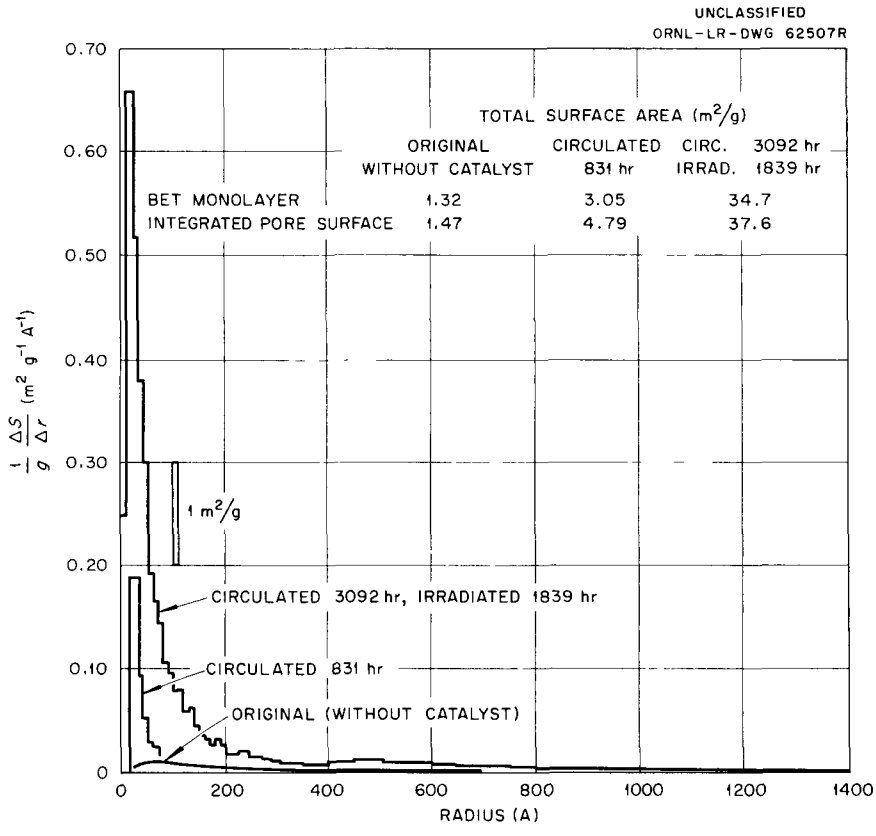

Fig. 15.4. Distribution of Surface Area as a Function of Pore Radius.

finely colloidal thoria particles would be gathered to existing slurry particles in the same fashion as corrosion products, catalyst-thoria preparations, and fission product oxides have been observed to do. A more flocculated slurry should result and has been observed.

Electron microscope photographs of samples of the irradiated circulated slurry from various stages of the experiment are shown in Fig. 15.5. The original particles were somewhat cubic and fairly regular in size. As irradiation time became greater, particle edges became more irregular and the proportion of fines steadily increased. A few larger masses, possibly agglomerates, are seen, which may have resulted from the gathering of fines of various types on larger particles as circulation was continued.

The relative influences of irradiation and pump circulation on the particle-size degradation were of interest. Autoclave experiment L5Z-155S, described subsequently, was carried out, irradiating slurry and catalyst from the same batches used in the loop experiment to similar fission doses, at similar temperatures, concentrations, etc. The results are shown in Table 15.4.

Table 15.4. Effects of Irradiation and Circulation on Particle Properties

	Original	Loop[a]	Autoclave
Fissions per gram of solids	0	4×10^{16}	4×10^{16}
Surface area, m^2/g	4–8	25	30
Crystallite size, A	1800	300	220
Average particle size, μ	1.7	0.3	1.6

[a]The loop sample corresponded to 1460 hr of irradiation.

UNCLASSIFIED
ORNL-LR-DWG. 58164R

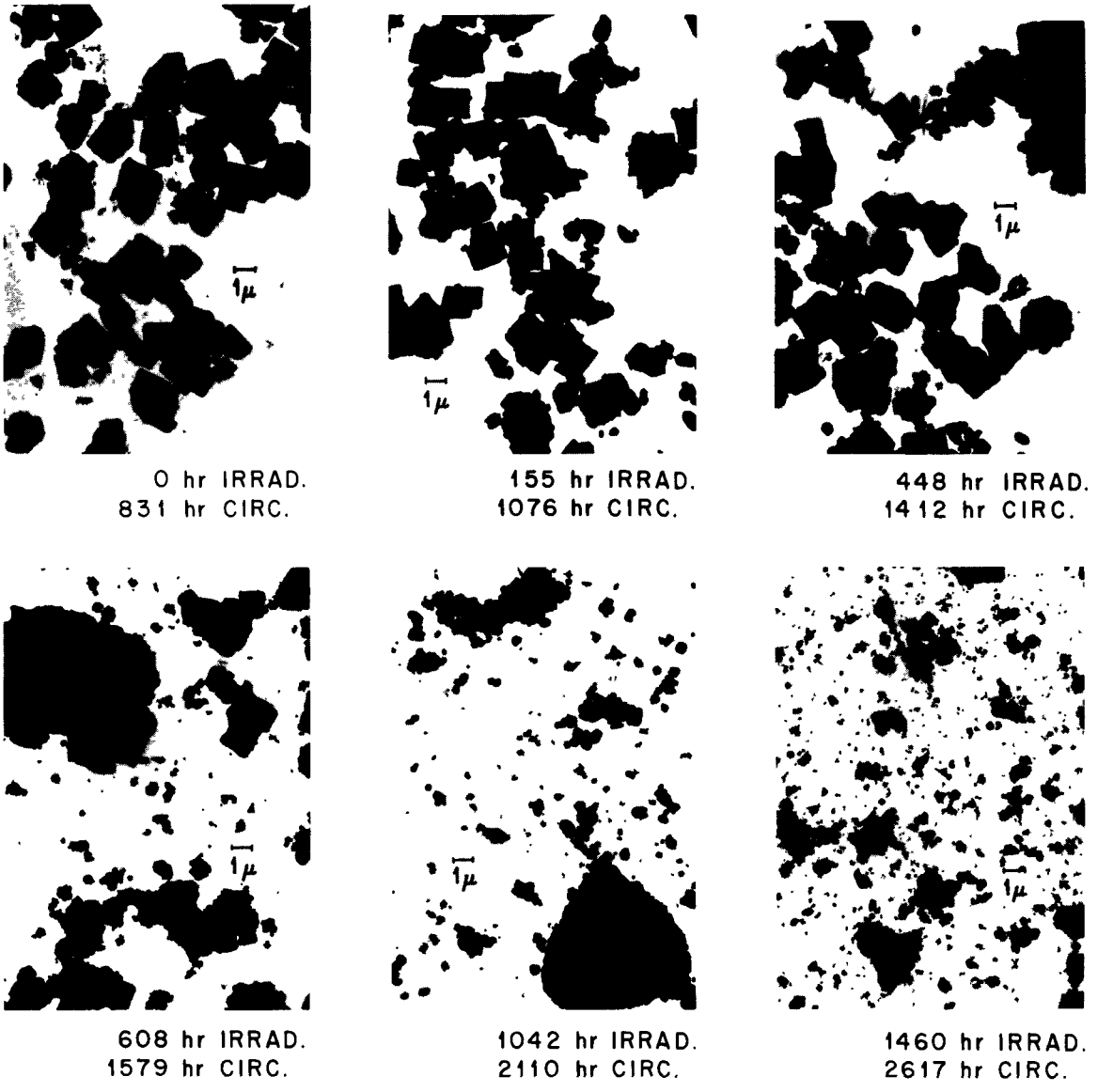

Fig. 15.5. Electron Photographs of Slurry from In-Pile Loop L-2-27S.

As may be seen, similar effects on surface area and crystallite size were found, but no effect at all on particle size resulted during the autoclave experiment. The combined action of circulation and fissioning in the slurry appears required to bring about the observed reduction in particle size.

Implications Regarding Reactor Applications. – The successful trouble-free operation of the loop demonstrated an effective tool for the examination of irradiation effects on slurries of interest for thorium power-breeder reactors. The lack of handling problems with the irradiated slurry in the loop experiment has indicated that the irradiation effects reported above do not necessarily preclude the utilization of thorium oxide slurries in breeder reactors.

16. Second In-Pile Loop Experiment

Following satisfactory completion of the first in-pile thorium oxide slurry loop experiment,[1,2] design and construction of a second in-pile loop experiment were initiated.

The primary objective of this loop experiment is to determine the combined effects of pumping and reactor irradiation on a pure thorium oxide slurry (ThO_2 dispersed in D_2O) in which a significant quantity of Th^{232} is converted to U^{233} in a manner simulating that for a thoria slurry circulated in an aqueous homogeneous breeder reactor. To meet this objective in a reasonable time, the loop was designed for operation in an experimental facility (beam hole HN-1) of the ORR, where the neutron flux is greater than that in the LITR.

Design, construction, and out-of-pile operation of the loop, as well as modifications to the experimental facility in the ORR, have been completed, and in-pile operation of the loop is scheduled to begin early in 1962.

LOOP DESIGN, CONSTRUCTION, AND TESTING

The second in-pile slurry loop, designated 0-1-28S, is shown in Fig. 16.1. Although its design is similar to that of the first slurry loop, L-2-27S,[2] several important modifications were made, based on experience gained from in-pile operation of L-2-27S and also because of the substantial increase in the radiation dose required to meet the objective of the second experiment.

The volume of the loop core section, which is closest to the lattice, was increased from 300 to 800 ml to increase from 35 to 60% the fraction of thoria exposed to the highest neutron flux. This was done by fabricating the core of concentric coils of $\frac{5}{8}$-in.-OD × 0.049-in.-wall tubing, as shown in Fig. 16.2.

Because of the mechanical failure of the sintered-metal filter in loop L-2-27S, two expansion bellows, one at each end of the filter tube, are used in the filter assembly of loop 0-1-28S. Only one bellows was used in L-2-27S, and the failure occurred at the fixed end of the filter. The sintered-metal filter (8-μ mean pore diameter) of type 347 stainless steel is used to provide a thoria-free filtrate as a pressurizer feed and as a pump-bearing purge. Satisfactory performance of this filter has been demonstrated in out-of-pile tests.

Changes to the horizontally mounted pressurizer included an increase in volume from 520 to 930 ml for additional expansion volume required when heating the larger loop slurry charge to operating temperature (280°C). In addition, the pressurizer was inclined slightly so that the outlet line is the lowest point in the pressurizer. This was done to minimize the possibility of gas entrainment into the pump purge in the event of low pressurizer liquid level.

Thirty-two corrosion test specimens of Zircaloy-2, titanium, and type 347 stainless steel are exposed to the circulating slurry in the loop main stream. These specimens are so located in the loop that duplicate specimen arrays are exposed at two flow velocities, 11 and 21 fps, and at two neutron flux levels.

Loop temperatures are monitored by 36 thermocouples, double the number in the previous loop. This will provide a great deal more information and knowledge about the performance of the loop and behavior of the slurry during in-pile operation

[1] H. C. Savage *et al.*, *In-Pile Loop Irradiation of Aqueous Thoria-Urania Slurry at Elevated Temperature. Design and In-Pile Operation of Loop L-2-27S*, ORNL-3222 (in press).

[2] E. L. Compere, H. C. Savage, *et al.*, *Reactor Chem. Div. Ann. Progr. Rept. Jan. 31, 1961*, ORNL-3127, pp 105–8 and Fig. 16.2.

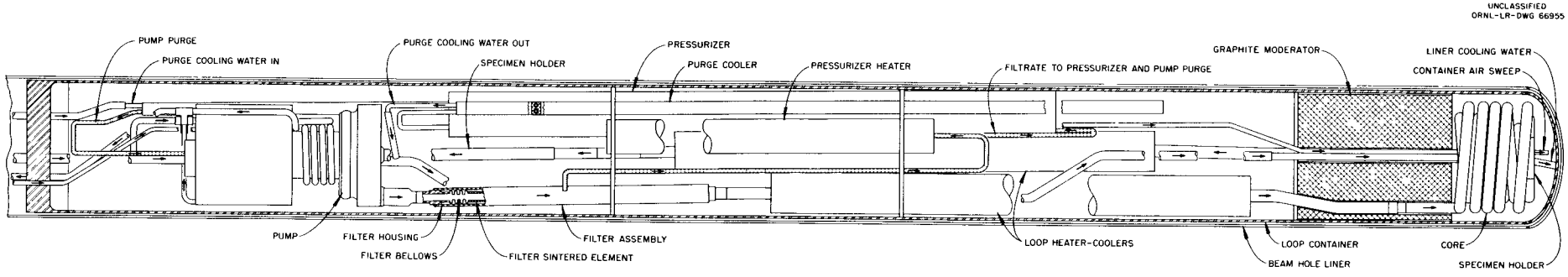

Fig. 16.1. In-Pile Slurry Loop 0-1-28S.

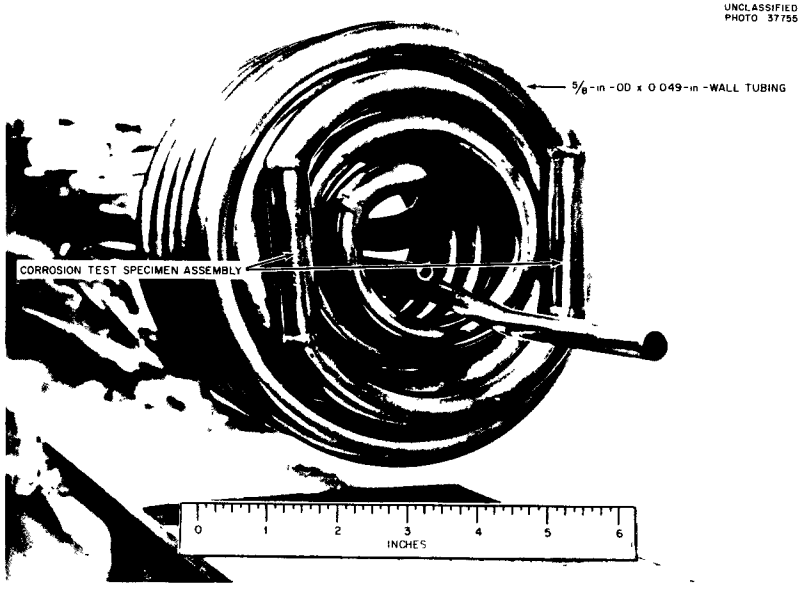

Fig. 16.2. Core Section for the ORR In-Pile Slurry Loop 0-1-28S.

EXPERIMENTAL FACILITY IN THE ORR

Slurry loop O-1-28S is to be operated in beam hole HN-1 of the ORR. This experimental facility was previously used for in-pile loop experiments with uranyl sulfate solutions.[3] However, several changes in the existing equipment were required for the shift to a slurry-loop experiment.

The stainless steel beam-hole liner was removed and replaced with a new liner of increased diameter ($4\frac{1}{2}$ in. to 8 in.) at the end adjacent to the reactor lattice. This increase in diameter was required to accommodate the enlarged core section of the loop, described above.

The loop will be charged with pure thoria rather than the thoria-urania ($\sim$0.4 wt % U^{235}) used in the first slurry loop experiment. To reach at least the fission fragment exposure of 7×10^{16} fissions per gram of solids attained in the previous experiment, the reactor fuel configuration in the vicinity of beam hole HN-1 will be rearranged to increase the neutron flux in the forward position of this beam hole. The best fuel arrangement was arrived at by flux-mapping experiments with various fuel loadings.[4]

Other modifications to the facility included the slurry sampling system, slurry addition system, a slurry dump tank equipped with a sintered-metal filter to retain all solids in the dump tank, and upgrading of the instrumentation to provide increased safety.

---

[3] H. C. Savage *et al., In-Pile Corrosion Test Loops for Aqueous Homogeneous Reactor Solutions,* ORNL-2977 (Nov. 10, 1960).

[4] A. J. Shor and T. H. Mauney, *Neutron Flux and Cd Ratio Measurements in the HN-1 Beam Hole for Three Fuel Loadings of the Oak Ridge Research Reactor,* ORNL TM-44 (Oct. 10, 1961).

17. In-Pile Slurry Autoclaves

In-pile slurry autoclave experiment L5Z-155S was performed[1] to compare the radiation effect of thoria-urania particles gently suspended in a rocking autoclave with that observed in slurry pumped in the in-pile slurry loop experiment L-2-27S. The Zircaloy-2 autoclave contained a thoria-urania slurry (~0.4 wt % U^{235}) prepared from the same batch (DT-22) used in the in-pile slurry loop experiment. The autoclave, loaded with slurry at a concentration of 996 g of thorium per kg of D_2O which was 0.014 *m* in Pd and with an oxygen overpressure, was operated for a total of 770 hr at 280°C. The autoclave was irradiated for 453 hr in the HB-5 facility of the LITR, achieving an effective full-flux time of 87% of this. Based on an average flux in the autoclave of 6.7×10^{12} thermal neutrons cm^{-2} sec^{-1} (corresponding to an *nvt* of 9.6×10^{18}), obtained from an activation of a cobalt flux monitor located inside the autoclave, the slurry particles developed 4.4×10^{16} fissions per g of solids.

Neutron captures by thorium, based on Pa^{233} counting, were 1.7×10^{17} captures per g of solids, leading to an estimated thorium cross section of 8.5 barns, which agrees favorably with the activation cross section of 7.7 ± 0.4 barns cited by Weinberg and Wigner.[2]

The autoclave was equipped with an Al_2O_3 filter to protect the capillary line to the pressure instrument. No indication of plugging of this line was noted during in-pile operation. However, a venting lag was encountered, and when the autoclave was later opened, the filter was found cracked off.

RADIOLYTIC GAS

Due to aberrations in temperature readings, caused by a faulty instrument cable, knowledge of the radiolytic gas generated was not very well defined. Some few observations which appear to be reliable indicate the absence of any radiolytic gas. It is believed that the catalytic and the gamma recombination were sufficient in the experiment to prevent the development of observable radiolytic-gas pressures.

CORROSION

Generalized corrosion was followed in the usual manner, by measuring the decrease in oxygen

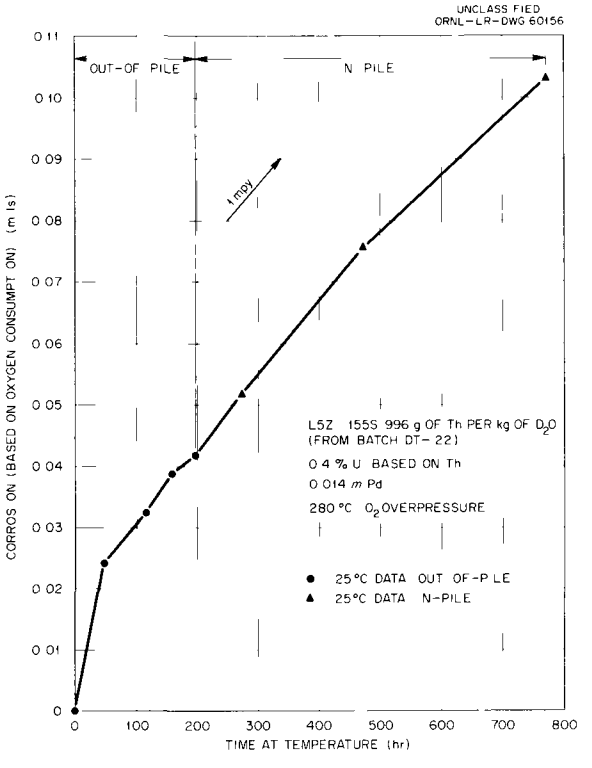

Fig. 17.1. Generalized Corrosion in Experiment L5Z-155S, Autoclave Control for In-Pile Slurry Loop L-2-27S.

[1] E. L. Compere *et al.*, *HRP Progr. Rept. Dec. 1, 1960, to May 31, 1961*, ORNL-3167, pp 87–91.

[2] A. M. Weinberg and E. P. Wigner, *The Physical Theory of Neutron Chain Reactors*, p 83, University of Chicago Press, Chicago, 1958.

pressure at periodic shutdowns. As indicated in Fig. 17.1, an out-of-pile corrosion rate of 4.4 mpy was observed for the first 48 hr. The rate decreased to 1 mpy for the remaining period out-of-pile. Upon irradiation the corrosion rate remained essentially constant at 1 mpy. Thus no effect of irradiation on the generalized corrosion was observed in this experiment.

Corrosion of coupon specimens (Table 17.1), determined from weight changes, was less than that indicated by oxygen measurements, possibly due both to the small amount of corrosion which actually occurred and to an inadequate technique for completely removing the Zircaloy-2 corrosion film from specimens for an accurate weight-loss determination. Stainless steel coupon corrosion was high, as in the loop experiment.

RECOVERY OF THE IRRADIATED SLURRY

A primary purpose of the experiment was the recovery of as much of the irradiated slurry as possible for the assessment of radiation effects. Since the irradiated slurry had settled for 30 days while its radioactivity decayed, resuspension was attempted by inverting the autoclave 100 times. The autoclave head was then removed and a 4.5-ml portion of the slurry was removed with a pipette. The autoclave was filled with distilled water, and its remaining contents were mixed by repeatedly drawing the slurry into the pipette and forcing it back into the autoclave. The autoclave was subsequently inverted over a funnel, and slurry remaining on the inside walls was rinsed with jets of water from small holes in a copper tube. A small amount of thickened slurry was noted on the autoclave head as it was removed.

All the recovered slurry was composited in a single beaker, and the water volume was reduced under a heat lamp. While the slurry was thoroughly agitated, two samples were removed for particle-size analyses. Then dried samples were removed for determination of surface area, crystallite size by x-ray diffraction, and pore-size distribution.

Table 17.1. Radiation Corrosion of Coupon Specimens in Zircaloy-2 Autoclave Experiment L5Z-155S

Temperature, °C	280
Concentration of slurry, g of Th per kg of D_2O	996
Enriched U, with respect to Th, wt %	0.4
Concentration of Pd catalyst, *m*	0.014
Atmosphere	Excess O_2
Type of autoclave	Zircaloy-2
Total hours at temperature	770
Hours irradiated	453
Effective full-flux irradiation time, fraction of 453 hr	0.872
Flux, thermal neutrons cm^{-2} sec^{-1} (in the fully inserted position)	6.7×10^{12}
Maximum power density, w/ml, at 280°C	0.9
Average power density while irradiated, w/ml, at 280°C	0.9
Autoclave generalized corrosion,[a] μin.	92
Coupon-specimen corrosion, μin.	
Zircaloy-2	3, 4, 10, 3
Ti-75A	5
Type 347 stainless steel	434

[a]Zircaloy-2 corrosion based on O_2 measurements after correction for oxygen uptake by type 347 stainless steel corrosion coupon.

EFFECT OF IRRADIATION ON PARTICLE INTEGRITY

The surface area of the original thoria-urania (92%) was 2 m^2/g, and that of the finely divided palladium-thoria catalyst (8%) was 53 m^2/g. The surface area of the unirradiated mixture (control) was 8 m^2/g. After irradiation, the surface area of the slurry was 30 m^2/g. Thus irradiation resulted in an increase in surface area similar to that shown by loop samples at an equivalent *nvt*.

Crystallite size of the slurry in the unirradiated mixture determined by x-ray diffraction was 1800 A. After irradiation the crystallite size of the slurry had diminished to 220 A, indicating radiation effects similar to those shown by loop samples.

The results of the particle-size analyses of the irradiated slurry and an unirradiated replicate mixture (control) are shown in Fig. 17.2. Although some agglomeration of fines was indicated in the irradiated slurry, as compared with the unirradiated material, no particular degradation of the slurry was seen.

In Figs. 17.3 and 17.4 the pore-size distribution of the slurry irradiated in autoclave L5Z-155S is compared with the distributions for the slurry circulated in loop L-2-27S for 831 hr without irradiation and for that circulated in the loop for 3092 hr and irradiated for 1839 hr. The pore-size distributions of the slurries irradiated in the loop and autoclave are similar, in that both slurries showed a marked increase in the number of pores of small radii as compared with the unirradiated slurry.

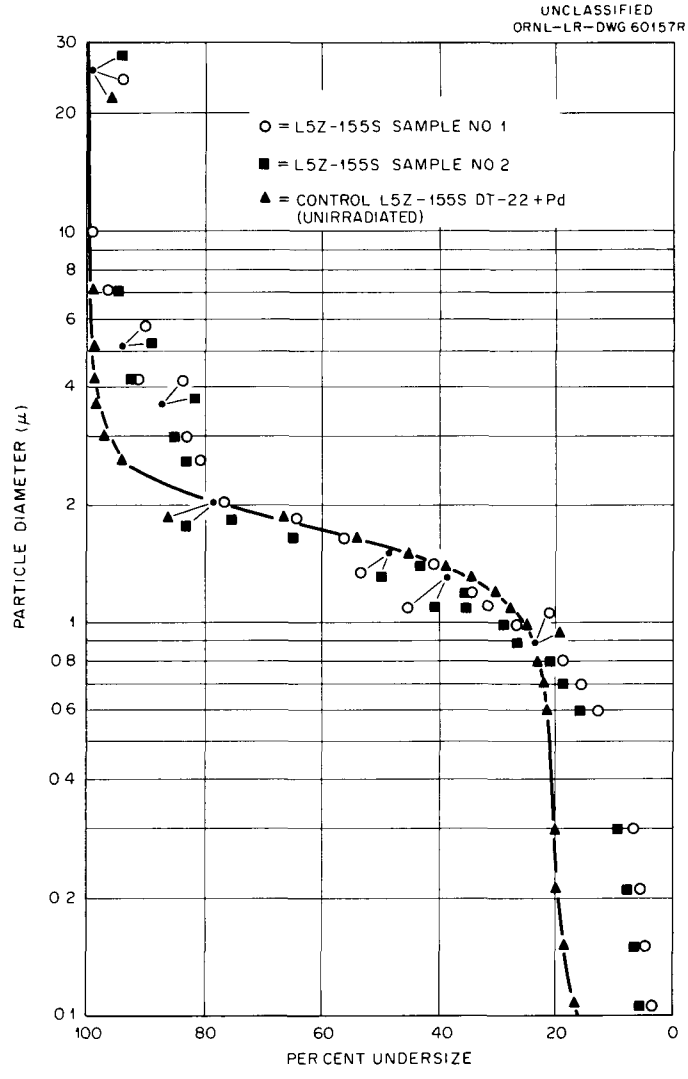

Fig. 17.2. Effect of Irradiation (10^{19} *nvt*) on Particle Size of Slurry Mixture.

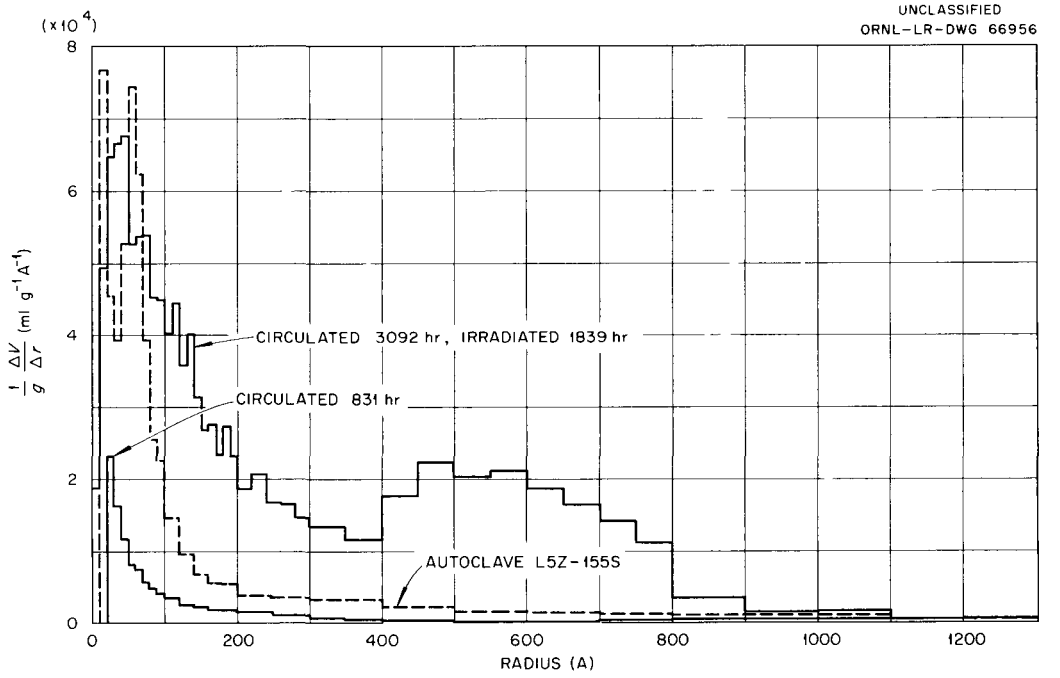

Fig. 17.3. Distribution of Pore Volume as a Function of Pore Radius.

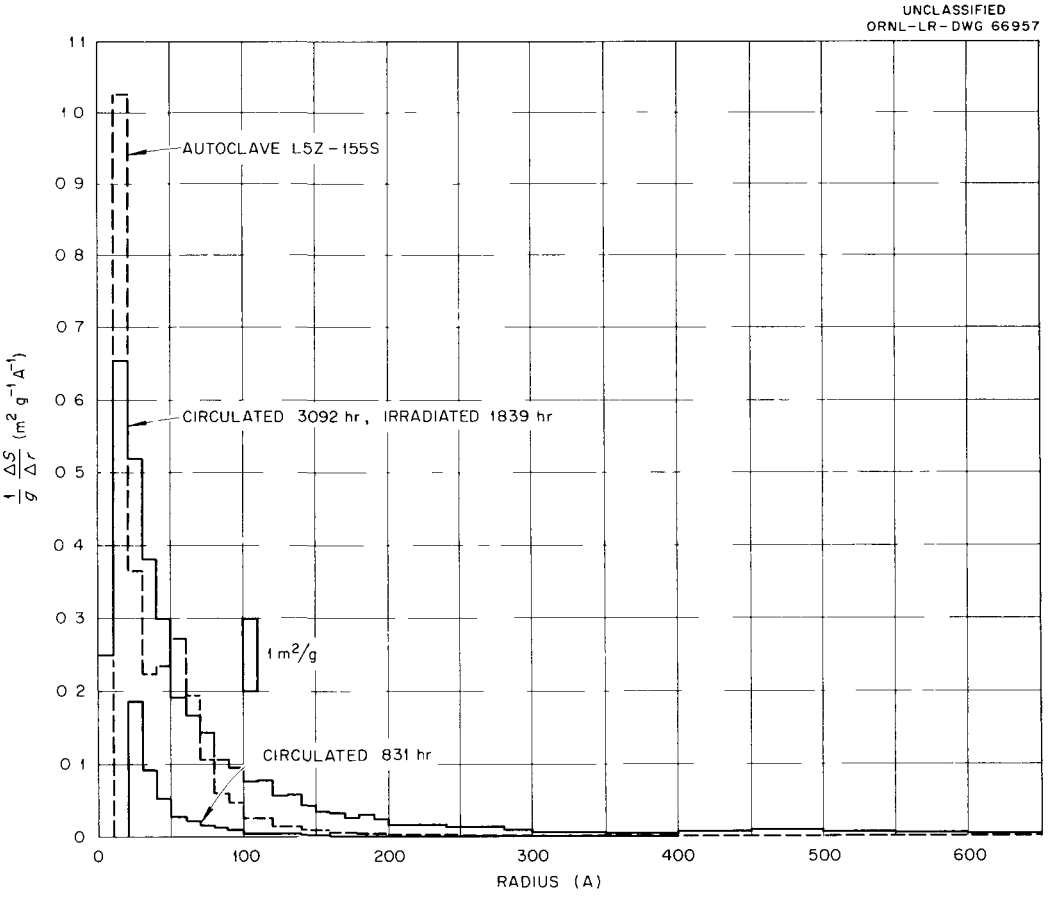

Fig. 17.4. Distribution of Surface Area as a Function of Pore Radius.

From the results of the physical measurements it is inferred that irradiation does indeed cause defects in the slurry particles, as observed by an increase in surface area, an increase in number of small pores, and a decrease in crystallite size, but that particle agitation more severe than that experienced in a rocking autoclave is necessary to break up the slurry particles.

SIMULATION OF FISSION DAMAGE TO $Th(U)O_2$ BY CYCLOTRON IRRADIATION

In an attempt to simulate fission damage to thoria-urania powders of interest in in-pile irradiation experiments, bombardments of dry targets of pure thoria (batch DT-46, to be used in in-pile slurry loop experiment O-1-28S) and thoria–0.4% enriched urania (batch DT-22, used in in-pile slurry loop experiment L-2-27S) have been made with the 28-Mev 63-in. nitrogen (3+) particle cyclotron and the 22.4-Mev 86-in. proton cyclotron. Because of the small size of the irradiated region (3×13 mm in the 63-in. cyclotron), crystallite size change was to be used as the criterion of irradiation degradation effects similar to those observed in in-pile experiments. Targets (both before and after irradiation) were transferred, without any disturbance of the thoria powder, to the x-ray diffraction apparatus, where x-ray line broadening was determined. Observation of line broadening in pressed targets before irradiation led to the adoption of slip casting and drying as the common preparation technique.

Targets were irradiated to achieve energy absorptions of $(1.5–6) \times 10^5$ w-sec per g of solids. The fission-energy absorption by slurry particles in in-pile slurry loop experiment L-2-27S is estimated to have been 2×10^5 w-sec per g of solids. Irradiation of the pure thoria target changed the color of the target region from white to robin's-egg blue. Irradiation of the thoria–0.4% urania changed the color of the target region from tan-white to gray.

In no case was any significant change in crystallite size observed in the dry thoria targets as a result of irradiation.

Part IV

Support for High-Temperature Solid-Fueled Reactors

18. Transport of Noble Gases in Graphites

J. Truitt N. V. Smith G. M. Watson R. B. Evans III E. A. Mason[1]

Gas-cooled reactors will benefit markedly if the ceramic fuel elements can be operated without impervious cladding and if, at the same time, the coolant (helium) stream can be kept relatively free of radioactive fission products. A possible configuration to achieve these contradictory requirements maintains the fuel elements within porous graphite sleeves through which helium bleeds from the main coolant stream to purge the radioactive gases into a side stream. Flow mechanisms and the applicability of various flow theories have, accordingly, been investigated for "back-diffusion" against a stream of helium flowing through porous materials.

The theoretical studies have advanced from isothermal uniform-pressure conditions to isothermal conditions where the pressure is nonuniform and, more recently, to conditions where the temperature is nonuniform. The experimental work has progressed at a somewhat slower pace than in the past, as the experiments are currently being carried out with low-permeability graphites which are slightly more difficult to handle than the highly permeable materials used in the initial experiments.[2-4] A detailed report of the theoretical and experimental progress attained during the last year is beyond the scope of the present report, and only the highlights are covered in the sections to follow. However, a special progress report,[5] which is detailed and complete, has been issued.

THEORETICAL STUDIES OF DIFFUSION MODELS APPLICABLE TO POROUS MEDIA

A model was derived for the diffusion of gases in porous media in the absence of temperature and pressure gradients, in which portions of the medium are visualized as a collection of uniformly distributed "dust particles" (giant molecules) which are constrained to be stationary.[6] Thus it was possible to derive all the desired results very simply from rigorous kinetic theory as special cases of multicomponent mixtures. The results apply over the entire pressure range from the Knudsen region to the normal diffusion region. This model permits the first satisfactory theoretical derivation of the experimentally discovered fact that the flux ratio for binary mixtures in a steady-state experiment is equal to $(m_2/m_1)^{1/2}$ at *all* pressures (not just in the low-pressure region) when pressure gradients are absent.

The effect of nonzero pressure gradients on the diffusion equations is to introduce into the fundamental kinetic-theory equations both a pressure diffusion term and an external force term.[7] Somewhat surprisingly, there is a considerable cancellation of terms, and the final diffusion

[1] Consultant, Institute for Molecular Physics, University of Maryland, College Park.

[2] R. B. Evans III, J. Truitt, and G. M. Watson, *Superposition of Forced and Diffusive Flow in a Large Pore Graphite*, ORNL-3067 (Feb. 24, 1961).

[3] J. Truitt, *Interdiffusion of Helium and Argon in Speer Moderator No. 1 Graphite (A Terminal Report on Large Pore Graphites -- Experimental Phase)*, ORNL-3117 (June 6, 1961).

[4] R. B. Evans III, J. Truitt, and G. M. Watson, *J. Chem. Eng. Data* 6(4), 522 (1961).

[5] J. Truitt *et al.*, *Transport of Noble Gases in Graphites (A Progress Report for the Period Jan. 31, 1961, to Jan. 31, 1962)*, ORNL-TM (in press).

[6] R. B. Evans III, G. M. Watson, and E. A. Mason, *J. Chem. Phys.* 35(12), 2076 (1961).

[7] R. B. Evans III, G. M. Watson, and E. A. Mason, "Gaseous Diffusion in Porous Media. II. Effect of Pressure Gradients," *J. Chem. Phys.* (in press).

equation has the same form as that for the uniform-pressure case. No additional parameters beyond those necessary to define a diffusing system at uniform pressure are thus required to compute the diffusion rates when pressure gradients are present.

A complete solution for the nonuniform-pressure case requires also a forced-flow equation giving J (the net flux) as a fuction of the pressure gradient. A forced-flow equation was derived on the basis of the "dusty gas" model, but one parameter must be made disposable in order to compensate for the fact that the model permits only a diffusive and not a viscous mechanism for flow. Good agreement was found between the model and available experimental data for highly permeable graphites. The model gives no quantitative a priori characterization of the porous medium itself, but if one gas mixture is measured in a given medium, then the behavior of other gas mixtures in the same medium can be predicted.

SUPPORTING EXPERIMENTAL WORK

Two sets of diffusion experiments were completed during the report period. The experiments involved the diffusion of helium and argon in two low-permeability graphites. Insofar as possible, the total pressure of the gases was maintained constant along the diffusion paths within the graphite pores. A diagram of the experimental apparatus is shown in Fig. 18.1. As opposed to our earlier experiments with high-permeability graphites, appreciable Knudsen effects were observed, not only in the permeability results but also in the diffusion results. These diffusion results have offered the first opportunity to test the validity of the rate equation developed through the model studies. The applicable rate equation [in terms of the atom flux J_i (atom cm^{-2} sec^{-1}), the diffusion coefficient D_{ij} (cm^2/sec), the superficial diffusion length in the graphite L (cm), the gas density $n = p/kT$ (atom/cm^3), the concentration at the boundaries $x_i(O)$ and $x_i(L)$ (atom fraction), and a new quantity δ_i] is:

$$J = \frac{nD_{HeAr}}{L} \ln \left[\frac{J_{He} - \delta_{He} J\, x_{He}(L)}{J_{He} - \delta_{He} J\, x_{He}(O)} \right], \quad (1)$$

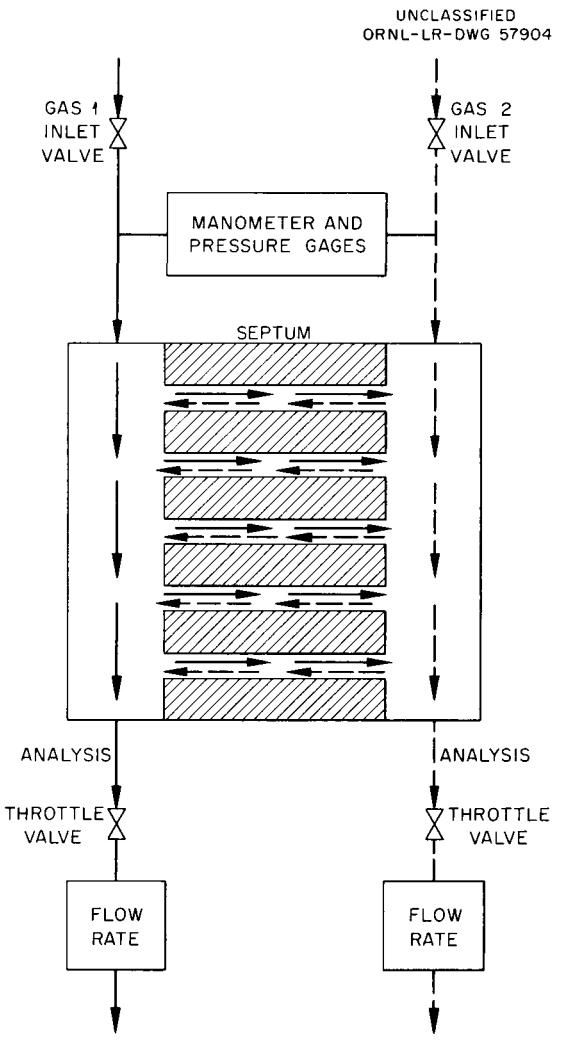

Fig. 18.1. Diagram of Steady-State Counter-Diffusion Experiment.

where

$$J = J_{He} + J_{Ar}, \quad (2)$$

$$\delta_{He}^{-1} = 1 + \frac{D_{HeAr}}{K_{He}(p \to 0)}. \quad (3)$$

Although $K_{He}(p \to 0)$, which is the intercept of the permeability coefficient versus p curve, and nD_{HeAr} do not vary with pressure, D_{HeAr} does; thus δ_{He} varies with pressure. The δ_{He} incorporates the contribution of the Knudsen effects on the diffusion behavior. It is interesting to note that this is the same equation (with $\delta_{He} = 1$) which was used to correlate the data for high-

permeability graphite. With $K_{He}(p \to 0)$ determined through permeability measurements and with interdiffusion data for two gases, one may determine D_{HeAr} through Eqs. (1), (2), and (3). Having determined these parameters, it is then possible to compute predicted curves for the diffusion behavior over a wide range of pressures under $dp/dz = 0$ conditions. A comparison of predicted and experimental results for one of the low-permeability graphites studied is shown on Fig. 18.2. The theoretical curve shows good agreement with the experimental data. Our current diffusion studies involve an extension of the low-permeability-graphite experiments from uniform-pressure to nonuniform-pressure conditions. The objective of these experiments is to determine the correct pressure dependence of the disposable parameter mentioned previously. In addition, the effects of graphite nonuniformity are under study.

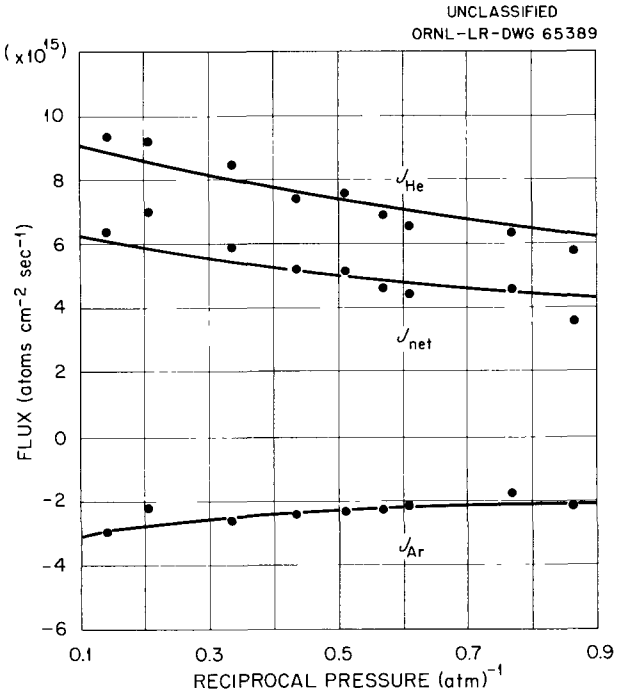

Fig. 18.2. Effect of Pressure on Diffusive Flux in Specimen III at 25°C.

CONCLUSIONS

A combination of the results of previous experiments with very permeable graphites and the results of classical treatments of kinetic theory of gases has led to the formulation of a gaseous diffusion model which is applicable to porous media in the absence of total-pressure gradients. Application of the model to earlier studies reveals that all conclusions made and equations used previously regarding uniform-pressure measurements remain valid. More important, the model appears applicable to all porous materials with a continuous porosity and over wide pressure ranges. The broad applicability of the model is suggested by theory and was verified recently by experiments with low-permeability materials. The interdiffusion characteristics of a given graphite can be readily defined by three parameters, D_{12}, δ_1, and δ_2. In addition to D_{12}, only one value of δ (actually D_{ik}) must be determined experimentally, and this can be done through permeability measurements. Recently, the theoretical treatment has been extended to cover nonuniform-pressure conditions. The results indicate that additional experimental data will be required to obtain complete verification of the extended theory.

19. Diffusion of Fuel and Nonvolatile Fission Products in Fuel-Graphite Systems

C. M. Blood R. B. Evans III

The proposed use of fuel elements composed of solid uranium dicarbide in contact with graphite in gas-cooled power reactors[1] (operating at 800 to 1200°C) suggests interesting solid-state diffusion problems. A knowledge of the rates of diffusion of nonvolatile solid fission products and of uranium through graphite would be useful information for the design of such a reactor. For this purpose, experimental solid-state diffusion studies have been started, with initial emphasis on porous AGOT graphites and with ultimate emphasis to be on pyrolytic carbon and/or graphites.

The diffusion of uranium for the UC_2–AGOT graphite system has been studied by Loch and co-workers.[2] This work has been examined to determine whether or not additional verification of the results is required and the advisability of applying the results to pyrolytic-carbon systems. It should be noted that a radical difference between the two carbon systems is not necessarily expected, and it has been deemed advantageous to review the older work in the light of recent reactor concepts.

The experimental work of Loch *et al.* covered a temperature range of 3300 to 4350°F. These investigators analyzed the concentration-penetration data on the basis of the equation:

$$C(x, t') = C_0 \operatorname{erfc} u , \qquad (1)$$

where

x = penetration distance in centimeters,

t' = exposure time in seconds for a fixed time interval,

$C(x, t')$ = concentration of uranium in graphite as a function of x and t',

$C_0 = \frac{1}{2} C_{UC_2}$ at $x = 0$ and $t = 0$,

$u = x/[2(Dt')^{1/2}]$, where D is the diffusion coefficient in square centimeters per second.

Such a treatment of the experimental data contains an anomaly; that is, the diffusion rates of uranium and carbon into graphites and UC_2, respectively, are assumed equal, though this equality is unlikely to exist.

The reported diffusion coefficients were obtained from the experimentally determined uranium concentration profiles. The concentration profiles were determined by assigning the uranium concentration for a given Δx volume increment to the midpoint of the increment; that is, the average uranium concentrations were assigned to the midpoints of Δx increments. This assignment of concentration values differs somewhat from the integral of the concentration profile. The values of D obtained by the method above ranged from 2.4×10^{-11} to 1.0×10^{-9} cm^2/sec at 3300 and 4250°F respectively.

Since there are some questions concerning the previous methods of correlation, these data have been reanalyzed by the present investigators on the basis of the fraction remaining which involves

[1] A. P. Fraas *et al.*, *Preliminary Design of a 10-Mu(T) Pebble-Bed Reactor Experiment*, ORNL CF-60-10-5 (Revised) (May 8, 1961).

[2] L. D. Loch, J. R. Gambino, W. H. Duckworth, "Diffusion of Uranium Through Graphite," p 145 in *Selected Papers from First Nuclear Engineering and Science Congress*, ed. by D. J. Hughes *et al.*, Pergamon Press, New York, 1957.

the integral of the concentration profile as follows:

$$M_{x_i \to \infty} = \int_{x_i}^{\infty} C(x, t')\, dV(x) , \qquad (2)$$

where $M_{x_i \to \infty}$ is the amount of uranium remaining after $M_0 \to x_i$ has been removed, C is a function of x and a fixed time (t'), and $dV = Adx$ is the volume as a function of x which is the linear diffusion direction normal to a constant area A.

Substitution of Eq. (1) into Eq. (2) for the semi-infinite case gives

$$M_{x_i \to \infty} = C_0 [2(Dt')^{1/2}]\, A \int_{x_i}^{\infty} \text{erfc } u\, du$$

$$= (C_0 A\, i \text{ erfc } u)\, [2(Dt')^{1/2}] , \qquad (3)$$

where u is that function in Eq. (1) referred to a fixed time t', and i represents the integral with the limits indicated.

It is desirable to rearrange Eq. (3) in some sort of dimensionless quantity in order to use available tabulated functions of erfc u versus u from which experimental values of $u = x/[2(Dt')^{1/2}]$ can be used to obtain D. For the self-diffusion of chromium in nickel-base alloys[3] employing Cr^{51} tracer, it was possible to use the dimensionless group $y = M_{x \to \infty}/M_{0 \to \infty}$ or fraction of the original total chromium, M, remaining from x to ∞. Calculations have shown that this fraction remaining became equal to i erfc u, which has been tabulated by Carslaw and Jaeger.[4] The quantity $M_{0 \to \infty}$ could be determined by counts before the initial electropolishing step, after which various $M_{x_i \to \infty}$ were obtained. The merit of this technique is that a determination of the concentration of chromium at the interface where $x = 0$ and $t = 0$ (and actually its precise location) is completely avoided. It would be somewhat difficult to obtain a value for the chromium concentration at the interface, since it depends on a determination of the location of $x = 0$. In similar calculations for the graphite–uranium carbide couple, the concentration of uranium at the interface must be estimated; one would not expect that the two layers could be separated at $x = 0$, where $C(x, t') = C_0$.

In order to obtain a dimensionless term like $y = M_{x \to \infty}/M_{0 \to \infty}$, both sides of Eq. (3) may be divided by $C_0 Ax$, forming the term $w = M_{x_i \to \infty}/C_0 Ax$. The relationship between w and the experimental data is shown as follows:

$$M_{x_i \to \infty}/C_0 Ax = \frac{1}{u}(i \text{ erfc } u) = w . \qquad (4)$$

The values for D calculated from this rigorous treatment were found to correlate well with those reported by Loch *et al.* For example, treating the data for specimen No. 20 at 4200°F (12 hr), a revised value of 6.9×10^{-10} for D was obtained (based on the second and third cuts), compared with the reported value of 7.4×10^{-10} cm^2/sec.

The predicted values for the groups $C(x, t')/C_0$, y, and w have been plotted vs u on Fig. 19.1 in terms of semilog coordinates. These plots show that the treated experimental data should be nearly a straight line analogous to that of a respective dimensionless group.

It is concluded that verification of the reported volume diffusion of uranium from UC_2 into AGOT graphite does not appear justifiable. A decision as to whether these results can be applied to pyrolytic-carbon systems will require an experimental investigation.

Loch *et al.* also reported that the depths of penetration of uranium by pore migration were ~100 times greater than those for the volume diffusion; however, the concentrations were very small. This kind of diffusion is not well understood, but may be possible in AGOT graphite. Further investigation of this phenomenon might be needed in view of problems related to solid fission products released. If migration of this type actually occurs in highly permeable materials, the use of highly permeable graphite even in fueled graphite bodies would be difficult to justify.

Considering the experimental technique of Loch and co-workers (where the concentration-penetration data were obtained by cutting depth increments of constant area normal to the interface), it becomes evident that amplification of the data would be very desirable. In their technique the interface was damaged in separating the components of the couple for the sampling procedure.

[3] R. B. Evans III, J. H. DeVan, and G. M. Watson, *Self-Diffusion on Chromium in Nickel-Base Alloys*, ORNL-2982 (Jan. 20, 1961).

[4] H. S. Carslaw and J. C. Jaeger, *Conduction of Heat in Solids*, Clarendon Press, Fair Lawn, N. J., 1947.

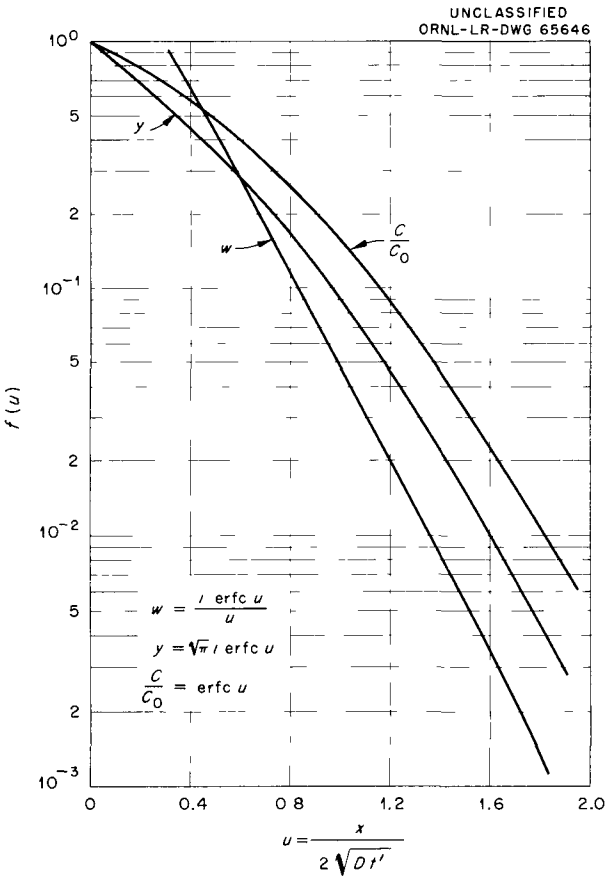

Fig. 19.1. Theoretical Relationship Between Diffusion Variables and the Diffusion Coefficient.

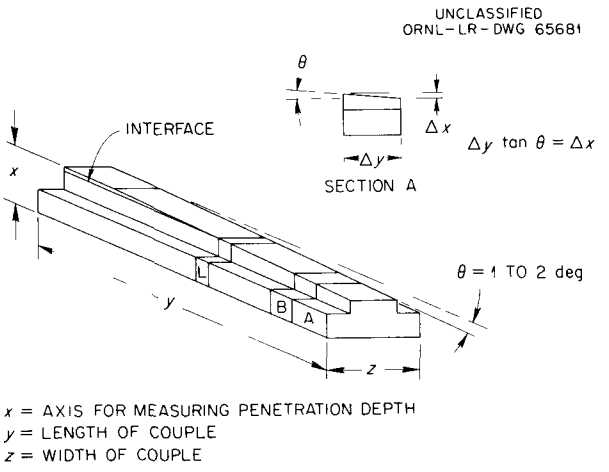

Fig. 19.2. Details of the Wedge Technique for Diffusion Couples.

The first cut was of no value and, generally, only the second and third cuts provided meaningful data.

In order to amplify the concentration-penetration data, the wedge technique (details shown in Fig. 19.2) was selected for use in the present experimental investigation. This technique, for an angle of 1 to 2° with the interface plane (which is parallel to the base plane), will provide a 50-fold amplification for the penetration distances. The amplification is obtained by measuring the length of parallel increments taken along the length of the couple and normal to the base plane. The concentration-penetration data obtained in this manner will require a similar dimensionless group like w for the calculation of D. A suitable solution for this method is being developed.

To verify this technique, the experimental work was begun with the diffusion of uranium from uranium carbide into AGOT-type graphite. A convenient experimental diffusion couple was designed, although considerable difficulty was encountered in the fabrication of the couples. The first couples were designed such that the infinitely thin layer method for linear diffusion might be employed. Uranium dicarbide was suspended in a molten paraffin solution and was then painted on the surface of a machined piece of graphite. Two such pieces were placed face to face, and the paraffin was removed by heating. Subsequent tests indicated that a uniform layer could not be placed on the face of the couple by using this technique. The next approach involved uranium metal, since it was decided that a uniform surface concentration was more important than the advantages offered by the infinitely thin layer. Two machined pieces of carbon separated by a uniform strip of uranium metal foil (as shown in Fig. 19.3) were heated in a small resistance-type vacuum furnace (see Fig. 19.4). The specimen was heated slightly below the melting point of the uranium, and then the temperature was raised to 1350°C. The resultant couple was completely welded together as shown in Fig. 19.3, and uniform distribution of uranium was ascertained by chemical and activation analyses. X-ray analysis of the carbide layer formed by this technique detected only the presence of UC. At higher annealing temperatures the conversion of UC to U_2C_3 and UC_2 might be expected according to the

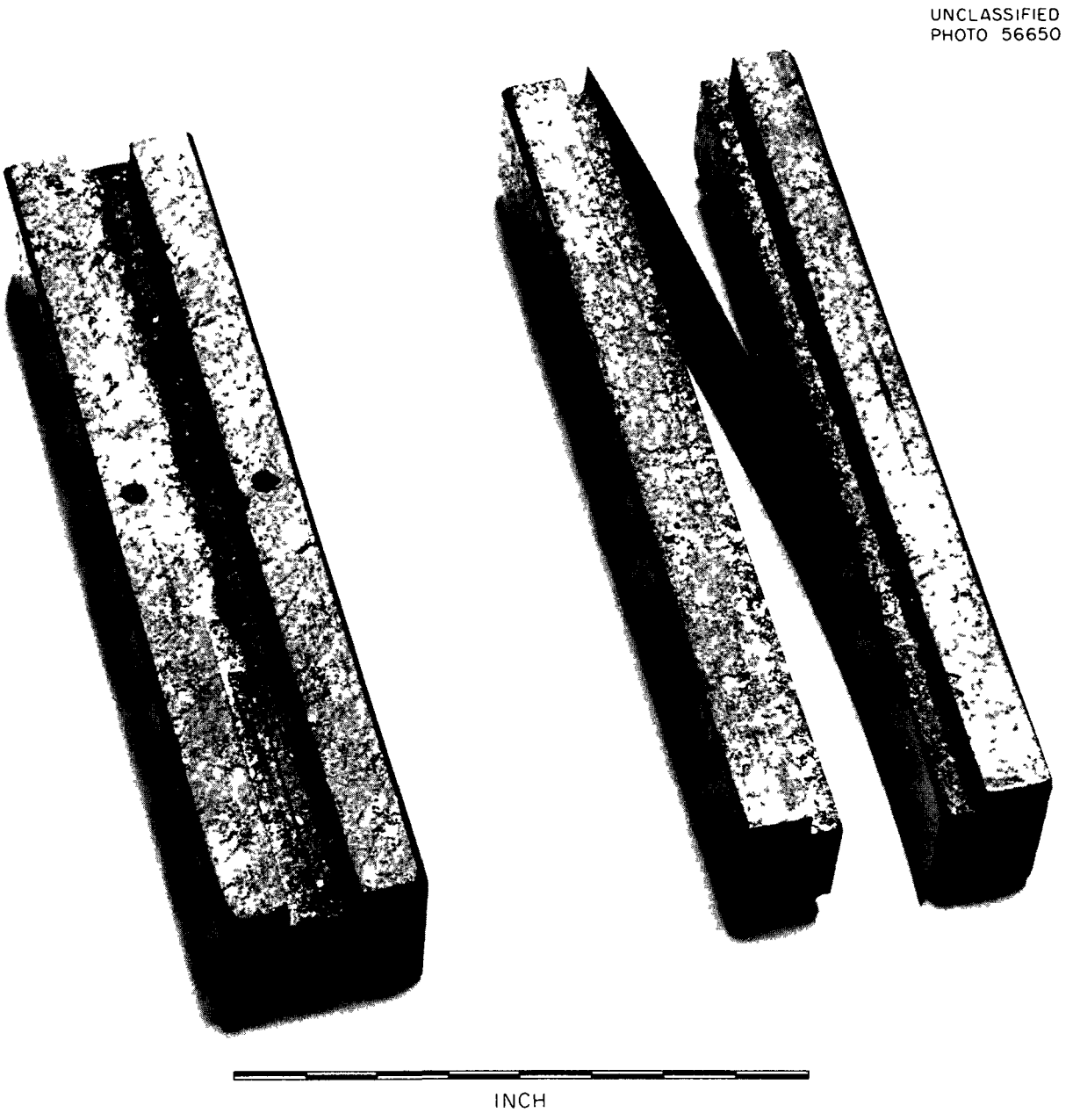

Fig. 19.3. Uranium Carbide–AGOT Graphite Diffusion Couple Fabricated at 1100 to 1350°C from Uranium Metal Foil Placed Between Two Graphite Sections.

phase studies of Mallet *et al.*[5] and the thermochemical properties of uranium compounds tabulated by Rand and Kubaschewski.[6]

Experimental results for the UC–AGOT graphite couple annealed at 1680°C for 120 hr have yielded a tentative diffusion coefficient of 3.0×10^{-12} cm^2/sec based on UC_2 at the interface. Metallographic examination of the uranium carbide layer detected that the carbide species present after annealing had the physical appearance of nearly pure UC_2 (see Fig. 19.5). This evidence confirms the expected conversion of UC to UC_2. The tentative value of D can be correlated with the results obtained at higher temperatures by Loch *et al.* for the UC_2–AGOT system, as shown by the temperature-dependence plot in Fig. 19.6. Whether this correlation is meaningful or not will depend on more experimental results; however, the method employed appears satisfactory.

[5]M. W. Mallet, A. F. Gerds, and H. R. Nelson, *J. Electrochem. Soc.* **99**, 197 (1952).

[6]M. H. Rand and O. Kubaschewski, *The Thermochemical Properties of Uranium Compounds*, AERE-R-3487 (1960).

UNCLASSIFIED
PHOTO 56647

Fig. 19.4. Graphite Resistance Vacuum Furnace Showing the Relative Loading Position of the Uranium Carbide–Graphite Couple Within the Cylindrical Heating Element, Which Is Surrounded with a Ta Heat Reflector.

Fig. 19.5. Uranium Carbide (UC_2)–AGOT Graphite Diffusion Couple Annealed at 1680°C for 120 hr.

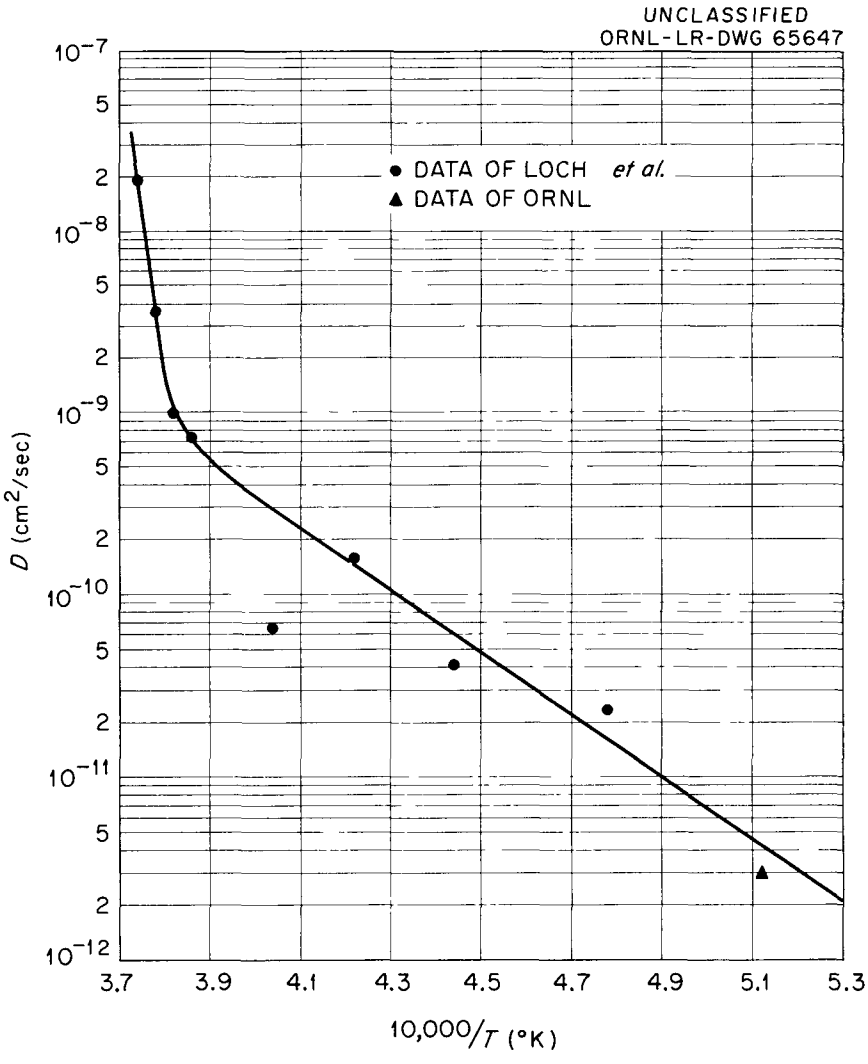

Fig. 19.6. Temperature Dependence of Diffusion Coefficients.

20. Compatibility of Special Fueled Graphites with Water Vapor

L. G. Overholser J. P. Blakely N. V. Smith

Reactor cores containing only ceramic materials with high-temperature stability are being considered in advanced designs of gas-cooled reactors in order to utilize coolant temperatures considerably above those imposed by the fuel or other core components in current use. A fuel body containing fuel particles (UC_2 core coated with pyrolytic carbon) in a graphite matrix has been proposed for use in the Pebble-Bed Reactor Experiment. Fission product retention is to be attained through use of the pyrolytic-carbon coating on the fuel particle and a siliconized silicon carbide or pyrolytic-carbon coating on the fuel body. The latter will also afford protection against oxidizing contaminants (H_2O, CO_2, O_2) present in the coolant (He). The coated particles, which are prepared by various procedures, have a nominal core size of 150 to 500 μ and a nominal coating thickness of 40 to 150 μ. The pyrolytic-carbon coating is usually deposited in either a laminar or columnar form, but can also occur as a composite of the two.

Inleakage of water from a ruptured tube in a steam generator may result in catastrophic attack of the hot-fuel body by water vapor if the fuel body is not coated or if the coating fails. In either case, water vapor would contact the fuel particles, and if the pyrolytic-carbon coating also fails fission products would be released into the main coolant stream.

Experimental studies to determine the integrity of the pyrolytic-carbon-coated fuel particles in contact with water vapor at various partial pressures in the temperature range 800 to 1200°C have been started. A nitric acid leach of the particles after exposure to water vapor and the subsequent determination of uranium in the leach solution are used to measure failure of the coating. The reaction rate of water vapor with the coating is obtained from the loss in weight of the particles and from the composition of the effluent gas. Uncoated fuel bodies are to be examined similarly to establish the reactivity of the graphite matrix with water vapor and the fate of the particles in the matrix.

Limited data[1] obtained at 900°C for two lots of coated particles by using helium containing 2.5 vol % of water vapor indicate that these two lots behave quite differently under comparable conditions. For example, an average reaction rate of 0.1%/hr was measured for one lot over a period of 100 hr, compared with 0.4%/hr for the other lot. This behavior undoubtedly arises from differences in fabrication methods.

---

[1] L. G. Overholser, J. P. Blakely, and N. V. Smith, "Compatibility of Special Fueled Graphites with Water Vapor," *GCR Quart. Progr. Rept. Dec. 31, 1961*, ORNL-3254 (in press).

21. Gas-Graphite Reactions

L. G. Overholser J. P. Blakely

Oxidation of the graphite components of a reactor by such oxidants as O_2, H_2O, and CO_2, which may be present as contaminants in the helium coolant, can result in serious operating difficulties. Burnout of the graphite may lead to deleterious effects on the mechanical properties and may increase the permeability of low-permeability graphite designed to contain fission products. The resulting CO may decompose to produce carbon deposits on the cooler surfaces of the reactor, particularly in the heat exchanger. Advancements in the technology of gas-cooled reactors have resulted in projected graphite temperatures of 1000°C or higher. The reaction rates of the oxidants with graphite at these temperatures are sufficiently high that in order to use graphite under these conditions the graphite must be protected either by an inert coating or by maintaining the concentration of the oxidants in the helium at very low levels through the use of a properly designed purification system. Since the design of such a purification system depends primarily on the reaction rates of the oxidants with graphite at some specified temperature, it is necessary to have suitable data relating the reaction rates to such variables as graphite temperature, partial pressure of the oxidant, flow rate, geometry of the system, and the effect of other gases, particularly reductants such as CO and H_2, in the system.

Although a large amount of data on oxidation of charcoal, coke, etc., is available, the results of only a few studies of the reaction of relatively pure graphites with H_2O and CO_2 at low partial pressures have been reported at temperatures around 1000°C.[1-4] The data given indicate that the reaction rates may vary markedly for various graphites and that the effect of pressure on the reaction rate is not clearly defined. Out-of-pile experiments appear to be justified by the general belief that in the temperature range of interest the rates of the thermal reactions are sufficiently higher than those of the radiation-induced reactions to make the latter unimportant.

An experimental program is being initiated to study the reactivity of oxidants such as CO_2 and H_2O present at low partial pressures (10 to 1000 volumes/million) in flowing helium with various grades of graphite in the temperature range of 800 to 1200°C. The reaction rates will be determined by measuring the change in weight of the graphite specimen and by analyses of the effluent gas. Spherical graphite specimens of various sizes cut from different grades of graphite will be used. The grades of graphite will include highly oriented pyrolytic types, graphitized reactor types, and poorly graphitized types, as found in the fuel bodies likely to be used in the Pebble-Bed Reactor Experiment. A single contaminant (CO_2 or H_2O) will be used in the initial studies; mixtures consisting of CO_2 + CO and $H_2O + H_2$ will be studied later.

---

[1] R. F. Strickland-Constable, *Trans. Faraday Soc.* 43, 769 (1949).

[2] F. Boulangier, Université de Nancy Thesis, July 1956.

[3] G. Blyholder and H. Eyring, *J. Phys. Chem.* 63, 693 (1959).

[4] J. E. Antill and K. A. Peakall, AERE-M/M-201 (August 1958); AERE-R-3070 (September 1959).

An Ainsworth semi-micro recording vacuum balance, model RV-AU-1, has been installed and checked out and will be used for measuring weight changes of the graphite specimens. A Burrell Kromo-Tog ionization model K-7 chromatograph is being checked out. It is anticipated that the use of this chromatograph will permit the measurement of very low concentrations of H_2, CO, and CO_2 in the effluent gas. The auxiliary equipment has been partially assembled.

22. Evolution of Gas from Graphite

L. G. Overholser J. P. Blakely

Additional studies were made of the degassing behavior of several commercial reactor-grade graphites. Detailed results of these studies are presented in several reports and publications.[1-5]

Samples of borated graphites (5 wt % B_4C) were found to evolve large volumes of gas [~150 cm^3 (STP) per 100 cm^3 of graphite] when heated to 1800°C.

Additional samples of EGCR graphite cut from monolithic columns were degassed to further characterize this moderator graphite. The release of sulfur compounds as a function of temperature and the volume-time relationships at temperatures not previously studied were of particular interest. It was demonstrated that SO_2 is evolved at temperatures as low as 200°C, but does not appear in the desorbate above 600°C. Small amounts of H_2S and CS_2 are evolved at temperatures ranging from 300 to 1400°C and above. The data given in Fig. 22.1 were obtained by degassing a single specimen of EGCR graphite at successively higher temperatures in the range 500 to 1000°C. A plot of volume vs log of time gives an essentially linear relationship at both 500 and 600°C. A similar relationship was reported[1] for 300°C. The nonlinearity of the curves reported for temperatures above 600°C indicates that a change in the desorption mechanism occurs upon increasing the temperature from 600 to 700°C. A marked increase in the H_2 concentration in the desorbate also occurs in this temperature range. The increases in the slopes with time observed at 700, 800, 900, and 1000°C are consistent with the behavior noted at 1000°C for many other grades of graphite.[4] It appears to be connected with an increase in the H_2/CO ratio in the desorbate, which occurs with prolonged degassing at constant temperature. The data illustrate the changes in the character of the degassing behavior which may occur when a single specimen of graphite is degassed at various temperatures for prolonged periods of time. Not only may the evolution process change with temperature, but also with time at a constant temperature. Although the rate of release is not completely described by the expression $v = A \log t + B$, it is useful for various time intervals at temperatures above 600°C. Plots of volume vs $t^{1/2}$, which were made for a number of cases, also resulted in curves with changing slopes, indicating that the rate of release also cannot be described by a simple diffusion mechanism. The effect of geometry appears to be relatively unimportant. No significant differences in the release rates were found for cylinders of EGCR graphite varying from 1 in. to 4 in. in length and from 1 in. to $2\frac{1}{4}$ in. in diameter.

[1] L. G. Overholser and J. P. Blakely, *GCR Quart. Progr. Rept. Mar. 31, 1961*, ORNL-3102, pp 216–24.

[2] L. G. Overholser and J. P. Blakely, *GCR Quart. Progr. Rept. June 30, 1961*, ORNL-3166, pp 169–77.

[3] L. G. Overholser and J. P. Blakely, *GCR Quart. Progr. Rept. Sept. 30, 1961*, ORNL-3210, pp 61–64.

[4] L. G. Overholser and J. P. Blakely, "The Degassing Behavior of Commercial Graphites," *Proceedings of Fifth Biennial Conference on Carbon*, Pennsylvania State University, June 19–23, 1961 (in press).

[5] L. G. Overholser and J. P. Blakely, "Evolution of Gas from High-Purity Graphites," *Proceedings of Second Conference on Nuclear Reactor Chemistry*, Gatlinburg, Tenn., Oct. 10–12, 1961, TID-7622.

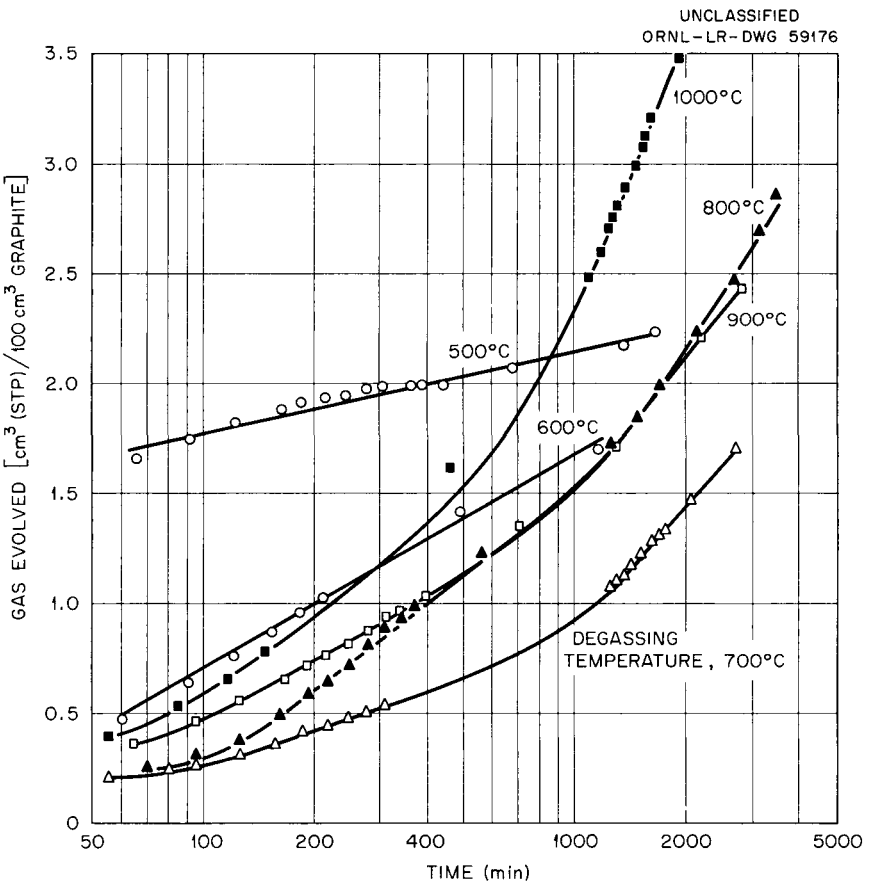

Fig. 22.1. Volume-Time Plots for EGCR Graphite in the Temperature Range 500–1000°C.

23. Measurement of Temperature in Reactor Environments

W. T. Rainey, Jr. R. L. Bennett H. L. Hemphill

BEHAVIOR OF BASE-METAL THERMOCOUPLES

The specification of Chromel-P–Alumel thermocouples for use as temperature sensors in the gas circuit of the EGCR has resulted in an extensive thermocouple research program. As previously reported,[1,2] large negative emf drifts have been observed when Chromel-P is used as a thermocouple leg in stagnant helium or air atmospheres at about 1000°C. The principal mechanism involved in the negative-emf-drift phenomenon has been shown to be the selective oxidation of chromium in the Chromel-P leg with resultant decrease in concentration of metallic chromium in the alloy. Such preferential oxidation occurred in a limited temperature range (700 to 900°C) and in atmospheres containing only trace quantities of oxidants (water or oxygen).

Additional tests have been conducted with a group of base-metal alloys which have been recommended as being more resistant than Chromel-P to selective oxidation. The test thermocouples were prepared from 24-gage bright wire and were tested in unpurged thermocouple protection tubes with a stagnant helium atmosphere at 1000°C. The several combinations tested are shown, along with alloy composition and mean drifts observed after an exposure of 600 hr (Table 23.1).

The comparatively large temperature drift of the Chromel-AA–alloy 875 thermocouple for a slight emf drift is due to the very low thermoelectric power of this couple at temperatures near 1000°C. When coupled with platinum, the Chromel-A and Chromel-AA showed about the same temperature drift (+4.0 and +6.0°C respectively).

Thermal-gradient emf profiles of the wires were plotted by slowly withdrawing the wires from an isothermal tube furnace. The profiles of the Chromel-A and Chromel-AA were similar and indicated only very small composition changes. Special and regular Chromel-P showed large negative emf errors in the sections exposed to the furnace thermal gradient. This type of profile has been associated with selective chromium oxidation in past experiments. The Special Chromel-P wire has been recommended as being more satisfactory than the regular Chromel-P in reducing and marginally oxidizing atmospheres.[3]

The Special Alumel wires showed only slight positive emf errors in profile, and the wires appeared to be physically sound. The regular Alumel wires were severely oxidized, even though they showed only slight positive emf errors in profile. The insignificant emf drifts are to be expected, because the emf output of Alumel is almost the same as that of pure nickel.

The alloy 875 was recommended[3] as the negative leg with Chromel-A and Chromel-AA under reducing atmospheric conditions. It appeared physically sound after use in the drift tests described. Emf error profiles showed that no appreciable composition changes occurred.

Bare, dull Chromel-P wires have been studied in the same assemblies as used in the 1000°C

[1] G. W. Keilholtz *et al.*, *Reactor Chem. Div. Ann. Progr. Rept. Jan. 31, 1961*, ORNL-3127, p 128.

[2] R. L. Bennett, W. M. McClain, and W. T. Rainey, *Symposium on Temperature, Its Measurement and Control in Science and Industry*, Columbus, Ohio, March 1961, paper B-3-10. To be published by Reinhold Publishing Co.

[3] *Chromel-Alumel Thermocouple Alloys*, Catalog M-61-Ca, Hoskins Manufacturing Co. (1961).

Table 23.1. Emf Drift Data in Stagnant Helium Atmospheres After 600 hr of Exposure

Thermocouple Alloys			Average Drift	
			mv	°C
Regular Chromel-P (90 Ni, 10 Cr)	vs	Regular Alumel (94 Ni, 3 Si, 2 Al, 1 Mn)	−1.76	−44
Special Chromel-P (Chromel-P + Nb)	vs	Special Alumel (Ni + 1–2 Si)	−2.33	−58
Chromel-A (80 Ni, 20 Cr)	vs	Alloy 875 (72 Fe, 23 Cr, 5 Al)	+0.05	+5
Chromel-AA (68 Ni, 20 Cr, 8+ Fe)	vs	Alloy 875 (72 Fe, 23 Cr, 5 Al)	+0.07	+25
Geminol-P (80 Ni, 20 Cr)			No data available	

tests, but with hot-junction temperatures as indicated in Fig. 23.1.[4] In all cases negative emf drifts were measured during exposure of the couples. In each case the nonhomogeneous section developed in the thermal-gradient region of the furnace. For the upper three temperatures the maximum error developed within a 29°C range (781 to 810°C). In the 770°C test the selective oxidation occurred even deep in the isothermal region of the furnace.

These tests substantiate data obtained previously, which indicated that the selective oxidation of chromium occurred predominantly in sections of wires exposed to stagnant helium atmospheres between 700 and 900°C. The selective oxidation of chromium occurred mainly in the thermal-gradient region of the assembly whenever the isothermal region was kept above 750°C. Otherwise, partial oxidation occurred even in the isothermal region. This pattern of behavior has been predicted by means of thermodynamic calculations on a simplified system containing oxidizing and reducing impurities at equilibrium with Ni-Cr solid solutions.[1]

It is concluded that the 80 Ni–20 Cr type alloy (Chromel-A and -AA, Geminol-P) is a more suitable type than the 90 Ni–10 Cr (regular and Special Chromel-P) type for use at temperatures above 700°C under marginally oxidizing conditions. This is especially important when the system geometry allows development of atmospheric

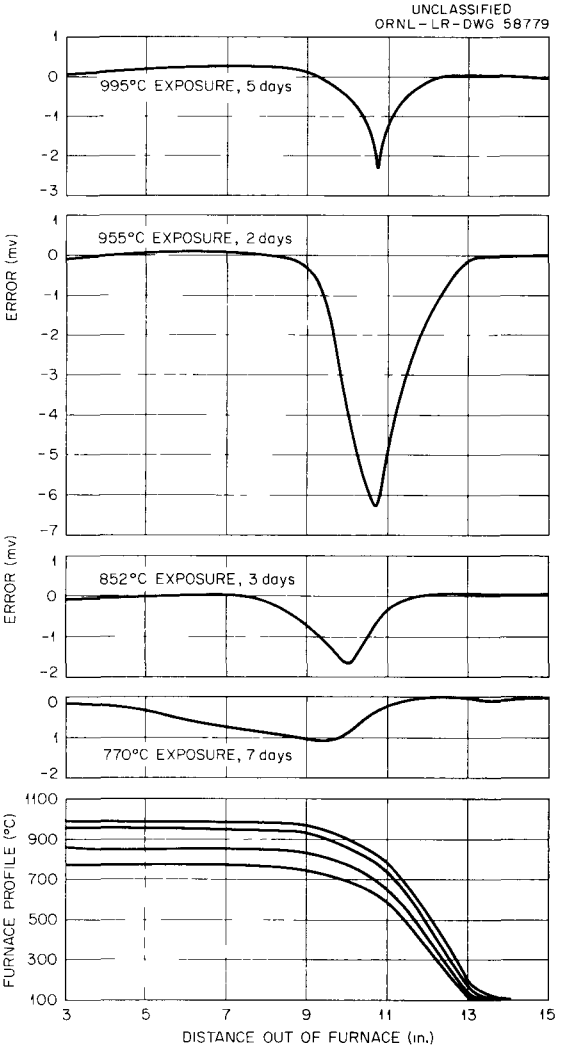

Fig. 23.1. Chromel-P EMF Profiles After Stagnant-Helium Exposure.

[4]G. W. Keilholtz *et al.*, *GCR Quart. Progr. Rept. June 30, 1961*, ORNL-3166, p 184.

gradients around the wire, as in long protection tubes of small bore. It is also concluded that the Special Alumel alloy was much more resistant to oxidative attack than the regular Alumel under these test conditions.

BEHAVIOR OF SHEATHED THERMOCOUPLES IN VARIOUS ATMOSPHERES

Chromel-P–Alumel thermocouples sheathed in stainless steel have been specified for measurement of temperature in the EGCR. Therefore such assemblies have been tested extensively under conditions approaching those expected in EGCR operation.

As previously reported,[5] abnormal emf outputs were obtained when these thermocouples were exposed at high temperatures to helium contaminated with gases desorbed from graphite. The emf errors were the result of selective oxidation of chromium in Chromel-P wires and appeared to be dependent upon the source of the thermocouple stock material as well as the external atmosphere.

Figure 23.2 is a composite of results from several series of experiments carried out in graphite-helium atmospheres at 870°C.[4] The sheathed thermocouples were inserted into holes drilled into an AGOT graphite cylinder contained in a stainless steel pressure can. A static pressure of 7 psig helium was maintained in the can during the tests. The complete assembly was installed in a Marshall tube furnace before heat was applied. Therefore all gaseous products desorbed from the graphite were left in contact with the couples during the test. Curve 1 is typical of all thermocouples protected from the graphite-helium atmosphere by stainless steel tubes open to air but mounted in the same test assembly. Thermocouples represented by curves 1, 5, and 6 were installed at the start of the test. Rapid negative emf drift was noted with couples, from vendor A, sheathed in type 304 stainless steel. A fresh group of these couples, curve 4, was inserted into the assembly after thorough outgassing of the graphite. During about three

[5]G. W. Keilholtz *et al.*, *Reactor Chem. Div. Ann. Progr. Rept. Jan. 31, 1961*, ORNL-3127, p 131.

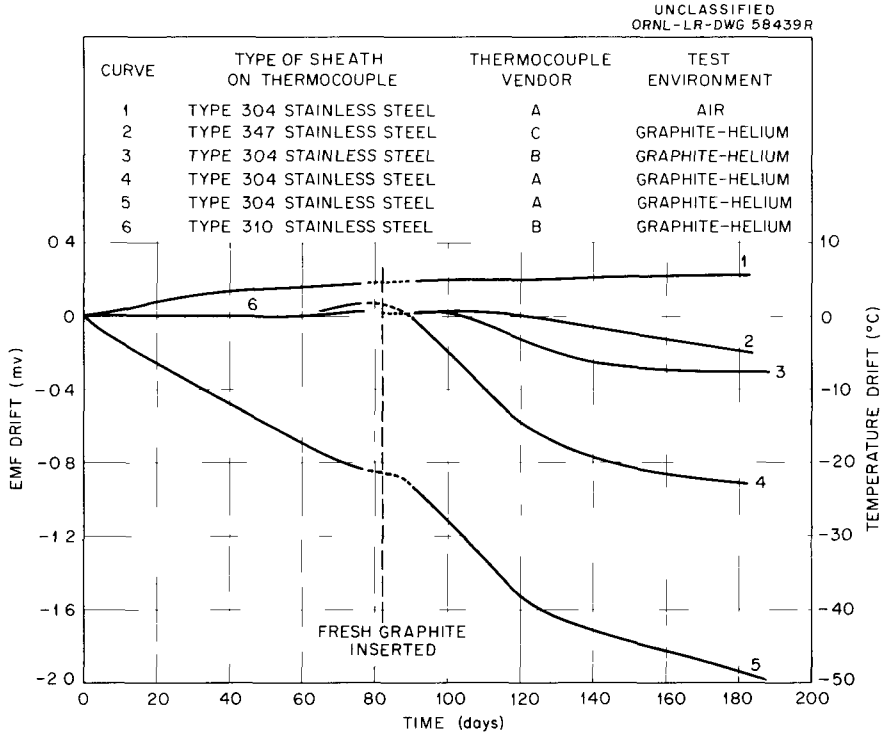

Fig. 23.2. Drift Data for Stainless-Steel-Sheathed Thermocouple.

weeks of exposure these couples showed only a slight positive emf drift.

After 82 days at temperature, a fresh AGOT graphite cylinder was installed. Couples represented by curves 1, 4, and 5 were reinserted along with two new sets, curves 2 and 3. The fresh graphite block resulted in (1) temporary increased rate of drift in curve 5, (2) start of negative drift in curve 4, and (3) no change in rate of drift in curve 1. It was interesting to note that couples sheathed in type 347 stainless steel (vendor C) and type 304 stainless steel (vendor B) indicated much less error at the end of the test than did those from vendor A after corresponding times.

Metallographic sections and thermal-gradient emf profiles[5] proved that selective oxidation of chromium in the Chromel wires occurred in those portions of wire exposed at about 750°C. The Alumel wires showed only slight surface oxidation.

Results to date indicate that the negative emf drift is closely associated with the desorption of gases from the graphite and with the source of thermocouple stock material. Under the conditions of these tests, hydrogen and carbon monoxide are the main desorbed gases. Figure 23.3 and ref 6 give data obtained from tests in which pure hydrogen and carbon monoxide atmospheres (7 psig) were maintained around type 304 stainless steel sheathed couples (vendor A) at 865°C. The couples exposed to hydrogen developed a total error of −3.84 mv (−96°C) after 155 days of exposure. Those exposed to carbon monoxide were +0.28 mv (7°C) in error after 194 days of exposure at 870°C. There was no tendency toward negative emf drift at any time during the test. However, recent thermal-gradient emf profile data have shown nonhomogeneous areas in these thermocouples near the hot junctions. It is probable that these composition changes were due to carburization of the Chromel wire. It is not unreasonable to expect carburization, with resultant diffusion of carbon through the sheath material, during such long times at high temperature.

Figure 23.4 shows a portion of the data obtained in the above cases, as well as data obtained to date in the high-pressure hydrogen and low-temperature graphite tests described below.

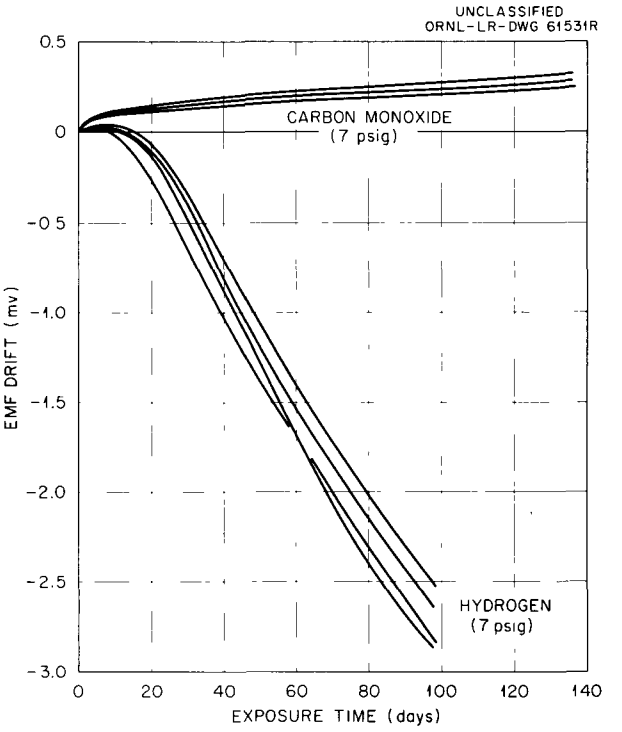

Fig. 23.3. EMF Drift Tests with Chromel-Alumel Sheathed Thermocouples in Hydrogen and Carbon Monoxide.

A set of type 304 stainless steel sheathed couples (vendor A) was installed as in previous tests, but was maintained at 700°C. After 98 days these couples averaged −0.08 mv (−2°C) error. The small drift in this test was not entirely unexpected, since temperatures in the range of 700°C were known to be on the border line of detectable selective oxidation.

A set of type 304 stainless steel sheathed couples (vendor A) was also installed in a high-pressure hydrogen assembly. These couples were exposed to 150 psig hydrogen pressure at 870°C for 64 days and showed an average emf drift of 0.00 mv. It is probable that hydrogen diffused through the sheath so rapidly that the inner atmosphere became strongly reducing before selective oxidation could occur.

Helium diffusion data indicate that the magnesia insulation is less densely packed in the product manufactured by vendor A than in those by vendors B and C. This may result in greater longitudinal diffusion of gases such that concentration gradients conducive to selective oxidation can be more easily formed. In addition, purity of

[6] W. T. Rainey and R. L. Bennett, *GCR Quart. Progr. Rept. Sept. 30, 1961*, ORNL-3210, p 215.

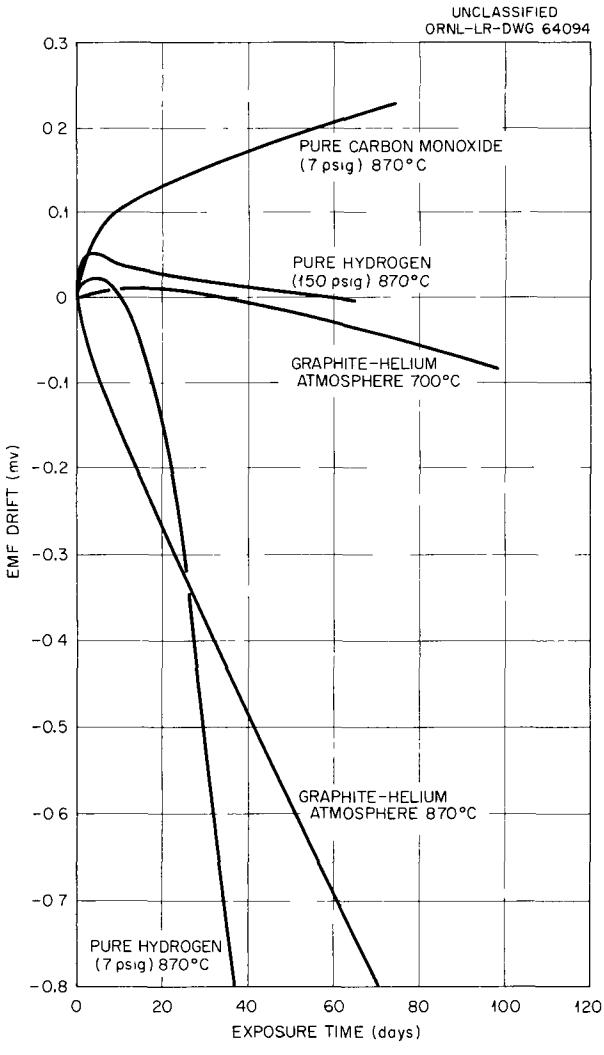

Fig. 23.4. EMF Drift Tests with Chromel-Alumel Sheathed Thermocouples.

magnesia; inclusion of air or moisture, presence of metal oxides, and method of fabrication may have influenced the results. Preliminary gas analyses have therefore been performed to determine whether gas or moisture content of the stock from vendor A differed markedly from the other stock. Results indicate that the total gas content of stock from vendor A is about three times that from vendor B. Quantitative composition of the gas has not been established, but nitrogen and hydrogen were the predominant components in both cases.

The presence of nitrogen might have been due to its use as an inert atmosphere for storage of magnesia before assembly of the stock. The lack of argon in the desorbed gases precludes the explanation that nitrogen was from air inclusion only. It is possible that the hydrogen was present as a result of reaction of moisture with metal during annealing and analytical outgassing. Recent incomplete gas analyses substantiate such an idea. Gases desorbed from the thermocouple stock at 600°C showed much higher percentages of hydrogen, water, and carbon dioxide than did those gases desorbed from the stock at 1200°C.

It is concluded that hydrogen penetration of the sheath was responsible for modifications of the atmosphere that resulted in selective oxidation. The variations in rate of drift were undoubtedly due to the differences in internal gas composition present when the assemblies were sealed at the factory. The results indicate that it is extremely difficult to write specifications for purchase of thermocouple stock with the complete assurance that such stock will perform satisfactorily under all kinds of operation conditions. In general, satisfactory operation can be expected from Chromel-P–Alumel thermocouples when used in oxidizing atmosphere. However, when used in atmospheres likely to contain hydrogen gas, Chromel-P–Alumel thermocouples sheathed in metal may give erroneous emf indication after use at temperatures over about 700°C. For use under such reducing conditions, it is recommended that a very tightly packed magnesia insulation be specified. In addition, manufacturing techniques should be rigidly controlled in order that as little moisture, air, and carbon oxide as possible be enclosed in the sheath before swaging. As indicated by the results from the bare-wire thermocouple test, the use of such alloys as Chromel-A or Geminol-P in place of the Chromel-P leg might be advisable under such conditions.

A complete discussion of the programs described above is to be found in a recent report.[7]

[7] W. T. Rainey, Jr., and R. L. Bennett, *Thermocouple Research Under EGCR Conditions*, ORNL CF-61-12-54 (Dec. 20, 1961).

24. Beryllium Chemistry Studies

REFRACTIVE INDEX OF BeO AS A FUNCTION OF RADIATION DAMAGE[1]

T. N. McVay[2] H. Insley[2]
R. E. Thoma H. A. Friedman
C. F. Weaver

Specimens of BeO irradiated at 120°C for a total of 1.5×10^{21} *nvt* showed the largest change in refractive index of all specimens exposed recently in the Engineering Test Reactor.[3] Hexagonal beryllium oxide is normally uniaxial positive with refractive indices $N_\omega = 1.719$, $N_\epsilon = 1.733$. The refractive indices of specimens irradiated to 1.5×10^{21} *nvt* at 120°C were $N_\omega = 1.700 \pm 0.003$, $N_\epsilon = 1.712 \pm 0.003$. Annealing experiments were conducted which reversed the radiation effects on the refractive indices of BeO at temperatures as low as approximately 650°C. The results of these experiments show that the determination of refractive indices with the petrographic method affords a rapid, quantitative, inexpensive, nondestructive method of measuring the extent of radiation damage to beryllium oxide and the extent to which thermal annealing effects a recovery of this property.

[1]Summary of published paper: *J. Am. Ceram. Soc.* 45, 48–49 (1962).

[2]Consultant.

[3]R. P. Shields, J. E. Lee, Jr., and W. E. Browning, Jr., *Effects of Fast-Neutron Irradiation and High Temperature on Beryllium Oxide*, ORNL-3164 (Mar. 19, 1962).

EXPERIMENTAL ATTEMPTS TO STABILIZE A CUBIC FORM OF BeO[4]

R. E. Thoma H. A. Friedman
T. N. McVay[2]

Binary mixtures of BeO with the oxides Al_2O_3, CaO, Li_2O, MgO, Sc_2O_3, TiO_2, Y_2O_3, and ZrO_2 were fired at temperatures above 2050°C in an attempt to produce a stabilized solid having the cubic crystalline modification of the BeO structure suggested by Rothman and Smith.[5] No evidence was observed in microscopic and x-ray-diffraction analyses of the cooled specimens that a cubic form of BeO had been produced in any of the experiments.

PREPARATION OF KILOGRAM QUANTITIES OF HIGH-PURITY BERYLLIUM OXIDE

R. E. Moore J. H. Shaffer
H. F. McDuffie

The availability of very nearly pure beryllium oxide is highly desirable for two principal reasons. First, it would permit the preparation of low-impurity-level spectrographic standards for analyzing beryllium and its compounds. Second, it would make possible an evaluation of the effects of small quantities of impurities and specific

[4]Abstract of published report: ORNL TM-94 (Dec. 22, 1961).

[5]A. J. Rothman and D. K. Smith (UCRL), unpublished work.

additives on sintering characteristics and irradiation behavior of BeO moderator material. The acetylacetone-EDTA solvent-extraction process for making high-purity beryllium oxide[6,7] has been developed to the point where a small-scale production operation has been demonstrated. In essence, this process, previously reported to be useful in analytical separations and decontamination procedures,[8-10] consists in extracting a solution of $Be(CH_3COCHCOCH_3)_2$, beryllium acetylacetonate, in carbon tetrachloride with an aqueous solution containing ethylenediaminetetraacetic acid (EDTA). Beryllium is largely retained in the organic phase, while most metallic impurities are complexed with EDTA in the aqueous phase. The beryllium is subsequently back-extracted into nitric acid, precipitated as hydroxide with ammonia, and calcined to purified beryllium oxide at 600 to 1000°C.

Altogether, a quantity of about 1280 g of high-purity oxide has been prepared in 24 batches. If all 24 batches were blended, the result would be a composite containing less than 10 ppm each of Ca, Al, Fe, and Si and less than 5 ppm each of Mg and Cu. All other metallic impurities were below the quantitatively detectable limit (5 or 10 ppm for most elements) in each of the 24 selected batches. A few of the batches contain a considerable amount of carbon as judged by a grayish coloration; most are definitely white, however, containing only a very few visible dark particles.

Several batches have already found use in the preparation of spectrographic standards. Other batches are scheduled for use in making sintered BeO bodies for irradiation experiments. Cracking and powdering of sintered BeO have been found to occur at low temperatures and high neutron dose.[3] The BeO used in these radiation studies was the best available commercial material, but it contained a total of 1200 ppm impurities (100 Al, 50 Ca, 20 Cr, 20 Fe, 100 K, 110 Si, and 800 S). The results of tests with material of higher purity will be useful in determining whether the radiation damage observed with the commercial-grade BeO is intrinsically characteristic of BeO or whether it may be attributed to the presence of impurities. The reports that the tensile strength of beryllia increases remarkably as the purity and crystal perfection are improved suggest that ultrapure BeO might display greater resistance to radiation damage.

Solubilities in the Extraction System

The solubility information in Table 24.1 was obtained to aid in the design of an efficient purification process. The data permit a wide choice of compositions which may be used in contact with an aqueous EDTA phase in a purification process. Compositions containing only a small amount of acetylacetone may be preferred in order to minimize the loss of this reagent to the aqueous phase. The pH of a saturated solution of beryllium acetylacetonate in water is approximately 7.1. The distribution coefficient (aqueous/organic) for beryllium at this pH, estimated from the ratio of solubilities in H_2O and CCl_4, is 0.0092.

Results of Batch Purification Process

The spectrographic analyses and percentage recoveries of purified oxide prepared in the program are given in Table 24.2.

Discussion of Results

The results of spectrographic analyses of the products show that in nearly every preparation there are certain elements reported to be present which should have been removed completely as judged by their distribution coefficients. There appears to be no correlation with the purity of the starting material or with washing procedures. In general, the impurities reported to be present are those expected as a result of dust and reagent contaminations, which are difficult to eliminate completely.

---

[6] R. E. Moore, *Reactor Chem. Div. Ann. Progr. Rept. Jan. 31, 1961*, ORNL-3127, pp 159–60.

[7] R. E. Moore, J. H. Shaffer, and H. F. McDuffie, "Preparation of High-Purity Beryllium Oxide," paper presented at the Second Conference on Nuclear Reactor Chemistry, Gatlinburg, Tenn., Oct. 10–12, 1961.

[8] J. A. Adam, E. Booth, and J. D. H. Strickland, *Anal. Chim. Acta.* 6, 462 (1952).

[9] I. P. Alimarin and I. M. Gibalo, *J. Anal. Chem. U.S.S.R. (English Translation)* 11, 405 (1956).

[10] J. D. Buchanan, *J. Inorg. Nuclear Chem.* 7, 140 (1958).

Table 24.1. Solubilities in the Extraction System

Compound	Solvent	Temp (°C)	Solubility (g per liter of saturated solution)
$Be(CH_3COCHCOCH_3)_2$	CCl_4	27	530
	$CH_3COCH_2COCH_3$	27	405
	50 vol % CCl_4 in $CH_3COCH_2COCH_3$	27	508
	H_2O	27	4.9
EDTA	H_2O	22	0.4
$CH_3COCH_2COCH_3$	CCl_4	27	∞
	H_2O	25	173[a]

[a]This value reported by J. F. Steinbach, thesis, University of Pittsburgh, NYO-6347 (1953).

Table 24.2. Preparations of Purified Beryllium Oxide

Preparation No.	Weight of BeO (g)	Percent Recovery	Color	Spectrographic Analysis[a] Reported Impurities (ppm)
A1	51.2	28.6	White	None
A2	49.2	28.3	Slight yellow	Mg <5 *T*, Na <10 *T*
A3	21.3	11.9	Slight gray	Si <25 *FT*, Mg 6, Fe 10
A4	53.3	31.4	Slight yellow	Mg <5 *FT*, Na <10 *T*
A5	40.9	22.9	Slight yellow	Si 10, Ca 10, Al 5, Mg 5, Fe 5
A6	56.5	31.9	White	Al <5 *T*, Ca 5, B <1 *T*
JA1	33.3	14.2	White	Li 30, Cu 2
JA2	67.9	29.2	Gray	Cu 2
JA3	73.8	31.7	Gray	Cu 2
JA4	72.9	31.3	Gray	Si 20, Mg 5, Cu 5
JA5	74.8	33.7	White	Al 7, Si 10, Mg 8, Cu <5 *T*
JA6	75.8	32.4	White	Al 5, Si 20, Mg 5, Cu 18
JA7	78.4	34.4	White	Al 5, Si 10, Mg 5, Cu 5, Ca <10 *T*
JA8	54.5	23.7	White	Al 5, Si 10, Mg 5, Cu 5, Ca <10 *T*
JA9	91.6	39.4	White	Si 15, Mg 5, Ca <10 *T*, B 2, Pt *FT*
JA10	59.8	25.9	White	Al 10, Si 10, Mg 5, Pt *T*
JA11	67.7	28.8	White	Si 10, Mg <5 *T*, Pt *T*
JA12	78.1	33.7	White	Si <10 *T*, Mg 5, Pt *FT*
JA13	37.6	16.3	White	Al 10, Si <10 *T*, Mg <5 *T*, Pt *T*

[a]The spectrographic analyses were reported by J. A. Norris, Z. Combs, and co-workers, Analytical Chemistry Division, ORNL. All impurities except those listed were not detected and were below the quantitatively detectable level, which was 5 or 10 ppm for most elements. The symbols *T* and *FT*, referring to trace and faint trace, mean that the element was detected but was present below the level indicated.

BERYLLIUM EXTRACTION STUDIES; ANALYTICAL METHOD

C. E. L. Bamberger[11] C. F. Baes, Jr.

To expedite further examination of the solvent-extraction process for the purification of beryllium,[12] a spectrophotometric method[13] has been developed for the simultaneous analysis of beryllium acetylacetonate [$Be(Ac)_2$] and acetylacetone (HAc) (the extractant) in carbon tetrachloride (the organic diluent). These compounds exhibit absorption peaks in the ultraviolet [294 and 272 mμ for $Be(Ac)_2$ and HAc respectively] which were found to obey Beer's law. The peaks are sufficiently separated so that measurement of sample absorbancy at two wavelengths (260 and 301.5 mμ) permits the determination of the concentration of each component by simultaneous solution of the following equations:

$$a_{260} = (A_{Be,260})\, C_{Be} + (A_{Ac,260})\, C_{Ac},$$

$$a_{301.5} = (A_{Be,301.5})\, C_{Be} + (A_{Ac,301.5})\, C_{Ac},$$

where

a_{260}, $a_{301.5}$ = measured absorbancies at the two wavelengths,

$A_{Be,260}$, $A_{Be,301.5}$ = molar extinction coefficients of $Be(Ac)_2$ at the two wavelengths (found to be 230 and 1493, respectively, for a 0.05-cm path length),

$A_{Ac,260}$, $A_{Ac,301.5}$ = molar extinction coefficients of HAc at the two wavelengths (found to be 403 and 63.5, respectively, for a 0.05-cm path length),

C_{Be} and C_{Ac} = molar concentration of $Be(Ac)_2$ and HAc respectively.

For mixtures in which one component concentration exceeds the other by less than a factor of 10, both concentrations could be determined with an accuracy of ±5% in the concentration range 5×10^{-5} to 10^{-3} *M*.

Appreciable absorption in this region of the ultraviolet was attributable to impurities in the solvent, the amount varying considerably for different brands and different batches of carbon tetrachloride. Also, a small but increasing absorption was noted to result from prolonged contact of the solvent with polyethylene containers. When care was taken to ensure that the reference solvent and the solutions were prepared from the same batch of carbon tetrachloride by similar treatments, these effects did not interfere with the method. Similarily no interference was found from the possible presence in the sample of varying small amounts of water, nitric acid, or EDTA.

[11] IAEA Fellow, Argentine Atomic Energy Commission.

[12] R. E. Moore, J. H. Shaffer, and H. F. McDuffie, "Preparation of High-Purity Beryllium Oxide," paper presented at the Second Conference on Nuclear Reactor Chemistry, Gatlinburg, Tenn., Oct. 10–12, 1961.

[13] Suggested by a spectrophotometric method for the analysis of beryllium alone, described in ref 8.

25. Effect of Radiation on Beryllium Oxide

G. W. Keilholtz J. E. Lee, Jr. W. E. Browning, Jr. R. P. Shields

The BeO irradiation program at ORNL[1] has yielded significant information during the past year. Experiments 1 through 5 are now complete, experiment 6 has been removed from the reactor for examination, and experiment 7 is in the ETR. Experiments 8 and 9, which are combined, are scheduled to begin about April 1, 1962. The status of the program is shown in Table 25.1.

In experiments 1–5[2,3] a total of 57 cylindrical BeO specimens were irradiated in the ETR from 10^{20} to 2.6×10^{21} *nvt* (>1 Mev) over the temperature range 100 to 1025°C. The specimens were encapsulated in stainless steel and installed within an annulus through which an argon-helium mixture was circulated to achieve temperature control. Two types of specimens were used: (1) hot-pressed samples with a density of 2.9 g/cm^3 made from oxide containing some impurities (spectrographic analysis showed the following composition, in percent: Si 0.6; Fe 0.1; Ca <0.08; Ni <0.09; and P, Cu, Cr, and Al <0.05); (2) cold-pressed and sintered samples with a density of 2.65 to 2.70 g/cm^3 made from Brush UOX grade BeO (spectrographic analysis, in ppm: Al and K 100; Si 110; Ca 50; Cr and Fe 20; Mg <70; Mo <50; and Mn and Ni <20).

After irradiation the specimens were observed by x-ray diffraction, petrographic microscopy, electron microscopy, and metallography; some specimens were dissolved for determination of helium and tritium. Severe damage occurred to specimens irradiated to high neutron dose at low temperatures. Specimens receiving as much as 1.5×10^{21} *nvt* at about 110°C disintegrated to powder. Fractures were observed in specimens irradiated at 2.6×10^{21} *nvt* at 800 to 950°C. Some specimens remained intact after exposure to intermediate doses and intermediate temperatures. Increases in linear dimensions from 0.5 to 4% were observed. This effect increases with neutron dose and decreases with temperature.

X-ray-diffraction examinations[4,5] of both types of specimens after irradiation show anisotropic lattice expansion ratios ($\Delta c/c_0 \div \Delta a/a_0$) of approximately 9. X-ray patterns of BeO irradiated at 120°C resemble those of irradiated graphite. The data may be interpreted as showing, in addition to isolated point defects, the presence of small disks of 10 to 20 interstitial atoms (such as Be, He, O) in semiregular array between closely packed planes. The strain energy in such a lattice should be high.

Petrographic examinations[6] of the irradiated specimens showed a decrease in the refractive index corresponding to the decrease in density (see "Refractive Index of BeO as a Function of Radiation Damage," this report). It was found that specimens irradiated in the 10^{21} *nvt* range, having a refractive index of 1.70, begin to anneal at 700°C, with complete annealing to the standard index of 1.72 at 1050°C.

---

[1] G. W. Keilholtz *et al.*, *Reactor Chem. Div. Ann. Progr. Rept. Jan. 31, 1961*, ORNL-3127, pp 153–54.

[2] R. P. Shields, J. E. Lee, Jr., and W. E. Browning, Jr., *Effects of Fast-Neutron Irradiation and High Temperature on Beryllium Oxide*, ORNL-3164 (Mar. 19, 1962).

[3] R. P. Shields, J. E. Lee, Jr., and W. E. Browning, Jr., "Irradiation Effects on BeO," in *Transactions of the American Nuclear Society, 1961 Winter Meeting*, November 7–9, vol 4(2).

[4] H. L. Yakel, Metallurgy Division, personal communication.

[5] R. E. Thoma, Reactor Chemistry Division, personal communication.

[6] T. N. McVay *et al.*, *J. Am. Ceram. Soc.* 45, 48–49 (1962).

Table 25.1. Beryllium Oxide Irradiation Experiments

Experiment No.	Number of Specimens	Type of Material	Nominal Dimensions		Density (g/cm^3)	Exposure ($nvt \times 10^{21}$)	Temp (°C)	State of Completion
			Diam (in.)	Length (in.)				
ORNL-41-1	3	Hot pressed	0.636	1.000	2.9	0.14	722	Complete
2	9	Hot pressed	0.636	1.000	2.9	0.11 – 0.35	219 – 500	Complete
3	3	Hot pressed	0.428	1.000	2.9	0.11 – 0.45	120 – 1025	Complete
	3	Hot pressed	0.636	1.000	2.9	0.11 – 0.45	120 – 1025	Complete
	6	Hot pressed	0.800	1.000	2.9	0.11 – 0.45	120 – 1025	
4	12	Cold pressed and sintered	0.800	1.000	2.65 – 2.70	1.8 – 2.4	120	Complete
5	21	Cold pressed and sintered	0.800	1.000	2.65 – 2.70	1.1 – 2.3	110 – 950	Complete
6	6	Cold pressed and sintered	1.180	3.000	2.65 – 2.70	0.2 – 0.5[a]	500 – 950	Irradiated and removed from ETR
7	40	Cold pressed and sintered	0.800	0.500	2.65 – 2.70	0.5 – 1.0[a]	550 – 1000	In progress
	8	Hot pressed	0.800	0.500	2.9	0.5 – 1.0	550 – 1000	
8–9	120	Cold pressed and sintered	0.500	0.500	2.7 and 2.9	1.0 – 10.0[b]	650 – 1100	Not started
	196	Cold pressed and sintered	0.250	0.250	2.7 and 2.9	1.0 – 10.0	650 – 1100	
	24	French	0.250	0.250	2.95	1.0 – 10.0	650 – 1100	
	10	French	0.250	0.500	2.95	1.0 – 10.0	650 – 1100	

[a]Estimated value.
[b]Proposed value.

The preparation of metallographic specimens revealed the presence of extensive intergranular fracture in the 10^{21} *nvt* range as evidenced by excessive pullout of material during polishing.

Electron microscopic examinations of irradiated BeO showed that voids 0.1 to 0.3 μ in diameter were present in the interior of the grains and at grain boundaries; these voids were not present in the original material. The voids were sometimes found in parallel alignment, suggesting a crystallographic relationship to the direction of helium diffusion. Heat treatment of the samples caused the voids to coalesce to form blisters.

The thermal conductivity of the samples decreased substantially as exposure progressed, as indicated by 50 to 100% increases in radial temperature differences. However, since there were no sudden changes in the temperature gradient and since more than 25 samples survived thermal cycling without cracking, thermal stress seems unlikely as a sole cause of failure.

Gas analyses[7] of irradiated BeO show that internally generated helium is retained even at high temperatures up to a fast-neutron dose of 1.6×10^{21} *nvt*. The scatter among the points plotted in Fig. 25.1 above this dose is probably caused by the release of helium by fracture of the pellets. Helium is produced through two nuclear reactions: (1) the $(n,2n)$ reaction in which the yield is proportional to *nvt*, and (2) the (n,α) reaction in which the yield is approximately proportional to $(nvt)^2$. The linear relationship seen in the plot indicates that the $(n,2n)$ reaction predominates over the (n,α) reaction, as is expected from the known cross-section values. The slope of the line in Fig. 25.1 gives a yield of 205 μl of He per g of BeO per 10^{21} *nvt*, which agrees well with the range 250 to 269 μl per g per 10^{21} *nvt* based on the data of Rich and Walters[8] for metallic beryllium but not with data reported by Ellis,[9] which shows a higher yield of 460 μl per g of BeO per 10^{21} *nvt*.

Since tritium is generated entirely through the (n,α) reaction, the yield should be approximately proportional to $(nvt)^2$. Gas analyses of tritium content plotted in Fig. 25.2 agree with the theoretical expectation at 120°C, but show that

[7] J. C. White and A. S. Meyer, Jr., Analytical Chemistry Division, personal communication.

[8] J. B. Rich and G. P. Walters, *The Mechanical Properties of Beryllium Irradiated at Various Temperatures*, AERE-R-3684 (1961).

[9] C. E. Ells, *The Swelling of Beryllium from Neutron Induced Gases*, CrMet-809 (1958).

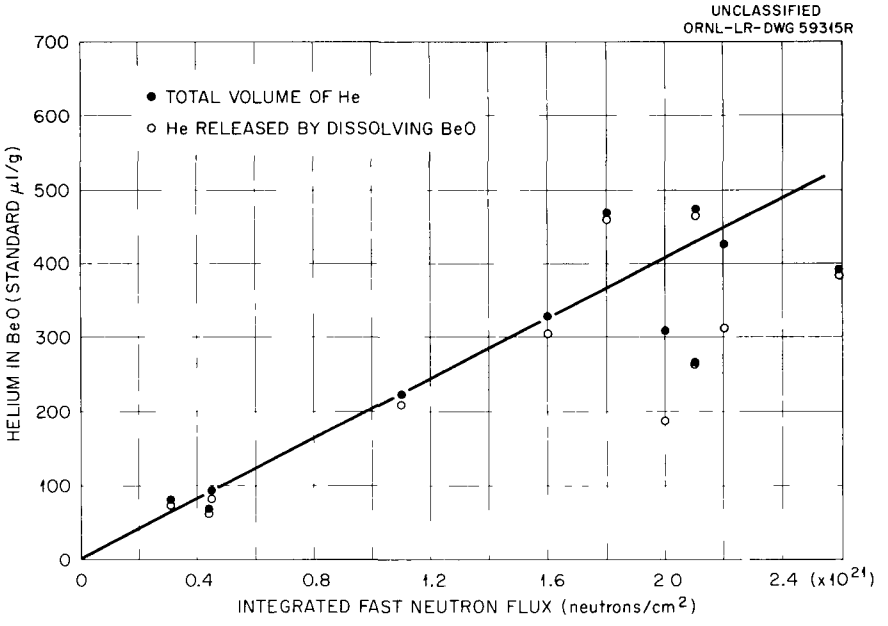

Fig. 25.1. Helium Concentration in Irradiated BeO vs Integrated Fast Neutron Flux (>1 Mev).

tritium is lost to an increasing degree at higher temperatures. Tritium content is very low in specimens irradiated at temperatures above 450°C.

Two processes which have been proposed to explain the failure of pellets under irradiation are (1) displacements of beryllium and oxygen atoms within the crystals (based on x-ray data indicating the formation of interstitial atoms between planes in the lattice) and (2) forces resulting from gas generation and formation of voids. Other experiments are designed to permit a better separation of variables in order to determine the relative importance of these and other possible processes. The experiment currently under irradiation contains samples which are being irradiated at high neutron dose at lower temperatures and at lower dose at higher temperatures, thus separating the competing dose and temperature factors. The next experiment (No. 8) is statistically designed to provide information on the following variables: exposure time, flux, temperature, pellet size, density, and grain size. The effect of density on irradiation damage, for example, may help to establish the importance of gas generation. Diffusion of generated gases from low-density pellets may be so rapid that there will be little or no retention and void formation. Under consideration for the future is a study of the effect of sample purity, in which irradiated pellets made from commercial BeO would be statistically compared with those made from ultrapure BeO, with sintering temperature also included as one of the variables.

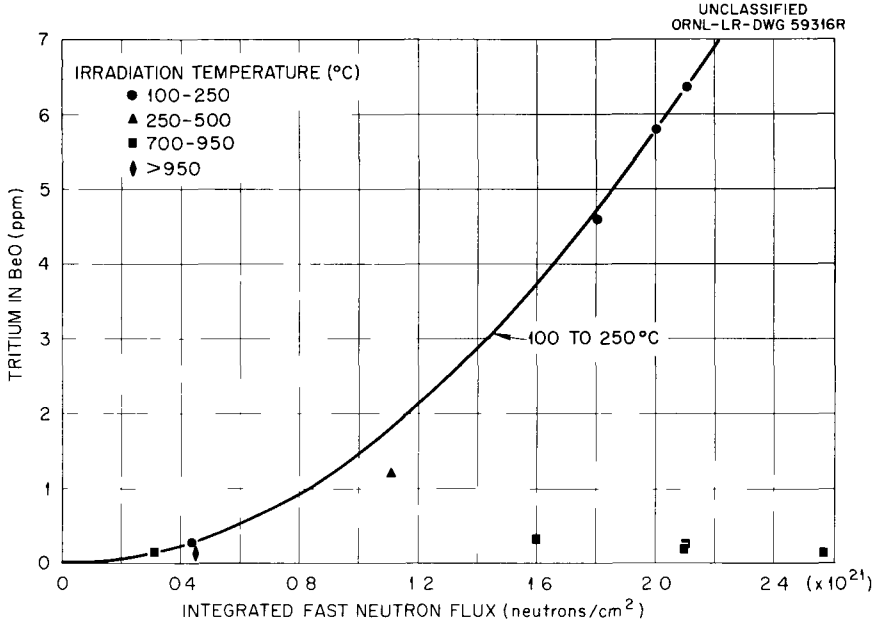

Fig. 25.2. Tritium Concentration in Irradiated BeO vs Integrated Fast Neutron Flux (>1 Mev).

26. Phase-Equilibrium Studies of the System UO_2-ThO_2-O_2

H. A. Friedman R. E. Thoma

The equilibrium-phase relationships in the system UO_2-ThO_2-O_2 are being studied because of their relevance to chemical factors involved in the preparation, performance, and processing of solid fuel elements based on thorium and uranium oxides. These elements can be in the form of massive shapes, pellets, or even slurry particles as small as fractions of a micron in diameter.

The experimental techniques involve heating coprecipitated oxides in air or in sealed systems in which the oxygen partial pressure can be measured; the oxygen contents of the products are determined by chemical analysis, and the crystallographic a_0 values are determined by x-ray diffraction.

EQUILIBRATION OF ThO_2-UO_{2+x} SOLID SOLUTIONS IN AIR

Specimen powders of compositions fixed at 10 mole % intervals from ThO_2 to UO_2 were prepared by coprecipitation, sintered in air at 1500°C to reduce their oxygen contents, and then allowed to reoxidize in air at temperatures from 200 to 1500°C. Periodic interruptions were made to remove samples for oxygen analysis. The oxygen/metal ratios found after equilibrium had been attained are shown in Fig. 26.1. The values for low-temperature equilibration are in some disagreement with results recently reported by Lynch,[1] who perhaps failed to reach equilibrium at these temperatures in the 48-hr test periods which he used; the present work involved equilibration periods up to 100 days.

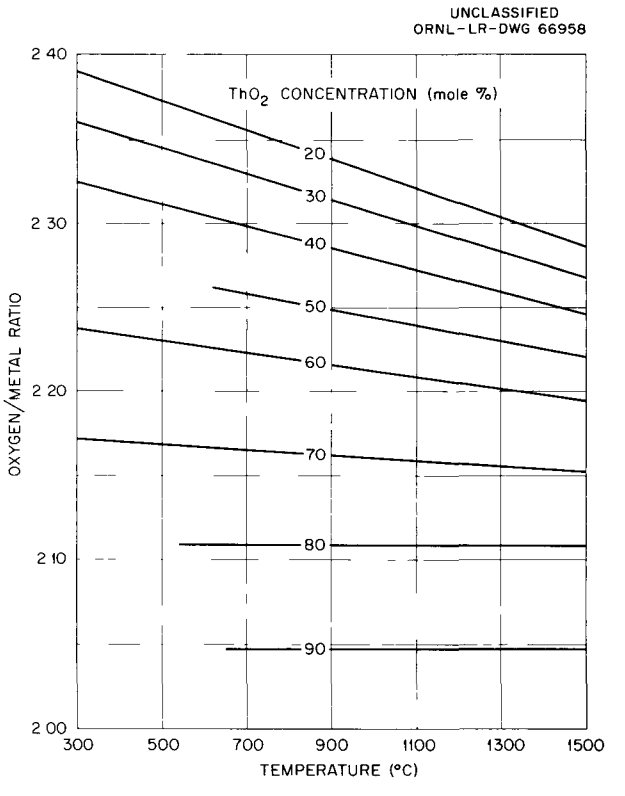

Fig. 26.1. Oxygen/Metal Ratios of Air-Sintered ThO_2-UO_{2+x} Solid Solutions.

Measurements of the unit-cell parameter, a_0, for the equilibrated samples, when plotted vs the oxygen/uranium ratio, revealed discontinuities in the a_0 values at uranium oxidation numbers between 4.0 and 5.0, as shown in Fig. 26.2. These are tentatively interpreted as indicating phase

[1] E. D. Lynch, "Oxidation and Phase Stabilities in Solid Solution Systems Containing Uranium Dioxide," presented at the Symposium on Characterization of Uranium Dioxide, ORNL (Dec. 13–14, 1961).

INTRODUCTION TO PART V

A reactor containment shell is a very prominent and rather expensive feature of large power-producing reactors. These shells are used in an effort to provide assurance that large amounts of radioactive materials, which are always present in operating reactors, will not endanger the health or welfare of people near the reactor in the event of a reactor accident. Lack of adequate information on the amounts and on the form of radioactive species that can be released by such accidents has led to the adoption of conservative hazards estimates which have an adverse effect on reactor costs and impose restrictions on reactor locations. The results of some types of nuclear excursions are being examined in experiments conducted elsewhere.

The purpose of a major part of the nuclear safety program described in this report is to provide data needed to assess the consequences of loss-of-coolant accidents in which overheated reactor fuel elements release fission products to the environment as the result of melting, diffusion, or reaction with components of the atmosphere to which they are exposed. Most of the attention is presently devoted to UO_2 fuels, since the majority of the newer power reactors are using this type of fuel. Information on the behavior of fission products after they are released and methods of collecting them is very pertinent to reactor hazards evaluations and is also needed in connection with the routine operation of some types of reactors. Studies of this type are included in this report.

27. Fission Product Transport Evaluations

C. J. Barton G. W. Parker

There is a lack of understanding of many factors which may affect the sedimentation of released fission products within reactor containment vessels and the fraction of these that may escape to the environment. A small-scale program to study some of these factors was initiated quite recently, but no data are available at present.

A large settling chamber (37 ft^3) is being constructed to study the sedimentation of radioactive particles emitted when irradiated UO_2 fuel specimens are melted in a hot cell by use of a dual-frequency generator. Particles collected in trays covering the floor of the chamber will be examined to determine their particle size and identify radioactive species present. The results will be compared with data from the examination of similar samples taken very near the emission point. Initial studies to establish proper operating conditions for the meltdown experiments will be performed with unirradiated particles of UO_2 or ThO_2 having a known size distribution. Methods are not presently available for direct identification of the chemical compounds in which the various fission-product species exist; development of such methods is one of the goals of this program.

28. Influence of Irradiation Level on Fission Product Hazards Associated with UO_2-Fueled Reactors

G. W. Parker G. E. Creek W. J. Martin

Laboratory measurements of fission product release have been performed in a continuing program sponsored by the Reactor Safety Section of the AEC Division of Reactor Development. As a part of this study, fission product release from irradiated UO_2 has been examined under out-of-pile conditions to permit maximum freedom in designing and conducting experiments. (Release studies performed under in-pile conditions are described in Chap. 29.) Studied so far have been diffusion of fission products into helium from solid materials at high temperature, release of fission products on oxidation of fuel material in air, release of fission products on melting of fuel in various atmospheres, and, finally, the effect of fission density or burnup on fission product release by each process. The effect of other variables, such as specimen size, environment, duration of heating, and overpressure, on the release of fission products during the melting of irradiated UO_2 will be considered in future studies.

RELEASE OF FISSION PRODUCTS ON OXIDATION OF UO_2 TO U_3O_8

A previous report[1] describes early results obtained in fission product release experiments performed with irradiated UO_2. Some of the previously reported data are included in the present report for ready comparison with more recent data. The percent of fission product activities released from PWR-type UO_2 (93% of theoretical density), irradiated at tracer level, is plotted in Fig. 28.1 as a function of temperature. Note that a distinct discontinuity is observed at intermediate temperatures (800 to 900°C), which is also the temperature range in which the minimum oxidation rate for UO_2 in air occurs. This anomalous behavior is believed to be associated with the occurrence of the maximum degree of plastic deformation of the U_3O_8 oxidation product at this temperature, thereby affording a maximum degree of surface-layer protection against further oxidation.

Release data obtained when UO_2 irradiated to 1000 Mwd/ton was heated in air to 1100°C and when UO_2 irradiated to 4000 Mwd/ton was heated to a maximum temperature of 900°C are shown in Fig. 28.2. Comparison of these release values with the data obtained with UO_2 irradiated at tracer level (Fig. 28.1) shows that, in general, release-rate values increase with increasing irradiation level. Data not reported here indicate that irradiated UO_2 oxidizes faster than unirradiated material under the same conditions. Since all the highly irradiated UO_2 material was received in the form of small fragments, these samples were made up of several small pieces having irregular shapes, while the tracer-level samples were single cylinders having smooth surfaces. The discontinuity observed at intermediate temperatures in Fig. 28.1 is missing in most of the release curves shown in Fig. 28.2, but it is still observable in the curve showing behavior of iodine. It is probable that fission product impurity defects in the UO_2 and the greater surface area of irradiated samples led to a higher oxidation rate and thus to higher release values.

[1] G. W. Parker, G. E. Creek, and W. J. Martin, *Chem. Div. Ann. Progr. Rept. June 20, 1961*, ORNL-3176, pp 68–72.

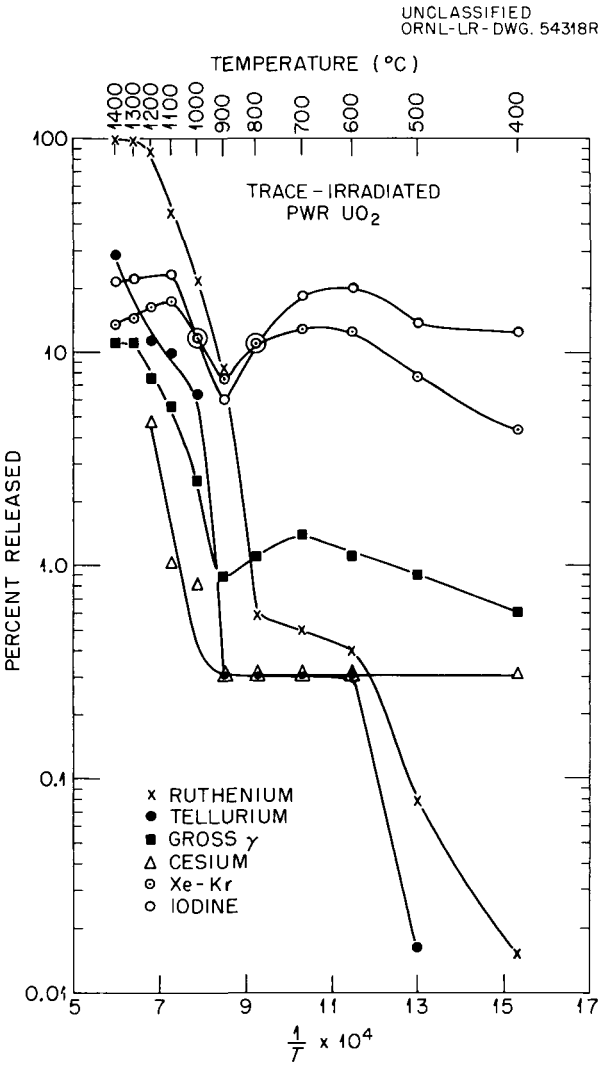

Fig. 28.1. Fission Product Release by the Oxidation of PWR-Type UO_2 to U_3O_8 in Air (Tracer-Level Irradiation).

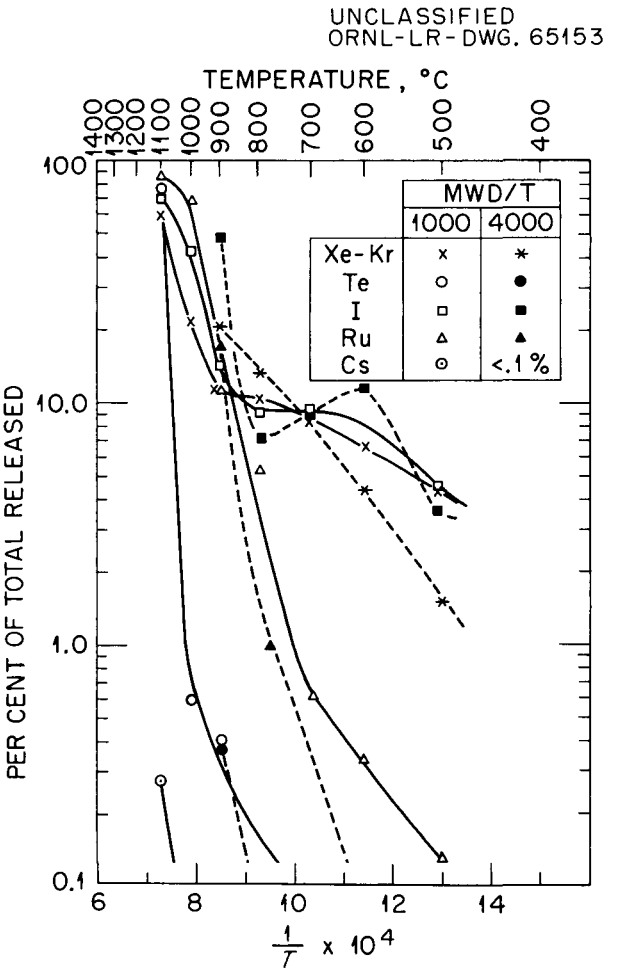

Fig. 28.2. Fission Product Release by Oxidation of Highly Irradiated UO_2 (1000 and 4000 Mwd/ton).

RELEASE OF FISSION PRODUCTS FROM UO_2 BY HIGH-TEMPERATURE DIFFUSION

Rates of fission product release by diffusion from solid UO_2 at high temperatures should probably increase with increasing burnup in a manner similar to rates of release on oxidation of UO_2. A series of diffusion experiments was conducted in which irradiated UO_2 specimens were heated in a stream of purified helium for 5.5 hr. An increase in irradiation level was found to be accompanied by an increase in fission product release. Data from a PWR-type compact (93% of theoretical density) and an EGCR-type compact (97% of theoretical density), both irradiated to 1000 Mwd/ton, and similar data obtained at the tracer irradiation level and at the 4000-Mwd/ton level for PWR-type compacts are illustrated in Figs. 28.3 and 28.4. The data in Table 28.1 permit a more direct comparison of the actual release values at a given temperature. The burnup effect is shown to be quite marked for all fission

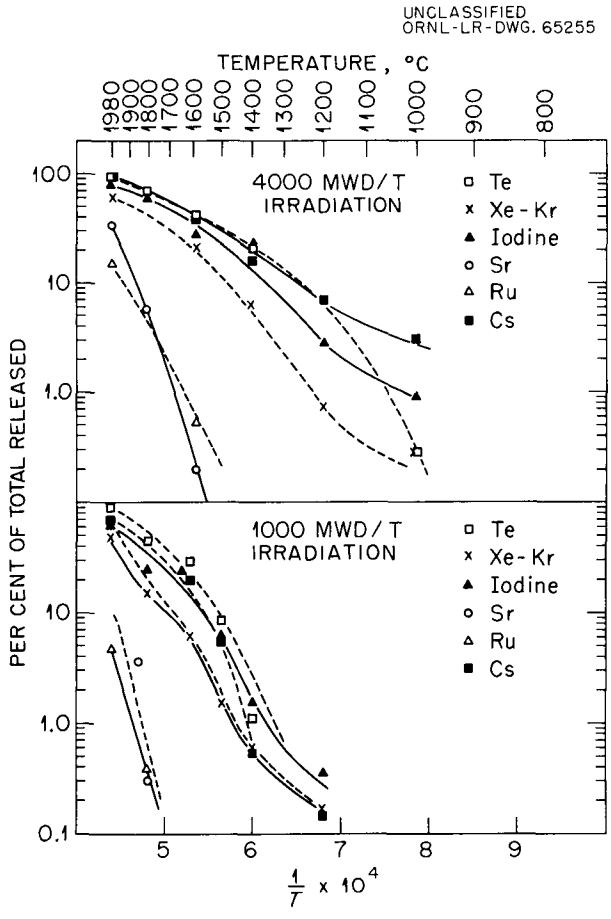

Fig. 28.3. Release of Fission Products by Diffusion from Highly Irradiated PWR-Type UO_2 Heated 5.5 hr in Purified Flowing Helium.

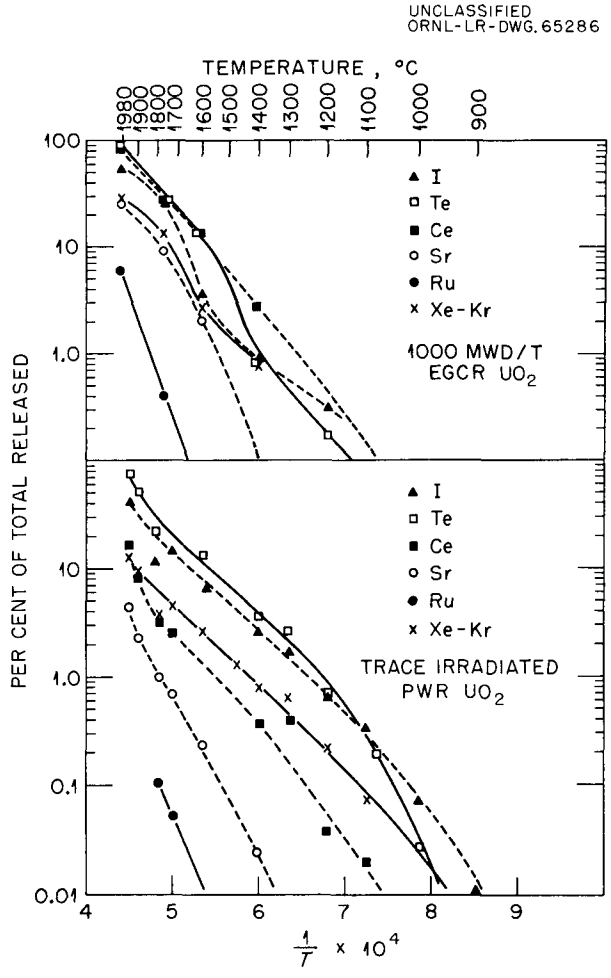

Fig. 28.4. Fission Product Release from Highly Irradiated EGCR UO_2 and from Trace-Irradiated PWR UO_2 by Diffusion into Pure Helium.

products except perhaps ruthenium; the greatest effect is found in cesium release where differences of an order of magnitude are observed. Differences between the two types of fuel at the 1000-Mwd/ton level are not pronounced in spite of the density variation.

RELEASE OF FISSION PRODUCTS FROM UO_2 MELTED IN HELIUM, AIR, AND CO_2

The usual hazards analysis for a loss-of-coolant accident to any large water-cooled reactor postulates melting of much of the fuel loading by decay heat. These hazards analyses unfortunately do not usually take into consideration the duration of the molten period, the velocity of movement of the gas cloud formed in the accident, or the composition of the gaseous atmosphere present during melting. It seems logical to assume that a large mass of UO_2 probably would not remain molten long. The material would probably flow out of the region of highest temperature under the influence of gravity, and it would soon solidify and entrap the remaining fission products. The melting experiments have accordingly been designed to maintain UO_2 in the molten condition for short periods in various atmospheres such as helium, air, and CO_2. The most important con-

dition for which no data have yet been obtained is a simulated meltdown in a steam atmosphere; however, it is felt that the release results obtained in steam would not differ greatly from those obtained in helium or CO_2.

The data in Table 28.2 show the effect of atmosphere and burnup on release of fission products during the melting of UO_2. Since the release values for the volatile fission products are ordinarily quite high even on melting tracer-level-

Table 28.1. Effect of Burnup Level and Density on Diffusion of Fission Products from Irradiated UO_2 into Pure Helium at Various Temperatures

Temperature (°C)	Irradiation Level (Mwd/ton)	Percentage of Individual Fission Products Released[a]						
		Xe-Kr	I	Te	Cs	Ru	Sr	Ba
1400	Tracer	0.8	4.0	3.9	0.02	0.02	0.001	
	1005 (EGCR)	0.8	0.9	0.8	2.6	0.001	0.1	
	1000 (PWR)	0.5	1.6	1.2	0.5	0.001	0.06	1.8
	4000 (PWR)	6.1	23	16	21	0.006	0.08	0.5
1610	Tracer	2.7	6.5	12.1	1.7	1.5	0.1	
	1005 (EGCR)	2.6	3.7	12.0	12.0	0.1	2.0	17.0
	1000 (PWR)	6.0	5.5	27	20	0.3	0.2	12
	4000 (PWR)	14	25	48	43	0.2	0.5	15
1780	Tracer	3.7	11.7	21.0	3.2	6.9	1.0	
	1005 (EGCR)	12.0	24.0	67.0	27.0	0.4	9.0	39.0
	1000 (PWR)	14	25.5	35	22	0.4	3.7	21
	4000 (PWR)	42.2	59.4	59.8	39.7	5.7	5.8	18.4
1980	Tracer	12.3	41.0	75.0	15.0	13.4	4.2	8.7
	1005 (EGCR)	29.0	53.0	74.0	84.0	6.0	15.0	57.0
	1000 (PWR)	48.5	63	90	69.5	4.8	~10	51
	4000 (PWR)	71.3	80.8	81	98.3	14.9	33.0	60.4

[a]Includes that portion adsorbed on crucible and reflector parts.

Table 28.2. Effect of Burnup Level and Atmosphere on the Release of Fission Products During the Melting of UO_2[a]

Atmosphere	Irradiation Level (Mwd/ton)	Sample Weight (g)	Number of Results	UO_2 Vaporized (%)	Percent of Individual Fission Products Released							
					Xe-Kr	I	Te	Cs	Ru	Sr	Ba	Rare Earths
Helium (impure)	Tracer	0.22	2		99.5	89.7	92.0	91.3	61.0	2.1	4.6	2.2
	2,800	0.03	3	21.2	99.9	92.2	98.2	98.5	90.4	2.1	6.6	5.1
	11,000	0.03	2	18.0	100.0	99.7	99.6	98.7	88.1	1.7	6.5	4.1
Air	Tracer	0.2	2		98.4	94.9	79.1	37.7	67.7	0.2	0.5	0.5
	2,800	0.04	3		100.0	99.7	93.6	92.5	95.0	0.4	1.8	3.0
	11,000	0.04	3	24.7	100	99.8	99.3	97.4	92.5	0.4	1.8	3.9
CO_2	Tracer	0.2	3	14.1	80.6	76.8	71.2	60.9	44.9	0.3	1.1	0.85
	2,800	0.02	3		99.9	98.7	98.6	90.2	74.3	0.5	2.5	2.8
	11,000	0.05	3		99.9	99.9	99.0	96.6	79.1	0.6	2.9	2.3

[a]EGCR UO_2 with an O/U ratio of 2.04 and an average density of 95% of theoretical.

irradiated UO_2, the burnup effect is not especially noticeable in these data.

PRODUCTION AND DEPOSITION OF PARTICLES ON MELTING OF UO_2

The size of particles released in a reactor accident affects the fraction of the released activity which will be deposited within the reactor containment shell before it reaches holes in the shell and the fraction of the remaining activity which will be deposited during passage through the opening. In Fig. 28.5 a particle-size analysis is given for the released uranium oxide particles volatilized in different atmospheres. Most of the particles had diameters ranging from 0.01 to 0.1 μ. An electron-microscope photograph of some of these particles is found in a previous report.[1]

An indication of the range in quantity of material which may be plated out (before reaching an absolute filter) as a function of the velocity of air passed over the sample during melting is given by the data in Table 28.3. Of particular interest is the range in quantity of iodine found to pass through the apparatus and filters and to be collected finally in activated charcoal. The data demonstrate that while most of the refractory fission product oxides are distributed to some extent in proportion to the amount of uranium oxides deposited, the more volatile iodine may be carried considerable distances by a rapid flow of gas. Up to 10% of the uranium may volatilize in a typical melting experiment, while an average of less than 1% of the strontium is volatilized in the process. This fact is very encouraging from the reactor hazards viewpoint.

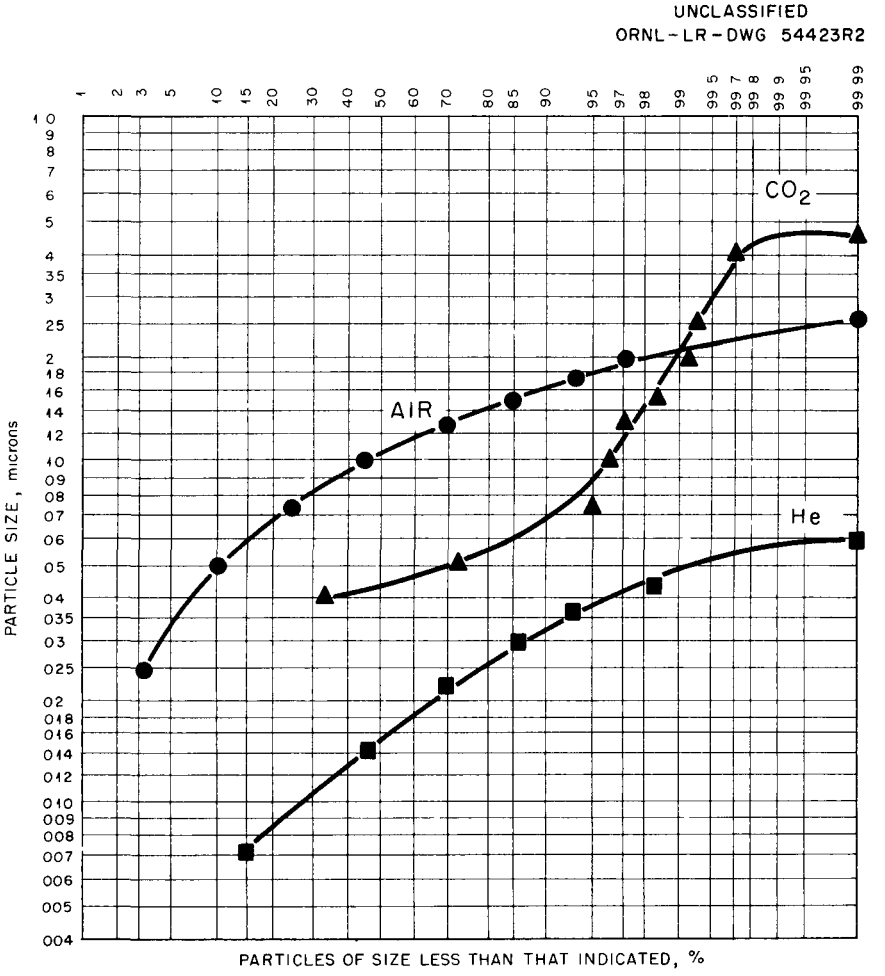

Fig. 28.5. Particle-Size Evaluation of Oxides Vaporized from Melted UO_2 (Arc-Image Furnace).

Table 28.3. Effect of Furnace Air Velocity on Deposition of Fission Products Released by Melting Modified UO_2 Specimens at 2650°C

	Percent of Total Activity and Its Location, with Velocity of Furnace Air as Indicated (lin ft/min)[a]							
	Furnace Tubes		Filters		Charcoal Trap		Total	
	0.3	5.0	0.3	5.0	0.3	5.0	0.3	5.0
Gross gamma	10.1	8.8	1.2	6.2	0.4	3.4	11.7	18.4
Rare gases					77.1	69.5	77.1	69.5
Iodine, γ	62.3	12.1	5.4	9.8	11.3	56.9	79.0	78.8
Tellurium, β^-	66.8	28.6	8.3	43.2			75.1	71.8
Cesium, γ	34.5	18.3	15.6	30.9			50.1	49.2
Ruthenium, γ	63.6	33.0	0.8	24.6			64.4	57.6
Cerium, β^-	0.24	0.17	0.11	0.37			0.35	0.54
Strontium, β^-	0.1	0.05	0.01				0.11	0.05
Barium, β^-	0.55	0.08	0.01	0.07			0.56	0.15
Zirconium, γ	0.02	0.02	0.01	0.01			0.03	0.03
Uranium[b]	6.4		1.4				7.8	

[a]Air flow = 200 cc/min or 0.3 lin ft/min or 3000 cc/min or 5 lin ft/min across sample; heating time = 90 sec.
[b]Vaporized as UO_3.

29. Release of Fission Products by the In-Pile Melting of Reactor Fuels

W. E. Browning, Jr. C. E. Miller, Jr.
R. P. Shields B. F. Roberts
W. H. Montgomery

A series of in-pile experiments in which miniature UO_2 fuel elements are melted by fission heat and the amounts of various fission products released are determined is being conducted in an effort to simulate a reactor accident in which the fuel elements are destroyed by melting or vaporization as a result of uncontrolled heat generation or loss of coolant in the reactor. Since heat is produced in the fuel specimens employed in these experiments by fission and gamma heat, as in a reactor, these experiments provide more realistic reactor accident conditions, in this respect, than can be furnished in out-of-pile experiments.

Miniature fuel elements are supported by a ThO_2 holder in a helium-filled ThO_2 cylinder. Thermal insulation surrounding the chamber consists of porous zirconium oxide, which is contained in two concentric vessels of stainless steel. The outer wall of the furnace assembly is cooled by reactor cooling water. A slow stream of helium is passed over the specimen during melting and is swept through filters and adsorbers to determine the amounts and forms of fission products released. The furnace and reactor facility have been described elsewhere in detail.[1,2]

Uranium dioxide, clad in stainless steel, was selected for the first series of experiments because it is so widely used in present-day power reactors and because it is difficult to melt in out-of-pile experiments. Two experiments have been performed in the ORR by using specimens of UO_2, 0.210 in. in diameter by 1 in. long, clad in stainless steel.

In the first experiment the UO_2 was 3% enriched and had a density of 94% of theoretical. It was irradiated (to accumulate tracer quantities of fission products) for 52 hr at a position in the reactor which produced a cladding temperature just below the melting point of stainless steel. The specimen was then further inserted into the lattice to a point of maximum flux, held at this point approximately 20 min, and retracted. Examination of material from this experiment in hot cells showed the UO_2 specimen to be intact (Fig. 29.1), but to contain a large central void over three-fourths of its length. The outer surface of the specimen consisted of pyramidal crystals, shown in more detail in Fig. 29.2. Figure 29.3

UNCLASSIFIED
R6841

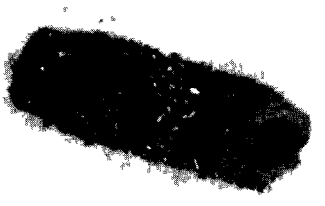

Fig. 29.1. Segment of UO_2 Specimen from Experiment 1 After Being Internally Heated to Melting Point of UO_2. Central void and crystalline surface indicate vaporization of UO_2.

[1] R. P. Shields *et al.*, *Reactor Chem. Div. Ann. Progr. Rept. Jan. 31, 1961*, ORNL-3127, pp 149–52.

[2] R. P. Shields *et al.*, "Release of Fission Products on the In-Pile Melting of Reactor Fuels," *Proceedings of the Second Conference on Nuclear Reactor Chemistry*, Gatlinburg, Tenn., Oct. 10–12, 1961, TID-7622.

Fig. 29.2. Crystalline Outer Surface of UO_2 Specimen from Experiment 1.

UNCLASSIFIED
R6519

UNCLASSIFIED
R6520

Fig. 29.3. Photomicrograph of Section of UO_2 Specimen from Experiment 1. The dashed line indicates the original surface of the specimen.

is a photomicrograph of a polished piece of the UO_2. The dashed line shows the estimated position of the original circumference of the specimen. There are large grains and voids visible, but the columnar growth often observed in UO_2 which has been subjected to high-temperature gradients is missing. The sharp well-defined crystals on the surface indicate that a considerable quantity of the UO_2 has passed through the vapor phase. This vapor, formed by the high temperature inside the specimen, migrated through the pores and cracks to the outside, where it crystallized on the cooler surface. The temperatures required to produce the effects displayed in the foregoing figures are consistent with the temperatures found by extrapolation from the temperature observed during irradiation.

In the second experiment a 25% enriched specimen of UO_2 was irradiated at 1200°C for 24 hr and then inserted to a position where the heat generation was estimated to be twice that required to melt the specimen. The experiment was retracted after 10 min. Examination of material from this experiment in the hot cell showed the fuel specimen to have completely vaporized or melted and to have collected as crystals throughout the inside of the ThO_2 cylinder. A considerable amount of material was deposited in the exit-gas tube. One wall of the ThO_2 holder apparently melted (see Fig. 29.4).

The first two experiments were intended to test the adequacy of the design and to reveal operational problems. They have shown that the furnace design is capable of carrying UO_2 specimens well above the melting point without overheating container materials. Temperatures observed agreed well with those calculated from flux and gamma-heat measurements. It is estimated that a temperature in excess of 3300°C was achieved in the second experiment. The reactor facility performed satisfactorily in positioning the experiment and in preventing release of fission products to the atmosphere.

These two experiments showed that UO_2 heated to its melting point or higher for only a few minutes is extensively transported by vaporization rather than collected in a compact melt. This behavior may have profound effects on the amounts and forms of fission products released during a reactor accident. Under such conditions fission products may be carried into the gas phase without regard to volatility. As the UO_2 vapor condenses it may scavenge fission products from the gas phase to deposit them on surfaces inside the reactor. On the other hand, the fission products may be carried in a form difficult to remove from gases. A further consequence of vaporization of UO_2 is the increased accessibility of fission products for chemical reaction with materials in the environment. Radioassay of various parts of the furnaces and their off-gas systems is being conducted to obtain information as to the amounts, nature, and behavior of fission products released. In the first experiment the fission product nuclides Ce^{144}, Zr^{95}, Y^{91}, and Sr^{90} were for the most part retained in the UO_2, while Xe^{133} and Ru^{106} were largely released. Partly released from the UO_2 were Ba^{140}, Sr^{89}, and Cs^{137}, all of which have volatile precursors. These results must be considered preliminary because they are based on only one experiment. Analysis of the second experiment is in progress.

Fig. 29.4. Photograph of ThO_2 Holder from Experiment 2 Showing Hole Where ThO_2 Melted or Dissolved in UO_2.

Further experiments will be conducted to determine the effects of various conditions on fission product release. Among the variables to be investigated is fission product concentration, since the tracer concentrations of fission products in the present experiments are much lower than those that exist in reactors. Toward this end, a facility has been designed and is being fabricated for long irradiation of fuel specimens to accumulate large concentrations of fission products prior to melting. This facility, which accommodates eight specimens, will occupy the F-3 position in the ORR. Meanwhile, several identical experiments are being run to establish reproducibility of operation, sampling, and analysis.

30. Removal of Radioactive Fission Products from Air and Other Gases

W. E. Browning, Jr. R. D. Ackley R. E. Adams

In the study of the removal of radioactive fission products from air and other gases, the radioactive materials considered include the gases krypton and xenon, iodine vapor, and finely divided particulate matter, which may consist primarily of fission products or which may be nonradioactive but may serve as a carrier for fission products and may promote or hinder their deposition.

REMOVAL OF RADIOIODINE VAPOR FROM GASES

Removal of Iodine from High-Temperature Helium

A study of the removal of iodine vapor from high-temperature helium streams was continued in support of the experimental loop program of the Gas-Cooled Reactor Project. The purpose of this study was to determine the feasibility of removing radioiodine vapor, by adsorption, from recirculating helium streams without reducing the temperature of the helium.

Previous study[1] revealed that one of the several types of charcoal tested exhibited markedly superior adsorption and retention of iodine vapor at elevated temperatures. This charcoal, Whetlerite ASC, is prepared commercially by impregnating Pittsburgh BPL charcoal with salts of silver, copper, and chromium. Efforts during the period covered by this report were directed toward study of the migration of iodine through relatively deep beds (~4 in.) of Whetlerite charcoal as a function of temperature to provide data more directly applicable to the EGCR loop conditions. Iodine vapor containing I^{131} was injected for a short time, and then the distribution of I^{131} in the test bed was monitored continuously over the duration of the run by a gamma scintillation crystal mounted on a traveling platform. Table 30.1 contains the results of this study. At temperatures up to 550°C the movement of iodine was hardly detectable. At 650°C the iodine was more mobile, but the 4.25-in. bed of Whetlerite charcoal delayed the iodine penetration for approximately six days. Whetlerite charcoal appears well suited for iodine vapor removal in the EGCR experimental loops without the necessity of reducing the temperature of the helium coolant.

Removal of Iodine from Steam-Air Mixtures

The removal of iodine from steam-air mixtures is being studied in support of the Maritime Reactors Program, specifically the NS "Savannah" Project. To provide control of radioiodine which may be evolved within the reactor containment vessel (and subsequently leak into the reactor compartment of the ship), an activated-charcoal iodine-adsorption unit will be used in the auxiliary ventilation system of the reactor compartment. While the existing experimental data are sufficient to demonstrate the feasibility of a design utilizing activated charcoal for the removal of iodine vapor from moist air streams near 100°C,[2] additional study is needed to ensure that the

[1] W. E. Browning, Jr., R. D. Ackley, and R. E. Adams, *Reactor Chem. Div. Ann. Progr. Rept. Jan. 31, 1961*, ORNL-3171, pp 142–43.

[2] R. E. Adams and W. E. Browning, Jr., *Removal of Radioiodine from Air-Steam Mixtures*, ORNL CF-60-11-39 (Nov. 14, 1960).

Table 30.1. Retention of Iodine Vapor by Whetlerite Charcoal in High-Temperature Helium Systems

Temperature (°C)	Helium Velocity (fpm)	Duration of Test (hr)	Total Migration of Iodine (in.)	Retention of Iodine (%)
325	38.8	468	0.06	99.99+
425	53.0	897	0.07	99.99+
550	53.7	602	0.15	99.99+
650	60.2	220	>4.25[a]	86.73

[a]A small portion of the iodine content emerged from the 4.25-in.-deep trap at ~143 hr.

iodine adsorbers as specified for the reactor-compartment ventilation system will provide the efficiency needed under the proposed operating conditions.

The experimental techniques being used in this study are essentially identical to those of previous iodine studies, with two exceptions: (1) iodine vapor injection is continuous rather than the pulse type used previously and (2) the mass concentration of iodine in the steam-air mixture is several orders of magnitude lower. Radiochemical analysis of the system after termination of the experiment provides the necessary information for computing the iodine vapor adsorption efficiency.

The program of study is divided into three phases. One phase involves small-scale testing of a sample of the charcoal (Pittsburgh BPL, 12/30 mesh) used in producing the full-size charcoal filters presently installed on the NS "Savannah." The purpose of these tests is to determine: (1) the iodine vapor removal efficiency under specified operating conditions, (2) ultimate iodine capacity under the stated operating conditions, and (3) the sensitivity of items (1) and (2) to changes in the operating conditions. If BPL charcoal does not perform satisfactorily, other types of activated charcoal are to be tested to ensure that the more efficient iodine vapor adsorbent be used in the shipboard iodine filters. The results of initial testing of Pittsburgh BPL charcoal ("Savannah" type) are in Table 30.2. Since the efficiencies observed were low, tests were run on Pittsburgh PCB charcoal. It appears from these few tests that the PCB is superior to the BPL type. Details of the tests are as follows: (1) continuous injection of iodine vapor at an estimated concentration in the steam-air mixture of 10^{-4} to 10^{-5} mg/m^3 of gas, (2) test duration of 5 hr, and (3) charcoal test bed 1 in. in diameter by 1.125 in. deep. Additional tests are in progress.

The second phase is concerned with larger-scale iodine tests involving charcoal units (11 × 11 × 1.125 in.) produced by the manufacturer with the same techniques which produced the full-scale iodine adsorber units installed on the NS "Savannah." Results from the small-scale tests will guide the experiments in this phase. The experimental facility for testing these prototype units under conditions of elevated temperatures (~100°C) and high humidity (~90%) is complete, and shakedown runs using radioactive I^{131} are in progress. The efficiency of the prototype units will be determined both by complete I^{131} analysis and by withdrawing gas samples before and after the charcoal unit. It is anticipated that some degree of correlation between the two techniques will be achieved.

The third phase concerns the development of a method for "in-place" testing of the installed shipboard charcoal units. This test (with I^{131} or a suitable substitute) will be designed to indicate (1) that the iodine unit is effectively mounted, with no bypass leakage occurring, and (2) when an iodine unit should be removed from service due to excess iodine penetration or lowered residual capacity for iodine. Experience gained with sampling apparatus and techniques during the tests involving the 11 × 11 in. prototype units will be useful during the "in-place" testing program.

Table 30.2. Retention of Iodine Under Simulated NS "Savannah" Conditions

Run	Charcoal Type	Temperature (°C)	Steam (% saturated)	Gas Velocity (fpm)	Efficiency (%)
1	Pittsburgh BPL 12/30 mesh	98	71.1	21.3	84.4
2	Pittsburgh BPL 12/30 mesh	98	77.3	21.8	93.7
3	Pittsburgh BPL 12/30 mesh	99	70.7	22.8	97.5
4	Pittsburgh BPL 12/30 mesh	97	83.8	33.8	97.0
5	Pittsburgh PCB 12/30 mesh	99	73.2	24.8	97.6–99.3[a]
6	Pittsburgh PCB 12/30 mesh	97	86.9	33.6	99.86
7	Pittsburgh PCB 12/30 mesh	98	79.2	28.4	99.71

[a]Amount of I^{131} very small. Most downstream samples below limit of analytical sensitivity; efficiency is within this range.

Environmental Air Monitoring for Iodine Vapor

Environmental monitoring for the presence of radioiodine in the various inhabited compartments of the NS "Savannah" will be accomplished by passing a measured volume of air through an activated-charcoal cartridge. Iodine radioactivity in the cartridge will then be determined by one of several types of radiation detection instruments such as a G-M survey meter, G-M scaler, or multichannel gamma spectrometer. Iodine-131 "standards" were fabricated at ORNL and supplied to New York Shipbuilding Corporation for determining the response of these instruments to amounts of I^{131} equivalent to 0.1, 1.0, 10, and 100 times the MPC_a for continuous exposure to I^{131}. The multichannel gamma spectrometer was able to detect 1 MPC_a while the G-M survey meter and scaler were applicable to the 10 to 100 MPC_a range.

To accomplish successful iodine monitoring by using the activated-charcoal cartridge, it is necessary to know the adsorption or collection efficiency under conditions of high gas velocity through the charcoal mass and at very low mass concentrations of iodine in air. A 1-in.-diam 1.25-in.-deep column of Pittsburgh PCB charcoal, 6/16 mesh, was studied at 24°C with a linear air velocity through the charcoal of 298 fpm. For a test period of 40 min, the iodine collection efficiency was determined to be 99.4%. This test was operated with iodine concentrations much larger than desired. Several methods are being considered for producing a concentration of iodine in air, equivalent to MPC_a conditions, for laboratory study.

TRANSPORT AND DEPOSITION OF RADIOACTIVE AEROSOLS

When radioactive materials appear in gases as gaseous components or true vapors, they can be removed by adsorbers, as described elsewhere in this report. When the radioactive burden of gases takes the form of particles 0.3 μ or larger in diameter, it can be removed by "absolute" filters. There is a range of particle sizes, however, smaller than 0.3 μ, where diffusion processes are too slow for efficient deposition on surfaces and particle masses are too small for efficient

filtration by inertial impaction. Particles of this size occur naturally in the atmosphere and may be produced by several processes, including the passing of gases over heated surfaces, a condition prevalent in nuclear reactors. These particles are usually of only indirect importance, for example, as condensation nuclei, but may still play an important role in the behavior of radioactive materials, because significant quantities of radioactivity may be associated with them. Fission products may form small particles directly or deposit on pre-existing particles and exhibit apparently anomalous behavior, penetrating both adsorbers and filters. Such anomalies have been observed and may be attributed to the presence of fine particles.

To characterize radioactivity carried in gases as to the particle size with which it is associated, measurements based on the radioactivity of the particles are necessary rather than those based on light scattering, condensation of supersaturated vapors, or optical or electron microscopy. The relative effectiveness of particles of different sizes and kinds for carrying radioactivity may differ from that indicated by other methods of measurement. Accordingly, an investigation concerned with the transport and deposition of fine particles has recently been undertaken. Also, consideration of the behavior of accompanying vapors such as iodine is included in the study (which is thus closely related to the preceding investigation on "Removal of Radioiodine Vapor").

An important mechanism in aerosol transport and deposition is that of diffusion, and an important characteristic of an aerosol, its particle diameter, is related to the diffusion constant. Townsend[3] measured the diffusion coefficients of ions in gases, and Nolan and Guerrini[4] and Thomas[5] adapted this method to determine the diffusion coefficient for a monodisperse aerosol. The initial emphasis in this study has been given to the application of diffusion as a means for determining the particle-size distribution of aerosols. At the same time, information helpful in understanding the mechanism itself is obtained.

Particle-Size Distribution of Aerosols by Diffusion Coefficient Measurements

Various investigators have derived expressions for the fraction of the entering particles, assumed uniform and in a flowing gas stream, penetrating rectangular or cylindrical channels. As the equations are rather cumbersome, only the functional relationships will be indicated. For rectangular geometry

$$N_g/N_0 = f(D, Q, Z, a, b) , \qquad (1)$$

where N_g is the number of particles remaining in the gas; N_0, the number entering; D, their diffusion coefficient; Q, the volumetric flow rate; Z, the channel length; and a is one-half the distance between parallel walls of height b. For a cylindrical tube, the diameter, in effect, cancels itself so that the corresponding equation for N_g/N_0 does not include diameter (or, of course, a or b). However, for the work described herein, these equations are not directly applicable, since the procedure being employed is to pass an aerosol through channels and then to determine the amount of deposition on definite increments of length of the inside walls of the channel as a function of channel length. Consequently, letting n_s represent the number of particles of a given species per unit length and letting N_s represent the cumulative number, the equations were modified to yield

$$n_s = \frac{\partial N_s}{\partial Z} = -\frac{\partial N_g}{\partial Z} = -N_0 f_z(Z) . \qquad (2)$$

For a spectrum of particles, having different diffusion coefficients, their distribution on the wall of a channel would be

$$\sum_i n_{s_i} = -\sum_i N_{0_i} f_z(D_i, Z) . \qquad (3)$$

The actual equations which have been employed are those of DeMarcus[6] and Gormley and Kennedy[7]

[3] J. S. Townsend, *Phil. Trans. Roy. Soc. London* 193A, 129–58 (1900).

[4] J. J. Nolan and V. H. Guerrini, *Proc. Royal Irish Acad.* 43A, 5–24 (1935).

[5] J. W. Thomas, *The Diffusion Battery Method for Aerosol Particle Size Determination*, ORNL-1648 (Dec. 14, 1953).

[6] W. DeMarcus and J. W. Thomas, *Theory of a Diffusion Battery*, ORNL-1413 (Oct. 13, 1952).

[7] P. G. Gormley and M. Kennedy, *Proc. Royal Irish Acad.* 52A, 163–69 (1949).

after modification as indicated above. For a rectangular channel, a single species, and a sufficient degree of deposition,

$$-f_z(Z) = 0.915\beta e^{-\beta Z} + 0.696\beta e^{-11.8\beta Z} + 2.08\beta e^{-80\beta Z}, \quad (4)$$

where

$$\beta = \frac{3.77\, bD}{aQ}. \quad (5)$$

The corresponding equation for a cylindrical channel is similar to Eq. (4), except that the numerical coefficients are different, and now

$$\beta = \frac{3.66\, \pi D}{Q}. \quad (6)$$

The approximate diffusion coefficient range of interest, for molecules or particles in air at normal conditions, is from 0.085 cm^2/sec for molecular iodine down to approximately 3×10^{-7} cm^2/sec for particles 1 μ in diameter. A close examination of Eqs. (4), (5), and (6), along with a consideration of the experimental factors involved, indicates that a cylindrical geometry would be convenient for the smaller particles, but that, for the larger ones, a rectangular geometry would be more useful. An IBM nonlinear regression code was utilized for processing the data in order to supply the D_i's and relative N_{0_i}'s in Eq. (3), weighted for radioactivity.

The more important experiments thus far performed have consisted in essence of passing air through a chamber in which an aerosol is being generated, then through I^{131} vapor, and next through one or two diffusion channels. Radioiodine was used because of its important role in nuclear safety problems and as a means of labeling particles to simulate other fission products. The particles used were formed by slow combustion of tobacco and/or by high-frequency discharge (4 Mc, 50 kv) across a spark gap made from aluminum wire. The estimated diameter for these particles is 0.25 μ for the tobacco smoke, from the value listed by Cadle,[8] and 0.004 μ for the aluminum oxide particles obtained by sparking aluminum wire, from a study by Dearth and Van den Akker.[9] A diagram illustrating one of the experiments is shown in Fig. 30.1. In another experiment, in which the spark

[8] R. D. Cadle, *Particle Size Determination*, p 1, Interscience, New York, 1955.

[9] L. R. Dearth and J. A. Van den Akker, *A Study of the Filtration and Permeability Characteristics of IPC 1478 Filter Paper*, DASA-1168, pp 37–38 (Feb. 13, 1960).

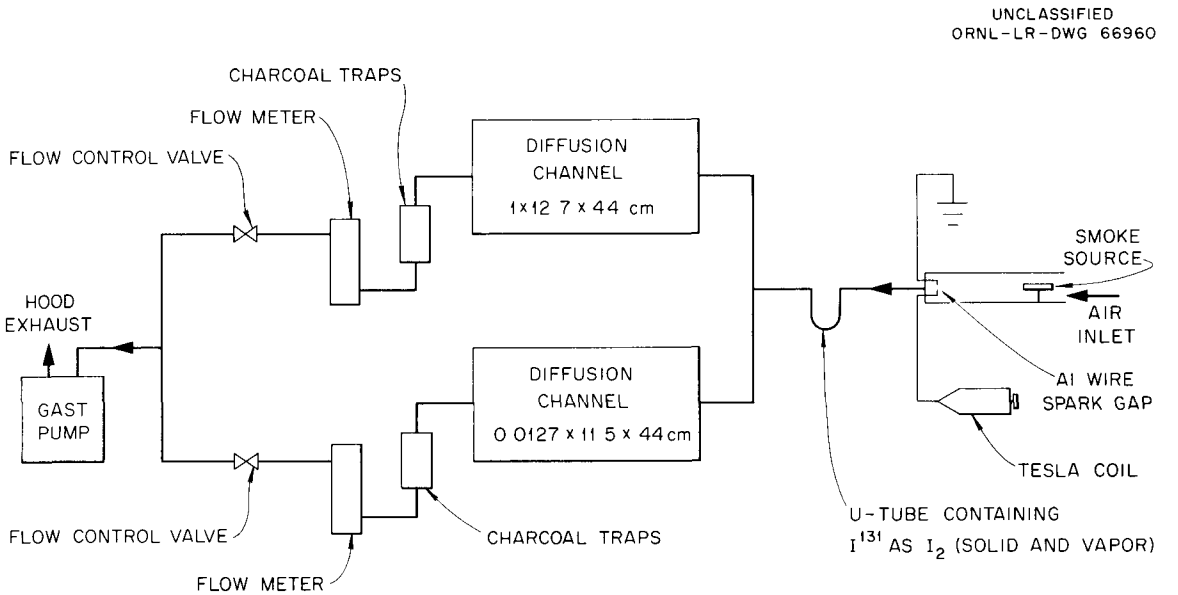

Fig. 30.1. Particle Diffusion Experiment with Rectangular Channels.

gap was employed, the rectangular channels were replaced by a single copper tube approximately 60 cm long and having an inside diameter of about 0.8 cm. Transport of elemental iodine alone was similarly studied, with a copper tube, by omitting aerosol generation. After exposure of the diffusion channels for a few hours, the distribution of activity on their walls as a function of length was determined by means of a gamma spectrometer. Some samples of the data obtained are shown in Figs. 30.2 and 30.3, along with selected theoretical curves. Regarding the experiment corresponding to Fig. 30.2 (and also Fig. 30.1), the IBM analysis of the data from the two channels actually gave a diffusion coefficient equivalent to the aforementioned value of 0.25 μ, although such agreement must be considered partially fortuitous. The deviation between observed and calculated values for the 1-cm-spaced

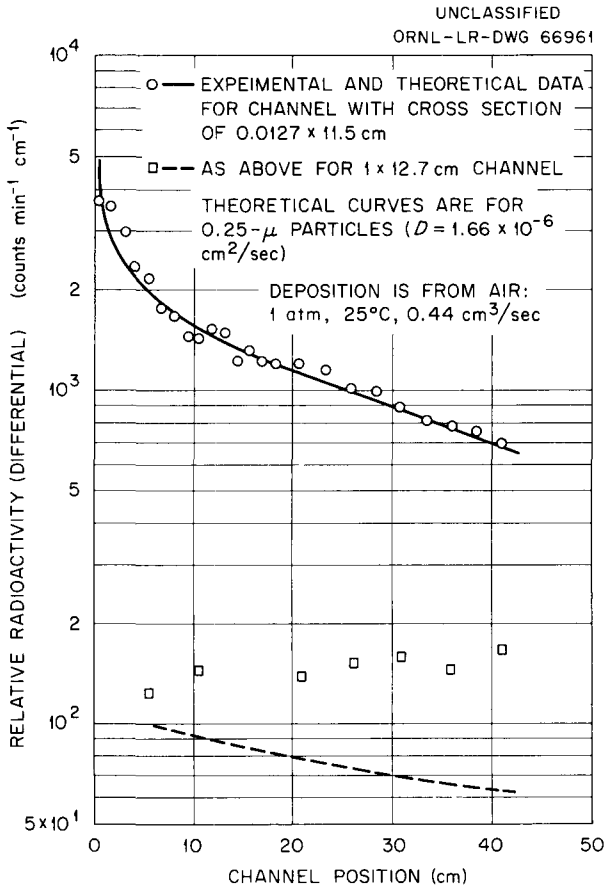

Fig. 30.2. Deposition of Smoke (~0.25 μ), Labeled with I^{131}, by Diffusion in Rectangular Channels.

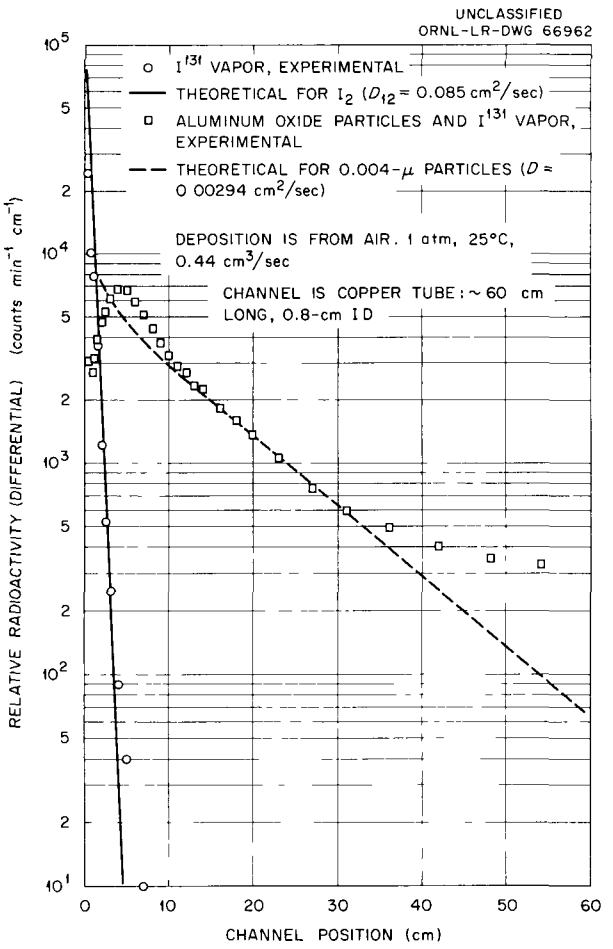

Fig. 30.3. Deposition of Molecular Iodine and Aluminum Oxide Particles by Diffusion in a Cylindrical Channel.

channel is associated with low counting rates and thus may not be as serious as it appears. Neither of the two channels showed evidence of elemental iodine or the presumed 0.004-μ particles; this observation is a result of their deposition prior to entering the rectangular diffusion channels. Data in Fig. 30.3 for iodine alone show good agreement with theory, and data for the aluminum oxide particles appear satisfactory except for an entrance effect, which may be a result of iodine vapor still being deposited on the particles. It is of interest to note the profound effect of 0.004-μ particles on deposition of radioiodine. Future experimental and testing arrangements will probably include a combination of

cylindrical and rectangular geometries, together with a more precise method for introduction of the air being sampled.

In summary, the results of the particle diffusion studies appear sufficiently promising from the standpoint of characterization of radioactive aerosols and vapors to warrant continued investigation.

REMOVAL OF RADIOACTIVE NOBLE GASES FROM CARRIER GASES

Work on removal of krypton and xenon from other gases[10] has continued, but at a lower level of effort. The method of removal receiving most of the attention is that based on physical adsorption; that is, an adsorber may delay the noble gases relative to the moving carrier gas, with resultant radioactive decay and disappearance of short-lived isotopes, or the adsorber may act as a concentrator or collector.

Equilibrium Adsorption of Noble Gases

While dynamic adsorption measurements under proposed operating conditions are desirable for adsorber design, and much of the previous work on noble gases has consisted of such measurements, equilibrium or static adsorption data, which are often more conveniently obtained, are also useful for this purpose. Previously, equilibrium krypton and xenon adsorption isotherms for four varieties of charcoal and for Linde molecular sieves type 5A were measured at 0, 25, and 60°C.[11] Plans are being made to extend such measurements to include a greater variety of adsorbents, noble gases, and temperatures. Some additional isotherms were recently obtained for one of the four types of charcoal mentioned above, and the detailed results will be published later. The isotherms included krypton at −45 and −78°C; xenon at −45 and −78°C; argon at 25, 0, and −78°C; and neon at −78 and −196°C. Radioargon, although not a fission product, can be a problem in the vicinity of reactors when air is irradiated; the interest in neon is mainly academic.

Thermal Conductivity of Charcoal-Gas Systems

In the design of adsorbers for use in situations in which the heat from radioactive decay of adsorbed fission product gases is appreciable, the thermal conductivity of the charcoal–carrier-gas system is an important parameter, since the design must provide for dissipation of the heat produced. Previous measurements on one type of charcoal[12] have been extended through use of the Northrup method, by members of the M.I.T. Practice School, to four additional types of charcoal with helium, nitrogen, and carbon dioxide, separately, in the voids. No pronounced differences in thermal conductivity were observed among the five varieties of charcoal (including the one studied earlier). The apparent thermal conductivity of charcoal-gas systems decreases in the order He, N_2, and CO_2, in accordance with the behavior of the pure gases. These recent results have been reported, both briefly[13] and in detail.[14]

Dynamic Krypton Retention at the Temperature of Liquid Nitrogen

Operation of adsorbers at liquid-nitrogen temperature, approximately −196°C, is frequently of interest, since equilibrium or static adsorption data indicate that dynamic holdup times for krypton or xenon would be extremely long. Therefore, since applicable dynamic data for temperatures in this region are very sparse, the experiment to be described was initiated. The adsorbent is 40 g of Columbia HCC, 12/28X, activated carbon, occupying 8.25 in. of length in a trap with an inside diameter of 0.95 in., at a temperature of about −196°C. The carrier gas is helium at 1 atm flowing at a rate of 360 cm^3 (STP)/min. The amount of krypton injected was about 7.5 cm^3 (STP) and included 800 mc of Kr^{85} to provide high counting sensitivity. The test has now been in progress for eight months with no evidence of breakthrough of Kr^{85}. For comparison, the average

[10] W. E. Browning, Jr., R. D. Ackley, and R. E. Adams, *Reactor Chem. Div. Ann. Progr. Rept. Jan. 31, 1961*, ORNL-3127, pp 144–47.

[11] R. D. Ackley and W. E. Browning, Jr., *Adsorption of Krypton and Xenon on Activated Carbon and Linde Molecular Sieves*, ORNL CF-61-2-32 (Feb. 14, 1961).

[12] W. E. Browning, Jr., R. D. Ackley, and R. E. Adams, *Reactor Chem. Div. Ann. Progr. Rept. Jan. 31, 1960*, ORNL-2931, pp 173–74.

[13] *GCR Quart. Progr. Rept. Mar. 31, 1961*, ORNL-3102, p 234.

[14] P. M. Roth and C. R. Wunderlich, *Determination of Effective Thermal Conductivities of Charcoal Beds*, KT-564 (Feb. 23, 1961).

krypton holdup time at room temperature for such a trap and flow rate would be 5 min. However, this result does not necessarily imply that traps for noble-gas fission products should usually be designed for a temperature as low as that of liquid nitrogen, since there are a number of disadvantages inherent in such operation.

Diffusion of Krypton and Xenon in Adsorbents

The importance of transport of radioactive krypton and xenon by longitudinal diffusion, in adsorbers where the carrier gas is moving at low velocity, has been mentioned previously. In addition, experimental diffusion coefficients have been presented for krypton diffusing through charcoal with helium in the voids.[15] A theory to account for these data has since been developed, resulting in the following equation, which is also regarded as applicable to the case of xenon diffusion:

$$D_e = D_{12} R_D E_D , \qquad (7)$$

where D_e is the effective diffusion coefficient, D_{12} is the gas-phase diffusion coefficient for the noble gas in the carrier gas, R_D is the ratio of gaseous noble gas to that adsorbed, and E_D is an efficiency factor which allows for tortuosity and the lower diffusivity in small pores. Verification of the theory was provided by a successful correlation of the aforementioned experimental diffusion coefficients which ranged from 0.0021 cm^2/sec at 0°C to 0.0141 cm^2/sec at 60°C. Equation (7) should permit, in the majority of situations, sufficiently accurate estimates to be made of effective diffusion coefficients for krypton and xenon, in adsorbers, utilizing available data and theory. Constants for the equations, together with certain restrictions and other details, have been reported elsewhere.[16]

---

[15] W. E. Browning, Jr., R. D. Ackley, and R. E. Adams, *Reactor Chem. Div. Ann. Progr. Rept. Jan. 31, 1961*, ORNL-3127, p 146.

[16] *GCR Quart. Progr. Rept. June 30, 1961*, ORNL-3166, pp 182–84.

Part VI

Preparation and Properties of Special Materials

31. Preparation of Pure Materials

PREPARATION OF SINGLE-CRYSTAL LiF

C. F. Weaver B. J. Sturm R. E. Thoma

Single crystals of lithium fluoride with differing isotopic abundance for the Li^+ are of considerable interest for a variety of solid-state researches. Accordingly, as part of a program for study of the properties of pure materials at the Oak Ridge National Laboratory and elsewhere, a program to produce large (>4-cm-diam) ultrapure crystals of Li^7F and Li^6F has been initiated. A slight modification of the Stockbarger technique,[1-3] in which the molten salt in a specially shaped crucible (of nickel in this case) is slowly lowered through a furnace containing a sharp thermal gradient, was applied in this study.

Preparation of LiF

Preparation of single crystals of LiF with minimum lattice distortion requires very pure starting material.[1-3] While many ions are rejected by the slowly growing crystal, Mg^{2+} and OH^- ions are accepted by the lattice with marked alterations of its properties. Therefore MgF_2 and LiOH must be reduced to low levels in the starting material. In addition, low sulfur content is desirable, even though S^{2-} is effectively excluded from the crystal, to avoid embrittlement and possible corrosion of the nickel container.

The raw material for studies to date has been $LiOH \cdot H_2O$ in which the Li^+ is 99.99% Li^7 and with the impurities shown in Table 31.1. This very pure material was dissolved in doubly distilled deionized water and was treated by extraction with perfluorooctanoic acid in diethylether to remove Mg^{2+} and other polyvalent cations by a modification of the method of Apple and White.[4] Lithium fluoride was precipitated in a 500-g batch by addition of this solution to a solution of HF prepared by dissolving HF gas in doubly distilled deionized water. The precipitate was recovered by filtration and dried in an oven at 115°C. Analysis of the product is shown in Table 31.1. This material was dehydrated by melting in a nickel container under a flowing mixture of anhydrous H_2 and HF. The melt was slowly cooled under dry helium. The clearest portions of the resulting crystalline aggregate were selected (in a helium-filled dry box) and were stored under dry helium until used. Impurities in the product material used for the single-crystal preparation are also shown in Table 31.1.

Preparation of Crystals from Melt

In a preliminary trial a crystal (1 in. in diam) of LiF was grown under an atmosphere of helium in a sealed nickel crucible with a relatively crude version of a Stockbarger furnace.[5] For this trial the LiF was commercial material (of normal isotopic abundance) which had been treated in the molten state with HF and H_2 to remove sulfur, moisture, and hydroxide ion, but not otherwise purified. The crucible and melt were moved

[1] D. C. Stockbarger, "Improved Crystallization of Lithium Fluoride of Optical Quality," *Discussions Faraday Soc.* No. 5, 299–306 (1949).

[2] D. C. Stockbarger, "The Production of Large Single Crystals of Lithium Fluoride," *Rev. Sci. Instr.* 7, 133–36 (1936).

[3] M. A. Vasilyeva, "Growing Lithium and Sodium Fluoride Single Crystals of High Transparency in the Ultraviolet and Infrared," p 191–96 in *Growth of Crystals*, vol. I, ed. by A. V. Shubnikov and N. N. Sheftal, translated from Russian, Consultants Bureau, New York, 1959.

[4] R. F. Apple and J. C. White, *Preparation of Essentially Pure Lithium Fluoride: Removal of Magnesium*, ORNL CF-61-6-31 (June 5, 1961).

[5] Preliminary work performed by J. E. Eorgan and B. F. Hitch.

Table 31.1. Spectrographic Analysis of Li^7-Containing Materials

Material	Element (ppm)								
	Al	B	Ba	Ca	K	Mg	Mn	Na	Si
Starting $LiOH \cdot H_2O$				200	150	<200		200	
Oven-dried LiF precipitate				40				<100	
Dehydrated LiF crystals									
Rejected	20	100	100	1000			500	100	2000
Used for runs				100					

through the furnace at 2 mm/hr, and the resulting crystal was removed from the system after a short annealing period.

The resulting single crystal contained some cloudy areas and some inclusions but was colorless throughout most of its volume. Analysis by emission spectroscopy showed less than 200 ppm calcium, less than 500 ppm magnesium, and less than 100 ppm sodium; analysis for sulfur by a turbidimetric method indicated less than 3 ppm. Strain was evident in some portions of the crystal under polarized light. The crystal had a refractive index of 1.393 ± 0.001 in sodium-D light, and the infrared and ultraviolet cutoff values were about 6.5 and 0.12 μ, respectively, with a few percent of the incident radiation transmitted at 8.0 and 0.11 μ. This crystal compared favorably with commercial LiF single crystals from the viewpoints of purity, strain, and light transmission. It appeared, however, that an improved furnace, slower growth rate, and longer annealing period would be beneficial.

The Stockbarger furnace shown in Fig. 31.1 was constructed and used for all tests with the Li^7F. Stockbarger[1] and Vasilyeva[3] recommend growth of LiF crystals under pressures of 10^{-3} to 10^{-4} mm Hg. This low pressure is supposed to permit easy volatilization of impurities such as AlF_3 and SiF_4 and to minimize inclusion of OH^- in the lattice by promoting the reaction

$$2LiOH \rightarrow Li_2O + H_2O .$$

An attempt to prepare a crystal under pressure carefully held in this range failed completely, however, and resulted in evaporation of all the charged LiF from the crucible. It condensed as a granular mass on a nickel surface the temperature of which was a few degrees below the melting point of LiF.

A modification of this technique, which outgassed the sample at 10^{-4} mm Hg and then maintained the melt under a helium pressure of 1000 mm, was satisfactory. The 300-g charge was lowered at a rate of 0.5 mm/hr through a thermal gradient of ~7°C/cm at the crystal face; the crystal was annealed for six days in a thermal gradient of 0 to 1°C/cm. The resulting mass, see Fig. 31.2, contains two crystals, which are clear except for the top 3 mm and which are strain free except near the interface between the two. These crystals have been sent elsewhere for cleaving and sample preparation.

The furnace is being altered to permit observation of the melt and to allow use of a controlled atmosphere of helium at pressures near 250 mm Hg.

Single Crystals of LiF from the Vapor Phase

The failure described above disclosed the possibility of distilling large quantities of LiF under easily attainable experimental conditions. Attempts to accomplish such distillations have yielded small single crystals of LiF condensed on surfaces of nickel. Figures 31.3 and 31.4 show such crystals grown at helium pressures of 1000 to 1300 mm Hg, LiF temperatures from 900 to 1000°C, and with natural convection of the helium. Crystals of $0.1 \times 0.1 \times 5$ mm have been obtained. Emission spectroscopy detects less than 100 ppm of magnesium in these crystals, which are strain free under polarized light. The crystals display very well formed (100) faces as identified by use of a precession x-ray-diffraction apparatus. Attempts to determine the Miller indices of the faces by cleavage were unsuccessful, because the crystals bent rather than cleaved. However, they provide (100) faces without the cleavage operation required for melt-grown crystals, and they may

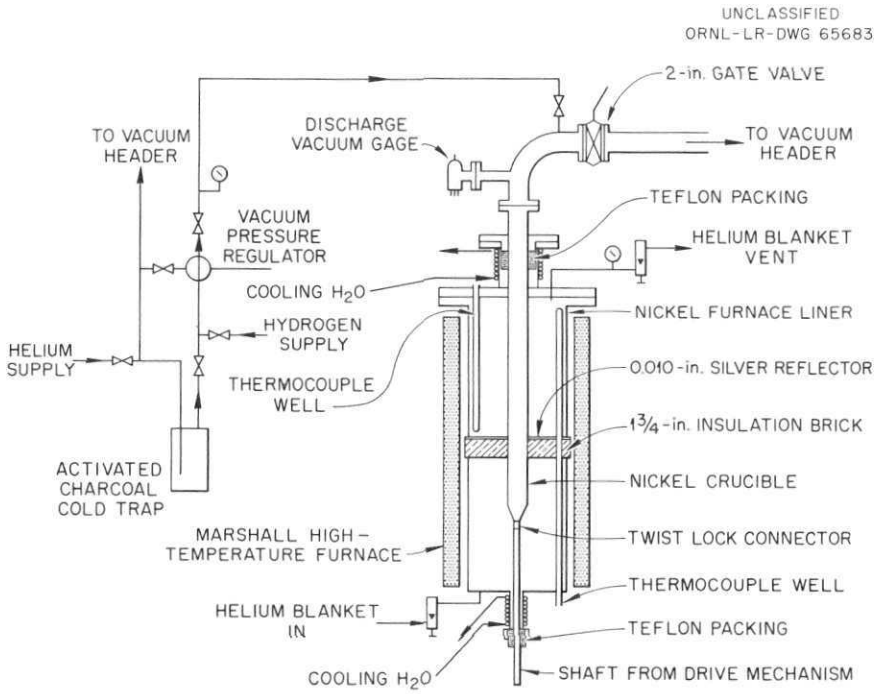

Fig. 31.1. Growing Apparatus for LiF Crystal.

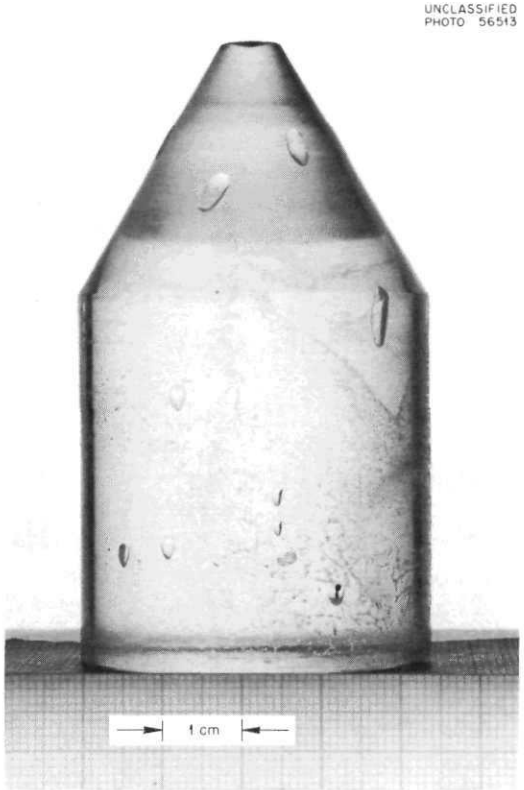

Fig. 31.2. Lithium-7 Fluoride Ingot Grown from Melt.

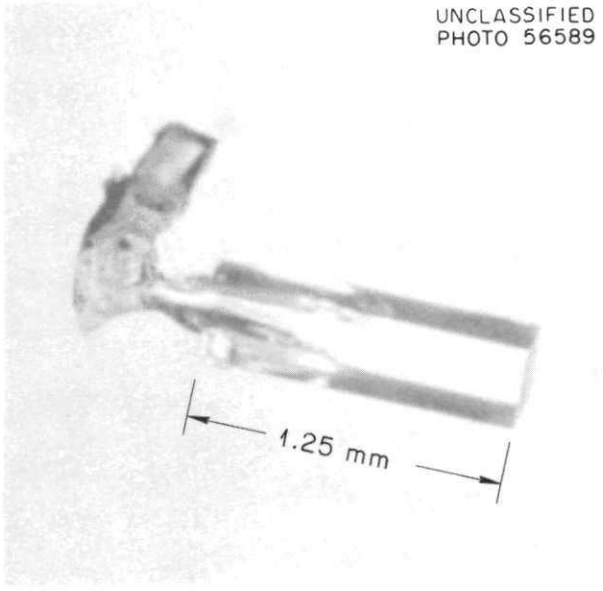

Fig. 31.3. Lithium Fluoride Crystal Grown from Vapor (Showing 100 Planes).

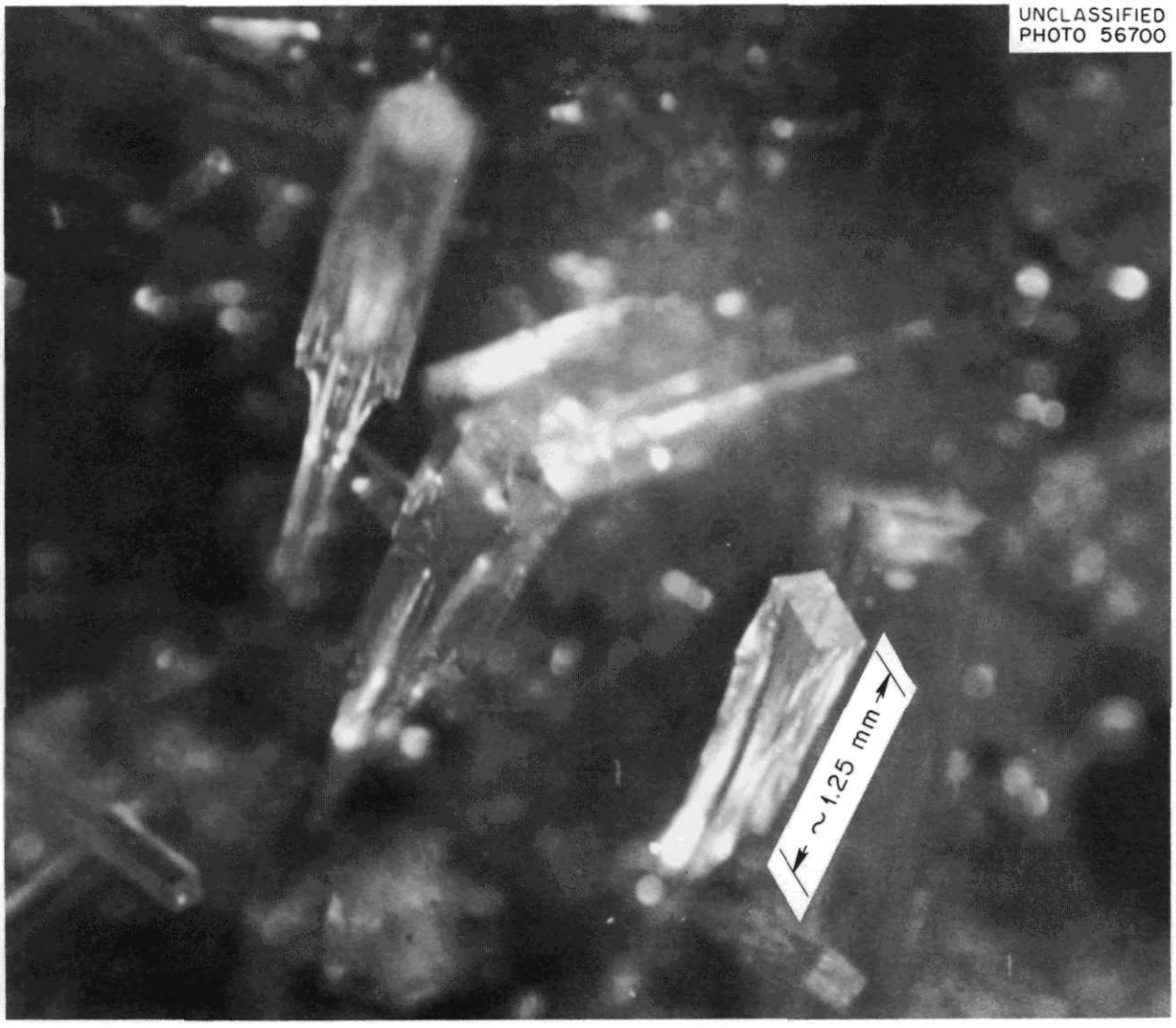

Fig. 31.4. Lithium Fluoride Crystals Grown from Vapor (in Place).

provide useful comparative material to evaluate the surface damage which occurs in the cleaving operation.

These crystals, which can be produced easily in a state of high purity and perfection, are now being used in x-ray photography as a standard to calibrate film shrinkage.

Growth of Refractory Compounds from Solutions

C. F. Weaver B. J. Sturm R. E. Thoma

Large pure single crystals of many compounds are normally prepared by slowly growing them from saturated solutions at modest pressures and temperatures. Refractory compounds – that is, those having quite high melting points – cannot be prepared by such methods because of their exceedingly low solubility in the solvents generally used at these pressures and temperatures. The experience obtained by ORNL in the study of phase equilibria involving high-temperature reactor materials suggested that valuable nonaqueous high-temperature solvent media for growth of single crystals of refractory compounds could be chosen from available phase-equilibrium information. With these nonaqueous, or molten salt, solvents, the

crystals would be grown at temperatures which are still far below the melting points of the pure compounds. Such growth of single crystals from a solvent requires:

1. a system in which adequate amounts of the solute can dissolve and from which it will precipitate on cooling as the uncomplex (pure) primary phase, and
2. experimental apparatus in which temperature, pressure, and atmosphere can be precisely controlled.

Growth from Oxide Solvents

Molybdenum trioxide, which has a convenient melting temperature (*ca.* 750°C), has been briefly examined as a possible solvent for preparation of oxide crystals of interest. It has been shown, however, that BeO, MgO, and ThO_2 form intermediate compounds with MoO_3. The existence of the compounds $2MoO_3 \cdot ThO_2$ (ref 6) and $MoO_3 \cdot MgO$ (ref 7) has been confirmed, and tentative optical and x-ray diffraction properties have been obtained for them. Both these compounds melt at temperatures higher than 814°C. In the system MoO_3-ThO_2 a eutectic invariant point exists at 782 ± 4°C and at less than 10 mole % ThO_2. It involves MoO_3 and $2MoO_3 \cdot ThO_2$ as the two solid phases.

The ceramic oxides UO_2, ThO_2, ZrO_2, and TiO_2 are appreciably soluble in, and form simple eutectic systems with, $Na_2B_4O_7$. Bard[8] has shown that UO_2 crystals up to 100 μ in diameter can be grown from this solvent. Some success with single crystals of each of these oxides has been achieved in preliminary experiments with less than optimum temperature control.

Crystals of ThO_2 about 1 mm on each edge and which appear to be optically perfect (see Fig. 31.5) have been grown by slowly cooling (10°C/day) solutions of this compound. Larger crystals (up to 3 mm) have been obtained in some attempts, but these are quite imperfect. It appears, however, that considerable improvement in the temperature control will permit growth of large high-quality crystals from this system.

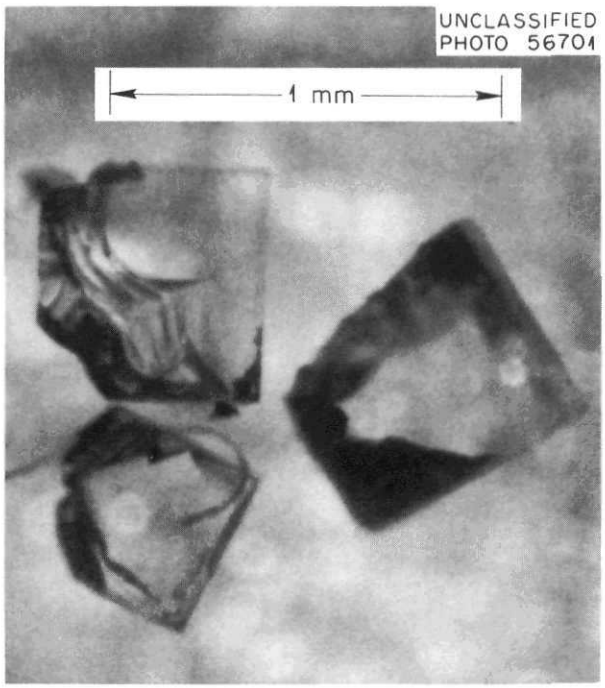

Fig. 31.5. Thorium Oxide Crystals Grown from Sodium Tetraborate.

Pronounced dendritic growth was observed in similar attempts with ZrO_2, though monoclinic crystals of this material (Fig. 31.6) have been obtained in sizes up to 0.1 × 0.1 × 1.5 mm.

Both ZrO_2 and ThO_2 seed crystals have been grown on platinum stirring rods at temperatures between 700 and 1200°C. This behavior may eliminate the substantial difficulty in mechanical attachment of very small crystals for use as seeds.

Rutile (TiO_2) needles several millimeters long have been grown (see Fig. 31.7). In some cases these were colorless and typical of the stoichiometric compound, while in others the crystals were brown. This color is probably, but not certainly, caused by iron accidentally introduced into the melt, since naturally occurring rutile is brown when contaminated by iron.[9,10]

[6] Identification by J. H. Burns.

[7] Data on chemicals for ceramic use from Bulletin No. 118 of the National Research Council, published by the University of Pittsburgh, p 137.

[8] R. J. Bard, *The Preparation of Uranium Dioxide Crystals*, LA-2076 (1957).

[9] A. N. Winchell and H. Winchell, *Elements of Optical Mineralogy*, p 66, Wiley, New York.

[10] T. N. McVay, personal communication.

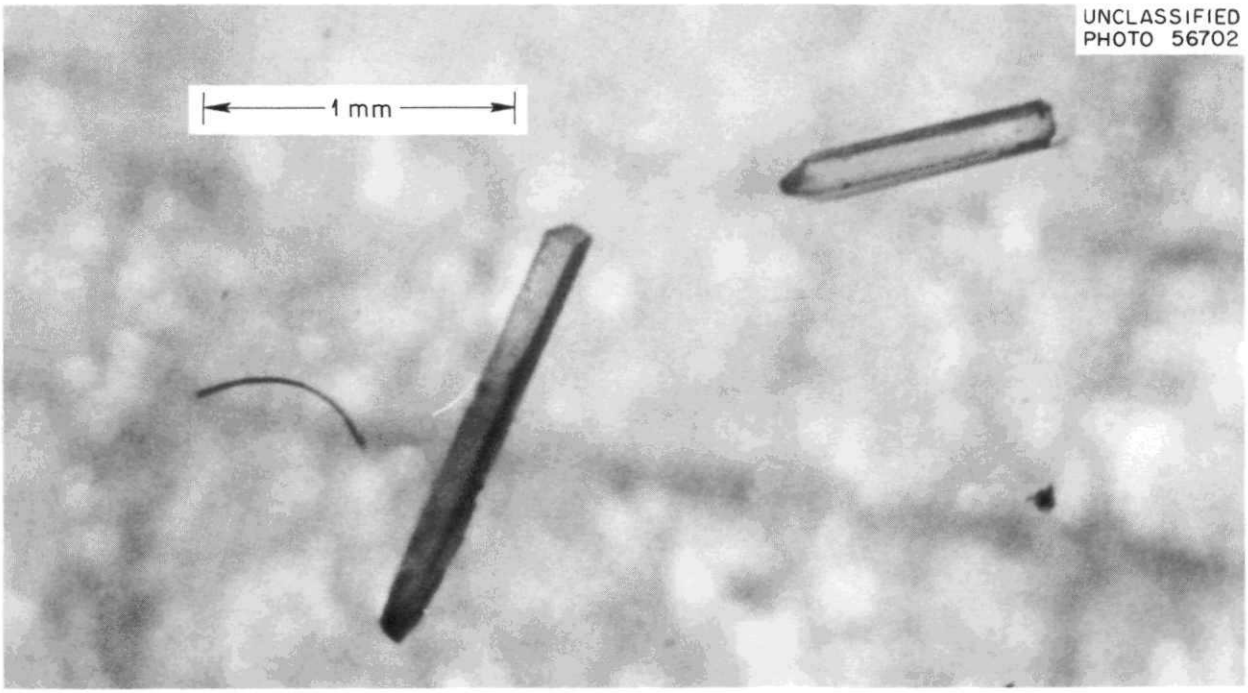

Fig. 31.6. Monoclinic Zirconium Oxide Crystals Grown from Sodium Tetraborate.

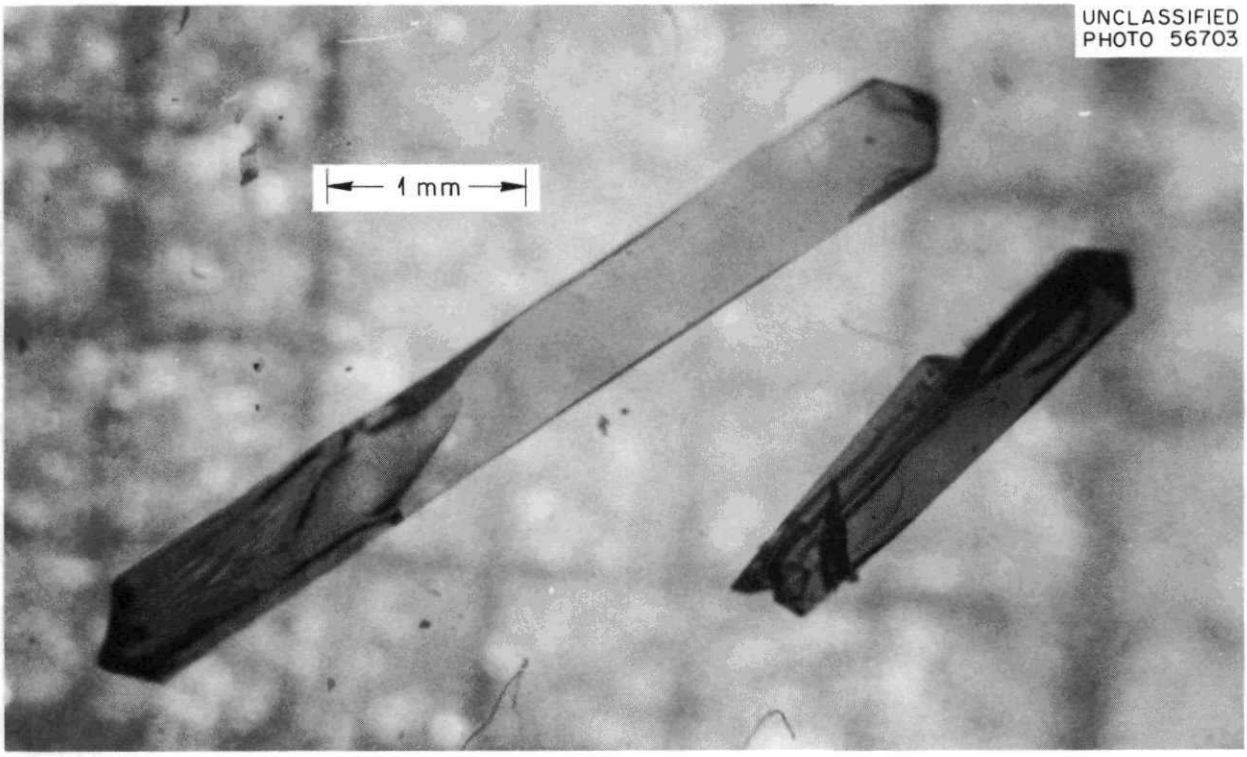

Fig. 31.7. Rutile Crystals Grown from Sodium Tetraborate.

Growth from Fluoride Solvents

Several ceramic oxides (monoclinic ZrO_2, UO_2, ThO_2, BeO) have been produced from mixtures of several fluorides to make use of the lower liquidus temperatures near eutectic compositions. A survey is being made to determine if the binary combinations expected to be stable diagonals are indeed so, and if intermediate compounds are formed. It has been found that the systems UF_4-UO_2, LiF-UO_2, LiF-ThO_2, LiF-ZrO_2, LiF-MgO, and LiF-TiO_2 are stable and that they do not form intermediate compounds or solid solutions. The possibility of growing crystals of these oxides from a lithium fluoride solvent is attractive, since LiF is available in a highly purified form which will not act as an impurity source.

Truncated octahedral crystals of MgO up to 0.35 mm on an edge (see Fig. 31.8) have been grown from LiF. Rutile grown from LiF was found to be dark blue, typical of an oxygen-deficient structure. Studies of these systems containing mixed oxides and fluorides may be of value in describing the behavior of MSRE fuels and coolants with significant oxide contamination, in addition to their value for the production of pure crystalline substances.

EXTRACTION OF METAL IONS BY DIALKYL PHOSPHORIC ACIDS[11]

C. F. Baes, Jr.

The extensive literature on extractants of the general formula $(RO)_2P(O)OH$, HX, has been reviewed. Their extraction behavior, osmotic behavior, and infrared spectra have shown that they are usually present in organic solvents as hydrogen-bonded dimers H_2X_2 which, at low loadings, extract metal cations M^{z+} to form complexes of the type $M(X_2H)_z$. The demonstrated wide occurrence of this simple cation-exchange mechanism – often

[11] Summary of a paper presented at the 140th Annual Meeting of the American Chemical Society, Chicago, September 1961. Submitted for publication in *Journal of Inorganic & Nuclear Chemistry.*

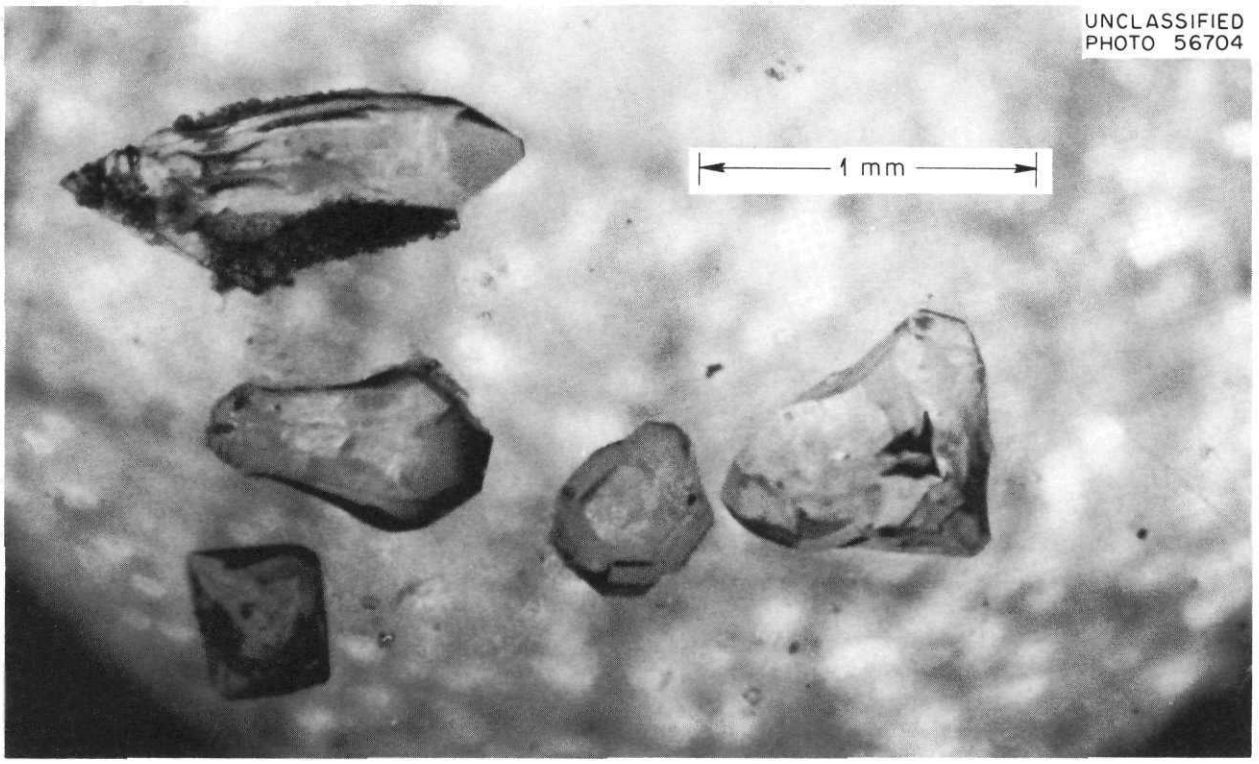

Fig. 31.8. Magnesium Oxide Crystals Grown from LiF.

free from complicating extensive association or anion extraction – offers an excellent opportunity to examine the effects of solvent, reagent structure, ion charge, ion size, and ion coordination properties on extraction.

The variation of the estimated equilibrium quotient

$$ {}^{z}K = \frac{[M(X_2H)_z]_{org}[H^+]^z_{aq}}{[M^{z+}]_{aq}[H_2X_2]^z_{org}} $$

for extraction of various cations at low loadings by di(2-ethylhexyl)phosphoric acid in toluene is shown as a function of the reciprocal of the ionic radius (r) in Fig. 31.9. In general, (log ${}^{z}K)/z$ increases fairly uniformly with z/r as one proceeds from the alkali-metal cations, through the alkaline-earth ions, to the trivalent ions of group III, the lanthanides, and the actinides. The MO_2^{2+} actinide ions are the most strongly extracted dipositive ions. The $MO_2(X_2H)_2$ complexes which these ions form may involve covalent bonding and/or a more highly coordinated structure than that (structure I) assumed for the other cations,

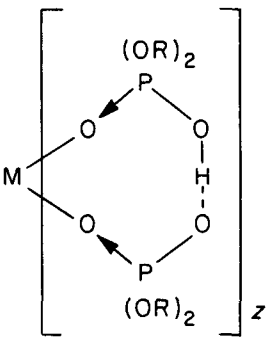

The Be^{2+} and Fe^{3+} show lower extractability than expected; this may be caused by the small size of these cations, which should result in oxygen-oxygen contact in tetra- and hexacoordination of the phosphate groups respectively.

Systems at high loading have shown more varied and complicated behavior involving polynuclear complex formation (UO_2^{2+}-HX) and anion extraction (Fe^{3+}-HX). The selective synergistic enhancement of uranium extraction found when dialkyl phosphoric acids are used in combination with neutral organophosphorous compounds is not sufficiently understood, especially in view of the much more general synergism which occurs when HX is replaced by TTA (thenoyltrifluoroacetone).

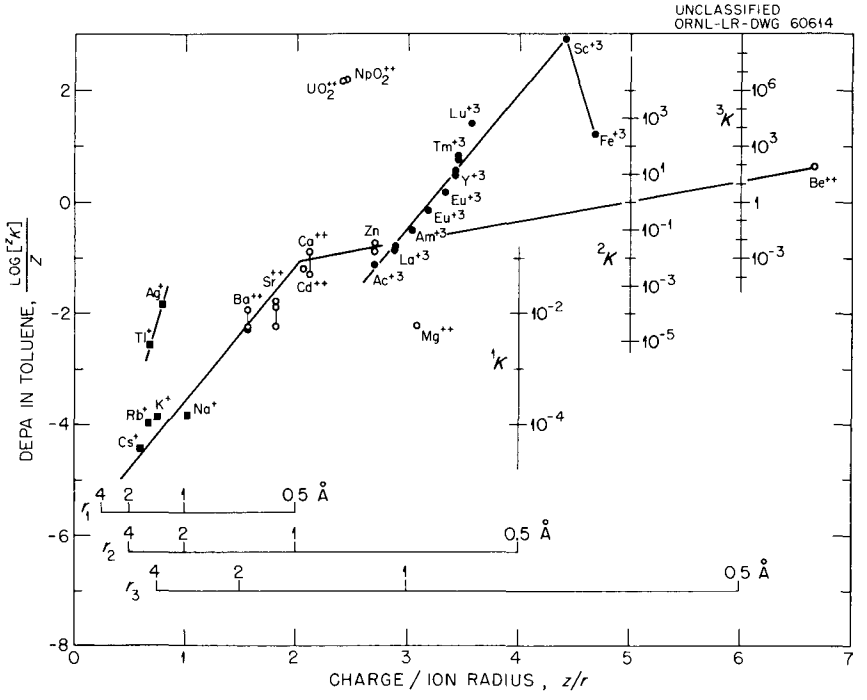

Fig. 31.9. Effect of Ion Charge and Ion Size on Extraction by Dialkyl Phosphoric Acids.

32. Radiation Chemistry of Organic Moderators

W. T. Rainey, Jr. L. B. Yeatts, Jr.

The state of knowledge on the thermal and radiation stability of organic molecules is inadequate at this time to permit the best choice of available organic materials as reactor moderators or coolants. Chemical kinetic studies of the pyrolytic and radiolytic decomposition of these materials should provide a better understanding of the relationship between molecular structure and chemical stability.

At this stage of development of organic nuclear reactors, it appears that, as a class of compounds, the polyphenyls offer the most promise as moderators and coolants. Specifically, biphenyl and the isomeric forms of terphenyl are of particular interest. Upon irradiation these compounds undergo pyrolysis and radiolysis simultaneously, thus complicating the chemical kinetic picture. Therefore research on the pyrolytic decomposition of biphenyl has been made the initial effort.

Samples of chromatographically pure biphenyl have been pyrolyzed in evacuated ampoules. Visible signs of decomposition occurred after exposure for 48 hr at 500°C (932°F). The samples at 300 and 400°C (572 and 752°F) showed no evidence of decomposition after 718 and 1212 hr, respectively, and were therefore heated at 525 and 550°C to decrease the time required for pyrolysis. Approximately 3.5 hr was sufficient time to produce decomposition in both instances, with a dark-brown to black tar forming after 4.75 hr at 550°C.

A vacuum line has given satisfactory separation of the pyrolytic products into three fractions: (1) low boilers, permanent gases and hydrocarbons boiling below room temperature; (2) intermediate boilers, hydrocarbons with boiling points between room temperature and the boiling point of biphenyl (256°C); and (3) high boilers, hydrocarbons boiling above 256°C.

An F and M Scientific Corporation model 500 chromatographic unit has been used for the identification of the pyrolytic products. The low boilers resulting from heating pure biphenyl at 490°C for 48 hr were analyzed on a 6-ft column of a molecular sieve (Linde No. 5A, 60–80 mesh) at room temperature with a helium flow rate of 37 ml/min. Only two components, hydrogen and methane, eluted during an analysis period of 40 min.

Dodecyl phthalate and silicone rubber columns proved unsatisfactory due to the formation of unsymmetrical chromatographic peaks caused by tailing. A 12-ft column of 30 wt % Apiezon L with 2 wt % Carbowax 20 M on Chromosorb P (35–80 mesh) showed excellent resolution of a seven-component mixture of benzene and its derivatives dissolved in acetone. At a helium flow rate of 29 ml/min with temperature programming between 125 and 250°C, only one pyrolytic product was eluted within 32 min. This product had a retention time of 4.1 min and was identified as benzene. The retention times of other materials falling within this boiling range and which might be anticipated upon pyrolyzing biphenyl are

Compound	Retention Time (min)
Benzene	4.2
Toluene	6.2
Phenylcyclohexane	20.0
Biphenyl	22.7

The high-temperature column, consisting of a eutectic composition of lithium, sodium, and potassium nitrates on Chromosorb P, was found to produce an unstable baseline during analysis. Also, at the higher temperatures required for an

analysis, it underwent decomposition, evolving N_2O_4 fumes. Therefore the components of the high-boiler fraction in benzene solution were resolved and, in some cases, identified through the use of a 12-ft column of 20 wt % lithium chloride[1] on Chromosorb P (35–80 mesh). The chromatogram produced at a helium flow rate of 29 ml/min with temperature programming between 200 and 350°C is shown in Fig. 32.1. Identities of peaks in the chromatogram were established by addition of internal standards. From the chromatogram it can be seen that nine components were present in addition to the benzene solvent and residual biphenyl. The component having a retention time of 5.5 min has been identified as biphenyl; 10.4 min, *o*-terphenyl; 13.7 min, *m*-terphenyl; 14.8 min, *p*-terphenyl. The last three compounds make up more than half the quantity of high boilers formed. Although the five additional compounds have not been definitely identified, they are all higher boiling than the terphenyls and are likely to be isomeric forms of quarter- and quinquephenyl.

The results thus far obtained indicate that the reaction mechanism for the pyrolysis of biphenyl must involve the rupture of the bond between phenyl groups, resulting in the formation of benzene and polymeric materials. The presence of methane further suggests the degradation of the benzene ring.

[1] P. S. Hudson and A. J. Moffat, *Organic Coolant Reactor Program Quarterly Report, Sept. 1–Dec. 31, 1960*, IDO-16675, pp 20–24.

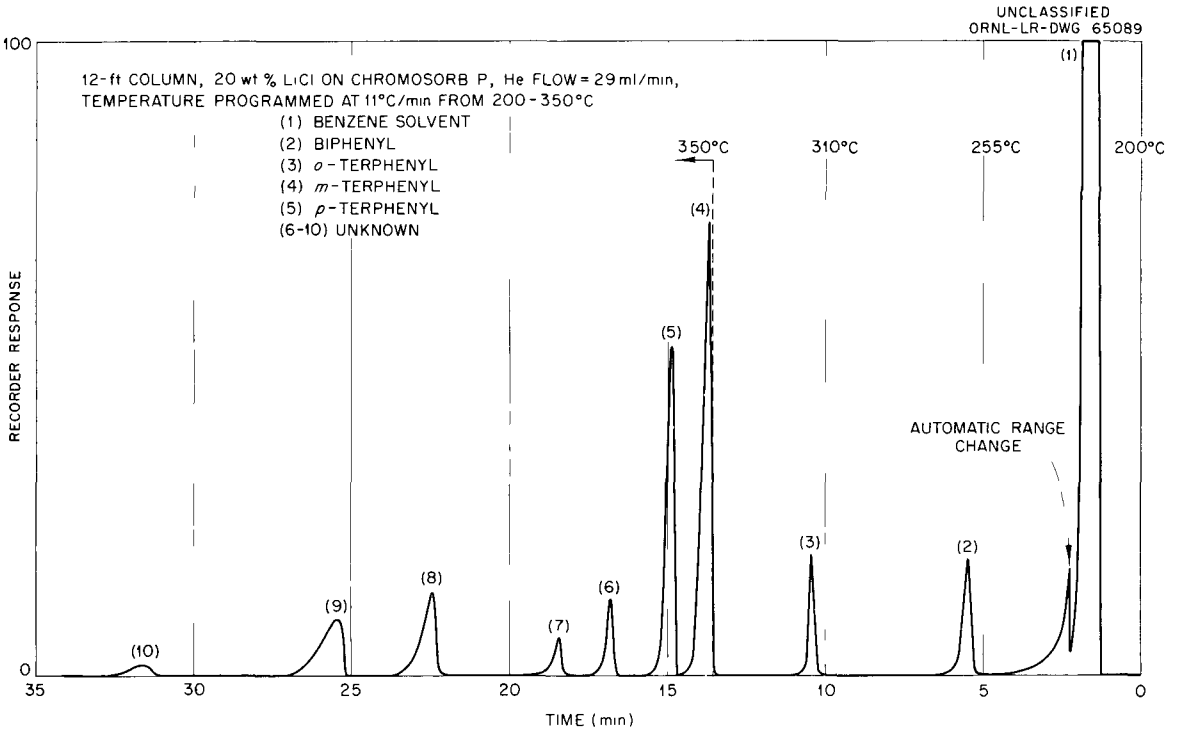

Fig. 32.1. Gas Chromatogram of Biphenyl High-Boiler Fraction with Temperature Programming.

Part VII

Chemical Support for the Thermonuclear Program

33. Sherwood Project Chemistry

The program of chemical support at ORNL for the Sherwood Project is one of materials research in a somewhat broadened sense. The basic "material" required by the plasma physics researches at present is excellent vacuum in large systems. Accordingly, studies of vacuum instrumentation, diffusion-pump fluids, and vapor-deposited titanium films have been conducted in order to assist in the meeting of current vacuum requirements. Initial information is presented concerning one set of experiments on the effect of bombardment of titanium by energetic deuterium ions. In addition, a summary of materials considerations pertaining to blankets for controlled thermonuclear reactors is given which outlines some of the functions that such a blanket may be expected to fulfill.

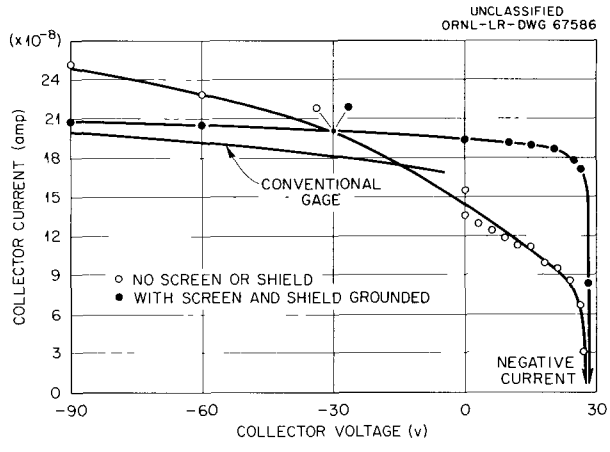

Fig. 33.1. Response of Unshielded and of Grounded-Screen Gages at 1.8×10^{-6} torr.

CALIBRATION OF ION GAGES

R. A. Strehlow J. D. Redman

A study of the response at very low pressure of ion gages without glass envelopes has been initiated. For this investigation a Veeco type RG-75 ion gage was modified by removal of the glass envelope and tubulation and by substitution of a copper screen of a geometry similar to that of the former envelope. The gage was mounted on a flange for insertion into a vacuum system of 4-in. glass piping in a manner such that the copper screen could be grounded or biased in voltage. Response and operating characteristics of the gage with the copper screen floating (electrically) were similar to those of the original enveloped gages; in such tests the copper assumed a potential of about +30 v.

Gage response with the screen grounded was similar to that of a conventional nude gage in metal vacuum system. Figure 33.1 shows the collector current as a function of collector voltage for this grounded-screen assembly in a system at 1.8×10^{-6} torr. The similar behavior of a conventional gage and that for the assembly without the screen are shown for comparison. The drop in current with decreasing negative potential for the unscreened assembly is probably a consequence of decrease in collector efficiency. When the grounded screen is added, positive ions are probably removed less effectively from the gage region; this difference appears to compensate to a considerable extent for the reduced collector efficiency, and response remains nearly independent of collector potential over a wide range.

A comparison of the collector current vs emission current at constant pressure (9.5×10^{-7} torr) and at constant collector potential (−30 v) has been made for a grounded-screen and a floating-screen assembly. In these tests, which produced the data shown in Fig. 33.2, the screen was of stainless steel. The superior linearity in response of the grounded-screen assembly is evident.

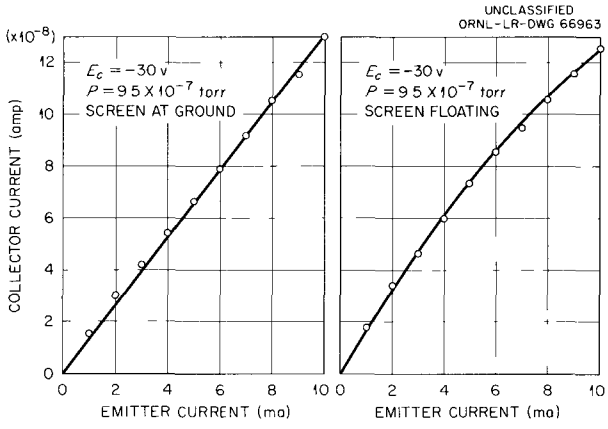

Fig. 33.2. Response of Grounded-Screen and Floating-Screen Gages at −30 v Collector Voltage and 9.5 × 10^{-7} torr.

Figure 33.3 shows typical plots of pressure read with conventional glass-enveloped ion gages vs those obtained with the floating-screen gage after 30 days in systems pumped with diffusion pumps using various oils.[1] Such comparisons show, in general, the effect of conditioning of the vacuum system, the presence of grounded surfaces near the screened gage, and other factors. In this study, in which the influence of such other factors was minimized, it is apparent that the (decomposition products of) pump oil affects the relative calibrations.

Each curve such as those of Fig. 33.3 can generally be fitted by an expression of the form $P_s = AP_E + B$, where P_s and P_E are pressures read by the screened and the enveloped gages, respectively, and A and B are constants. The pressure-insensitive term, B, which accounts for curvature of the log-log plots, appears (see Fig. 33.4) to diminish with decreasing emission current; a control unit, which will permit use of emission currents of about 2 μa and which may eliminate the curvature from these plots, is under examination. The pressure-sensitive factor, A, which obviously varies with pump oil composition, is not well understood.

Polyphenyl ethers, which have vapor pressures of 2 × 10^{-11} mm Hg at 25°C, have been shown

[1]The data for Convoil-20 is from C. E. Normand, *Calibration of Nude Ionization Gauges*, ORNL CF-61-5-109, suppl 2 (Nov. 24, 1961).

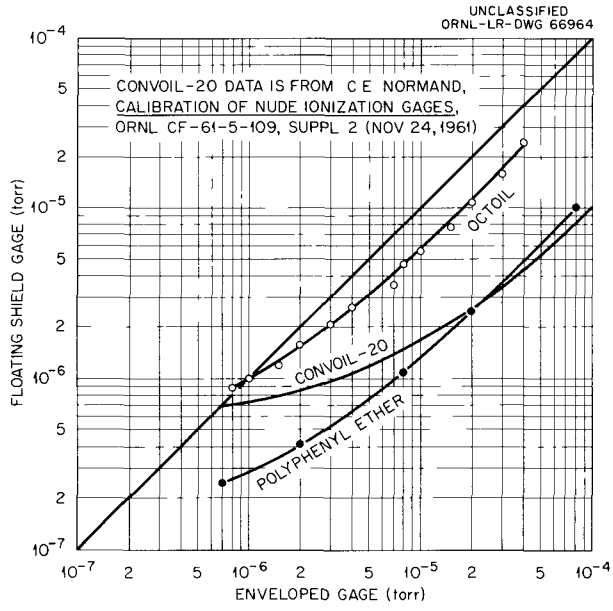

Fig. 33.3. Relative Pressure Readings from Enveloped and Floating-Screen Gages in Systems Pumped 30 Days with Various Diffusion-Pump Oils. Convoil-20 data were taken from *Thermonuclear Div. Progr. Rept. Feb. 1, 1961, to Oct. 31, 1961*, ORNL-3239, pp 85–95.

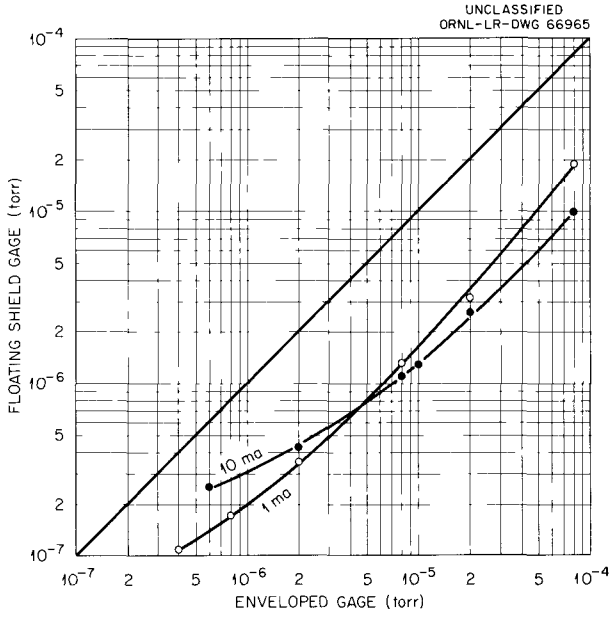

Fig. 33.4. Relative Pressure Readings from Enveloped and Floating-Screen Gages at Controlled Emission Current.

(see section below) to be significantly more stable to thermal decomposition than other common oils. Comparative tests with polyphenyl ether and with Octoil in a Consolidated Vacuum Company pump PMC-720 (unmodified but with a slightly higher wall temperature necessary with the polyphenyl ether) yielded data on pressure vs time shown in Table 33.1. It is clear that lower pressures can be obtained with the better oil at all times; the optimum pressure attainable after conditioning of the oil has been reached in a few days with the Octoil, but may not have been realized after 90 days with polyphenyl ether.

Table 33.1. Pressures Attainable in Unmodified PMC-720 Pump with Octoil and with Polyphenyl Ether

Pumping Time (days)	Pressure (torr)	
	Octoil	Polyphenyl Ether
1	1.2×10^{-5}	1.4×10^{-6}
2	2×10^{-6}	1×10^{-6}
9	1.2×10^{-6}	8.4×10^{-7}
29	1.2×10^{-6}	7×10^{-7}
60		4×10^{-7}

EVAPORATIVE PUMPING

R. A. Strehlow J. D. Redman

Removal of gases at low pressure by sorption on vapor-deposited films of titanium is under continued study by personnel associated with the Thermonuclear Program. The status of these studies, only a portion of which were done by the Reactor Chemistry Division, was recently described in some detail.[2,3]

Experiments have been performed in the small-scale (6-in.-diam) test facility to establish sorption rates (pumping speeds) for H_2 on titanium films deposited on water-cooled copper substrates. It was shown that films deposited in the presence of He or Ar at a pressure of 2 to 10 μ Hg gave sorption rates higher by about threefold than similar films deposited under high vacuum. The sorption rates, however, in these experiments did not exceed about 15% of the theoretical value. Larger-scale studies by other investigators in the ORNL program[3] have shown much higher (0.8 × theoretical) initial values for titanium films deposited in the presence of low pressures of inert gas on substrates held at liquid-nitrogen temperature.

BOMBARDMENT OF TITANIUM BY D^+

R. A. Strehlow

Eleven samples of titanium (6 × 3.5 × 0.125 in.) were separately bombarded with D^+ ions accelerated to 10–25 kv.[4] Background pressure of D_2 was 2 to 3 × 10^{-5} mm Hg during these tests. The total dosage was about 1.7 × 10^{21} particles to each target. Data from these tests, given in Table 33.2, show that a substantial fraction of the bombarding beam entered and was retained by the target. In agreement with previous observations, no sputtering of the titanium could be observed. Some unknown part of the target weight increase can be attributed to pickup by the specimen after the beam was turned off. Assuming a value of 10^{-14} ev cm^2 atom^{-1} for the stopping cross section of titanium for deuterons, one would expect the direct penetration to be of the order of 300 A. Figure 33.5 shows a cross-sectional view of a different titanium specimen, which had been bombarded for 2500 ma-hr at 25 kev at a current of 50 to 60 ma. Deuteride formation is apparent. X-ray diffraction patterns yield peaks characteristic of $TiD_{(1.97)}$ with very little discrepancy. The TiD_2 extends to a maximum depth of about 0.04 in. The thickness of the two-phase region, based on microscopic examination, is close to 0.01 cm. A diffusion constant of 10^{-6} cm^2/sec and a concentration difference of 10^{23} atoms of D per cm^3 lead to a flux of 10^{19} atoms cm^{-2} sec^{-1}. The bombarding beam at even 150 ma is but 1.5 × 10^{17} atoms cm^{-2} sec^{-1} and for the present experiment is no more than 3 × 10^{16} atoms cm^{-2} sec^{-1}.

[2] C. E. Normand *et al.*, *Thermonuclear Div. Progr. Rept. Feb. 1, 1961, to Oct. 31, 1961*, ORNL-3239, pp 85–95.

[3] R. E. Clausing, *A Large-Scale Getter Pumping Experiment Using Vapor Deposited Titanium Films*, ORNL-3217 (Oct. 24, 1961).

[4] O. C. Younts, Thermonuclear Division.

Table 33.2. Absorption of Energetic Deuterons by Titanium

Current (ma)	Energy (kev)	ma-hr	Power Density (w/cm^2)	Input Beam Accounted for by Weight Increase (%)
28	10	829	15	15
55	15	897	34	24
48	15	721	30	93
27	20	854	22.5	45
48	20	717	40	80
55	20	844	45.5	85
90	20	1132	75	86
150	25	905	150	57
94	25	1099	97	78
51	25	807	54	92
74	20 (D_2^+)	813	36	69

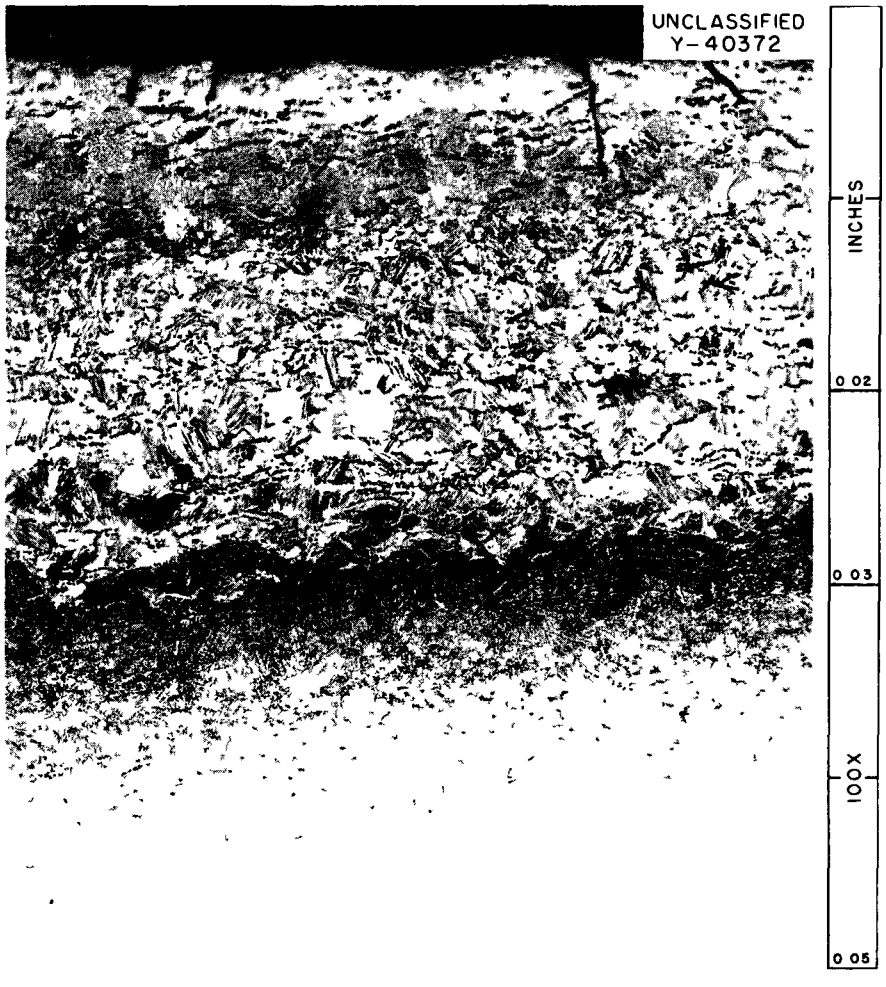

Fig. 33.5. Photomicrograph Showing the Formation of Titanium Deuteride at the Surface of a Titanium Specimen Bombarded with 25-kv D^+ at 50 to 60 ma for 2500 ma-hr.

It seems that the process of bombarding the surface allows the deuteron to penetrate the usual surface layer, thus allowing diffusion into the specimens.

CONSIDERATIONS OF BLANKETS FOR THERMONUCLEAR REACTORS

R. A. Strehlow C. J. Barton

A survey was made of proposed blanket assemblies for thermonuclear reactors. Achievement of controlled thermonuclear power requires the solution of the very difficult problem of confining a stable energetic plasma. Concentration of research effort on this problem has resulted in the past in virtual exclusion of consideration of questions relating to energy extraction from a stable contained plasma. Although many uncertainties exist regarding the design of a successful thermonuclear reactor, the fact remains that some fraction of the energy of thermonuclear neutrons must be removed or recovered as heat. This consideration alone makes necessary the presence of a heat recovery or removal blanket surrounding the reactor, but the production of tritium is an equally necessary function of the blanket for a deuterium-tritium-fueled (D-T) reactor.

A confined thermonuclear plasma will yield energy in accordance with the following equations:

$$ {}_1D^2 + {}_1D^2 \rightarrow {}_2He^3\ (0.82\ \text{Mev}) + {}_0n^1\ (2.45\ \text{Mev}), \quad (1) $$

$$ {}_1D^2 + {}_1D^2 \rightarrow {}_1T^3\ (1.01\ \text{Mev}) + {}_1H^1\ (3.02\ \text{Mev}), \quad (2) $$

$$ {}_1D^2 + {}_1T^3 \rightarrow {}_2He^4\ (3.5\ \text{Mev}) + {}_0n^1\ (14.1\ \text{Mev}), \quad (3) $$

$$ {}_1D^2 + {}_2He^3 \rightarrow {}_2He^4\ (3.8\ \text{Mev}) + {}_1H^1\ (14.7\ \text{Mev}), \quad (4) $$

$$ 3\,{}_1D^2 \rightarrow {}_2He^4\ (3.6\ \text{Mev}) + {}_0n^1\ (8.3\ \text{Mev}) + {}_1H^1\ (8.8\ \text{Mev}). \quad (5) $$

The reactions in a deuterium-fueled (D-D) reactor can be described approximately by the sum of Eqs. (1) through (4), or by Eq. (5) if the intermediate ${}_2He^3$ can be contained in the plasma long enough for the $He^3(d,p)He^4$ reaction to take place. The difference of 0.9 Mev between 21.6 Mev and the sum of these figures is the kinetic energy of the intermediate ${}_1T^3$ and ${}_2He^3$ nuclei. The deuterium-tritium (D-T) reaction is described by Eq. (3) alone, and it is apparent that 80% of the total energy released in this type of thermonuclear reactor accompanies the neutrons. In a D-D reactor, from 34 to 50% of the total energy released will be in the form of energetic neutrons, depending on the fraction of He^3 which reacts according to Eq. (4). Since in a D-D reactor the fraction of the total energy released which is associated with charged particles will be much larger than for a D-T reactor, there is a greater incentive to exploit some, as yet undemonstrated, method for directly converting the energy contained in a D-D reactor plasma into electrical power. While it is obviously desirable to recover the neutron energy in a D-D reactor, it is clear that development of a method for recovering the neutron energy is *essential* for the success of a D-T reactor.

Equations (1) and (2) occur at approximately equal rates over a wide range of deuteron energies, while Eq. (3) occurs at a much faster rate at all energy levels. The D-He^3 reaction [Eq. (4)] is slower than the other three reactions at low energy levels, but its rate equals that of the D-D reactions at about 120 kev. The technological problems associated with the attainment of a successful D-T reactor appear distinctly less formidable than for a D-D reactor. The neutrons liberated by the D-T reaction, after they have been slowed down to recover most of their energy, must be employed as efficiently as possible to produce the tritium needed to provide fuel for the reactor. The most obvious method for doing this is by reaction with Li^6, which makes up 7.5% of naturally occurring lithium, according to the reaction

$$ {}_3Li^6 + {}_0n^1 \rightarrow {}_2He^4 + {}_1T^3 + 4.8\ \text{Mev}. \quad (6) $$

Some neutron losses are considered inevitable, and it is therefore necessary to compensate for

these losses by use of $(n,2n)$ reactions. A number of these reactions (with lead, tungsten, or other materials with a Z greater than 40 or 50) are worthy of consideration, but the only material that has been discussed to any extent in the literature on this subject is beryllium. The nuclear reaction involved in tritium production from beryllium is

$$ {}_4Be^9 + {}_0n^1 \rightarrow 2\,{}_0n^1 + {}_4Be^8 \rightarrow 2\,{}_2He^4 + 2\,{}_0n^1 . \quad (7) $$

Another reaction of neutrons with beryllium results in the production of Li^6, which will in turn produce tritium, but at a cost of two neutrons per atom of tritium produced. Fortunately, the cross section for reaction (7) is much larger than for the reaction producing either Li^6 or Be^{10}.

Since design details of a successful thermonuclear power device are not known, it appears advisable to consider only the two principal functions which a blanket assembly will be called upon to perform and to discuss factors which are pertinent to the fulfillment of the functions. The functions can probably be most readily performed by fluid blanket components which will allow heat extraction at reasonably high temperatures. Some factors that must be considered in choosing a suitable breeding and heat removal blanket are:

1. provision for neutron multiplication;
2. moderation of neutrons to low energy and their adsorption in ${}_3Li^6$;
3. small parasitic neutron capture;
4. absorption of secondary gamma rays;
5. extraction of heat at useful temperatures;
6. recovery of tritium;
7. stability and chemical compatibility;
8. compatibility of the blanket with magnetic requirements, small electrical loss;
9. the pressure of the system, which should be low at the operating temperature;
10. minimum induced radioactivity;
11. minimum thickness.

In addition to serving the function of providing a vacuum container, the wall exposed to vacuum will have a significant effect on the neutrons that pass through it, and thus the basic longer-range vacuum problem is tightly coupled to blanketing considerations.

THERMAL STABILITY OF VACUUM-PUMP OILS

W. T. Rainey, Jr. L. B. Yeatts, Jr.

The use of organic compounds as pumping oils in vacuum diffusion pumps has resulted in the development of a series of oils with reasonably satisfactory physical properties. Available oils have sufficiently low vapor pressure and adequate thermal stability for normal high-vacuum technology. However, in the ultrahigh-vacuum systems which are necessary in the controlled thermonuclear experiments, the presence of any extraneous molecules is extremely undesirable. It is especially important to avoid simple molecules such as carbon monoxide, hydrogen, methane, etc., which are difficult to adsorb in traps, interfere in plasma studies, and are often formed in the pyrolytic decomposition of organic molecules.

Therefore, several series of tests have been carried out to determine the relative thermal stabilities of several diffusion oils. Samples of the oils were heated in evacuated Pyrex ampoules. The samples were inspected periodically, and samples were removed at the first visible signs of decomposition. Other samples were left at temperature for longer times, as indicated in Table 33.3.

The decomposition products will be analyzed for all gaseous or volatile liquid components. Such analyses are of utmost importance, since stability as measured by visible signs of decomposition would not necessarily be the same as when measured by formation of gaseous products.

It is concluded that the order of stability is: polyphenyl ether > esters > aliphatic hydrocarbons. The purity of the crude polyphenyl ethers is not known, and thus it is not possible to suggest reasons for the apparent greater stability of the crude pentaphenyl ether. The ester oils were similar in stability, and the formation of solid decomposition products was not entirely unexpected. Formation of free acids and anhydrides has been noted in such cases.

Table 33.3. Qualitative Observations of Thermal Decomposition of Diffusion-Pump Oils

Compound	Temperature (°C)	Time (hr)	Results
Aliphatic hydrocarbons			
Convoil-20	250	1.0	Light yellow[a]
	250	360	Light yellow
	400	1.0	Light yellow
	400	7.5	Brown
Esters			
Di(2-ethylhexyl) phthalate,	250	360	No change
Octoil	400	3.3	No color; crystals at room temperature
	450	0.75	Yellow; crystals at room temperature
	450	2.3	Light brown; crystals at room temperature
Di(2-ethylhexyl) sebacate,	250	360	No change
Octoil-S	400	2.3	Light yellow; crystals at room temperature
	400	48	Light yellow; crystals at room temperature
	450	1.0	Light yellow; crystals at room temperature
Polyphenyl ethers			
m-Bis(*m*-phenoxy-phenoxy) benzene			
(*a*) Crude	400	104	Faint yellow
	400	424	Deep yellow
	450	9.0	Faint yellow
	450	360	Light yellow
(*b*) Purified (by distributor)	400	34	Faint yellow
	400	475	Light yellow
	450	1.9	Faint yellow
	450	7.5	Yellow
	500	1.5	Light yellow
	500	3.3	Yellow-brown
m,*m*′-Bis(*m*-phenoxy-phenoxy) diphenyl ether, crude	400	13	Faint yellow
	400	232	Light yellow
	450	0.5	Light yellow
	450	15	Light brown

[a]Intensity of yellow: faint yellow < light yellow < yellow < deep yellow.

Publications

AUTHOR(S)	TITLE	PUBLICATION
Adams, R. E., and W. E. Browning	Deposition of Radioactive Materials from Gases	*Nuclear Safety* 3(2), 46 (1961)
Bacarella, A. L.	Electrochemical Measurements of Corrosion Rates on Zirconium and Zircaloy-2 at Elevated Temperatures	*J. Electrochem. Soc.* 108, 331 (1961)
Baes, C. F., and N. J. Meyer	An Investigation of Uranyl Ion Hydrolysis at Elevated Temperatures Using the Glass Electrode	TID-7610, p 135 (1961)
Baker, J. M., and S. E. Bolt	Titanium Pump Loop for Aqueous Solutions at High Temperatures	ORNL-3187 (November 1961)
Barton, C. J.	A Review of Glove-Box Construction and Experimentation	ORNL-3070 (May 1961)
Barton, C. J.	Beryllium Hazards in Nuclear Operations	*Nuclear Safety* 3(2), 51 (1961)
Barton, C. J., and R. A. Strehlow	Phase Relations in the System $LiF-PuF_3$	*J. Inorg. & Nuclear Chem.* 18, 143–47 (1961)
Barton, C. J., J. D. Redman, and R. A. Strehlow	Phase Equilibria in the Systems $NaF-PuF_3$ and $NaF-CeF_3$	*J. Inorg. & Nuclear Chem.* 20, 45–52 (1961)
Blander, M.	Quasi-Lattice Model of Reciprocal Salt Systems A Generalized Calculation	*J. Chem. Phys.* 34, 432 (1961)
Blander, M.	Some Calculations for a One-Dimensional Salt Mixture	*J. Chem. Phys.* 34, 697 (1961)
Bohlmann, E. G.	Activity Buildup in Pressurized-Water Reactor Systems	*Nuclear Safety* 3(2), 20 (1961)
Browning, W. E., R. E. Adams, and R. D. Ackley	Removal of Volatile Fission Products from Gases	TID-7610, p 44 (1961)
Burns, J. H.	Unit Cell and Space Group of $LiBrO_3$	*Acta Cryst.* 15, 89 (1962)
Cantor, Stanley	Freezing Point Depressions in Sodium Fluoride. Effect of Alkaline Earth Fluorides	*J. Phys. Chem.* 65, 2208 (1961)
Davis, R. J., G. H. Jenks, E. G. Bohlmann, V. A. DeCarlo, S. E. Bolt, and H. C. Savage	In-Pile Autoclave Test of Zircaloy-2 Corrosion in $UO_2(NO_3)_2$ Solution and of Solution Stability	ORNL-3171 (Dec. 29, 1961)

AUTHOR(S)	TITLE	PUBLICATION
English, J. L., L. Rice, and J. C. Griess	The Corrosion of Aluminum Alloys in High-Velocity Water at 170 to 290°C	ORNL-3063 (June 1, 1961)
Evans, R. B., III, J. Truitt, and G. M. Watson	Superposition of Forced and Diffusive Flow in a Large-Pore Graphite	ORNL-3067 (Feb. 24, 1961)
Evans, R. B., III, J. Truitt, and G. M. Watson	Interdiffusion of Helium and Argon in a Large-Pore Graphite	*J. Chem. Eng. Data* 6, 522 (1961)
Evans, R. B., III, G. M. Watson, and E. A. Mason	Gaseous Diffusion in Porous Media at Uniform Pressure	*J. Chem. Phys.* 35, 2076 (1961)
Franck, E. U.	Hydrolysis in Supercritical Steam	TID-7610, p 137 (1961)
Gill, J. S., and W. L. Marshall	High-Pressure Vessel Incorporating a Teflon Gasket for Use to 500°C and 1000 Atmospheres	*Rev. Sci. Instr.* 32, 1060 (1961)
Gill, J. S., and W. L. Marshall	Aqueous Systems at High Temperature. I. The Compound $CuO \cdot 3UO_3$	*J. Inorg. & Nuclear Chem.* 20, 85 (1961)
Griess, J. C., H. C. Savage, T. H. Mauney, J. L. English, and J. G. Rainwater	Effect of Heat Flux on the Corrosion of Aluminum by Water: Part II. Influence of Water Temperature, Velocity, and pH on Corrosion-Product Formation	ORNL-3056 (Feb. 10, 1961)
Griess, J. C., H. C. Savage, T. H. Mauney, J. L. English, and J. G. Rainwater	Effect of Heat Flux on the Corrosion of Aluminum by Water. Part III. Final Report on Tests Relative to the High-Flux Isotope Reactor	ORNL-3230 (Dec. 5, 1961)
Griess, J. C., H. C. Savage, T. H. Mauney, and J. L. English	The Corrosion of Aluminum Under Conditions of High Heat Flux	TID-7610, p 61 (1961)
Grimes, W. R., G. M. Watson, J. H. DeVan, and R. B. Evans III	Diffusion of Chromium in Nickel-Base Alloys	TID-7610, p 63 (1961)
Hill, D. G., and M. Blander	EMF Measurements in the System $AgNO_3$ and NaCl in Equimolar $NaNO_3$-KNO_3 Mixtures and Their Comparison with the Quasi-Lattice Theory	*J. Phys. Chem.* 65, 1866 (1961)
Jenks, G. H.	Radiation Corrosion of Zircaloy-2	TID-7610, p 113 (1961)
Jenks, G. H.	Review and Correlation of In-Pile Zircaloy-2 Corrosion Data and a Model for the Effect of Irradiation	ORNL-3039 (July 6, 1961)
Kelly, M. J., J. W. Landry, T. S. Mackey, and R. W. Stelzner	Inline Applications of Gamma Monitoring and Uranium Colorimetry	*IRE Trans. Nuclear Sci.* NS-8, 89 (1961)
Kelly, M. J., W. L. Marshall, and H. F. McDuffie	Recent Developments in Aqueous Homogeneous Reactor Fuel Solution Chemistry	TID-7610, p 122 (1961)
McDuffie, H. F.	Safety in Source Handling	*Nuclear Safety* 3(2), 8 (1961)
McVay, T. N., R. E. Thoma, H. Insley, H. A. Friedman, and C. F. Weaver	Post-Irradiation Examinations of BeO	*J. Am. Ceram. Soc.* 45, 48 (1962)

AUTHOR(S)	TITLE	PUBLICATION
Neumann, P. D.	The Corrosion of Aluminum Alloys in the Oak Ridge Research Reactor	ORNL-3151 (June 23, 1961)
Parker, G. W., G. E. Creek, and W. J. Martin	Fission Product Release from UO_2 Under Simulated Reactor Accident Conditions	TID-7610, p 26 (1961)
Quist, A. S., and H. S. Frank[a]	Ice VIII – An Acetone Hydrate	*J. Phys. Chem.* 65, 560 (1961)
Quist, A. S., and H. S. Frank[a]	Pauling's Model and the Thermodynamic Properties of Water	*J. Chem. Phys.* 34, 604–11 (1961)
Quist, A. S., and C. E. Vanderzee[b]	The Third Dissociation Constant of Orthophosphoric Acid	*J. Phys. Chem.* 65, 118 (1961)
Saunders, A. R.	A Study of Fission Product Transport Mechanisms in High Temperature Gas-Cooled Reactor Fuel Elements	ORNL-3145 (June 29, 1961)
Savage, H. C., *et al.*	In-Pile Loop Irradiation of Aqueous Thoria-Urania Slurry at Elevated Temperature. Design and In-Pile Operation of Loop L-2-27S	ORNL-3222 (Jan. 29, 1962)
Schulze, R. C., W. H. Cook, R. B. Evans III, and J. L. Crowley	INOR-8–Graphite–Fused Salt Compatibility Test	ORNL-3124 (June 1, 1961)
Secoy, C. H., and H. F. Holmes	Electrokinetic Transport Properties of Thoria Surfaces in Dilute Aqueous Electrolytes	TID-7610, p 119 (1961)
Shaffer, J. H., W. R. Grimes, G. M. Watson, D. R. Cuneo, J. E. Strain, and M. J. Kelly	The Recovery of Uranium and Protactinium from Molten Fluoride Systems by Precipitation as Oxides	TID-7610, p 157 (1961)
Shields, R. P., J. E. Lee, Jr., and W. E. Browning, Jr.	Irradiation Effects on BeO	ORNL-3164 (June 7, 1961); *Trans. Am. Nuclear Soc.* 4(2), 338 (1961)
Thoma, R. E., C. F. Weaver, H. A. Friedman, H. Insley, L. A. Harris, and H. A. Yakel, Jr.	Phase Equilibria in the System $LiF-YF_3$	*J. Phys. Chem.* 65, 1096 (1961)
Thoma, R. E., and T. S. Carlton	Phase Equilibria in the System $CsF-ThF_4$	*J. Inorg. & Nuclear Chem.* 17, 88 (1961)
Thoma, R. E., H. A. Friedman, H. Insley, and C. F. Weaver	Phase Behavior of Molten Fluoride Fuels	TID-7610, p 147 (1961)
Truitt, Jack	Interdiffusion of Helium and Argon in Speer Moderator No. 1 Graphite	ORNL-3117 (June 6, 1961)
Weaver, C. F., R. E. Thoma, H. A. Friedman, and G. M. Hebert	Phase Equilibria in the System $BeF_2-UF_4-ThF_4$	*J. Am. Ceram. Soc.* 44, 146 (1961)

[a]Work performed at Department of Chemistry, University of Pittsburgh.
[b]Work performed at Avery Laboratory of Chemistry, University of Nebraska.

Papers Presented at Scientific and Technical Meetings

AUTHOR(S)	TITLE	PLACE PRESENTED
Adams,* R. E., and W. E. Browning, Jr.	The Removal of Iodine from Gas Streams	Conference on Air Cleaning, AEC, 7th, Brookhaven National Laboratory, Oct. 10–12, 1961
Baes, C. F.	Experimental Studies of Hydrolysis and Ion Association Equilibria in Aqueous Solutions at Elevated Temperatures	ORINS Lecture at Georgia Institute of Technology, October 1961
Baes, C. F.	The Extraction of Metallic Species by Dialkylphosphoric Acids	American Chemical Society, Chicago, Sept. 3–8, 1961
Baes,* C. F., and N. J. Meyer	Acidity Measurements at Elevated Temperatures: I. Uranium(VI) Hydrolysis at 25°C and 94°C	American Chemical Society, Chicago, Sept. 3–8, 1961
Blander, Milton	Association in Molten Salts	University of Minnesota, Chemistry Department Seminar, May 2, 1961
Blander, Milton	Interpretation and Evaluation of Higher Association Constants from EMF Data	Gordon Research Conference, Meriden, N.H., Aug. 30, 1961
Blankenship, F. F., and W. R. Grimes*	Recent Developments in the Chemistry of the Molten-Salt Reactor Experiment	Conference on Nuclear Reactor Chemistry, 2nd, Gatlinburg, Tenn., Oct. 10–12, 1961
Blankenship, F. F.	Fused Salts	Navy Research and Development Clinic, Raton, N.M., Sept. 29, 1961
Braunstein,* J., and R. M. Lindgren	The Association of Cadmium Ion with Bromide and Iodide Ions in Molten Equimolar $NaNO_3$-KNO_3	American Chemical Society, Chicago, Sept. 3–8, 1961
Braunstein, J.	Molten Salts	University of Mississippi, Chemistry Seminar, Mar. 24, 1961
Braunstein, J., M. Blander,* R. M. Lindgren, and Alba R. Alvarez-Funes	Activity Coefficients and Association in Molten Salt Solutions	International Congress of Pure and Applied Chemistry, 18th, Montreal, Aug. 6–12, 1961

*Speaker.

AUTHOR(S)	TITLE	PLACE PRESENTED
Braunstein, J.	EMF Measurements with Silver–Solid Silver Halide Electrodes in Molten Nitrates	Gordon Research Conference, Meriden, N.H., Aug. 30, 1961
Browning,* W. E., Jr., and H. L. Hemphill	Measurement of the Surface Temperature of Nuclear Fuel Elements	Symposium on Temperature, Its Measurement and Control in Science and Industry, 3rd, Columbus, Ohio, Mar. 27–31, 1961
Burns, J. H.	The Crystal Structure of $LiSbF_6$	American Crystallographic Association, Boulder, Colo., July 31–Aug. 1, 1961
Cantor, Stanley	Cryoscopy in Sodium Fluoride	Gordon Research Conference, Meriden, N.H., Aug. 29, 1961
Cantor, Stanley	Cryoscopy in Molten Salts	American Chemical Society, Wilson Dam Section Meeting, Mar. 14, 1961
Compere, E. L., A. J. Shor, H. C. Savage,* V. A. DeCarlo, J. M. Baker, and D. T. Jones	In-Pile Loop Irradiation of Aqueous Thoria-Urania Slurry at Elevated Temperature. Part I. Loop Package Design and In-Pile Operation	American Nuclear Society, Pittsburgh, Pa., June 4–6, 1961
Compere,* E. L., A. J. Shor, L. F. Woo, and H. C. Savage	Irradiation Effects on Thoria-Urania Slurries	Conference on Nuclear Reactor Chemistry, 2nd, Gatlinburg, Tenn., Oct. 10–12, 1961
Grimes, W. R.	Molten Fluorides as Nuclear Reactor Fuels	Alfred University, Seminar, Feb. 7, 1961
Grimes, W. R.	The Chemistry and Problems Associated with the Use of Molten Salts as Solvents	National Science Foundation Short Course for Teachers of Science, Butler University, June 30–July 1, 1961
Grimes, W. R.	Molten Fluoride Systems as Fuels and Blankets for Nuclear Reactors	Gordon Research Conference, Meriden, N.H., Sept. 1, 1961
Grimes, W. R.	Some Chemical Problems of Molten Salt Reactors	ORINS Lecture, Purdue University, Nov. 16, 1961
Kelly,* M. J., J. W. Landry, T. S. Mackey, and R. W. Stelzner	Inline Applications of Gamma Monitoring and Uranium Colorimetry	Joint Nuclear Instrumentation Symposium, Raleigh, N.C., Sept. 6–8, 1961
Kelly,* M. J., W. W. Johnston, and C. D. Baumann	The Effects of Nuclear Radiation on Thermocouples	Symposium on Temperature, Its Measurement and Control in Science and Industry, 3rd, Columbus, Ohio, Mar. 27–31, 1961

*Speaker.

AUTHOR(S)	TITLE	PLACE PRESENTED
Kelly,* M. J., G. L. Johnson, and D. R. Cuneo	Reactions of Aqueous Thorium Solutions with Hydrogen Peroxide	American Chemistry Society, Regional Meeting, New Orleans, La., Dec. 7–8, 1961
Moore,* R. E., J. H. Shaffer, and H. F. McDuffie	Preparation of High-Purity Beryllium Oxide	Conference on Nuclear Reactor Chemistry, 2nd, Gatlinburg, Tenn., Oct. 10–12, 1961
Overholser,* L. G., and J. P. Blakely	Evolution of Gas from Graphite	Conference on Nuclear Reactor Chemistry, 2nd, Gatlinburg, Tenn., Oct. 10–12, 1961
Overholser,* L. G., and J. P. Blakely	The Degassing Behavior of Commercial Graphites	Conference on Carbon, 5th Biennial, Pennsylvania State University, June 19, 1961
Parker, G. W., G. E. Creek,* and W. J. Martin	Release of Fission Products from Reactor-Grade UO_2 by Diffusion, Oxidation, and Melting	Conference on Nuclear Reactor Chemistry, 2nd, Gatlinburg, Tenn., Oct. 10–12, 1961
Parker, G. W., G. E. Creek, and W. J. Martin*	Fuel Element Decomposition Products	Conference on Air Cleaning, AEC, 7th, Brookhaven National Laboratory, Oct. 10–12, 1961
Parker,* G. W., G. E. Creek, and W. J. Martin	Fission Product Release from Reactor-Grade UO_2 by Oxidation, Diffusion, and Melting	IAEA Panel on Siting of Reactors, Vienna, Oct. 3–Nov. 3, 1961
Rainey,* W. T., R. L. Bennett, and W. M. McClain	Drift Studies on Chromel-P/Alumel Thermocouples in Helium Atmospheres	Symposium on Temperature, Its Measurement and Control in Science and Industry, 3rd, Columbus, Ohio, Mar. 27–31, 1961
Shields,* R. P., C. E. Miller, Jr., R. A. Lorenz, and W. E. Browning, Jr.	Release of Fission Products on the In-Pile Melting of Reactor Fuels	Conference on Nuclear Reactor Chemistry, 2nd, Gatlinburg, Tenn., Oct. 10–12, 1961
Shields, R. P., J. E. Lee, Jr.,* and W. E. Browning, Jr.	Irradiation Effects on BeO	American Nuclear Society, Chicago, Nov. 7–9, 1961
Shor,* A. J., and E. L. Compere	Corrosion in an In-Pile Aqueous Thoria-Urania Slurry Loop	Corrosion Symposium, 10th Annual AEC, San Diego, Calif., May 9–11, 1961

*Speaker.

AUTHOR(S)	TITLE	PLACE PRESENTED
Soldano, B. A.	Is Planck's h Gravitational in Origin?	American Physical Society, New York, Jan. 31–Feb. 4, 1961
Sturm, B. J.	A Study of Phase Equilibria in the System CrF_2-CrF_3	Tennessee Academy of Science, Martin, Tenn., Nov. 24, 1961
Thoma,* R. E., H. Insley, H. A. Friedman, and C. F. Weaver	Phase Equilibria in the System NaF-ThF_4-UF_4	American Ceramic Society, 63rd Annual Meeting, Toronto, Canada, Apr. 23–27, 1961
Watson, G. M.	The Chemistry and Problems Associated with the Use of Molten Salts as Solvents	National Science Foundation Short Course for Teachers of Science, Butler University, June 29, 1961
Watson,* G. M., R. B. Evans III, and Jack Truitt	A Diffusion Model for the Transport of Gases in Porous Media	Conference on Nuclear Reactor Chemistry, 2nd, Gatlinburg, Tenn., Oct. 10–12, 1961

*Speaker.

ORNL-3262
UC-4 – Chemistry
TID-4500 (17th ed.)

INTERNAL DISTRIBUTION

1. Biology Library
2. Reactor Division Library
3. ORNL – Y-12 Technical Library, Document Reference Section
4-6. Central Research Library
7-26. Laboratory Records Department
27. Laboratory Records, ORNL R.C.
28. C. E. Larson
29. A. M. Weinberg
30. J. P. Murray (K-25)
31. R. G. Jordan (Y-12)
32. J. A. Swartout
33. G. E. Boyd
34. F. R. Bruce
35. W. H. Jordan
36. H. G. MacPherson
37. A. H. Snell
38. A. L. Boch
39. R. B. Briggs
40. J. A. Lane
41. W. D. Manly
42. H. C. McCurdy
43. D. S. Billington
44. F. L. Culler
45. J. H. Frye, Jr.
46. M. T. Kelley
47. E. H. Taylor
48. S. E. Beall
49. M. A. Bredig
50. L. T. Corbin
51. J. E. Cunningham
52. J. H. Crawford
53. A. P. Fraas
54. R. N. Lyon
55. A. J. Miller
56. J. C. White
57. M. J. Skinner
58. W. R. Grimes
59. E. G. Bohlmann
60. H. F. McDuffie
61. G. M. Watson
62. F. F. Blankenship
63. C. H. Secoy
64. C. F. Baes
65. C. J. Barton
66. M. Blander
67. W. E. Browning
68. R. E. Thoma
69. S. Cantor
70. E. L. Compere
71. R. B. Evans III
72. J. C. Griess
73. G. H. Jenks
74. G. W. Keilholtz
75. M. J. Kelly
76. W. L. Marshall
77. L. G. Overholser
78. G. W. Parker
79. W. T. Rainey
80. H. C. Savage
81. J. H. Shaffer
82. R. A. Strehlow
83-93. G. C. Warlick
94. E. V. Jones (Consultant)
95. Farrington Daniels (Consultant)
96. F. T. Miles (Consultant)
97. F. T. Gucker (Consultant)
98. Leo Brewer (Consultant)
99. H. Insley (Consultant)
100. J. E. Ricci (Consultant)
101. D. G. Hill (Consultant)
102. G. W. Morey (Consultant)
103. Henry Eyring (Consultant)
104. M. G. Fontana (Consultant)
105. R. M. Fuoss (Consultant)
106. Norman Hackerman (Consultant)
107. H. S. Harned (Consultant)
108. E. A. Mason (Consultant)
109. T. N. McVay (Consultant)
110. George Scatchard (Consultant)
111. T. F. Young (Consultant)
112. J. W. Cobble (Consultant)
113. P. H. Emmett (Consultant)
114. R. F. Newton (Consultant)

EXTERNAL DISTRIBUTION

115. R. W. McNamee, Union Carbide Corp.
116. Division of Research and Development, AEC, Washington
117. Division of Research and Development, AEC, ORO
118. Division of Reactor Development, AEC, Washington
119. Division of Reactor Development, AEC, ORO
120-706. Given distribution as shown in TID-4500 (17th ed.) under Chemistry category (75 copies – OTS)